POLITECNICO DI MILANO

Scuola di Ingegneria Industriale e dell'Informazione

Corso di Laurea Magistrale in Ingegneria Chimica

Experimental and numerical study of heat transfer
in open cell metal foam as catalyst support

Relatore: Prof. Enrico Tronconi

Correlatore: Prof. Gianpiero Groppi

Dr. Carlo Giorgio Visconti

Dr. Pedram Aghaei

Tesi di Laurea Magistrale di

Cavallini Tommaso   Matricola: 786881

Anno Accademico 2013-2014

Summary

Index of figures

Riassunto

Scopo di questo lavoro di tesi è lo studio delle schiume metalliche come supporto per reattori catalitici. Tali supporti catalitici sono di interesse in quanto consentono di intensificare i processi in cui il trasferimento di calore gioca un ruolo principale, ossia in cui avvengono reazioni catalitiche eterogenee fortemente esotermiche e endotermiche, come ad esempio il processo di *steam reforming* o la sintesi di *Fischer-Tropsch*. In questo contesto, le schiume metalliche sono di particolare rilievo poiché presentano un'alta superficie di scambio, alta frazione di vuoto e alti coefficienti di trasferimento di calore e materia, il tutto con perdite di carico ridotte. Tuttavia, ancora oggi è difficile valutare le prestazioni dei reattori impaccati con schiume, dal momento che non esistono ancora né dati né correlazioni soddisfacenti per descrivere il fenomeno. Durante questo lavoro si è cercato di raccogliere un alto numero di prove sperimentali in modo da poter avere un sufficiente numero di dati per poi provare a descrivere quantitativamente lo scambio termico nelle schiume. Sono stati studiati campioni con diversa conducibilità, diversa porosità, e diversa densità dei pori per determinare e valutare il ruolo dei diversi meccanismi di trasferimento di calore in tali supporti.

Dopo una breve introduzione all'argomento (Capitolo 1), nel Capitolo 2 è stata effettuata un'approfondita caratterizzazione geometrica e gravimetrica delle schiume. La caratterizzazione geometrica è necessaria al fine di definire i diametri di cella e dei pori e le dimensioni dei ligamenti, ed è stata svolta tramite la microscopia ottica, mentre la caratterizzazione gravimetrica serve a misurare la densità dei campioni, utilizzando una bilancia ad immersione. Nel capitolo successivo è descritta in modo particolareggiato la procedura sperimentale con i relativi problemi riscontrati. La parte sperimentale ha previsto lo svolgimento di test volti a raccogliere profili di temperatura a differenti coordinate radiali e assiali di otto tipi diversi di schiume; il campione da testare viene posto all'interno di un tubo posizionato in una camera termostatica, al cui interno viene flussata una portata nota di azoto o elio. Raggiunta la condizione di stazionarietà, si procede con la raccolta dei profili di temperatura a differenti coordinate radiali (r = 0, r = 1/2 R e r = 2/3 R) e assiali (ogni 5 mm per un totale di 100 mm). Nel Capitolo 4 viene descritto il modello usato per stimare i parametri termici, si tratta di un modello 2D, sotto l'ipotesi di fase pseudo - omogenea e geometria assialsimmetrica scritto in *Athena*, un ambiente software per la modellazione matematica che utilizza il linguaggio *Fortran*. I dati sperimentali per le misure di trasferimento di calore sono poi presentati nel Capitolo 5. Inoltre, sono stati analizzati gli effetti di diverse portate, tipi di gas, tipi di schiume, temperature della fornace sui profili di temperatura. Infine sono stati esaminati i parametri stimati dal modello, studiandone l'andamento in base alle diverse condizioni operative.

Abstract

The purpose of this thesis is the study of metal foam as a support for catalytic reactors. Such catalytic supports are interesting since they allow to intensify the processes in which the heat transfer plays a main role, i.e. in heterogeneous catalytic reactions, both highly exothermic and endothermic, such as steam reforming or the Fischer-Tropsch synthesis. In this context, the metal foams are particularly important since they have a high exchange surface area, high void fraction and high coefficients of heat and mass transfer with a very low pressure drop. However, it is still difficult to assess the performance of the reactors packed with foam, since there are not yet any data or any satisfactory correlations to describe the phenomenon. During this work a large number of experimental tests have been performed in order to have a sufficient number of data and then to try to quantitatively describe the heat transfer in foams. Samples with different conductivity of the solid bulk material, different porosity, and different pore density were investigated to determine and evaluate the role of the different heat transfer mechanisms in such supports.

After a brief introduction to the topic (Chapter 1), in Chapter 2 a detailed characterization of geometric and gravimetric foams has been carried out. The geometric characterization is required in order to define the cell and pore diameters and the size of the struts, and it was carried out by optical microscopy, whereas the gravimetric characterization serves to measure the density of the samples, using a buoyancy balance. The following chapter describes in detail the experimental procedure with their problems. The experimental part consists in conducting tests aimed to collect temperature profiles at different radial and axial coordinates of eight different types of foams; the sample is placed inside a tube inserted in a thermostatic chamber, where a known flow rate of nitrogen or helium is fluxed in. Once the steady state condition is reached, the temperature profiles are collected at different radial coordinates (r = 0, r = 1/2 R and r = 2/3 R) and different axial coordinates (every 5 mm for a total of 100 mm). In Chapter 4 the model used to estimate the thermal parameters is described. This is a 2D model, made under the assumption of pseudo - homogeneous phase and axial symmetric geometry, written in *Athena*, a mathematical modeling software which uses a *Fortran* code. The experimental data for the measurements of heat transfer are presented in Chapter 5. Moreover, the effects of different flow rates, gas types, types of foams, the temperature of the furnace, on temperature profiles have been analyzed. Finally, the parameters estimated by the model have been examined in order to study the results under different operating conditions.

1.   State of art

1.1   Introduction

Open-cell foams, also called solid sponges are irregular structures made of different materials, both metals or metal alloys and ceramics [1]. In this project the attention will be focused on the metal foams. These cellular materials, due to their structure with high porosity - typically 75-95% of the volume consists of void space - and specific surface area, offer excellent potential for higher performance in terms of resistance to flow, i.e. low pressure drops, high gas-solid mass transfer, and in case of metallic foams, high heat transfer efficiency [2, 11]. Furthermore, in comparison to honeycomb monoliths, metal foams improve mass and heat transfer thanks to the flow turbulence produced by their spongy structure allowing the radial mixing [3].

Figure 1.1 - Samples of commercial open-cell foams.

In general, there are three types of solid foams: close-cell foams, open-cell foams and a combination of the two [4]. Recently, a novel structure has been developed, known as lotus-type growth, which consists of long cylindrical pores aligned in one direction [5]. Closed-cell foams are composed by isolated cells linked together by a continuous and impermeable wall [4]. Such features make these foams applicable to be used in insulation, energy absorption, and structuring items. In contrast, the open cell incorporate interconnected pores, whereas close cell pores are surrounded by a metallic wall [4]. The fundamental unit consists of pores communicating through windows [6]. In this type, as shown in figure 1.2, it is possible to recognize three component: strut, cell, and pore (window). Struts are composed of solid material; cells are the void part, often spherical in shape, enclosed by struts; finally, pores are openings which connect the cells to each other. Open-cell metal foams structures involve a high surface and volume ratio that make

them attractive for different applications, i.e. heat exchangers, fuel cell electrodes, high temperature filters, electron emitters, and catalyst supports [4, 12].
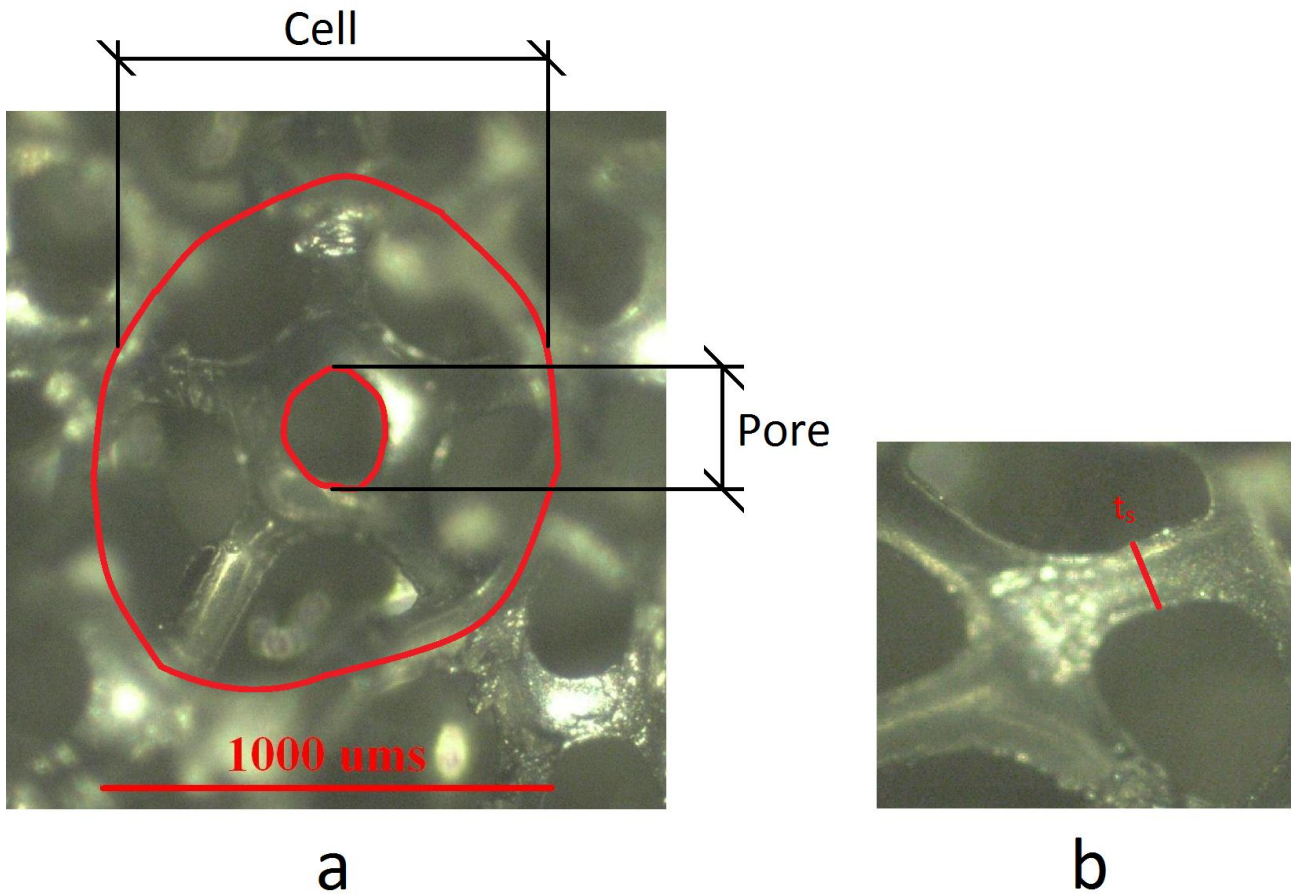
Figure 1.2 - (a) Identification of cell and pore diameters in the foams samples; (b) average strut thickness in the middle.

In the last three decades, several processes have been developed to introduce pores, almost uniformly distributed, in metallic materials [4]. Two common processes are used for manufacturing metal foams: the liquid metal route which foaming is accomplished by direct foaming of melt with gas, or some foaming agent, and the powder metallurgy route which manufacturing is done by foaming a sintered compact. Used gases usually are air, nitrogen or argon which precipitate during solidification and if they are not allowed to escape, they will give rise to a foamed structure [4]. Other ways for manufacturing metal foams include sintering of hollow spheres, and pressing the material around a filler followed by sintering with subsequent filler dissolution or decomposition [4]. If the production is carried out in microgravity conditions is possible stabilize the foam and obtain highly porous structures [4]. In figure 1.3 it is possible to see the most important methods by which metallic foams can be produced.
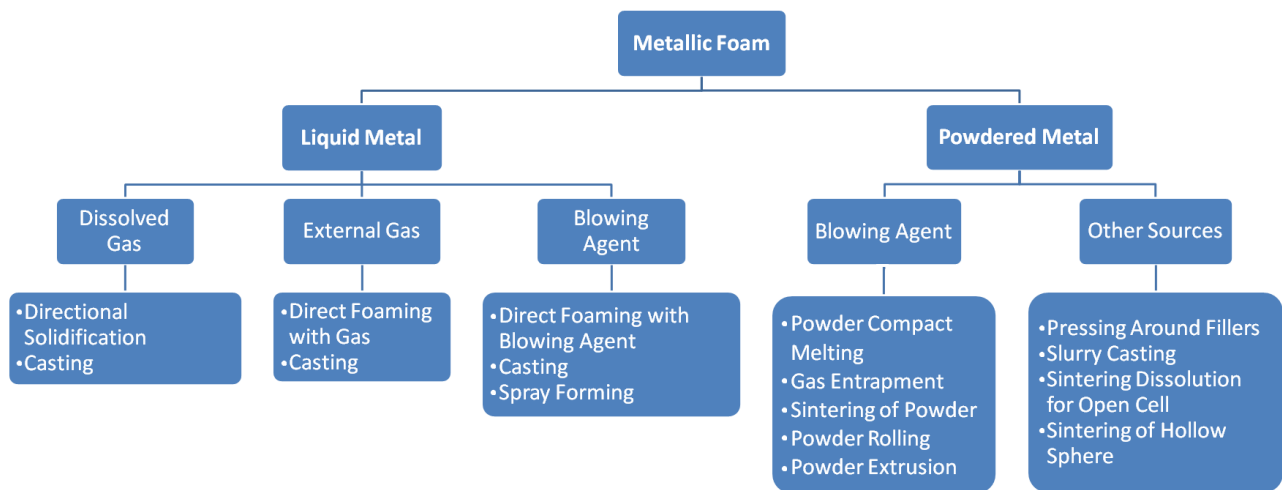
Figure 1.3 - Processing map for metallic foam [4].

Typically different kinds of materials are used to manufacture solid foams exist: metal, ceramic, polymer and carbon, and they are applied in a wide range of applications. The principal materials of ceramic foams are α-alumina, zirconia and cordierite; instead, for the metal foams, copper, aluminum, nickel, iron-chromium alloy, nickel-chromium, cobalt, stainless steel, lead, titanium, tin, and zinc are used [7, 8]. Obviously, different materials mean different intrinsic characteristic and consequently different applications. For examples a ceramic open-cell foam will give a low pressure drop, but not a high heat exchange efficiency, differently from the metal one.

Open-cell metal foams, as catalyst supports, offer the advantage of radial mixing and a better mass and heat transfer in comparison to honeycomb monoliths [9, 10]. Moreover, they have a high contact surface between active catalyst and reactants. Reducing pressure drop process energy costs are decreased and large space velocities are provided. Consequently it becomes possible to produce more compact units than the conventional reactors [11].

These cellular materials exhibit the unique combination of physical and mechanical properties such as high rigidity, low specific weight, and high gas permeability [4]. The most important applications of these materials are in the area of automotive industries, light weight construction materials, silencers, flame arrester, heaters, and electrochemical applications [12-15]. Their high thermal conductivity also make them an interesting candidate as catalyst support, in particular in the both exothermic and endothermic reactions, which a high thermal control is needed [2]. Open-cell metal foams as catalyst carriers can also minimize the appearance of hot spots in the catalysts, and prevent mechanical-strength and thermal-shock limitations. Another advantage is the possibility to manufacture metal foams which match with the shape and size of reactor, simplifying the assembling of many long and narrow tubes. These properties suggest replacing conventional packed-bed catalysts with the metal foams. In fact, using foams as catalyst supports, smaller reactors could be produced, obtaining higher yields and selectivities, particularly in heat-transfer-

limited processes and improving temperature controller and heat management [3, 16]. For conventional packed-bed reactors the needed surface for heat transfer, into or from the process, is accomplished by multiple long tubes with a very small diameter causing a significant pressure drop. To avoid this issue the catalyst pellets should be used larger, increasing the radial heat transfer too, but decreasing the effectiveness factor [3]. All these issues can be solved by employing metal foams as supports, because they fit with the tube and are made of a highly conductive material, so high heat transfer is delivered. Because of complex interactions between technical and economic factors, evaluations for replacing packed particles with structured foam supports must be considered case by case.

As mentioned, above metallic foams are very suitable in heat-transfer-limited processes. In chemical industry, a large number of reactor operations are heat-transfer-limited, and they require an accurate heat exchange control. Many reactions, interesting from the industrial viewpoint, are highly endothermic, like dehydrogenations (cyclohexane to benzene or ethyl benzene to styrene) and steam reforming (to product synthesis gas); or strongly exothermic like hydrocarbons partial oxidation, where the desired product is an intermediate and a short contact time is provided, alkylation (benzene to ethyl benzene), oxychlorination such as acetic acid to vinyl acetate, and hydrogenations as methanol and Fisher-Tropsch synthesis [3]. All of these features would enable substantial intensification of many crucial catalytic processes, which could be run with greatly enhanced performances and in much more compact units as compared to conventional reactors, particularly in critical areas related to energy conversion and environmental protection, like distributed H_2 generation, with the development of efficient small-scale reformers or fuel cells; local exploitation of biomass and biogas, i.e. conversion to clean liquid fuels in compact and transportable reactors; improved after treatment of polluting emissions from vehicles, trains and ships, typically affected by severe volume constraints, with a significant reduction of the size of catalytic converters [11].

In spite of the great potential of industrial implementation of open-cell metal foams as structured catalyst supports, however, there are still some challenges to be addressed to improve the applicability of these materials as catalysts supports.

1. To fully exploit the superior physical and mechanical characteristics of these materials, engineering correlations which describe mass and heat transfer properties, representing quantitatively the dependence of these phenomena on the geometry of the adopted supports, on their thermal conductivity and on the associated flow dynamics, are needed. There is not enough data available to conduct an effective investigation on this subject and the existing data often are contradictory [11].

2. The metal foam supports must be stable during long term reactions at high temperature. Neither support composition nor the catalyst deposition process should cause the deactivation due to the

poisoning, ion migration, sintering, and interaction between the support and the catalytic layer at elevated temperatures [17].

3. The catalyst preparation is still problematic, due to the impurities which might be added during this process and cause catalyst poisoning. Also, some bare metal on the foam surface might be accessible if the metal foam is not fully covered by the washcoat. This can reduce the catalytic activity [17].

4. Proof-of-concepts and demonstrations at a representative process scale are still lacking [11].

5. Finally, the commercially available metal sponges, originally designed for other applications, i.e. energy absorption, filtration, and noise reduction, do not necessarily be endowed with optimal structural characteristics for catalytic applications in terms of both fabrication material and geometry, and also are associated with high manufacturing costs [4, 11, 12, 18]. However, to consider metal foams attractive as catalyst supports, the manufacturing cost should be comparable to that of pellets [3, 11].

1.2 Heat transfer mechanism in open cell metal foam

Most of the previous studies on heat transfer in porous matter are based on the Darcy's law, which is only valid for Reynolds number inferior of 10. [20] Under such conditions, the fluid and the solid matrix can be assumed to be in local thermal equilibrium, so everything can be treated as a continuum. But going to higher flow rates, which are typical for industrial-scale reactors, in metal foam, heat transfer is caused by fluid convection and mixing. The thermal conductivity of the two phases is replaced by an effective thermal conductivity ke, which is determined by the combination of the physical properties of the two phases, the catalyst geometry, the reactor geometry and the operating conditions. It is possible to define different mechanisms for heat transfer in metal foam:

- Conduction through the solid (foam - tube);
- Radiation between surfaces of foam (specially at high temperature);
- Conduction within the fluid;
- Convection by the fluid in axial direction;
- Axial and radial mixing of the fluid;
- Fluid-solid heat transfer;
- Conduction through the fluid film near contact points.

The bulk of the fluid flows axially and causes convective transport in this direction. Inside the foam fluid flows chaotically in empty spaces between the solid part, thereby causing additional heat transport in axial and radial direction; mixing of the fluid is due to the turbulence and molecular conduction. At high flow rates, , this contribute additional to the convective transport is referred to as heat dispersion. If the

temperature of the solid is different to that of the fluid flowing within the bed, an additional heat exchange contribute must be taken into account. The contribution of heat conduction through the solid can be significant depending on the conductivity of the solid and the fluid velocity. Heat transfer occurs even through radiation between part of the foam. Since there are a lot of contributes, estimation of the heat transferred by the foam is not an easy task. However this can be divided in two directions, radial and axial. The radial direction is the most important and it is defined by the sum of static contribute and convective contribute:

$$k_{er} = k_{er}^s + k_{er}^c \tag{1.1}$$

The static contribute is definable as sum of three different terms:

$$k_{er}^s = k_{rad}^s + k_f^s + k_{solid}^s \tag{1.2}$$

Where k_f^s is the conductivity of the flowing gas, k_{solid}^s is the conductivity of the foam material and k_{rad}^s the contribute due to radiation.

For the heat transfer at the wall is possible to do the same approach. It can be defined by a sum of a static contribute and a contribute which depends on the flow rate:

$$h_w = h_w^s + h_w^f \tag{1.3}$$

The static contribute is definable as sum of three different terms:

$$h_w^s = h_{gas}^s + h_{rad}^s + h_{cond}^s \tag{1.4}$$

Where h_{gas}^s is the heat transferred by the fluid, h_{rad}^s is the contribute of radiation and h_{cond}^s is due to the conduction between foam and wall. It is possible to define two different Nusselt numbers, related to the different contributes to the wall heat transfer coefficient:

$$Nu_w^s = \frac{h_w^s d_c}{k_f} = cost \tag{1.5}$$

Since the Nusselt number is only a function of the gas conductivity and the foam geometry configuration is constant.

$$Nu_w^f = \frac{h_w^f d_c}{k_f} = f(Re) \tag{1.6}$$

This contribute, since depends on the flow rate can be defined as a function of Reynolds number. The main contribute to heat transfer at the wall is due to the pure conduction through the fluid film at the interface. At high fluid velocities, a temperature drop at the wall can be observed,; this causes a change in the

effective mixing length in heat dispersion and an increase of the axial velocity. Heat transfer resistance at the wall is a function of the effective radial conductivity of the bed and of a true fluid film resistance developing at the interface. Empty foams made of highly conductive materials show a great effective radial conductivity due to a high conductivity of the solid metal matrix, but since they have not a perfect contact with the wall cannot present high wall heat transfer coefficients.

This work has to be considered as a continuation of Bianchi thesis work [2, 44]. In those studies 5 different metal foams were analyzed, two made of FeCrAlY and three made of Al with the properties reported in the following table.

Table 1.1 - Properties of foams studied by Bianchi.

Material	Hydraulic porosity [-]	Total porosity [-]	Cell diameter [mm]	Pore diameter [mm]	Strut thickness [mm]
FeCrAlY	0.94	0.949	5.09	2.20	0.45
FeCrAlY	0.931	0.937	1.55	0.86	0.14
Al-6101	0.89	0.89	2.03	0.86	0.28
Al-6101	0.897	0.897	3.59	1.83	0.44
Al-6101	0.945	0.945	2.00	0.81	0.27

With a similar experimental procedure which will be adopted here, Bianchi collected the axial and radial temperature profile, and using a model written in *Fortran*, estimated three parameters: the axial and radial effective conductivity and the wall heat transfer coefficient. For this parameters he found that the effective radial conductivity can be nearly described by the Lemlich theory:

$$k_{Lemlich} = \frac{(1 - \varepsilon_T)}{3} k_s \tag{1.7}$$

But, especially for lower conductive material, it is not enough to explain the phenomenon, since it doesn't take into account the radial and convective effects. However what had been found is that the Lemlich theory is a good starting point. As far it concerned the wall heat transfer coefficient, starting from equation 1.5, 1.6 and then 1.3, Bianchi found the following correlation:

$$h_W = \frac{k_f}{d_c}(7.18 + 0.029 Re^{0.8}) \tag{1.8}$$

Valid for Reynolds number between 4 and 255, with a good agreement with the experimental data.

The foams studied in this work have a bigger porosity with a small cell diameter, so they have an higher PPI. The purpose is to augment the experimental data available, and for this reason a huge experimental campaign has been conducted.

What will be done here is to collect new sets of experimental data and analyze the heat transfer parameters estimated by the model; in the future works will be to see if these correlations are still valid and if they are not, try to modify them or propose new ones.

2. Properties of tested samples

2.1 Foam materials

Samples investigated in this work are open-celled metal foams made of cobalt, copper, iron-chromium alloy, and nickel-chromium alloy supplied by Alantum Europe GmbH in two different nominal cell diameters, 580 μm and 1200 μm, as shown in figure 2.1, shaped as disks.
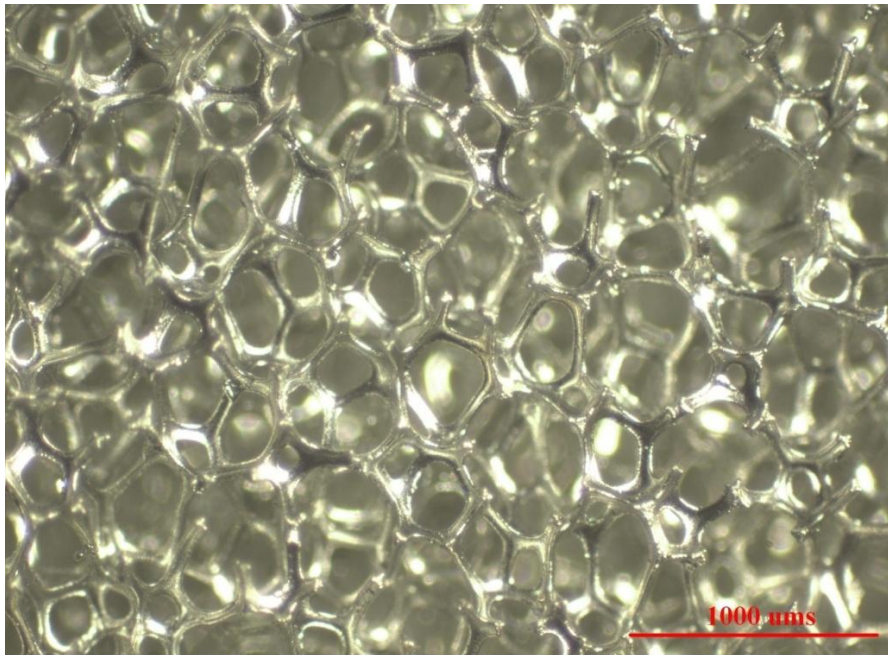
Co 580 μm
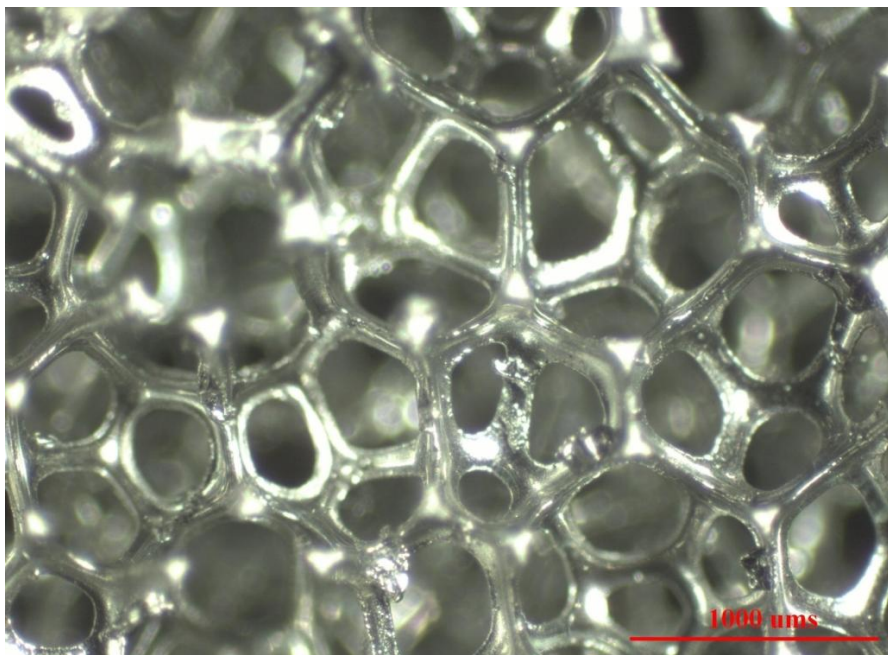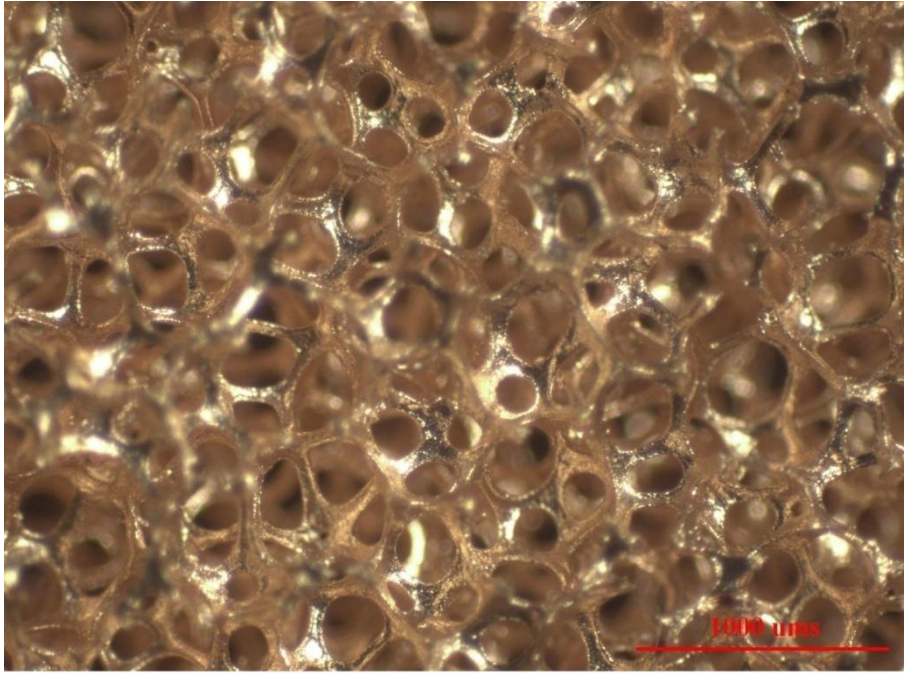
Co 1200 μm

Cu 580 μm
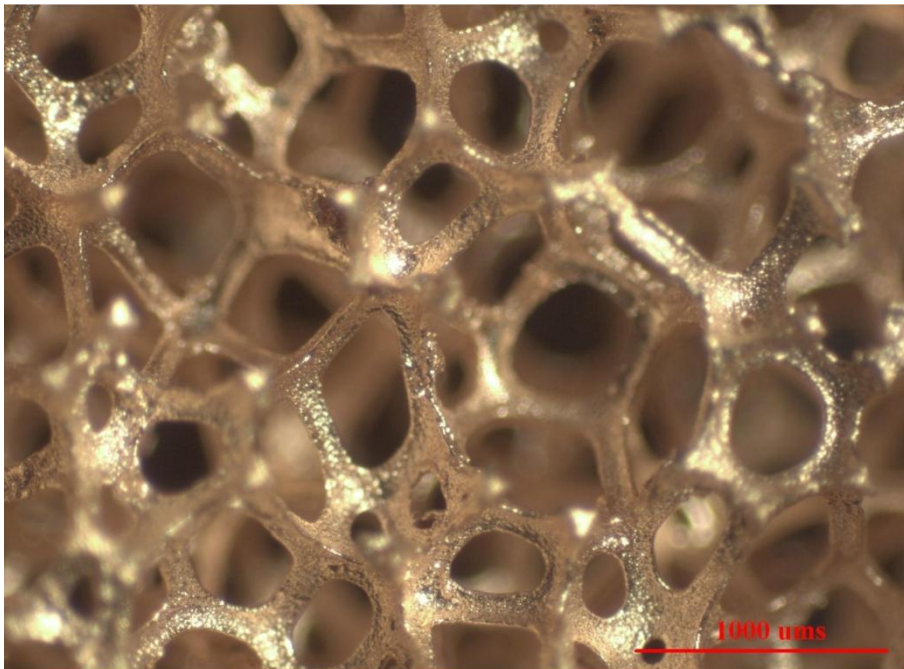
Cu 1200 μm
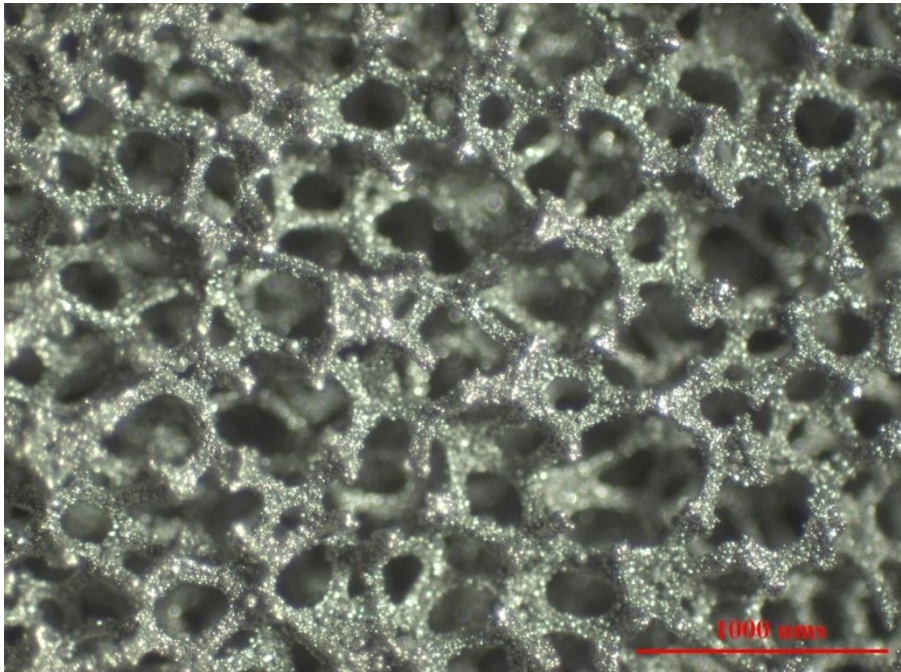
FeCr Alloy 580 μm
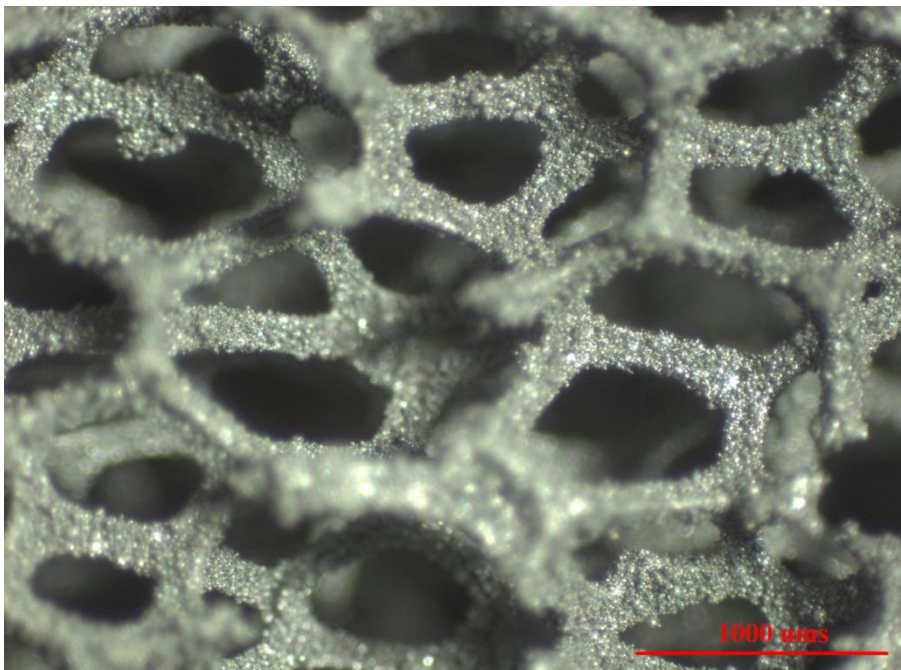
FeCr Alloy 1200 μm
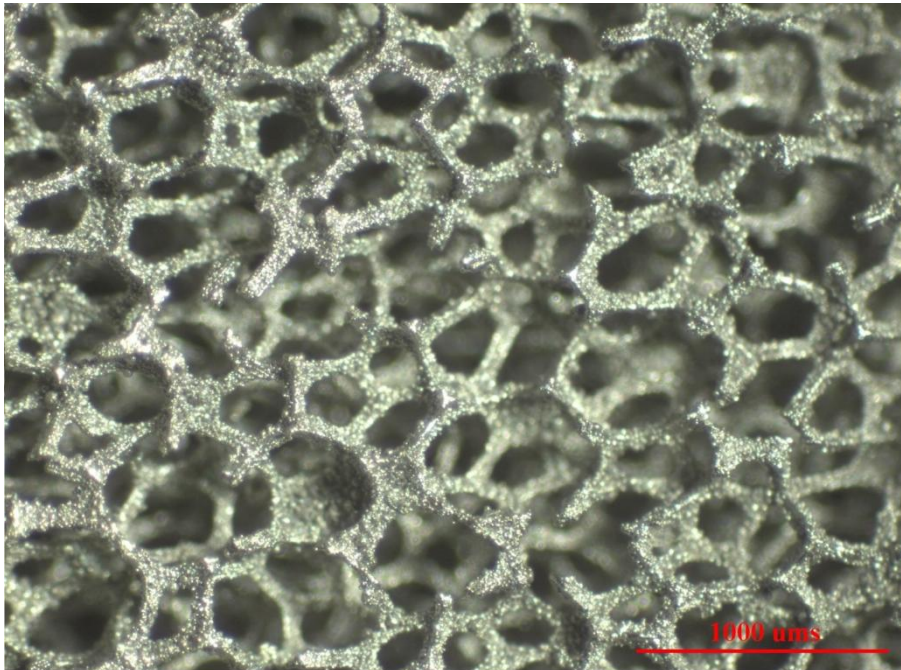
NiCr Alloy 580 µm
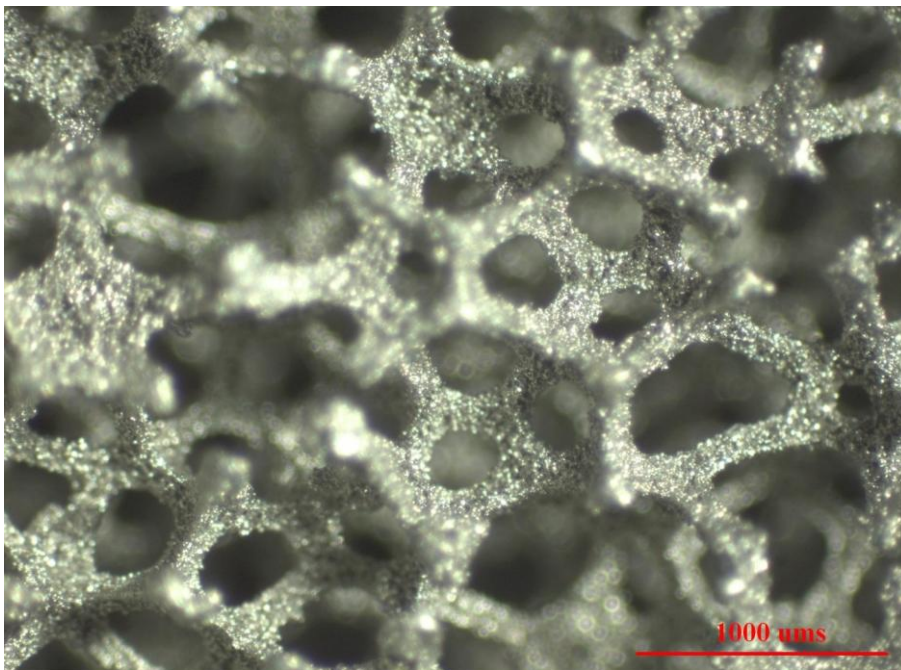
NiCr Alloy 1200 µm

Figure 2.1 - Cellular structure of tested foam samples. Images obtained with optical microscope with a magnification of 40.

2.2 Morphological characterization

A good knowledge of cell configuration and characteristic dimension of solid foams is needed to illustrate and to understand correctly the transport properties. However, because of the geometrical complexity and random orientation of the solid phase and the average porous, the real geometry of foams is not easy to be characterized without sophisticate methods like magnetic resonance or X-ray micro-computed tomography [19]. Here, in order to characterize the structures of the foams, an optical microscope is used to measure the average cell and pore diameter and average strut thickness in the middle.

2.2.1 Geometrical characterization

In order to propose a suitable model to describe satisfactorily the cell shape, many studies have been made. Thus, starting from a simple cubic structure [20], firstly it has been suggested a rhombic dodecahedron shape by Plateau [21], which however doesn't minimize the surface to volume ratio of the foam. Furthermore Kelvin supposed a tetrakaidecahedron framework [22]; and finally Wearie and Phelan [23,6], suggested a cell with 12-14 pentagonal or hexagonal faces which definitively represents, as a geometric idealization, the open-celled foams shape [23, 2]. Once the fundamental cell configuration is decided, foams can be ideally characterized by their porosity based on microscopic geometrical parameters such as pore, cell diameter, or strut thickness [2]. Figure 2.2 shows the different discussed cell models.
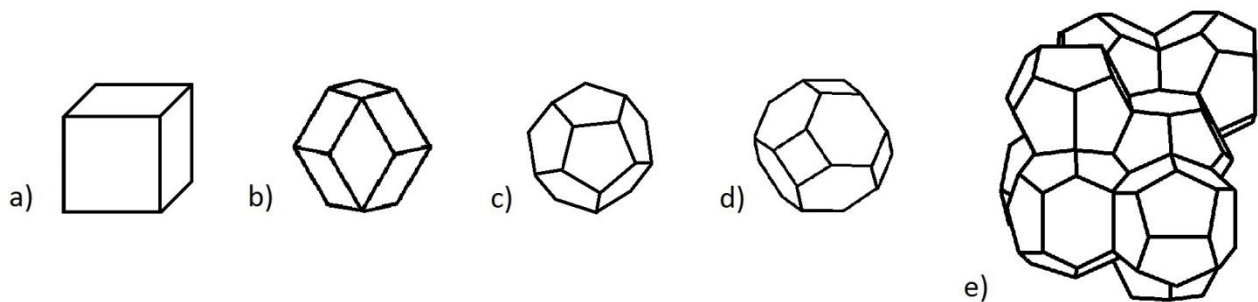
Figure 2.2 - Different cell models: a) cube; b) rhombic dodecahedron; c) dodecahedron; d) tetrakaidecahedron; e) Weaire-Phelan structures

Metal foams are composed by three elements: strut, cell and pore. Differently from other studies (Bianchi et al. [2]) that simplified pore and cell to a circular shape, in this work we have considered them as an ellipse, thus we have taken two measures for each of them, the major and the minor axes and made the average of this two. In any given cell the pores can be of different size, but they are generally simplified to a single average size. The number of these pores that underlie one linear inch is used by manufactures to indicate the foam pore density (pores per inch, PPI). In such way an average pore diameter is between 30% and 70% of the diameter of its parent cell [2]. The struts thickness is not constant, but it changes from the centre, where it is less thick, to the intersection with other struts. In this work an average strut in the middle is measured. Since the strut cross section may be of different shapes (as it shown in figure 2.3b), the

measured value is the diameter of the strut in case of cylindrical one, while it is the length of a side of triangle for struts of triangular shape. Strut shapes of investigated samples are shown in figure 23a.
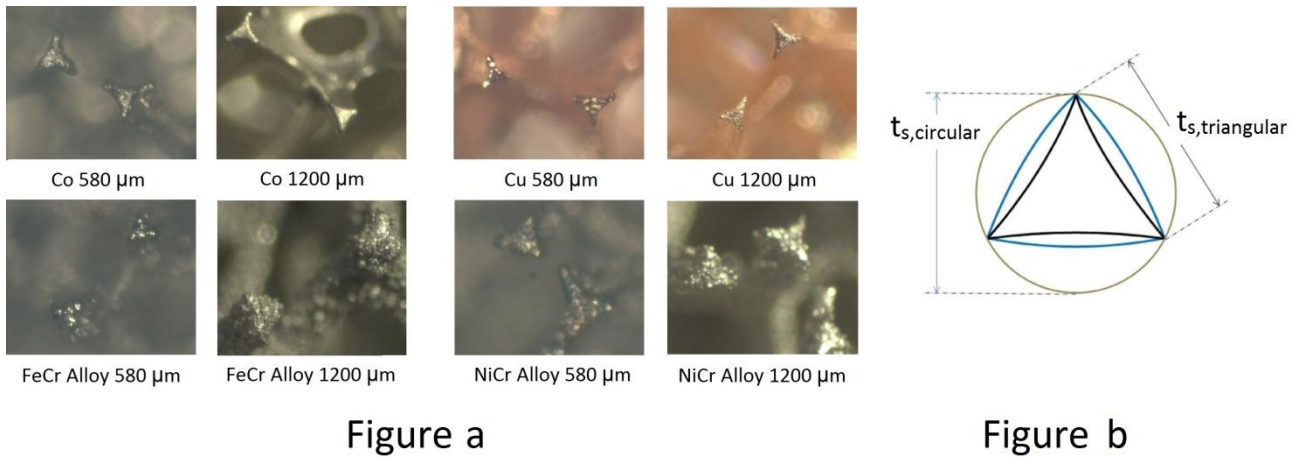
Figure 2.3 - (a) Identification of struts shape for each foam sample with a magnification of 40 for the 1200 μm nominal cell diameter samples and with a magnification of 50 for the 580 nominal cell diameter samples; (b) strut thickness for every shape

As it is possible to see in figure 2.3a, all struts of samples have a concave triangular shape, at least triangular, even if in case of FeCr alloy is quite difficult to identify them, due to the roughness formed by alloy. Averaged measures of characteristic sizes of foams and their standard deviation (σ) are reported in table 2.1. Micrographs are taken with an optical microscope (*Olympus SZ-CTZ 40*) with a magnification of 40, lengths are measured with PC software *Image Pro Plus 5.0*.

Table 2.1 - Geometrical properties of the investigated metal foam samples. Average measurements of cell ($\bar{d}_c$), pore ($\bar{d}_p$), and strut ($\bar{t}_s$) diameter and their corresponding standard deviation (σ_{d_c}, σ_{d_p}, and σ_{t_s}).

Optical Microscope Analysis						
Foam Material	Nominal Cell Diameter [μm]	Cell Diameter [μm]		Pore Diameter [μm]		Average Strut Thickness in the Middle [μm]	
		$\bar{d}_c$	σ_{d_c}	$\bar{d}_p$	σ_{d_p}	$\bar{t}_s$	σ_{t_s}
FeCr Alloy	580	608,19	92,95	194,45	69,75	82,81	11,45
FeCr Alloy	1200	1312,77	257,97	492,80	221,46	178,01	24,15
NiCr Alloy	580	626,66	109,93	224,61	77,92	72,96	11,33
NiCr Alloy	1200	1109,76	154,89	295,95	100,93	142,86	36,74
Co	580	596,64	82,63	256,19	106,87	68,36	13,95
Co	1200	1051,22	121,78	335,95	115,75	122,91	18,73
Cu	580	648,02	105,32	205,46	65,76	73,58	15,52
Cu	1200	1089,46	160,07	339,59	146,78	128,93	18,40

In table 2.1, each geometrical parameter of the studied foams is the average of at least 40 measurements to make sure of an error range less than 10% at confidence level α=0,95 [2]. Making some calculations with this measures it is possible to notice that average pore diameter is 31% - 42% of the diameter of its parent cell, and the average strut thickness is between 11% and 13% of the diameter of its parent cell too.

The specific surface area can be considered as a geometrical property of open-cell foams. This feature can be assessed by scanning the foam sample with an X-ray micro-computed tomography machine, then a 3D image is created whereby geometrical measure are taken, such as described in detail by Bianchi et al. [2]. However, many models are developed to predict the specific surface (S_V) of open-celled foams. All of them are functions of the characteristic dimensions, such as pore, cell or struts diameter, and functions of the hydrodynamic porosity, which represents the accessible void space in a foam. First a model for cell should be chosen, then a correlation for a single unit can be proposed and finally this can be extrapolated to the whole foam. For example, Lacroix et al. [25] proposed the following model, considering the single cell as a cube:

$$S_V = \frac{4}{t_s}(1 - \varepsilon_H) \tag{2.1}$$

Where, ε_H is the hydrodynamic porosity. As Giani et al. [24] reported:

$$t_s = d_c \left[\frac{4}{3\pi}(1 - \varepsilon_H)\right]^{\frac{1}{2}} \tag{2.2}$$

so the surface area can be rewritten:

$$S_V = \frac{2}{d_c}\sqrt{3\pi(1 - \varepsilon_H)} \tag{2.3}$$

As in the cubic model pore and cell have the same diameter, d_c can be replaced by d_p [2]. Calmidi et al. [26] suggested a formula suitable for a dodecahedra cell shape:

$$S_V = \frac{3\pi t_s}{(0.59 d_c)^2}\left[1 - exp\left(-\frac{(1 - \varepsilon_H)}{0.04}\right)\right] \tag{2.4}$$

Inayat et al. [27] advised a model for the tetrakaidecahedron configuration which also takes into account the different cross section of struts:

$$S_V = \alpha \frac{\left[1 - 0.971(1 - \varepsilon_H)^{\frac{1}{2}}\right]}{d_p}(1 - \varepsilon_H)^{\frac{1}{2}} \tag{2.5}$$

Where, α is equal to 6.49 for concave triangular struts, 5.62 for triangular struts, and 4.867 for cylindrical struts.

Finally Grosse et al. [19] used the Weaire-Phelan structure to model open-celled foam, obtaining the semi-empirical correlation:

$$S_V = \frac{4.84\sqrt{1 - \varepsilon_H} - 2.64(1 - \varepsilon_H)}{(d_p + t_s)}$$

$$(2.6)$$

Where, the coefficients (4.84 and 2.64) are defined by an empirical fitting procedure based on their experimental data. These correlations should be applied to predict the experimental data, but they always need to be compared with the empirical results because they don't always represent correctly the real surface area as made by Bianchi et al. [2]. Specific surface areas of every foams are calculated using the described correlations and reported in the following table.

Table 2.2 - Comparison between specific geometrical surfaces calculated from literature correlations.

Foam Material	Nominal Cell Diameter [μm]	Specific Surface Area [m^{-1}]					
		Lacroix et al. [25]	Giani et al. [24]	Calmidi et al. [26]	Inayat et al. [27]		Grosse et al. [19]
					Triangular Strut	Concave Triangular Strut	
FeCr Alloy	580	5067,02	3269,74	5621,16	6416,97	7410,34	4655,04
FeCr Alloy	1200	1451,60	1188,75	2240,39	2183,21	2521,18	1579,61
NiCr Alloy	580	5082,24	2983,13	4534,62	5365,91	6196,58	4129,75
NiCr Alloy	1200	1898,36	1440,63	2564,03	3694,46	4266,37	2464,09
Co	580	2732,59	2223,88	3581,57	3745,85	4325,72	2842,84
Co	1200	1109,76	1078,57	1727,49	2535,24	2927,71	1751,60
Cu	580	2712,69	2116,55	3381,48	4784,91	5525,63	3402,52
Cu	1200	1163,42	1091,36	1789,30	2602,17	3004,99	1789,17

Without doing X-ray microcomputed tomography analysis it is not possible to say which of these correlations is the best, because there are not measured parameters to compare. Bianchi et al. [2] indicate the Inayat's correlation [27] as the one with the best agreement but this could not be the same for the foams which are considered in this work.

2.2.2 Gravimetric analysis

Another important parameter to characterize the foams is porosity which is defined as the ratio between the void volume and the total volume. From other studies [2, 24-28], it can be noticed that the struts might be hollow. This derives from the way in which foams are produced [29]. Thus, it is possible to calculate two different porosities; the total porosity ε_T, which considers all kind of porosities, and the hydrodynamic porosity ε_H, which consists of the macroscopic reachable void part [30]. This last one is particularly important to evaluate the transport phenomena [24]; instead the total porosity is needed in effective heat conductivity calculation [2]. These two porosities can be expressed as:

$$\varepsilon_H = 1 - \frac{\rho_{FOAM}}{\rho_{HS}}$$

$$(2.7)$$

$$\varepsilon_T = 1 - \frac{\rho_{FOAM}}{\rho_{SOLID}}$$

$$(2.8)$$

Where, ρ_{FOAM} is the foam density, ρ_{HS} is the hollow struts density and ρ_{SOLID} is the density of the solid (in this case metal or alloy) phase. The foam density can be determined by dividing the weight of the samples by its volume:

$$\rho_{FOAM} = \frac{W_{FOAM}^{in\,Air}}{V_{FOAM}} \tag{2.9}$$

Where the volume is computed knowing that the sample has a cylindrical shape; $W_{FOAM}^{in\,Air}$ is the weight of the foam disc in air, D_{FOAM} the diameter and h_{FOAM} the height of the foam sample. To calculate the density of the hollow struts a hydrostatic balance (*Sartorius YDK 01*) is used, based on the Archimedean principle: a solid immersed in a liquid is exposed to the force of buoyancy. The value of this force is the same as that of the weight of the liquid displaced by the volume of the solid, with this balance, which enables to weigh a solid in air as well as in solvent, it is possible to determine the specific gravity of a solid when the density of the liquid causing buoyancy is known:

$$\rho_{HS} = \frac{W_{FOAM}^{in\,Air}\,\rho_{EtOH}}{W_{FOAM}^{in\,Air} - W_{FOAM}^{in\,EtOH}} \tag{2.10}$$

Where, $W_{FOAM}^{in\,EtOH}$ is the weight of the foam immersed in pure ethanol, and ρ_{EtOH} is the ethanol density which is tabulated in different temperature. Ethanol is chosen as solvent instead of water because of the ability to access to the entire void volume without creating air bubbles attached to the struts [31]. In our study, unlike the cited publications [2, 24-28] in which the hollow struts are clearly visible in optical microscope images, the foam samples, don't exhibit this peculiarity clearly. This might be due to the laser cutter used to slice the metal foams in shape disk that has melted the far end of the struts. However a very careful inspection demonstrated the existence of hollow struts in our FeCr alloy samples (Figure 2.4).
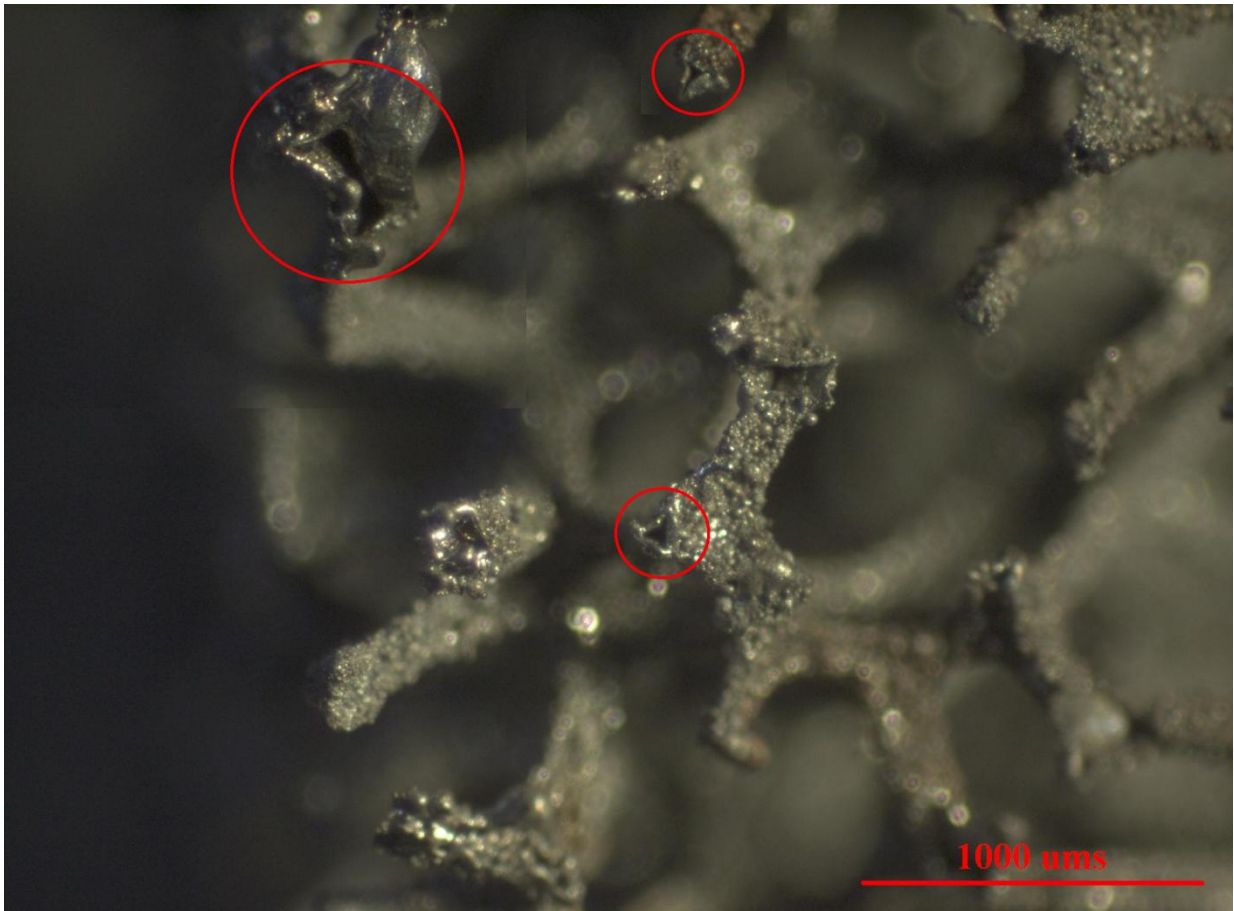
Figure 2.4 - Presence of hollow struts in FeCr alloy 1200 μm sample (magnification of 40).

Anyway, the measured densities reveal the presence of hollow struts in foams. The densities and porosities of measured samples are reported in the following table, where the estimated parameters are the average of three different experiments, to increase the reproducibility.

Table 2.3 - Density and porosity of the investigated samples. Estimated parameters are the average of three different experiments. Measurements of mass density of bulk material (ρ_{SOLID}), foam mass density (ρ_{FOAM}), mass density of hollow struts (ρ_{HS}), hydrodynamic porosity (ε_H) and total porosity (ε_T) are reported.

Gravimetric Analysis						
Foam Material	Nominal Cell Diameter [μm]	ρ_{SOLID} [g/cm^3]	ρ_{FOAM} [g/cm^3]	ρ_{HS} [g/cm^3]	ε_H [-]	ε_T [-]
Co	580	8,9	0,2983	6,4250	0,9533	0,9665
Co	1200	8,9	0,1753	5,4488	0,9659	0,9803
Cu	580	8,96	0,4164	8,5702	0,9501	0,9535
Cu	1200	8,96	0,2663	7,1068	0,9625	0,9703
FeCr Alloy	580	7,65	0,6058	5,7757	0,8951	0,9208
FeCr Alloy	1200	7,65	0,4044	6,3290	0,9354	0,9471
NiCr Alloy	580	8,4	0,5848	6,3898	0,9073	0,9303
NiCr Alloy	1200	8,4	0,4365	6,6195	0,9322	0,9480

The above measurements, confirmed by the manufacturer, show an amazing high porosity, in the range of 93% to 98%. As mentioned, metal foam are produced for several different uses. In particular, these foams

are created for electric use, as supercapacitors [32]. In these applications high porosity is requested because it greatly enhances the efficiency making them attractive for a improvement of batteries and fuel cells [33-35].

All the complete measurements which are shown in this chapter, are reported in the Appendix B, section 1 (page 96).

3. Experimental

In this section, a full description of the experimental setup and procedure for heat transfer measurements is reported. All the experiments were performed in the *Laboratory of Catalysis and Catalytic Process* (LCCP) at the Politecnico di Milano, both in Leonardo and Bovisa campus.

3.1 Experimental setup

All the experimental thermal tests are carried out with the same plant which is already used in the previous studies [2, 36]. The idea here is to keep the experimental procedure and setup as similar as possible to Enrico Bianchi's work [2], to conduct a good comparison between the experimental results of both works.
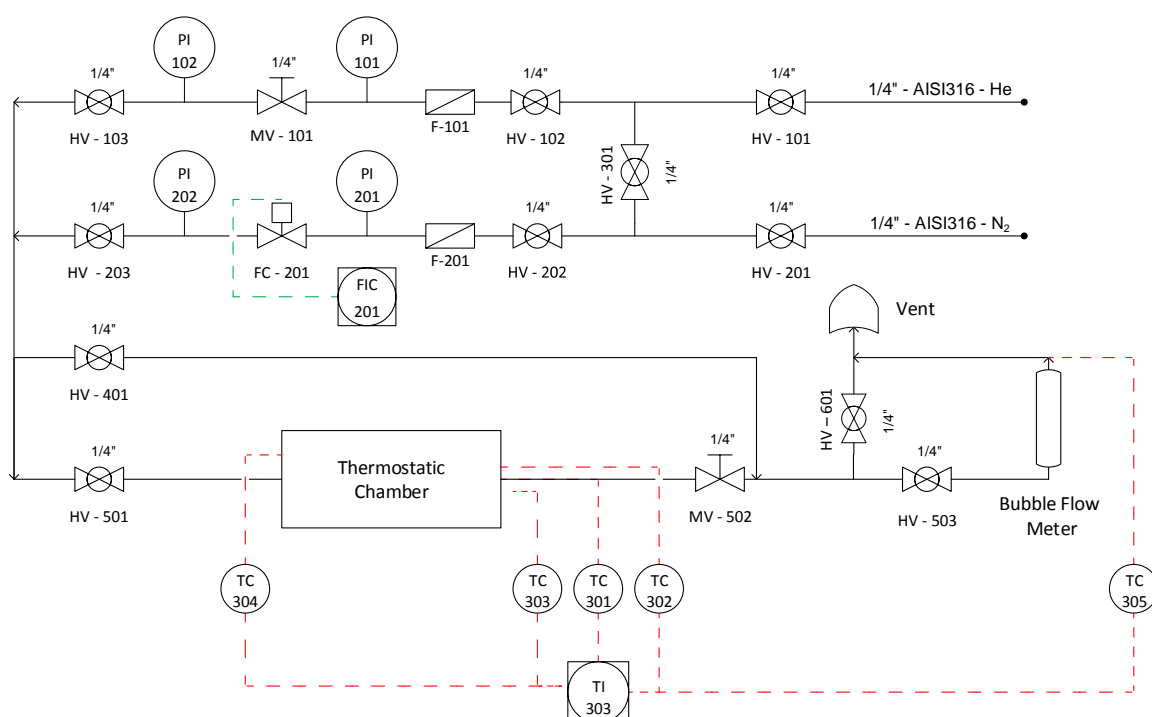
Figure 3.1 - P&I of the heat transfer rig.

Figure 3.1 shows the P&I scheme of the heat transfer setup. All the elements are connected by stainless steel AISI 316 pipes with diameter of 1/4 inch. As described in figure 3.1, there are two feed lines, one for nitrogen and one for helium. Nitrogen is stored as liquid in a tank connected to an evaporator placed in the underground of the department. This is enough to provide the nitrogen request of all plants present in the department. The helium gas comes from a 40 liters cylinder with initial pressure of 200 bar. The heat transfer rig has a dedicated helium line since helium is used continuously by all other plants in the laboratory as carrier gas in chromatography system. Gas lines arrive to the laboratory, where pressure reducers are placed, then gases come in the plant: here five ball valves are put in order to select the desired gas and by-pass one of the flow controllers fitted on the two lines or to use both of them simultaneously.

Successively, gases pass through filters to remove impurities and dust before being introduced to the setup. Then, there is the section dedicated to control the flow rate (figure 3.2).

Figure 3.2 - Digital photograph of control section of the setup with a mass flow controller in parallel with a needle valve.

As shown in the figure 3.2 and figure 3.1, a mass flow controller (Brooks) is installed in parallel with a needle valve which can be sued to regulate the needed flow rate. This is a different configuration compared to Bianchi's setup [2], where two mass flow controller in parallel are used, one with maximum flow rate of 40 SLM and one with maximum flow rate of 15 SLM. In the previous study [36], the aim was to work with 60 SLM which could not be reached with the previous (Bianchi's) configuration, therefore the needle valve is installed instead of the Brooks with 15 SLM nominal flow rate to overcome this issue. Furthermore in the configuration, there are two non-return valves and two ball valves which can isolate this section from the rest of flow control section. Also, pressure gauges are placed before and after the flow controllers and the non-return valves. Here, the gas can either flow through a bypass and goes directly to the fume hood (exhaust gas) or to setup (heating part, which consists of a preheater, not employed in these tests, and the thermostatic chamber. The preheater and the oven are both electric with built-in temperature controllers and are connected by an insulated line. The oven (thermostatic chamber) in which the heating tube

containing the foam is placed is a *Mazzali Thermotest* an oven with forced air recirculation managed by a proportional-integrative-derivative controller (figure 3.3)

Figure 3.3 - Digital photograph of Mazzali thermostatic chamber.

It is possible to send the gas directly to the fume hood or through the bubble flow meter and then to the fume hood. The bubble flow meter is used to verify the gas flow and set the hand-operated needle valve and the brooks. After opening the brooks of a wanted percentage, gas is let flow through the oven and to the bubble flow meter. Here, by measuring the time which a bubble take to cover a known volume is it possible to calculate the flow rate. The radial and axial experimental temperature can be read by selecting the desired channel through the dedicated switch in the control temperature panel. Five different channels are available, each representing a different thermocouple which correspond to five different positions, three are used to measure the foam temperature, one is used to measure the heating tube wall temperature, and the last is placed on the top of the bubble flow meter, to measure the gas temperature.

3.2 Heating tube

In this section a description of the tube used for the measurement is presented. Figure 3.4 shows all the components used to assemble the heating tube.
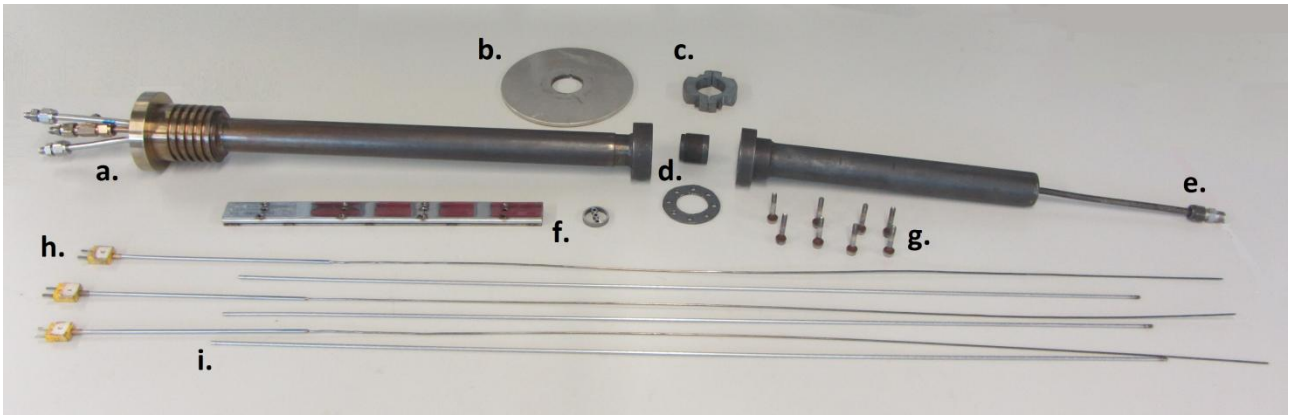
Figure 3.4 - Digital photograph of the heating tube set up, with: a) tube head; b) fin; c) steel ring; d) threaded ferrule and graphite gasket; e) measuring tube; f) two different available spacers; g) screws for connecting the two parts of heating tube; h) thermocouples; i) thermowells.

Going deeper, here is presented the figure 3.4, showing only the tube where metal foams are placed.

Figure 3.5 - Digital photograph of unassembled heating tube.

The heating tube consists of a stainless steel (AISI 316L) pipe with an external diameter of 33 mm. Section *d*, where the foam will be placed, has 28 millimeters of inner diameter. The outer diameter of the foam sample is equal to the inner diameter of the experimental section heating tube (section d), to ensure a good thermal contact between the foam and the tube and to avoid bypass at the wall.. The guides for the thermowells are shown in figure 3.5 section *a*. The pipe segment (figure 3.5, b) provides a connection wide enough to accommodate the three thermowells between the main section (figure 3.5, d) and the gas outlet section. The safety threaded ferrule and graphite gasket shown in the figure 3.5 section c, are placed to seal the section *b* and *d* through a flange joint avoiding any gas leak. The heating tube is equipped with eight external aluminum fins to enhance the heat transfer with the thermostatic chamber, between one fin and the other a steel ring is put, to keep them at the same distance (figure 3.6a). The optimal contact of the fins with the heating tube being ensured by a thin copper foil rolled around the tube. Each fin is equipped with a hole (channel) in order to let the thermocouple slide on the external part of the tube and measure the wall temperature, shown in figure 3.6b.

a.
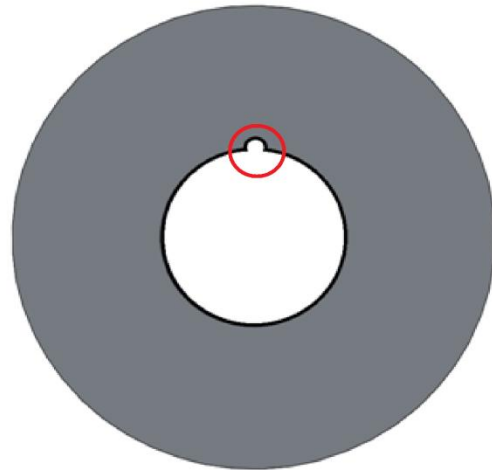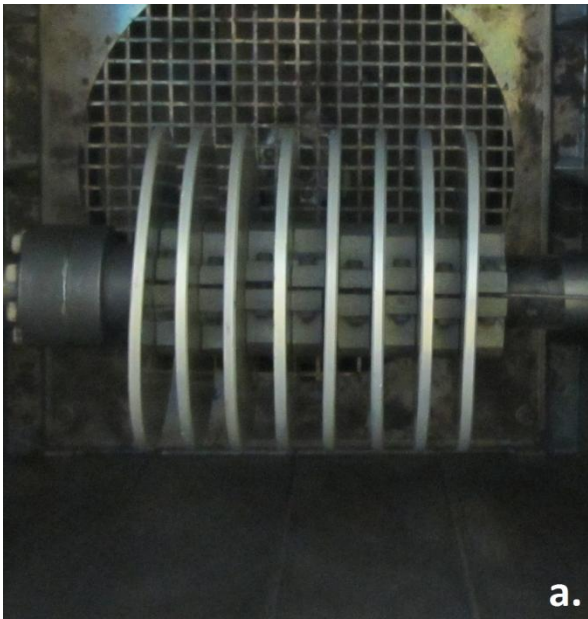
b.

Figure 3.6 - Digital photograph and schematic representation of the heating tube with fins inside the oven; a) Fins position and b) Schematic representation of a fin equipped with the channel for sliding the outer thermocouple.

Another point where pay attention is the insulation of the external parts of the tube: the downstream end of the pipe has to be wrapped by a Teflon tape; while the part where gas comes in has to be filled by glass wool, in order to avoid heat losses, as shown in figure 3.7.

Figure 3.7 - Digital photograph of the insulation part, with the channel for the fourth thermocouple (pipe at the left) and gas inlet (central pipe).

Four K-type thermocouples are used to collect the experimental data: three are placed in the thermowells that pass through the foam, and one, as already described, is placed on the outer surface of the tube. The three inner thermocouples measure the temperature of the foam in axial direction in three different radial positions, central, 1/2 radius and 2/3 radius (figure 3.8).
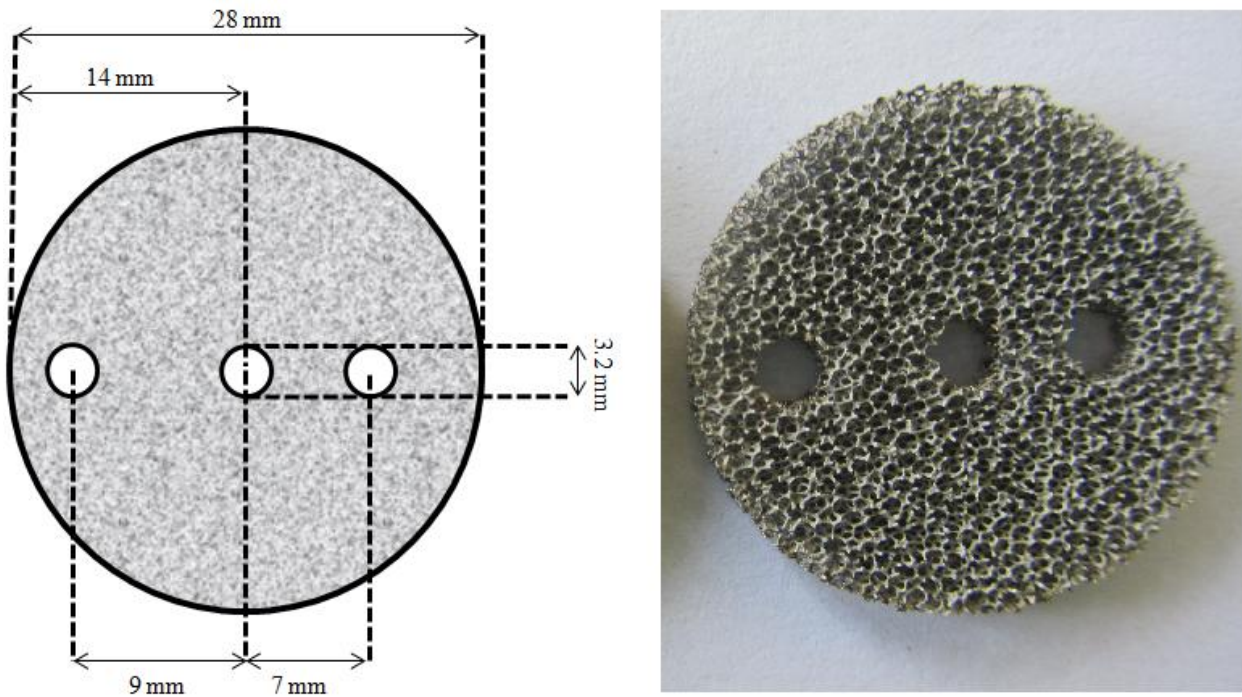
Figure 3.8 - Digital photograph and schematic representation of foam disk sample with the three through holes positioned at 0 - 7 - 9 mm from the center.

Foam samples are supplied by Alantum [32] in shape of disks with diameter of 28 millimeters and different thickness depending by material and cell diameters. To obtain a length of 100 millimeters for each foam bed, a minimum of 30 disks for cell diameters of 1200 μm and at least 60 disks for cell diameters of 580 μm are needed. In this case, care must be taken to ensure that the foam disks are packed after each other with no space among them. To solve this issue, in this work, the tube is fully loaded by foam disks (FeCr alloy disks with different cell diameter) and then closed by the threaded ferrule showed in figure 3.5c. These disks are equipped with three different holes with 3.28 millimeters diameter, in order to allow the passage of three thermowells of 1/8 inch of diameter through the foam. The thermowells are indispensable to let the thermocouple slide through the foam without problem. The presence of three holes slightly affects the porosity of the samples, which is not significantly increase since it is only a local negligible effect. The following sketch shows the heating tube and exact position of the foam bed (measuring zone) inside the heating tube (figure 3.9).
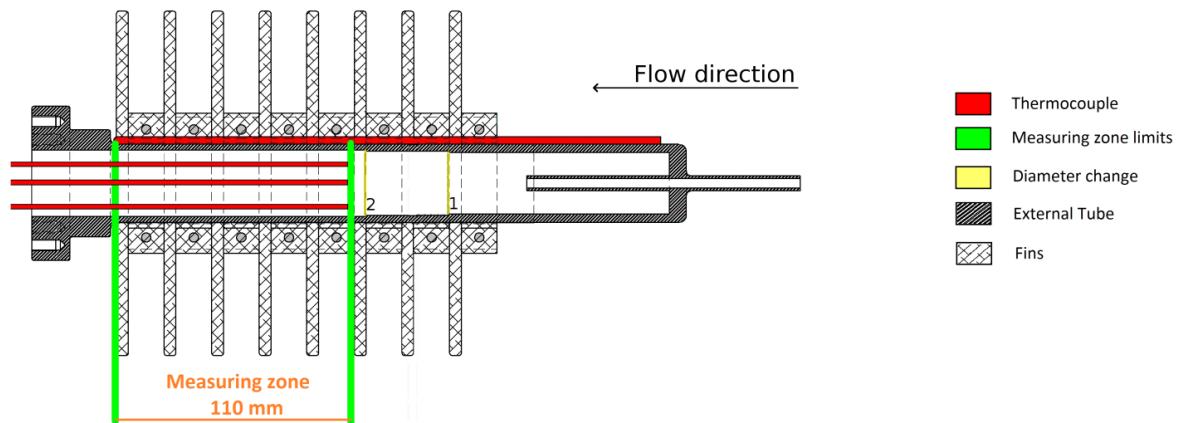
Figure 3.9 - Schematic representation of the heating tube section with foam bed (measuring zone), thermocouples and fins.

The length of the foam bed (measuring zone) consists in 100 millimeters of sample foam and 5 millimeters of FeCr alloy foam used upstream from the test samples to have a uniform gas flow and temperature distributions and after this zone. Figure 3.9 shows also that the internal diameter of the heating tube is not constant along the tube and it changes from 26 centimeters in the direction of the flow to 27 centimeters at point 1, then again changes to 28 centimeters at point 2 shown in the figure 3.9. This means that the foam samples having diameter of 28 centimeters, cannot go deeper than the limit indicated with number 2. From figure 3.9, it is possible to see that even if the length of the samples are quite different, and the upstream configuration is different, the beginning of the measuring zone is the same for all the samples studied. Downstream the sampling zone, gas flows until it reaches the outlet section; this part is made by a three way connector used to allocate the central thermowell, and then goes to the fume hood. Figure 3.10 shows the outlet section of the heating tube.
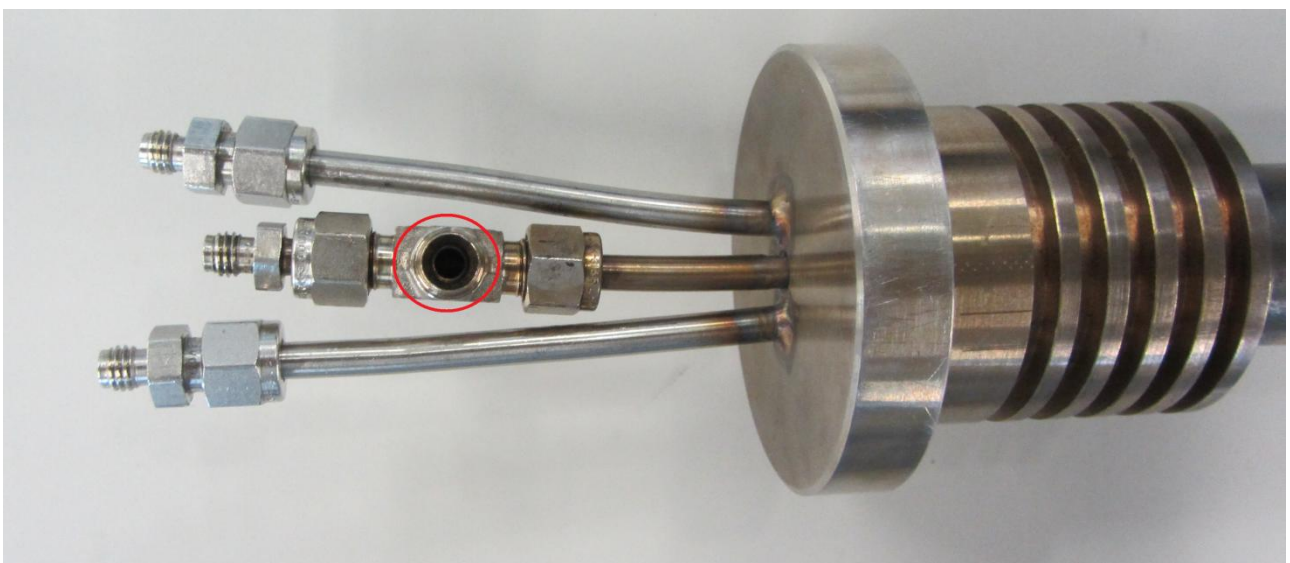
Figure 3.10 - Digital photograph of the outlet section of the tube with channels used to allocate thermocouples at different radial positions; the red circle shows the three way connector used to direct the exhaust gas.

Figure 3.10 demonstrates also the three 1/4 inch tubes where the 1/8 inch thermowells are inserted in. These tubes are bent to make it easier to tight the nuts but this bending makes the thermowells to bend as well. Figure 3.11 shows the three thermowells after being used in the heating tube; it is interesting to focus on how the 1/2 radius thermowell is bent.
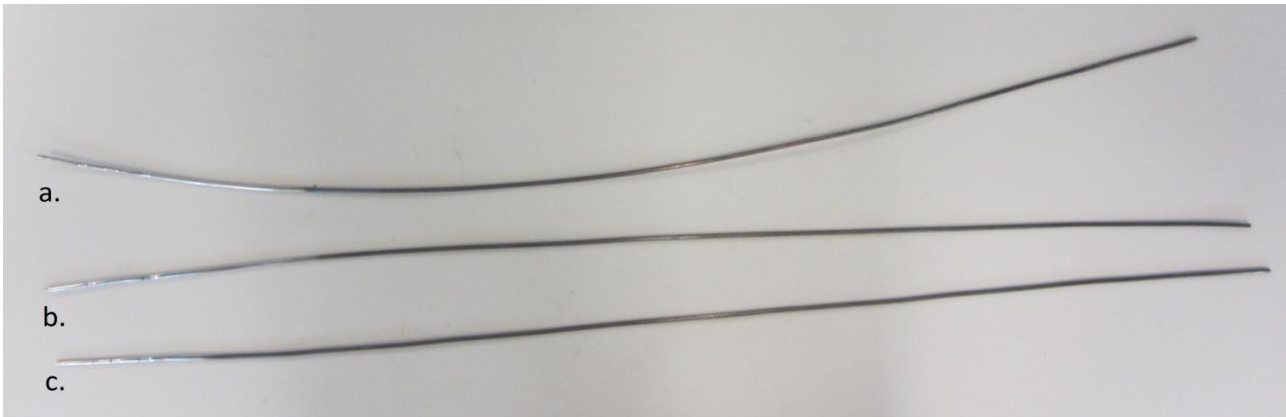
Figure 3.11 - Digital photograph of 1/8 inch thermowells used inside the heating tube, a) 1/2 radius; b) central; c) 2/3 radius.

This unparalleled position of the thermowells damages the three through holes of the foam disks, making them wider, especially in case of very soft foam materials, such as copper and cobalt. To avoid this issue two spacers shown in figure 3.12 have been ideated in order to keep the thermowells in the correct position.
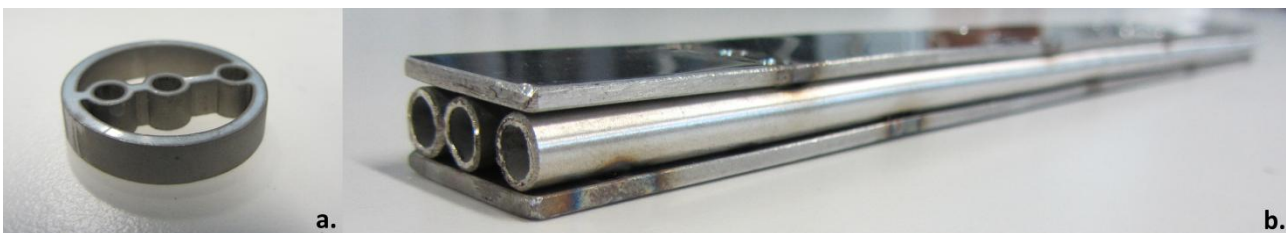
Figure 3.12 - Digital photograph of the two used spacers: a) spacer made in titanium by water jet of 5 mm thickness; b) spacer made in stainless steel of 30 cm length.

The first spacer (figure 3.12a) is made by cutting titanium plate by water-jet in the shape of the foam disks, starting from a cylinder of titanium. The second spacer consists of three 1/4 inch stainless steel tubes welded in two stainless steel plates is shown in figure 3.12b. By using these spacers, the configuration is the one described in figure 3.13.

Figure 3.13 - Sketch of tube configuration with the two spacers.

However, when the long stainless steel spacer (figure 3.12b) is used with the cobalt foam, an unreasonable axial temperature profile of the 2/3 radius has been found. By repeating the measurement without the long stainless steel spacer and only using the titanium spacer in the downstream region the measured temperature profile seems more reasonable, as it is possible to see in figure 3.14.
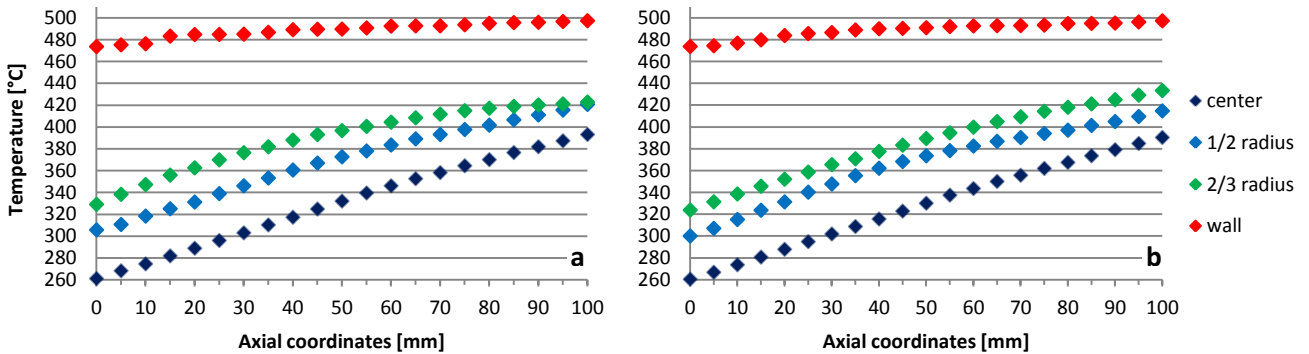
Figure 3.14 - Axial temperature profiles of cobalt foam at 500 °C and 30 SLM: a) measurements taken with the long stainless steel spacer; b) measurements taken without the stainless steel spacer only using the titanium spacer at the downstream.

Figure 3.14a shows the axial temperature profiles for the heat transfer measurements conducted for cobalt foam with cell diameter of 1200 µm, at oven temperature of 500 ˚C, flow rate of 30 SLM, and nitrogen gas. In this figure, the 1/2 radius temperature profile (cyan diamonds) and the 2/3 radius temperature profile (green diamonds) are getting to close to each other at the end of the foam bed. This could be due to the presence of the stainless steel spacer placed downstream, at the end of the foam bed (close to the end of the foam bed, figure 3.13). The long stainless steel spacer might conduct during the heat transfer measurement specially quite close to the end of the foam bed. Trying to remove this spacer and repeating the experiment only with the Ti ring spacer the problem disappear and the profile seems more reasonable, as shown in the figure 3.14b.

3.3 Different loading configurations

In this section, different sketches of all loading configurations are applied for different foam samples in the heating transfer measurement are presented. The three thermocouples used for measuring the radial temperature of them foams are not shown here in order to simplify the sketches. In the following figures, the flow directions are from right to left. The aluminum fins are made start at the end of the thermocouple which measure the wall temperature; the number of them is enough to cover all the measuring section plus 2.5 centimeters in order to guarantee the correct line up. The section represents the one placed in the thermostatic chamber. In all the different loading, a short packed bed of 24 millimeters of length made of glass spheres of 3 millimeters diameter placed upstream is used to ensure an uniform temperature and flow distribution. Thin sintered nickel foam disks are used to block the glass spheres from one side and the thermowells in the other side. In this part three sintered nickel foams are used and between them one FeCr alloy 1200 µm foam disk is placed to avoid them to turn inside the heating tube and be bent by the

thermowells. An inlet zone of 5 millimeters of FeCr alloy foam (one disk of FeCr 1200 μm cell diameter and one of FeCr 580 μm diameter) are placed upstream to guarantee the correct lineup of the three thermowells. These 5 millimeters represent also the inlet temperature profile used by the model described in the next chapter. Then, the sampling foam bed starts. At the end of the foam bed (close to downstream) four or six FeCr alloy foam disks are used to ensure the packing of all the foam sample disks together. The number of disks changes because the thickness of foam disks varies for each kind of foams and it is really important to have a good packing in order to avoid the foam movements inside the tube during the measurements.

In the following paragraphs a detailed description of the tube configuration is reported, for each kind of studied foams.

3.3.1 FeCr alloy foam with 1200 μm cell diameter
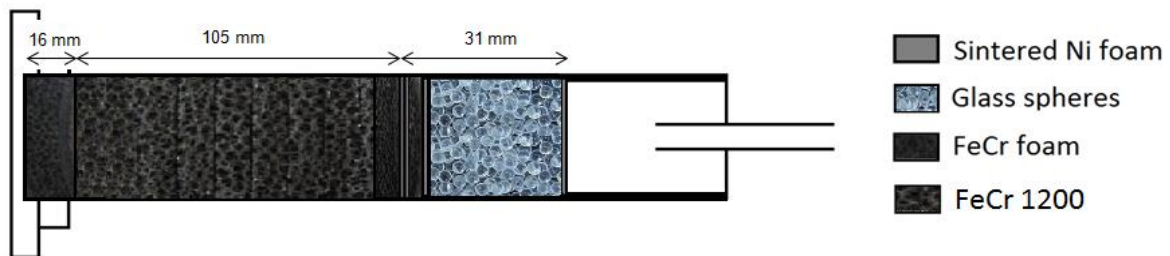
Figure 3.15 - Sketch of heating tube with FeCr 1200 μm.

- **Pre-mixer zone (31 mm length):**

1 sintered nickel foam (to block the glass spheres) + glass spheres (d_s = 3 mm, 24 mm length) + 1 sintered nickel foam (to block the glass spheres on the other side) + 1 FeCr alloy foam disk (d_c = 1200 μm) + 2 sintered nickel foam (to block the thermowells)

- **Upstream (5 mm length):**

1 FeCr alloy foam disk (d_c = 580 μm) + 1 FeCr alloy foam disk (d_c = 1200 μm)

- **Foam bed (100 mm length):**

33 FeCr alloy foam disks (d_c = 1200 μm)

- **Downstream (16 mm length):**

1 FeCr alloy foam disk (d_c = 580 μm) + 4 FeCr alloy foam disks (d_c = 1200 μm) + 1 FeCr alloy foam disk (d_c = 580 μm)

3.3.2 FeCr alloy foam with 580 µm cell diameter
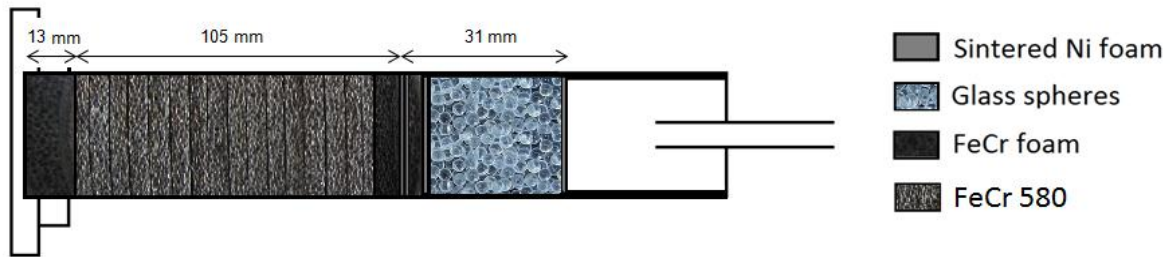
Figure 3.16 - Sketch of heating tube with FeCr 580 µm.

- **Pre-mixer zone (31 mm length):**

1 sintered nickel foam + glass spheres + 1 sintered nickel foam + 1 FeCr alloy foam disk (d_c = 1200 µm) + 2 sintered nickel foam

- **Upstream (5 mm length):**

1 FeCr alloy foam disk (d_c = 580 µm) + 1 FeCr alloy foam disk (d_c = 1200 µm)

- **Foam bed (100 mm length):**

53 FeCr alloy foam disks (d_c = 580 µm)

- **Downstream (13 mm length):**

1 FeCr alloy foam disk (d_c = 580 µm) + 3 FeCr alloy foam disks (d_c = 1200 µm) + 1 FeCr alloy foam disk (d_c = 580 µm)

3.3.3 NiCr alloy foam with 1200 µm cell diameter
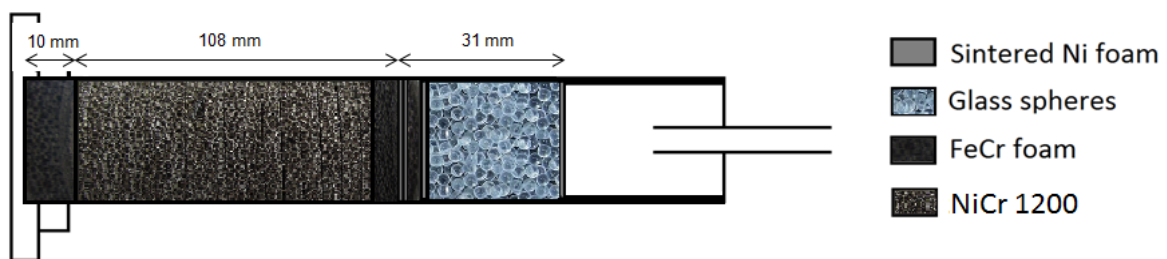
Figure 3.17 - Sketch of heating tube with NiCr 1200 µm.

- **Pre-mixer zone (31 mm length):**

1 sintered nickel foam + glass spheres + 1 sintered nickel foam + 1 FeCr alloy foam disk (d_c = 1200 µm) + 2 sintered nickel foam

- **Upstream (5 mm length):**

1 FeCr alloy foam disk (d_c = 580 µm) + 1 FeCr alloy foam disk (d_c = 1200 µm)

- **Foam bed (103 mm length):**

35 NiCr alloy foam disks (d_c = 1200 µm)

- **Downstream (10 mm length):**

1 FeCr alloy foam disk (d_c = 580 µm) + 2 FeCr alloy foam disks (d_c = 1200 µm) + 1 FeCr alloy foam disk (d_c = 580 µm)

3.3.4 NiCr alloy foam with 580 μm cell diameter
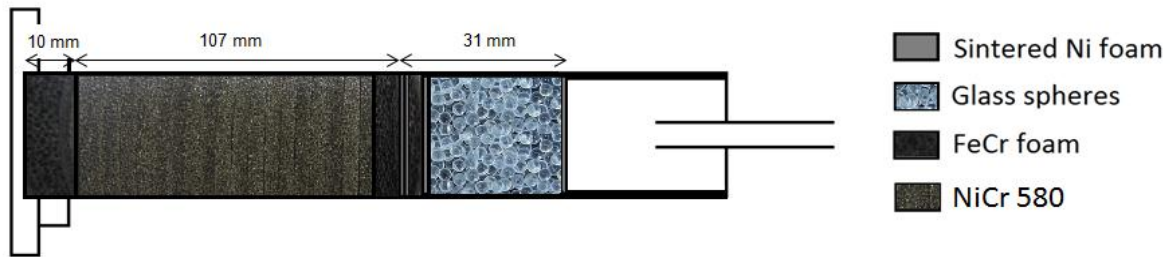
Figure 3.18 - Sketch of heating tube with NiCr 580 μm.

- **Pre-mixer zone (31 mm length):**

1 sintered nickel foam + glass spheres + 1 sintered nickel foam + 1 FeCr alloy foam disk (d_c = 1200 μm) + 2 sintered nickel foam

- **Upstream (5 mm length):**

1 FeCr alloy foam disk (d_c = 580 μm) + 1 FeCr alloy foam disk (d_c = 1200 μm)

- **Foam bed (102 mm length):**

57 NiCr alloy foam disks (d_c = 580 μm)

- **Downstream (10 mm length):**

1 FeCr alloy foam disk (d_c = 580 μm) + 2 FeCr alloy foam disks (d_c = 1200 μm) + 1 FeCr alloy foam disk (d_c = 580 μm)

3.3.5 Co foam with 1200 μm cell diameter
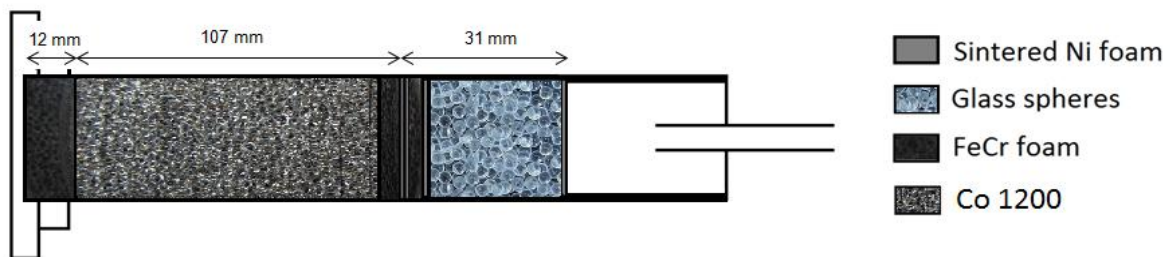
Figure 3.19 - Sketch of heating tube with Co 1200 μm.

- **Pre-mixer zone (31 mm length):**

1 sintered nickel foam + glass spheres + 1 sintered nickel foam + 1 FeCr alloy foam disk (d_c = 1200 μm) + 2 sintered nickel foam

- **Upstream (5 mm length):**

1 FeCr alloy foam disk (d_c = 580 μm) + 1 FeCr alloy foam disk (d_c = 1200 μm)

- **Foam bed (102 mm length):**

35 Co foam disks (d_c = 1200 μm)

- **Downstream (12 mm length):**

1 FeCr alloy foam disk (d_c = 580 μm) + 2 FeCr alloy foam disks (d_c = 1200 μm) + 2 FeCr alloy foam disks (d_c = 580 μm)

Two titanium spacers at 5 cm of distance to each others

3.3.6 Co foam with 580 µm cell diameter
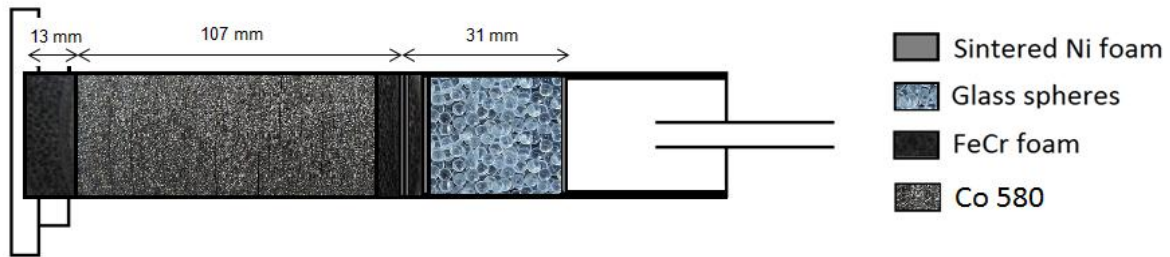
Figure 3.20 - Sketch of heating tube with Co 580 µm.

- **Pre-mixer zone (31 mm length):**

1 sintered nickel foam + glass spheres + 1 sintered nickel foam + 1 FeCr alloy foam disk (d_c = 1200 µm) + 2 sintered nickel foam

- **Upstream (5 mm length):**

1 FeCr alloy foam disk (d_c = 580 µm) + 1 FeCr alloy foam disk (d_c = 1200 µm)

- **Foam bed (102 mm length):**

58 Co foam disks (d_c = 580 µm)

- **Downstream (13 mm length):**

1 FeCr alloy foam disk (d_c = 580 µm) + 3 FeCr alloy foam disks (d_c = 1200 µm) + 1 FeCr alloy foam disk (d_c = 580 µm)

Two titanium spacers at 5 cm of distance to each others

3.3.7 Cu foam with 1200 µm cell diameter
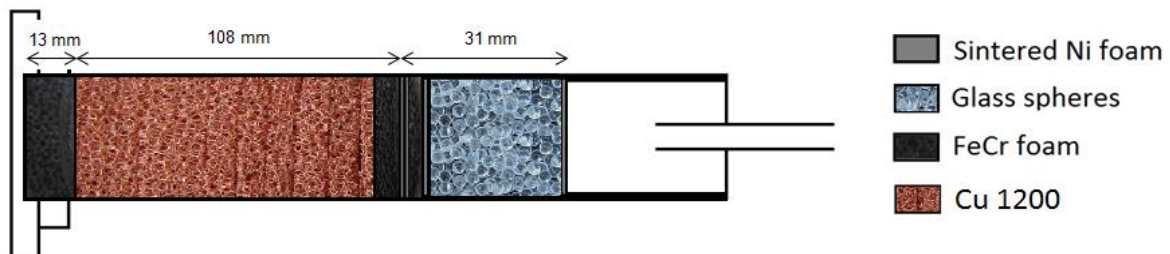
Figure 3.21 - Sketch of heating tube with Cu 1200 µm.

- **Pre-mixer zone (31 mm length):**

1 sintered nickel foam + glass spheres + 1 sintered nickel foam + 1 FeCr alloy foam disk (d_c = 1200 µm) + 2 sintered nickel foam

- **Upstream (5 mm length):**

1 FeCr alloy foam disk (d_c = 580 µm) + 1 FeCr alloy foam disk (d_c = 1200 µm)

- **Foam bed (103 mm length):**

38 Cu foam disks (d_c = 1200 µm)

- **Downstream (13 mm length):**

1 FeCr alloy foam disk (d_c = 580 µm) + 3 FeCr alloy foam disks (d_c = 1200 µm) + 1 FeCr alloy foam disk (d_c = 580 µm)

Two titanium spacers at 5 cm of distance to each others

3.3.8 Cu foam with 580 μm cell diameter
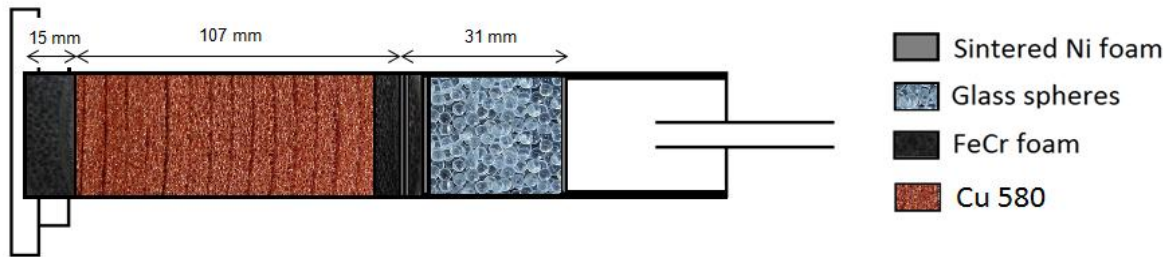
Figure 3.22 - Sketch of heating tube with Cu 580 μm.

- **Pre-mixer zone (31 mm length):**

1 sintered nickel foam + glass spheres + 1 sintered nickel foam + 1 FeCr alloy foam disk (d_c = 1200 μm) + 2 sintered nickel foam

- **Upstream (5 mm length):**

1 FeCr alloy foam disk (d_c = 580 μm) + 1 FeCr alloy foam disk (d_c = 1200 μm)

- **Foam bed (102 mm length):**

60 Cu foam disks (d_c = 580 μm)

- **Downstream (15 mm length):**

1 FeCr alloy foam disk (d_c = 580 μm) + 3 FeCr alloy foam disks (d_c = 1200 μm) + 2 FeCr alloy foam disks (d_c = 580 μm)

Two titanium spacers at 5 cm of distance to each others

3.4 Experimental tests

Thermal experiments were performed under different flow rate conditions, in order to investigate different Reynolds number. To study the effect of gases with different thermal conductivity, two kind of gases are used, nitrogen (k_f = 0.026 $\frac{W}{mK}$ NPT) and helium (k_f = 0.147 $\frac{W}{mK}$ NPT). Different gases are also chosen as representative of a gas of low thermal conductivity, such as air, and a gas with high thermal conductivity, such as synthesis gas, respectively, in order to carry out measurements representative of the operation of the most common strongly exothermic and endothermic processes. During the experimental tests the thermostatic chamber is set at two different temperatures:

- 300 °C (573.15 K)
- 500 °C (773.15 K)

Generally, since a sufficient thermal gradient is needed, tests using helium and setting the thermostatic chamber at 300°C aren't performed. Gases are fed to the system with different flow rates:

- 10 SLM
- 15 SLM
- 20 SLM
- 25 SLM

- 30 SLM
- 35 SLM

For the same reason, tests with helium with flow rate of 10 SLM and 15 SLM and oven temperature of 500 °C are not carried out, these conditions have been used only with FeCr alloy, with useless results. Tests at 35 SLM have been made only with nitrogen. In this work, eight kind of foams are studied:

- FeCr Alloy, d_C = 580 µm
- FeCr Alloy, d_C = 1200 µm
- NiCr Alloy, d_C = 580 µm
- NiCr Alloy, d_C = 1200 µm
- Co, d_C = 580 µm
- Co, d_C = 1200 µm
- Cu, d_C = 580 µm
- Cu, d_C = 1200 µm

3.5 Experimental procedure

Once time the heating tube is loaded and everything is connected with no leakages, the plant can be turned on. First of all, a very low flow rate is flushed and then the thermostatic chamber is turned on and set to the desired temperature. The oven has two programs: the first is a programmed temperature, which allows reaching the set temperature with a certain velocity, expressed in terms of K/min; the second is aimed at keeping the desired temperature inside the thermostatic chamber. When the temperature set point is reached, it is possible to start to calibrate the flow. In Leonardo, if the flow rate is lower or equal to 30 SLM, the mass flow controller can be used alone; if the flow rate is higher the needle valve has to be used, because the mass flow controller at high flow rate starts to oscillate. This is due to a that not allow to work with very high flow rate. This problem disappeared by moving in Bovisa. However, each time the flow rate is measured and verified using a bubble flow meter; this device is based on a simple principle: by measuring the time taken by a bubble to cover a known volume it is possible to calculate the flow rate as the ratio of the known volume and the time. Since the flow rate is affected by the gas temperature, this ratio have to be corrected. Starting from the perfect gas law:

$$P\dot{V}_1 = \dot{n}RT_1 \tag{3.1}$$

Where $\dot{V}_1$ is the desired flow rate in SLM and T_1 the standard temperature (25 °C). Since the gas is at different temperature T_2:

$$P\frac{V_2}{t} = \dot{n}RT_2 \tag{3.2}$$

Where V_2 is known volume of the bubble flow meter, in this case 1.5 liters, and t the time in minutes taken by the bubble to cover V_2, which is around 10 seconds for 10 SLM and 2.5 seconds for 35 SLM. Dividing equation (3.1) for equation (3.2):

$$\dot{V}_1 = \frac{T_1}{T_2} \cdot \frac{V_2}{t} \tag{3.3}$$

Which represents the flow rate measured by the bubble column flow meter.

After calibrating the flux, the steady state has to be waited, this is considered reached when the temperature of the central thermocouple doesn't change its measure in five minutes. Then the temperature profile are collected by sliding every thermocouple of 5 mm and measuring the corresponding temperature. Each test is run at least twice in order to ensure the reproducibility of that. A difference of more than 1 °C in two measures is not accepted and test is repeated. Experiments consist in collect temperature at different axial and radial positions, results of thermal tests are reported in dedicated diagrams in this work. Finally, when the experiments are finished the oven can be turned off. Till it doesn't go down 60 °C a low flow rate is let flush into the plant.

3.5.1 Foam oxidation

The described precaution, which takes more than 3 hours, is adopted after the first experiment with copper which after the experiment has been found oxidized, as showed in figure 3.23; this might be due to some air that has been sucked in the plant during the cooling down of the system. As is possible to see in the two photos, the color is not constant but it changes from red in downstream, to violet. Second photo represents four disks taken in four different position of the bed.

Figure 3.23 - Digital pictures of oxidized copper.

By using this procedure the problem was quite solved as it is possible to see in figure 3.24, where the pale reddish color of the copper sample (figure 3.24b) probably could be due to some impurity present in the

nitrogen line, however the situation is clearly better than the previous one and it indicates that the new precaution is good and prevent a total oxidation even in case of higher oven temperature.
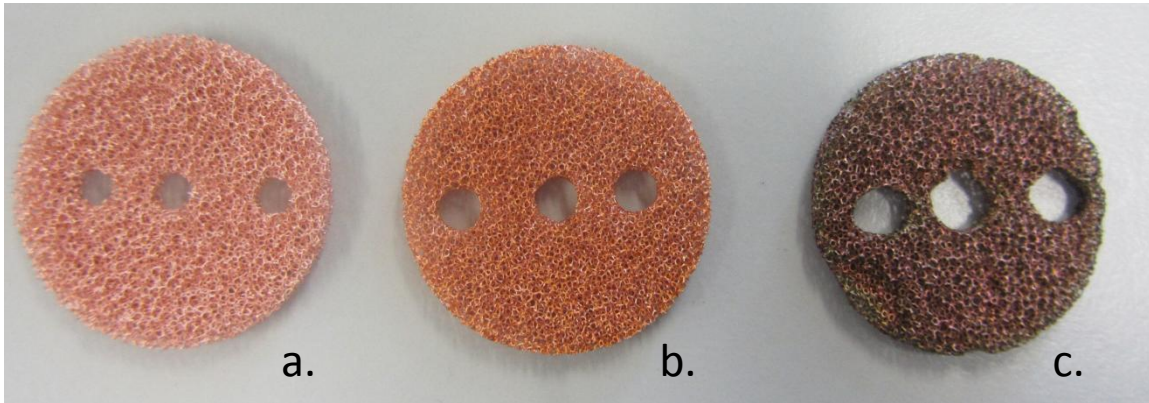
Figure 3.24 - a) copper before treatment; b) copper after new treatment (T$_{oven}$ = 500°C); c) copper oxidized first time (T$_{oven}$ = 300°C).

3.5.2 Problem with helium

During the first test using helium, a difficult to reach the steady state temperature was found, specially at high flow rate (from 25 to 30 SLM): the temperature increased continuously, as shown in the following graph (figure 3.25).
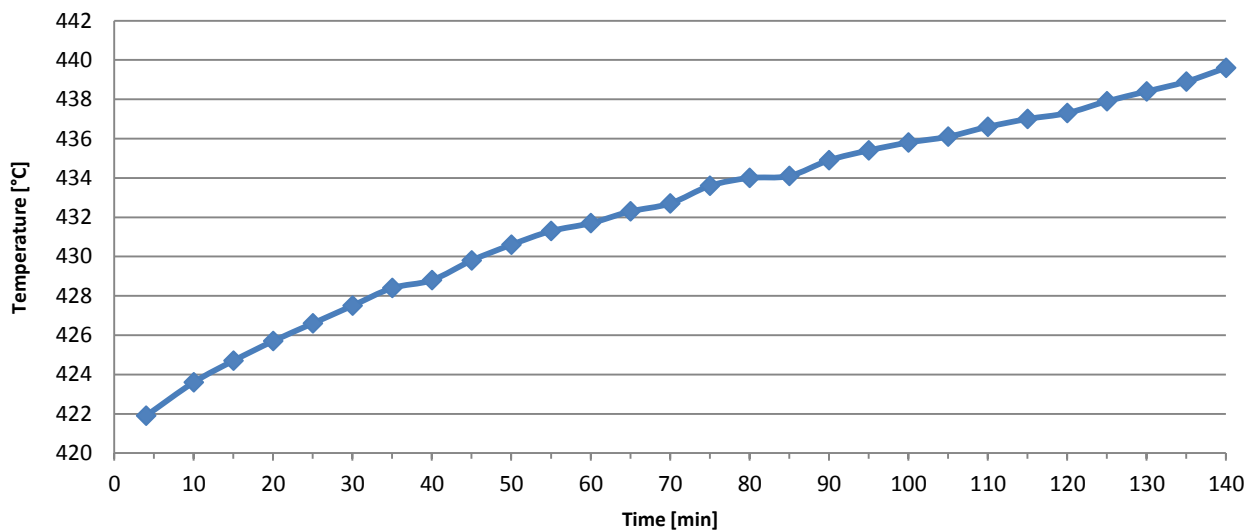
Figure 3.25 - Temperature profile in helium test.

At the same time a decreasing of the pressure in the pressure gauge placed on the plant has been noticed. The following graph (figure 3.26) describes the pressure trend of helium cylinder, the pressure reducer placed on the cylinder and the two pressure gauges.
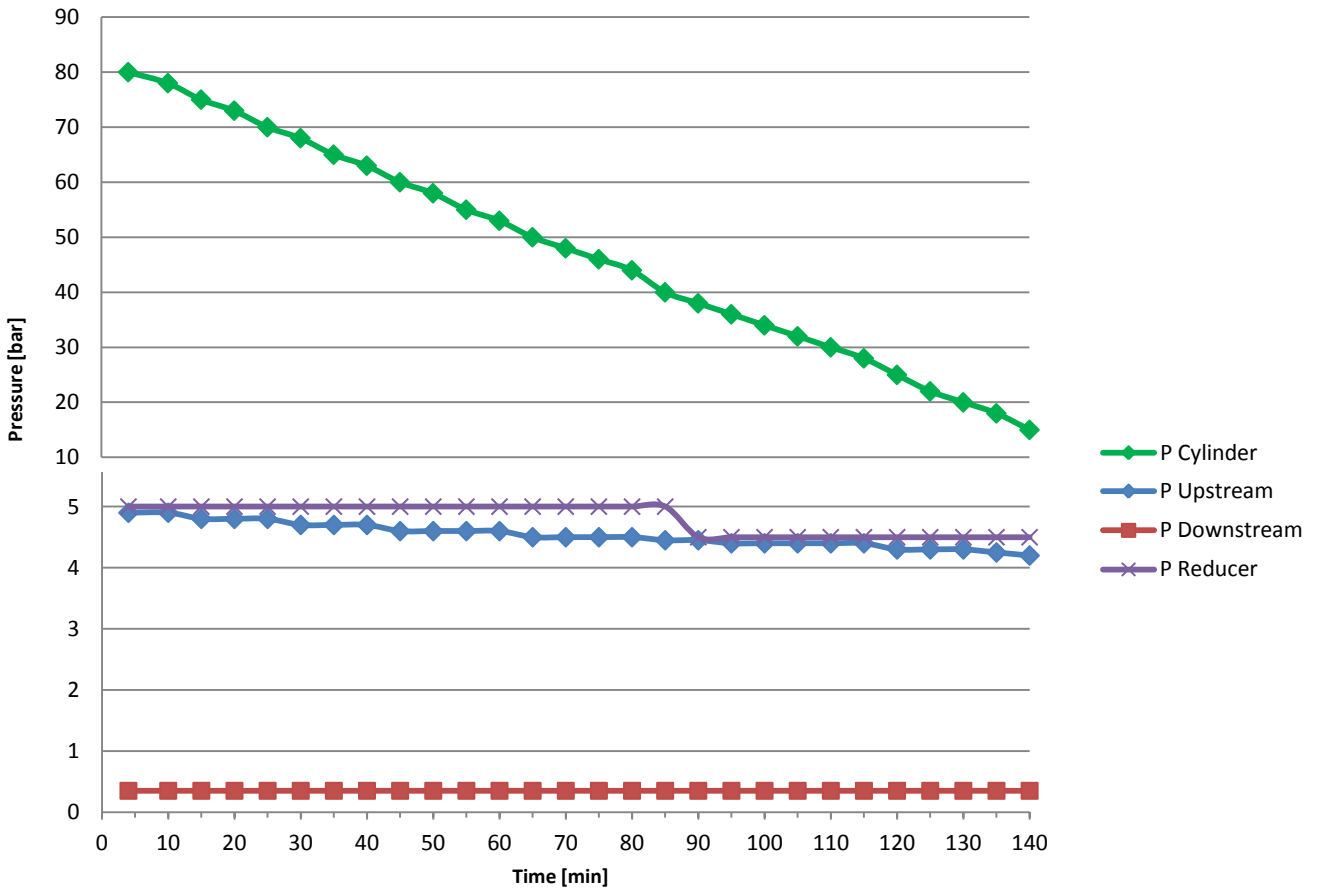
Figure 3.26 - Pressure profile: cylinder (green diamonds); reducer (violet crosses); upstream gauge (cyan diamonds); downstream gauge (red squares).

As it should be, pressure of cylinder decreases, in fact is an indicator of the cylinder consumption; on the contrary, the other pressures should keep constant. Since a pressure decreasing and a temperature increasing might mean a flow rate decreasing, this has been measured six time during the 2 hours and 20 minutes (figure 3.27).
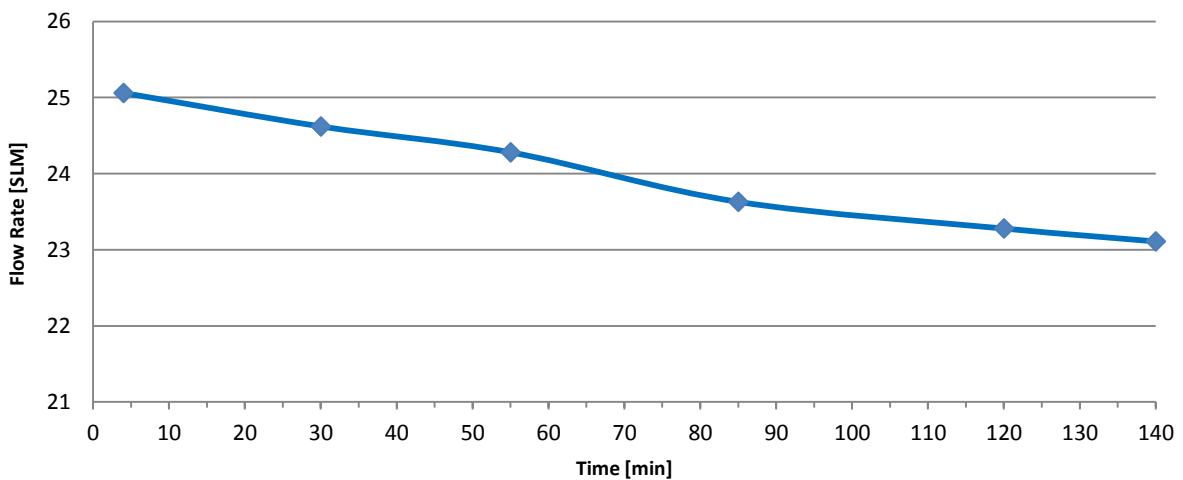
Figure 3.27 - Measured flow rate in helium test.

This is a very critical point because in that way the control on the flow rate is not working well. The cause has been found in the reducer situated on the helium cylinder. The rig works at 5 bar as inlet pressure gas, but the supplied reducer was an high-high, which means a full scale of 100 bar. In that condition to set exactly 5 bar becomes very difficult. Moreover, as the graphs show, the reducer is not able to keep this pressure, which is very low for that scale, constant. Once the reducer was changed with a more appropriate high-medium, the problem has been solved.

3.5.3 Reproducibility

In experimental campaigns the reproducibility of the experiments is one of the most important parts of the work and should always be done. In our case this is assured by repeating each test two times. Moreover, since during the work the plant has been moved from Leonardo to Bovisa, a further control about the reproducibility became necessary. For this reason measures of FeCr alloy with 1200 μm cell diameter, at 300 °C oven temperature with nitrogen have been redone at 10, 25 and 35 SLM three times, one in Leonardo, and two in Bovisa in two different months, July and September, with the following results which are represented in graphs where the triangular shape symbolizes the wall temperature, the circles represent the 2/3 radius position, the square shape the 1/2 radius place and the crosses depict the central position; different color represents the three different tests.
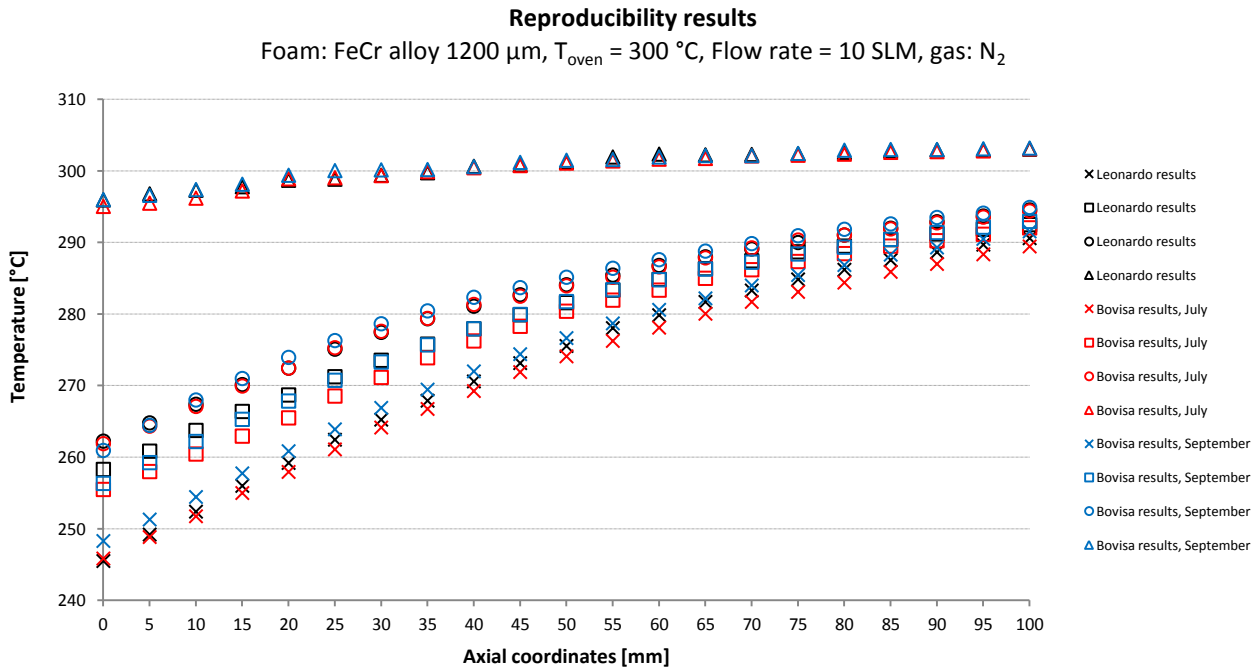
Figure 3.28 - Comparison between measurements taken in Leonardo and in Bovisa; Foam: FeCr alloy, T = 300°C, Flow rate: 10 SLM, Gas: Nitrogen.
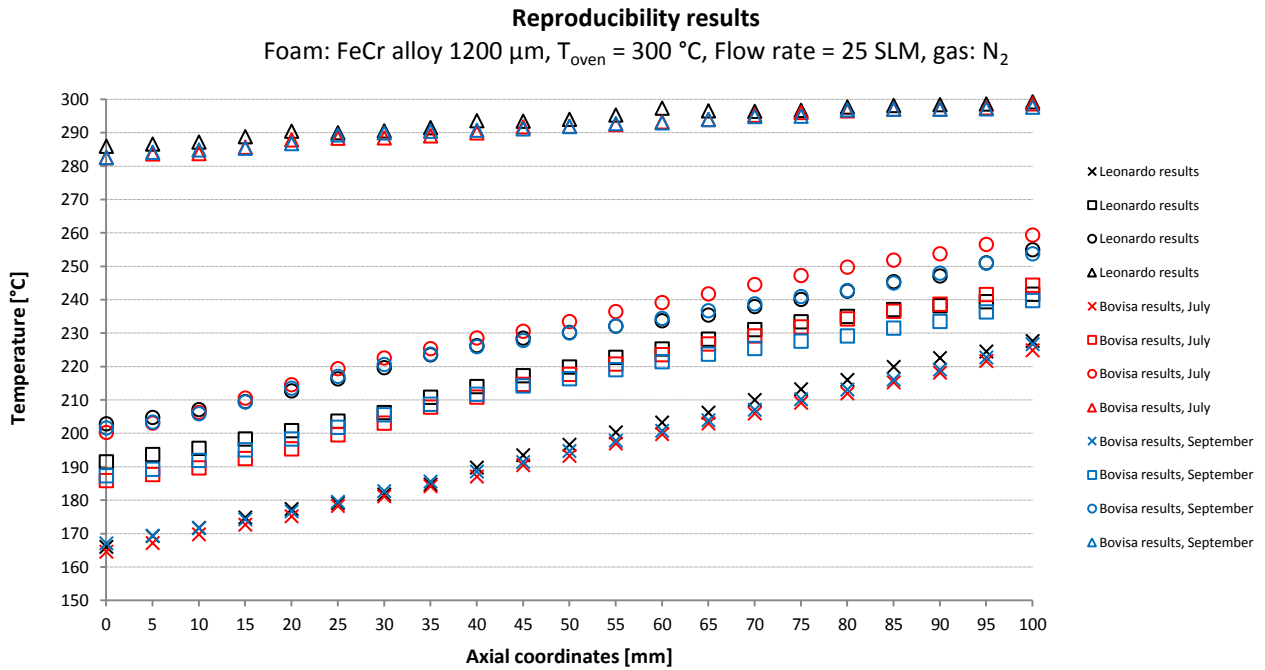
Figure 3.29 - Comparison between measurements taken in Leonardo and in Bovisa; Foam: FeCr alloy, T = 300°C, Flow rate: 25 SLM, Gas: Nitrogen.
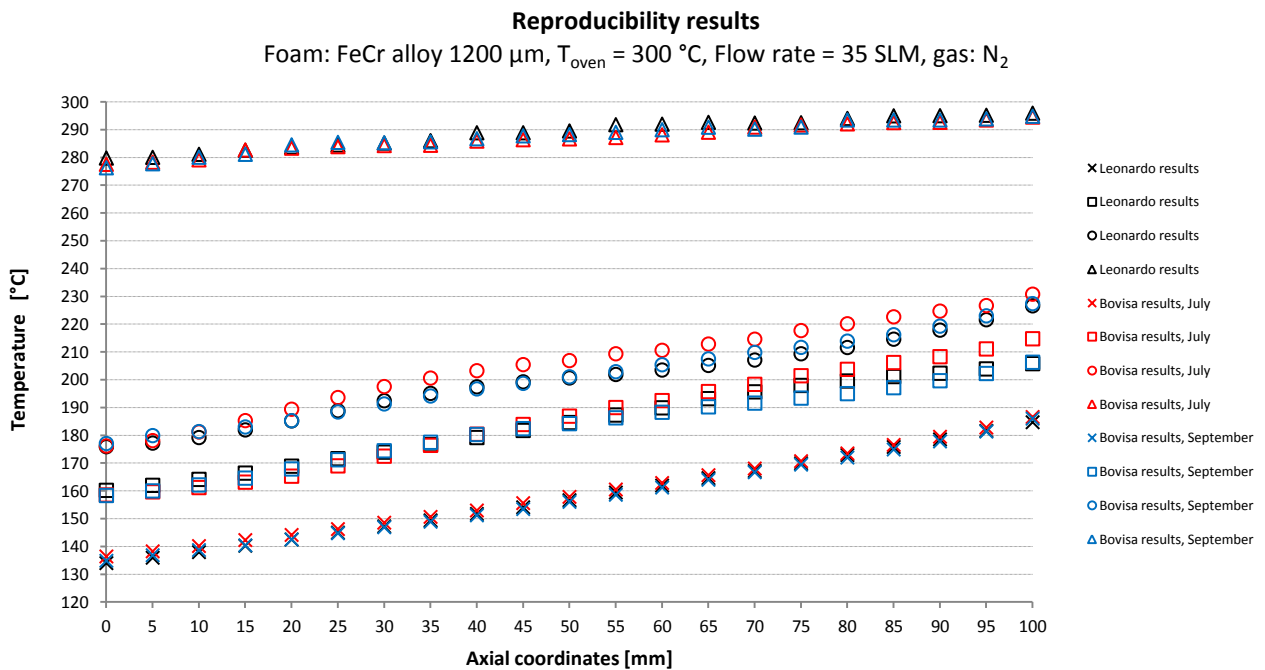
Figure 3.30 - Comparison between measurements taken in Leonardo and in Bovisa; Foam: FeCr alloy, T = 300°C, Flow rate: 35 SLM, Gas: Nitrogen.

As it is possible to see the matching between the three different tests are quite good, especially the measurements taken in Leonardo and the ones taken in Bovisa in September. However the differences are very little and can be considered in the range of experimental error.

4. Model

The obtained experimental data from the heat transfer measurements are used to numerically calculate the optimal values for the radial effective conductivity (k_{er}), axial effective conductivity (k_{ea}), and wall heat transfer coefficient (h_w). In this section a description of the model is illustrated.

4.1 2D heat transfer model

A two dimensional heat transfer model is adopted to estimate the heat transfer parameters based on the optimal fit for the obtained experimental data. The energy balance of the differential element of the foam is set under these assumptions:

- System is in steady state, which means no variation of temperature over the time, mathematically: $\frac{\partial T}{\partial t} = 0$.

- A fast heat transfer between the gas and metal occurs inside the foam during the heat transfer experiment, resulting in absence of a temperature difference locally between the foam material and the gas. This assumption has been made according to Giani et al. [37] reporting a high interphase (gas/solid) heat transfer coefficient in the foam. In this paper it was reported that the differences between gas and metal solid in the foam in each local position are negligible, i.e. less than 1 ˚C.

- The metal foam and gas inside the foam are a single pseudo-homogeneous phase.

- Axial symmetric geometry.

- Heat generation due to the friction of the flowing gas through the porous foam is negligible, thus neglecting viscous dissipation and pressure work. The temperature increase of this frictional heat generation is negligibly small due to the small pressure drop and the large heat input into the foam from the heating tube wall.

- No chemical reactions occur inside the heating tube.

Accordingly, the energy balance in the foam with cylindrical coordinates is expressed:

$$W_{in} c_P \frac{\partial T}{\partial x} = k_{er} \left(\frac{1}{r} \frac{\partial T}{\partial r} + \frac{\partial^2 T}{\partial r^2} \right) + k_{ea} \left(\frac{\partial^2 T}{\partial x^2} \right) \tag{4.1}$$

Where, W_{in} is the specific mass velocity, and c_P the specific heat capacity. Since the equation (4.1) is a second-order PDE equation, two boundary conditions in both radial and axial directions are required. For the radial direction a symmetrical boundary condition at the centerline is assumed. This means that at the centerline there is no gradient in the temperature:

$$\frac{\partial T}{\partial r} = 0, \ \ at: r = 0 \tag{4.2}$$

Also, for the radial direction a boundary condition applies considering the steady state condition at the surface of the metal foam; it is assumed that the heat flux leaving the foam outer surface, $k_{er}\left(\frac{\partial T}{\partial r}\right)$ is equal to the heat transfer from the foam outer surface to the heating tube wall, $h_w\left(T_{x,w} - T_{x,r=R}\right)$:

$$k_{er}\left(\frac{\partial T}{\partial r}\right) = h_w\left(T_{x,w} - T_{x,r=R}\right), \quad at: r = R \tag{4.3}$$

Equations (4.2) and (4.3) represent the two boundary conditions for the radial direction.

For the axial direction boundary condition at the end of the foam adiabatic condition is assumed since heat exchange at the end of the foam with the surroundings is neglected. This implies no temperature gradient at the foam outlet or in another words no heat loss towards the foam downstream zone:

$$\frac{\partial T}{\partial x} = 0, \quad at: x = L \tag{4.4}$$

Moreover, a Danckwerts boundary condition is assumed at the axial coordinate at the beginning of the foam. It is assumed that the heat flux at the entrance due to the axial condition, $k_{ea}\left(\frac{\partial T}{\partial x}\right)$, is equal to the heat transport into the foam by conduction. In other words, the heat loss due to the axial conduction towards the upstream zone is proportional to the temperature difference between the beginning of the foam (x = 0) and the undisturbed zone. In this work it is considered as undisturbed zone the position at axial coordinate x = -0.5 cm, which is the only experimental available measurement.

$$k_{ea}\left(\frac{\partial T}{\partial x}\right) = W_{in}c_P\left(T_{x=0,r} - T_{x=-0.5,r}\right), \quad at: x = 0 \tag{4.5}$$

Equations (4.4) and (4.5) represent the two boundary condition for the axial direction. The model is solved numerically applying the finite difference method of second order in the axial direction and the orthogonal collocation method in the radial direction [38]. The controlling parameters for solving this model are the effective radial conductivity (k_{er}), the axial effective conductivity (k_{ea}), and the wall heat transfer coefficient (h_w). These three parameters are applicable in the whole foam (global parameter) and include contributions of conduction, convection, and radiation. A non-linear regression, which is the minimization of the sum of squared differences between experimental and model data, is used to obtain the optimal estimates of these three parameters for each individual heat transfer experiment. For this the regression routine performs repeatedly a simulation while adapting the estimated value of these three parameters (k_{er}, k_{ea}, and h_w) during the search for the global optimum. The complete experimental dataset used for the parameter estimation and regression contains experimentally measured temperature profiles in the radial and axial direction of the foam bed. The radial positions are located at the center, 1/2 radius, and 2/3 radius and axial positions are located at each 5 mm starting from -5 mm (inlet temperature) to 100 mm (end of the foam). The experimental data are obtained in 120 heat transfer experiments at various

conditions, 4 different foam materials, 2 different cell diameters, 15 different conditions (flow type, temperature, and flow rate). The parameter estimation and regression is carried out using the software package Athena Visual Studio [39].

4.2 Inlet temperature profile

From the boundary conditions (equation 4.5) it appears the relevance the -0.5 axial position as input data to the solver routine. This profile however cannot be obtained from experimental tests. In fact, by using only three thermocouples at different radial coordinates, it is not possible to know the correct function fitting the inlet temperature profile. This is a problem that must be solved, since the solution strongly depends on this profile. In order to do so, is necessary to create a function suitable to describe values of temperature at different radial locations, corresponding to the different radial collocation points of the solver routine, at the axial position corresponding, in this work, 5 mm before the beginning of the foam. Here, FeCr alloy metal foam (1 foam disc 580 um and 1 foam disc 1200 um to reach 5 mm length) is loaded in the upstream zone to improve further, in addition to the glass spheres, the uniformity of the inlet gas flow rate and temperature over the radius.

The radial inlet temperature profile is calculated with the following exponential equation:

$$T = T_{r=0} + a \left(\frac{r}{R}\right)^b \tag{4.6}$$

Where, T is the local temperature in Kelvin; $T_{r=0}$ the temperature at r=0 and x = -0.5 cm in Kelvin; a, b are fitting parameter; r is radial position at the inlet and R the foam external radius, which is 14 mm. This equation $T_{r=0}$, a and b, whereas there are four conditions available at the axial coordinate of x = -0.5 cm and at the different radial positions:

    (i)   temperature measured at r = 0 (center, T_0),

    (ii)   temperature measured at r = 1/2 R ($T_{1/2}$),

    (iii)   temperature measured at r = 2/3 R ($T_{2/3}$),

    (iv)   temperature measured at the wall (T_w).

Since the radial locations 1/2 R and 2/3 R are very close to each other, it was decided to take the average of these two points in order to end with three equations with three unknowns to determine the inlet radial temperature profile. Therefore, temperature at the axial coordinate x = -0.5 cm and radial coordinate of $r_{av} = \frac{\left(\frac{1}{2}R + \frac{2}{3}R\right)}{2} = \frac{7}{12}R$, is taken as:

$$T_{av} = \frac{T_{1/2} + T_{2/3}}{2} \tag{4.7}$$

Which using equation (4.6), and remembering how r_{av} was just defined, can be rewritten:

$$T_{av} = T_{r=0} + a \left(\frac{7}{12}\right)^b \tag{4.8}$$

The temperature T_1 is assumed for the position of x = -0.5 and $r = R$, where R is the external radius of the foam. In other words, the temperature of the foam external surface at the inlet (x = -0.5 cm) is assumed to be T_1. This temperature, from the boundary condition 16, can be defined:

$$T_w - T_1 = \left(\frac{k_{er}}{h_w}\right)\frac{\partial T}{\partial r} \tag{4.9}$$

By using the equation (4.6):

$$T_w - T_1 = \left(\frac{k_{er}}{h_w}\right)\frac{\partial T}{\partial r} = \left(\frac{k_{er}}{h_w}\right)\frac{ab}{R} \tag{4.10}$$

Also calculating T_1 from the equation (4.6) at ($r = R$):

$$T_1 = T_{r=0} + a \tag{4.11}$$

Combining the two equations (4.10 and 4.11), it follows:

$$T_w = T_{r=0} + a \left(1 + \left(\frac{k_{er}}{h_w}\right)\frac{b}{R}\right) \tag{4.12}$$

The value of $\frac{k_{er}}{h_w}\frac{1}{R}$ in the inlet zone has not been estimated by e.g. literature correlations, but defined as an additional unknown parameter to be estimated in the fitting procedure. It is called "Par (4)" since it is the 4th parameters in each regression, which is thus calculated by the model based on the best fit for the inlet temperature profile and the optimal fit for the whole foam. Therefore, "Par (4)" is treated just as a fitting parameter and not a realistic estimate of the ratio $\frac{k_{er}}{h_w}$. This fitting parameter can adequately account for the effect of the deviation of the inlet gas flow from plug flow behavior.

This finally yields three equations with three unknowns $T_{r=0}$, a, and b which are solved by the Athena solver:

$$T_{r=0} = T_0 \tag{4.15}$$

$$T_{av} = T_{r=0} + a \left(\frac{7}{12}\right)^b \tag{4.14}$$

$$T_w = T_{r=0} + a \left(1 + \left(\frac{k_{er}}{h_w}\right)\frac{b}{R}\right) \tag{4.15}$$

By solving these three equations it is possible do define an inlet temperature profile which cover all the radial position of the foam at the axial coordinate -0.5.

In order to investigate how the model uses the three experimental points to calculate the radial profile at the inlet zone (x = -0.5), radial profile of FeCr 1200 µm, FeCr 580 µm and Co 580 µm has been analyzed at different operative conditions. It is important to notice, as described in chapter 3, that at the axial position x = -0.5 the foam there is always one disk of FeCr 1200 µm and one of FeCr 580 µm, so the radial profile at the same operative condition should have the same curves. In all the following figures the three blue points are the experimental measured temperature of the foam, the red point is the experimental wall temperature, and the cyan line is the simulated radial profile.

Figure 4.1 shows radial temperature profiles of FeCr 1200 µm at different flow rate, flowing gas and oven temperature.

T = 500 °C, flow rate = 20 SLM, gas: He.

T = 500 °C, flow rate = 25 SLM, gas: He.
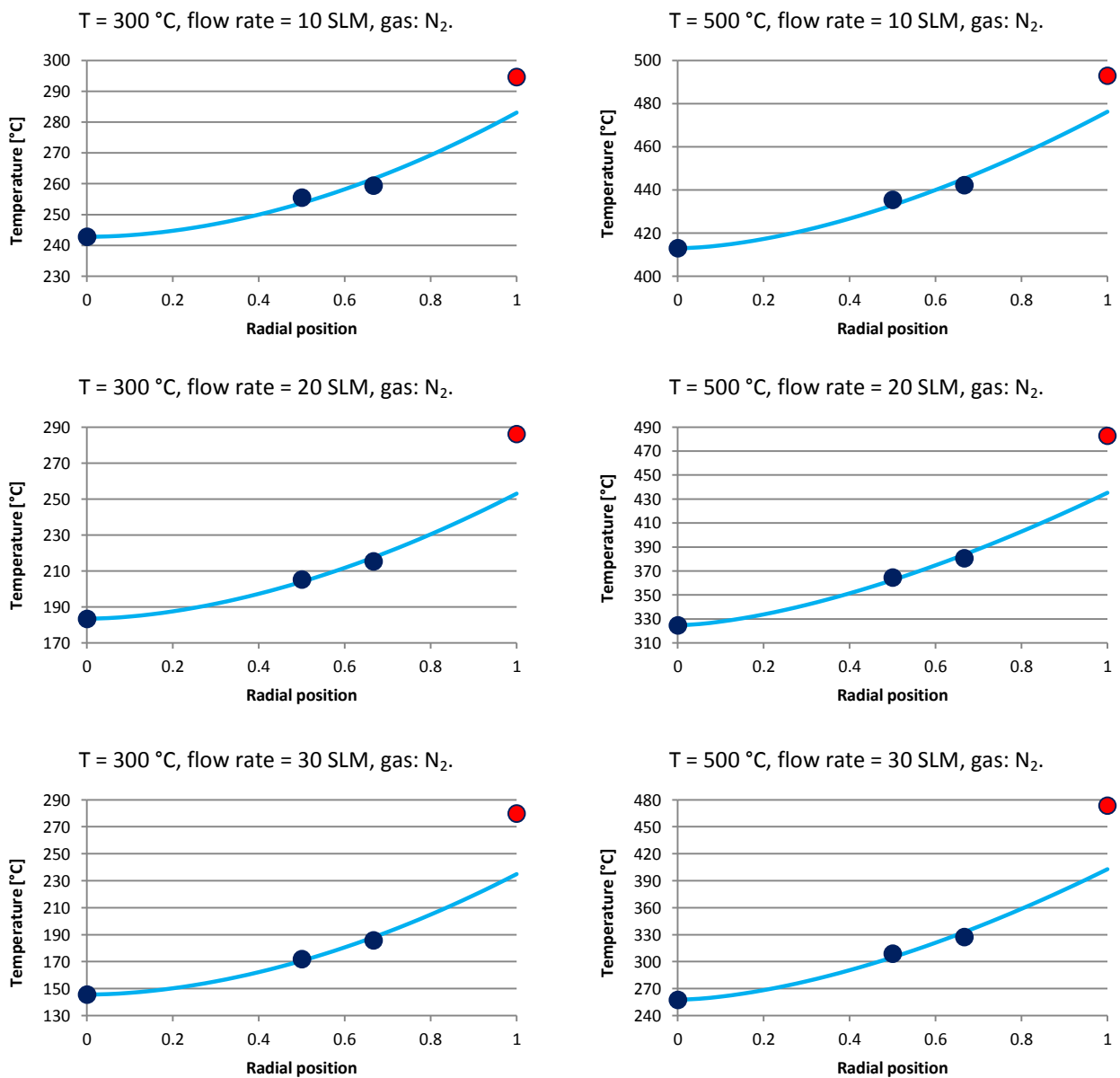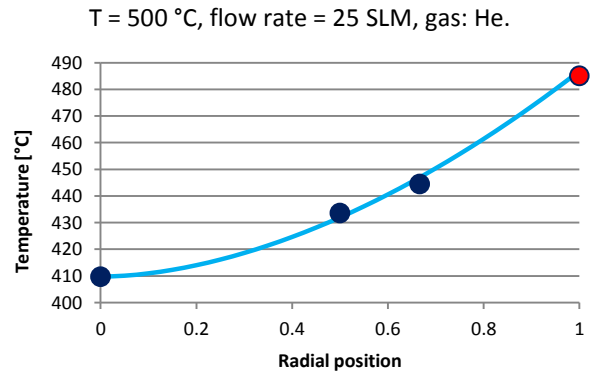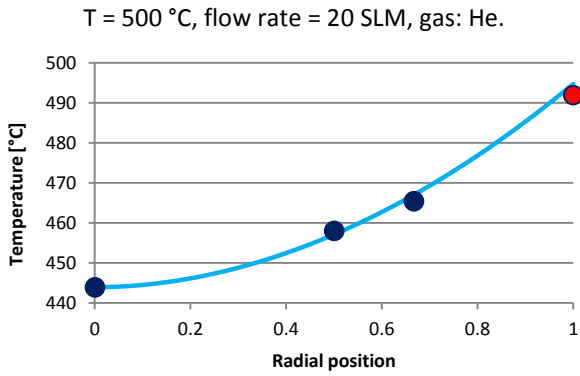
Figure 4.1 - Radial temperature profiles at axial coordinate x = -0.5 of FeCr 1200 µm at different operative conditions.

These plots shows that increasing the flow rate the inlet temperature decrease and increasing the oven temperature the temperature raises. These effects will be analyzed in detail in the next chapter. What is important to notice here is that even by changing the thermostatic temperature set point the profile shape at same flow rate doesn't change. The two presented profile with helium show an irregularity: at r =1 the internal temperature estimated by the model overcomes the red point, which is external. This is probably due to the par(4), estimated to be equal to 0, which means $h_w = \infty$; and this could be due to the very small gradient between the temperature at r = 0 and the wall temperature.

Figure 4.2 compares the radial temperature profiles of FeCr 1200 µm and FeCr 580 µm at different flow rate, flowing gas and oven temperature.

T = 300 °C, flow rate = 15 SLM, gas: N_2, FeCr 1200 µm

T = 300 °C, flow rate = 15 SLM, gas: N_2, FeCr 580 µm

T = 300 °C, flow rate = 35 SLM, gas: N_2, FeCr 1200 µm

T = 300 °C, flow rate = 35 SLM, gas: N_2, FeCr 580 µm

53
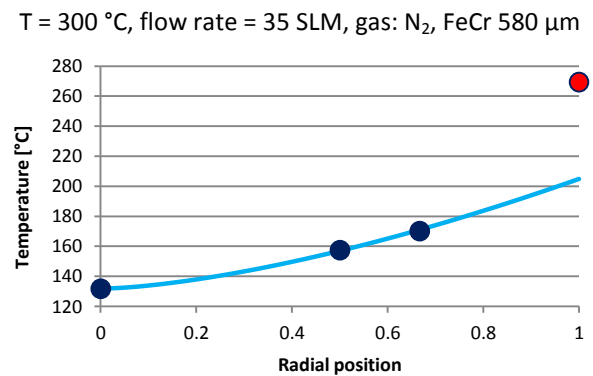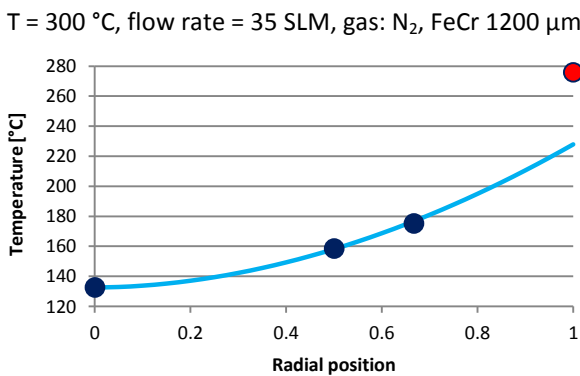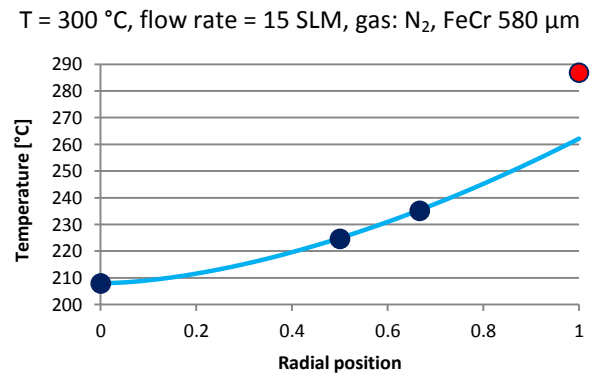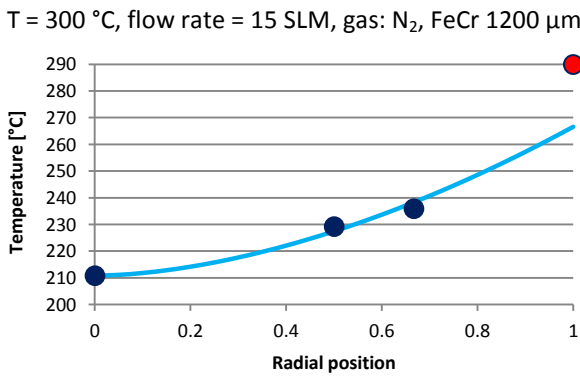
T = 500 °C, flow rate = 25 SLM, gas: N$_2$, FeCr 1200 µm

T = 500 °C, flow rate = 25 SLM, gas: N$_2$, FeCr 580 µm

Figure 4.2 - Comparison of radial temperature profiles at axial coordinate x = -0.5 between FeCr 1200 µm and FeCr 580 µm at different operative conditions.

The last comparison is made between FeCr 1200 µm and Co 580 µm. Figure 4.3 shows the results.

T = 300 °C, flow rate = 10 SLM, gas: N$_2$, FeCr 1200 µm
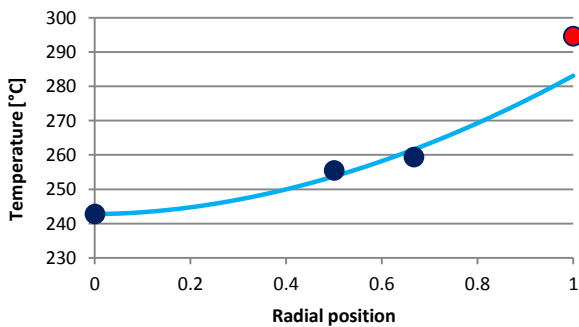
T = 300 °C, flow rate = 10 SLM, gas: N$_2$, Co 580 µm
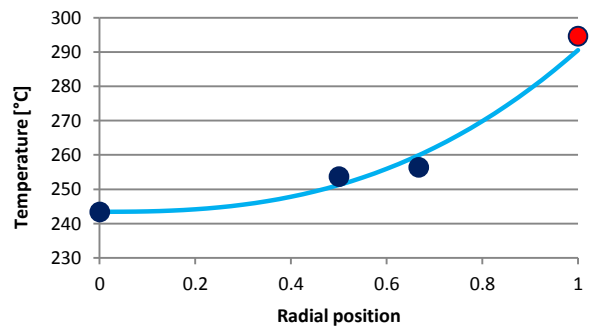
T = 500 °C, flow rate = 20 SLM, gas: N$_2$, FeCr 1200 µm
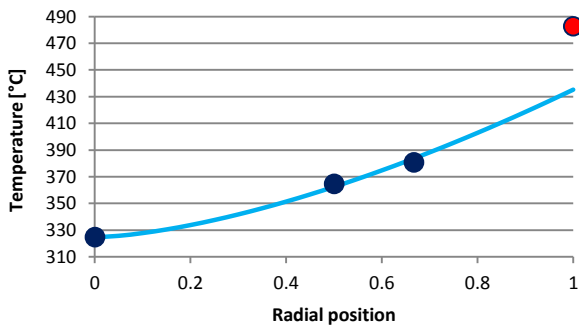
T = 500 °C, flow rate = 20 SLM, gas: N$_2$, Co 580 µm
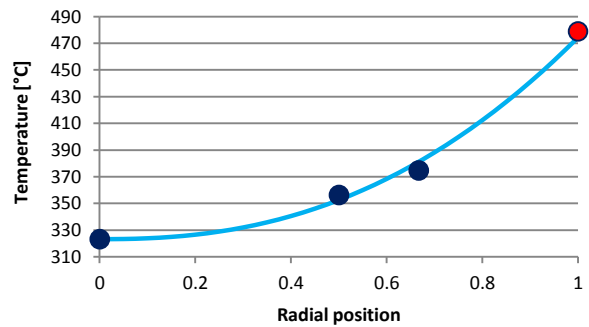
T = 500 °C, flow rate = 20 SLM, gas: He, FeCr 1200 µm
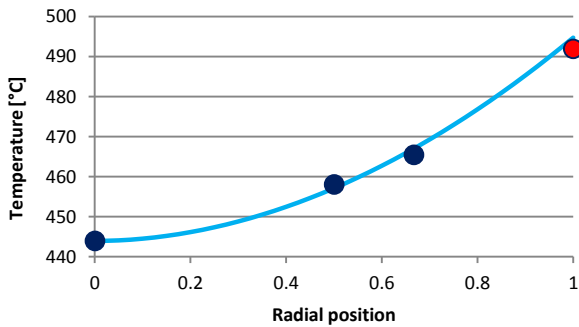
T = 500 °C, flow rate = 20 SLM, gas: He, Co 580 µm
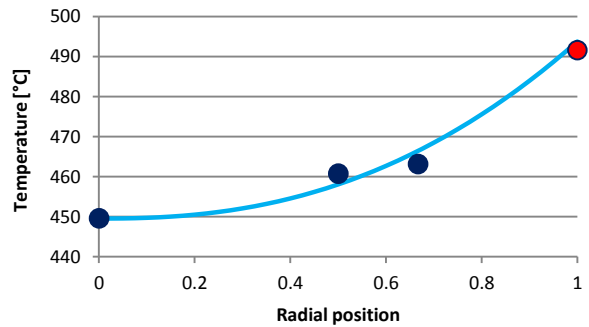
Figure 4.3 - Comparison of radial temperature profiles at axial coordinate x = -0.5 between FeCr 1200 µm and FeCr 580 µm at different operative conditions.

Figure 4.2 and 4.3 demonstrate the reproducibility of the inlet profile at given flow rate, gas type and oven temperature conditions. As expected, since the upstream preheating and flow distribution section has been kept unchanged in all the tests, experimental inlet profile obtained at the same operative conditions with different foams are quite similar. On the other hand, some difference are evident between the fitted profiles, especially in figure 4.3, where foams made of different materials and with different porosities are compared. Such differences originates from manipulation associated with the overall data fitting procedure.

5. Results

In this chapter, experimental and modeling results of all the heat transfer measurements in different operative conditions are presented. First of all some single experimental tests, then comparative graphs, in order to investigate the effect of various parameters on the temperature profiles, will be reported. Once the experimental results have been illustrated, the experimental axial temperature profiles with the regression analysis based on the optimal fit for each foam are shown and parameters estimated by the model are discussed.

5.1 Experimental results and analysis

As already described in chapter 3, four different foam materials have been experimentally studied in this work: FeCr alloy, NiCr alloy, Co and Cu metal foams. Each metal foam with two different nominal cell diameters: 580 µm and 1200 µm. Next table reports, the properties for each foam.

Table 5.1 - Properties of studied foams.

Foam Material	Cell [mm]	Pore [mm]	Struts thickness in the middle [mm]	Hydraulic Porosity [-]	Total Porosity [-]	Solid Conductivity [W/(m K)]
FeCr	1.2	0.49	0.18	0.9414	0.9449	16 [40]
	0.58	0.19	0.08	0.8977	0.9251	
NiCr	1.2	0.3	0.14	0.9465	0.9482	17 [41]
	0.58	0.22	0.07	0.9193	0.9305	
Co	1.2	0.33	0.12	0.9720	0.9799	68 [42]
	0.58	0.25	0.07	0.9484	0.9707	
Cu	1.2	0.39	0.13	0.9647	0.9715	369 [42]
	0.58	0.2	0.07	0.9469	0.9562	

Experiments with foams have been conducted at 300 °C and 500 °C using nitrogen and varying the flow rate from 10 to 35 SLM, and at 500 °C with helium, varying the flow from 10 to 30 SLM, however, by running tests with helium at low flow rate, the temperature profiles developed themselves in a range of less than 10 degrees, as shown in figure 5.1.
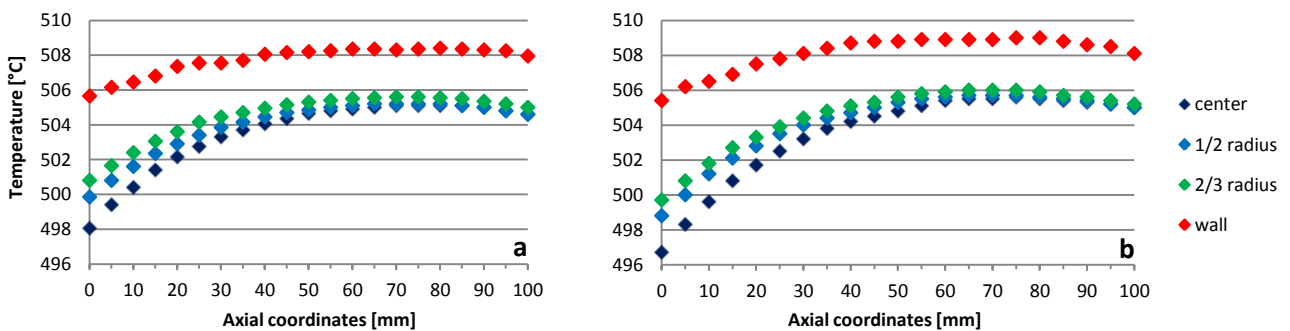
Figure 5.1 - Axial temperature profiles of FeCr alloy at 10 SLM, 500 °C, He, a) d_c = 1200 µm, b) d_c = 580 µm.

The profiles shown in figure 5.1 make any considerations useless, since temperatures differences are well within the experimental error. Moreover, the profiles at the end of the bed start to slightly decrease, this

might due to the proximity of the foam to the flange of the tube, which could affect the measurement, making it faulty. By this way, as the FeCr has the worst heat exchange, tests with helium at low flow rate aren't performed again. All the experimental data are available in appendix B section 2, (page 106), however, here are reported some experimental graphs for every foams, at the lowest and highest flow rate and with the two different flowing gas.

Experimental data, T_{oven} = 300 °C, Flow rate = 10 SLM, Gas: N_2, d_c = 580 µm
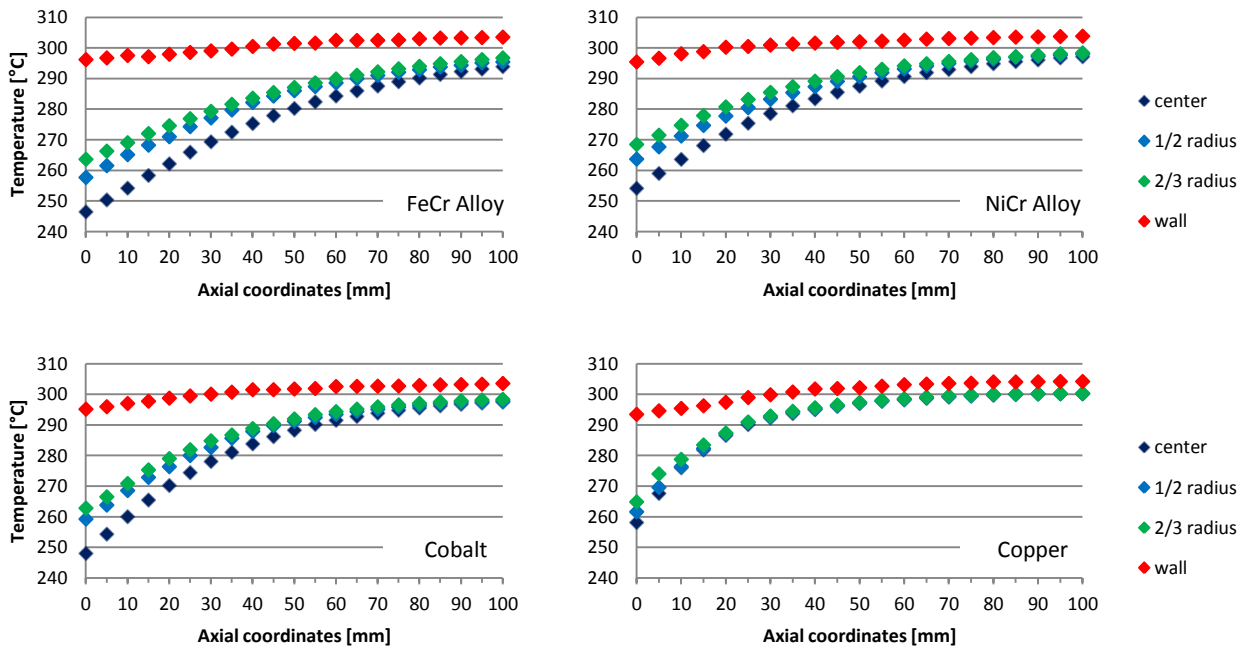
Experimental data, T_{oven} = 500 °C, Flow rate = 35 SLM, Gas: N_2, d_c = 1200 µm

Experimental data, T$_{oven}$ = 500 °C, Flow rate = 30 SLM, Gas: He, d$_c$ = 1200 µm
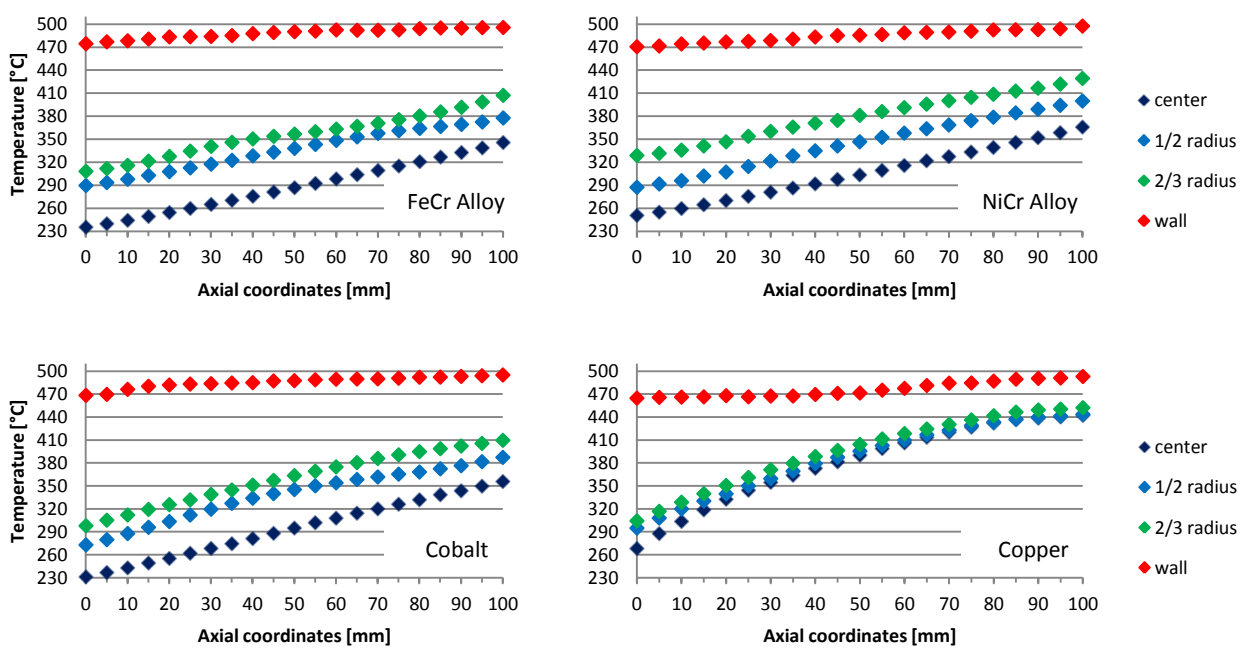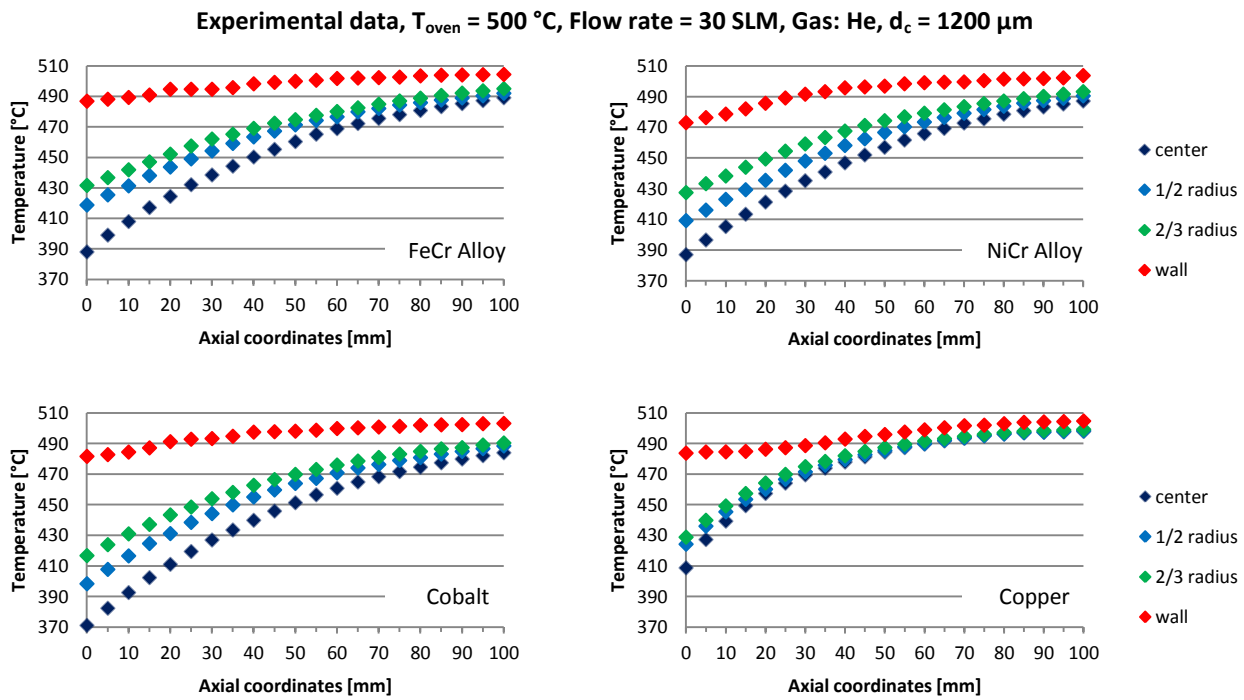
Figure 5.2 - Experimental data of sample foam at: 10 SLM with nitrogen at 300 °C, 35 SLM with nitrogen at 500 °C and at 30 SLM with helium at 500 °C.

It is interesting to see that radial profiles in copper are much closer than the others. they also reach the highest temperature and an evident concavity is always present. These phenomena and the influences of operative condition are discussed in the next paragraphs. The irregularity of internal profile which could be noticed at high flow rate are considerable as little uncertainty of position of thermocouples inside the thermowells. It is also worth noticing that the temperature profiles of the wall temperature show irregularities; this is due to the fact that these profiles are collected on the outer surface of the experimental section pipe. Even though fins and stainless steel rings are such that the thermocouple has the best contact with the surface, there are still some zones where contact is imperfect. These issues have been encountered also in the previous works [2, 36].

5.1.1 Influence of radial and axial position

As it was possible to see from the previous graphs, the three different radial positions provide in three different temperature profiles, always in the same order, starting from the central, which is the coolest one, to the 2/3 radius, which is the hottest one. This is very easy to explain, in fact the central profile is the farest from the tube wall, so it receives the lowest part of the heat produced by the oven; on the other hand, the 2/3 radius position is the closest to the tube and for this reason it has the hottest measured profile. Radial conduction heat transfer from the outer surface of the heating tube into the foam over the foam length occurs as well, as shown in figure 5.3a. This sketch qualitatively explains the temperature distribution in a radial section of the foam, where on the left is located the 2/3 radius position, on the left the 1/2 radius position. In addition, the temperature of the gas flow increases moving along the axial

direction from the beginning of the foam sample to the end (0 mm to 100 mm) since the gas heats up in its way inside the heating tube reaching the end of the foam bed. This convection heat transfer results in increase in the radial temperature measurements (center, 1/2 radius, 2/3 radius) along the axial direction, as it is possible to see in figure 5.3b. The above axial temperature profiles also show that the wall temperature which is measured by the 4th thermocouple placed on the outer surface of the heating tube in each test measures the oven set point temperature, either 300 °C or 500 °C. However, in the beginning of the foam length (axial direction), the wall temperature is lower than the oven temperature due to the colder gas flow.
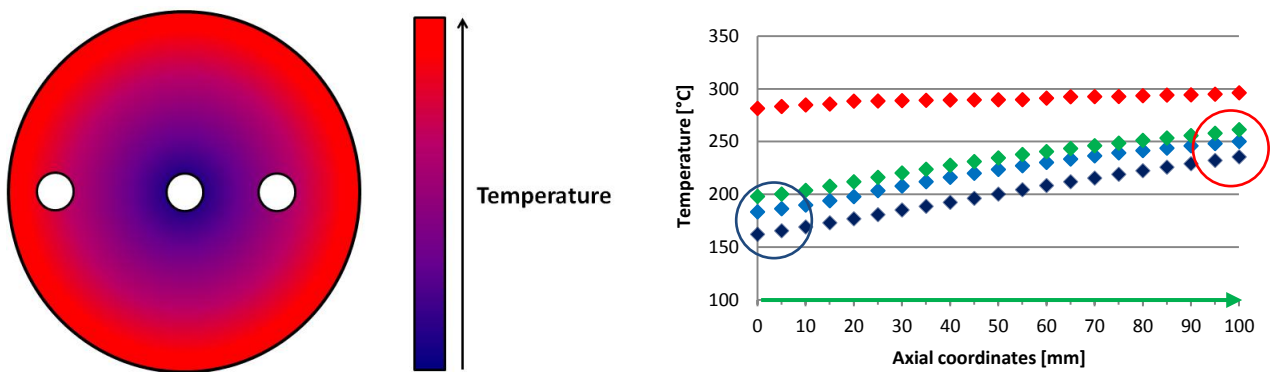
Figure 5.3 - a) Qualitative temperature arrangement in the foam radial section during the heat transfer experiment, conduction heat transfer; b) An example of axial temperature profile for schematically describing the heat transfer occurs inside the foam sample.

5.1.2 Influence of thermal conductivity of material on the relative radial and axial position

The just described phenomena are not always the same. By changing the foam material the relative position of the radial profile changes, in other words, the gradient of radial profiles of ferrochrome foam is bigger than the one of copper foam, whose three radial temperatures are closer to each other. To make it easier and clearer to analyze, a ratio between the central temperature and the others has been calculated. The following graphs (figure 5.4 and figure 5.5) report this ratio for the four different materials, using temperatures taken in the middle of the bed and using foam with cell diameter of 580 µm and 1200 µm at two different operative conditions.
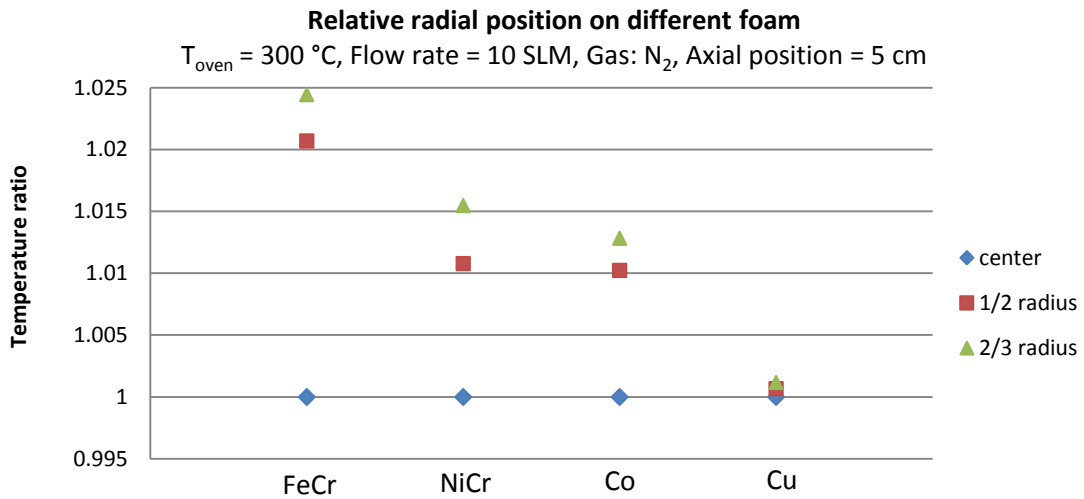
Figure 5.4 - Effect of conductivity on the relative radial position of each foam, T = 300 °C, flow rate = 10 SLM, gas: N$_2$, axial position = 5 cm, cell diameter = 580 µm.

By increasing the flow rate from 10 to 35 SLM, the relative distance of the three radial position grows but however, as shown in figure 5.5, even by changing the oven temperature and the cell diameter, the situation still remains the same.
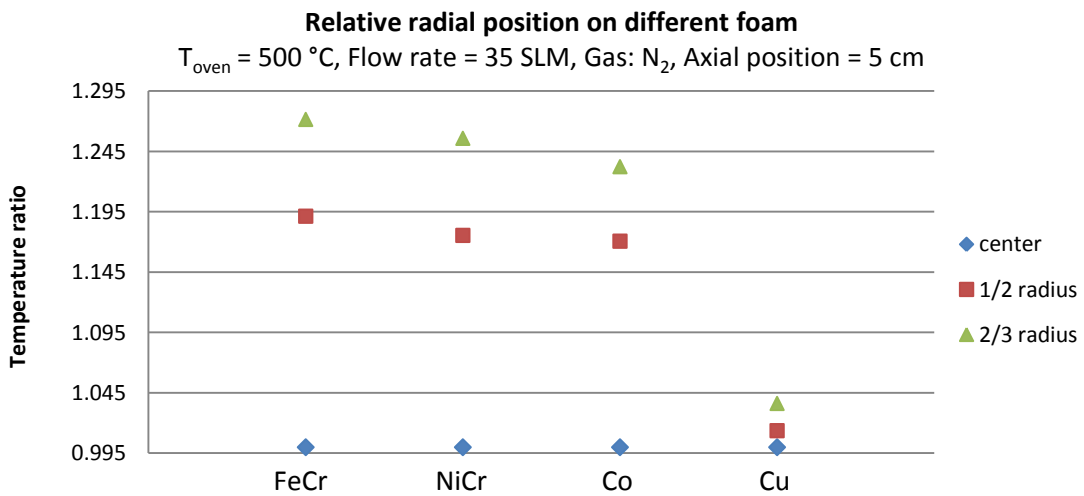
Figure 5.5 - Effect of conductivity on the relative radial position of each foam, T = 500 °C, flow rate = 35 SLM, gas: N$_2$, axial position = 5 cm, cell diameter = 1200 µm.

Moreover, materials affects also the axial temperature profiles. Figure 5.6 shows the four profiles, corresponding the four materials, collected in the same operative conditions, i.e. setting the furnace at 300 °C, 35 SLM and using nitrogen. To make it clearer, only the central profile is reported.
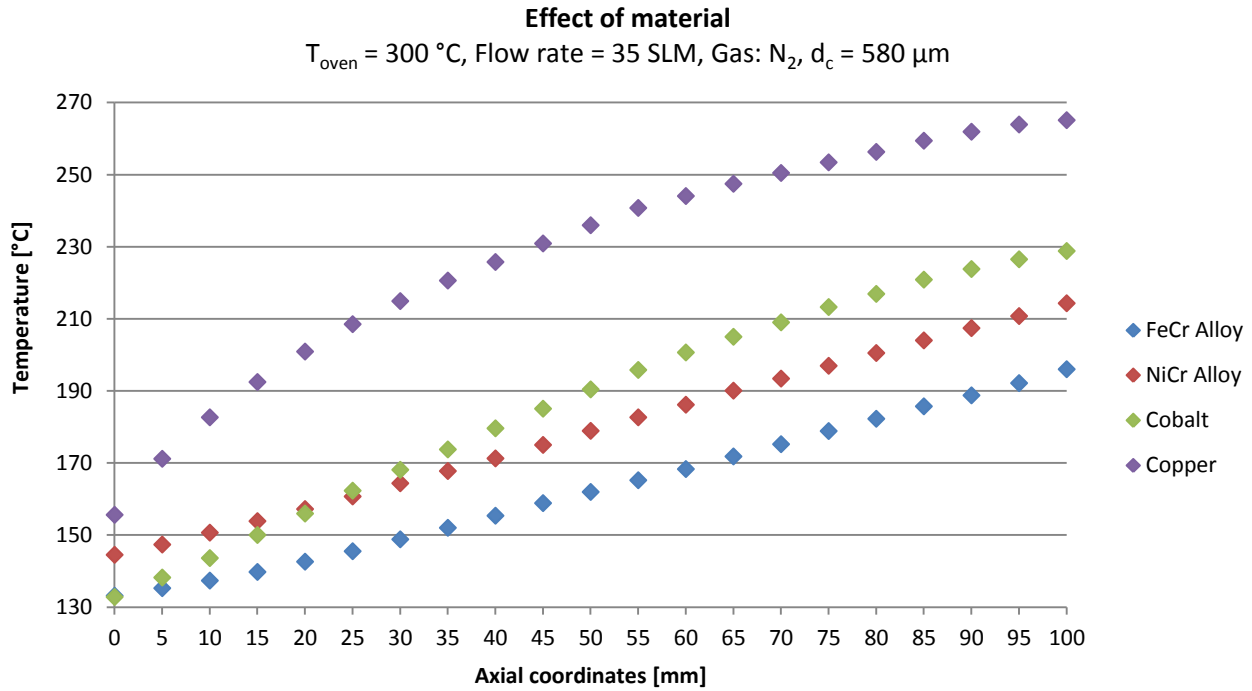
Figure 5.6 - Effect of foam material, T = 300 °C, flow rate = 35 SLM, gas: N$_2$, cell diameter = 580 µm.

These effects are both due to the conductivity of the material of the foam, since it is:

$$k_{Cu} \gg k_{Co} > k_{NiCr} > k_{FeCr}$$

and the higher is the conductivity the closer are the two profile. In fact foams with high conductivity present an higher thermal resistance to the flow, which cannot cool down enough the foam, leaving it closer to the wall temperature. Foam made of copper reaches, at the end of the bed, the highest temperature, then it is followed by the cobalt foam, which, even starting at a lower temperature of the nickel chrome one, overcomes it, and the lowest temperature profile belongs to the ferrochrome foam.

The conductive heat transfer is directly proportional to the material thermal conductivity. That means by increasing the material conductivity (k_s), heat transfer by conduction increases. However, it is important to consider the positive effect of material thermal conductivity and negative effect of total porosity (ε_T) on conduction heat transfer, accordingly to the Lemlich's theory:

$$k_{cond} = \frac{(1 - \varepsilon_T)}{3} k_s \tag{5.1}$$

It is also interesting see that this is a strong dependence, in fact the conductivity of copper, which is extremely high compared to the others, brings the foam at a very higher temperature comparatively to other temperatures.

5.1.3 Influence of different flow rates

In order to carry out a clear analysis of the effect of flow rate, temperature profiles measured with all the studied flow rate have been compared in figure 5.7. Temperature profiles reported in this plot are collected by setting the oven temperature at 300 °C (573.25 K) and using nitrogen as flowing gas.
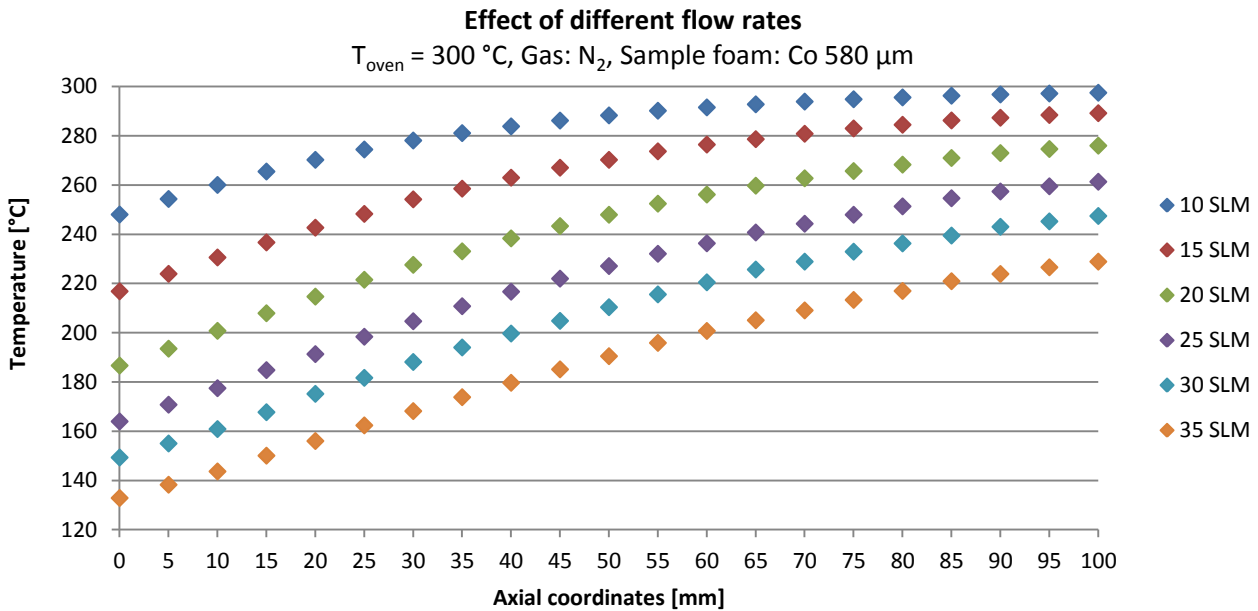
Figure 5.7 - Effect of different flow rates on temperature profile, T = 300 °C, gas: N$_2$, sample foam: Co 580 µm.

First of all, as it is possible to see from figure 5.7, the inlet temperature of the gas is higher than the room temperature. This is explained considering the heat exchange, which cannot be avoided, from all the parts used upstream the foam. Analyzing the plot it can be noticed that the increase of the flow rate entail a decrease of the temperature of the foam: by increasing the flow rate it also grows the flowing heat capacity and, for this reason, a lower temperature is obtained. Another thing which is possible to notice from this graph is the effect of the flow rate on the shape of the temperature profile, in particular, the concavity of the profile decreases by increasing the flow rate. In this system the heat is distributed from the periphery to the center of the pipe, and at high flow rate the system cannot achieve the thermal equilibrium, target which can be reached when the flow rate is low.

5.1.4 Influence of different flowing gases: N$_2$ and He

In this experimental campaign two different gases have been studied, in order to study the effect of gases with different thermal conductivity, nitrogen (k_f = 0.026 $\frac{W}{mK}$ NPT) and helium (k_f = 0.147 $\frac{W}{mK}$ NPT). Different gases are also chosen as representative of a gas of low thermal conductivity, such as air, which is a reference situation for selective oxidation processes, and a gas with high thermal conductivity, such as synthesis gas which is a reference for processes which produce (as steam reforming) or consume (Fischer

Tropsch synthesis) syngas, respectively. Here, a comparison graph (figure 5.8) is reported to evaluate the effect of different flowing gases. In this case, the temperature is set at 500 °C (773.15 K).

Effect of different flowing gases
T_{oven} = 500 °C, Sample foam: Co 580 µm
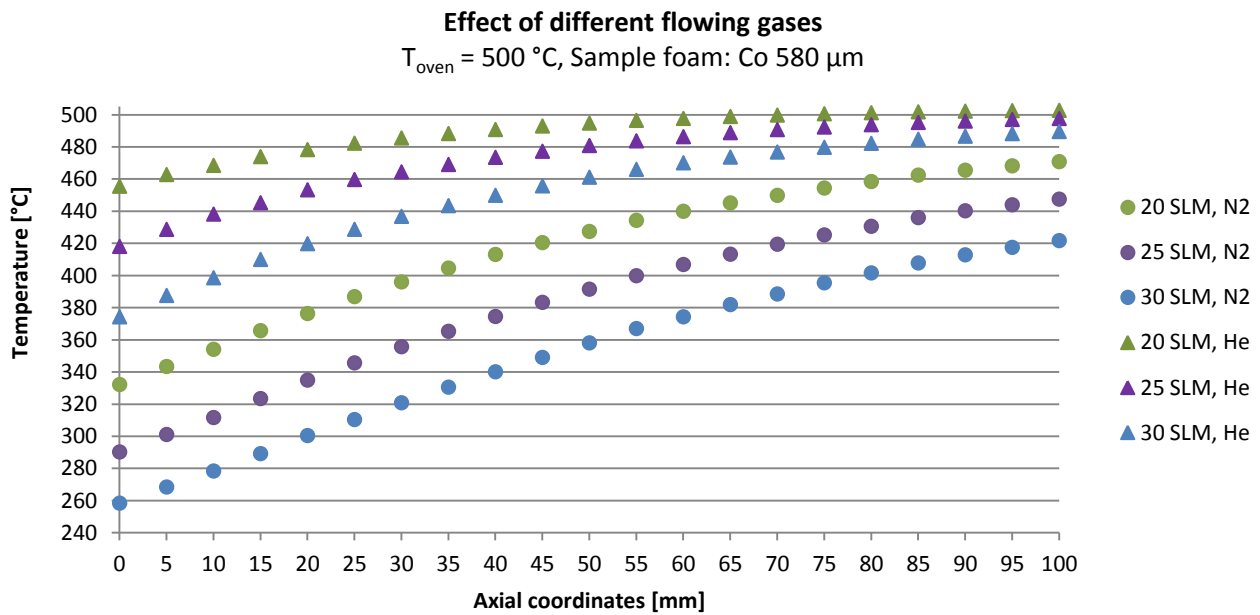
Figure 5.8 - Effect of different flowing gases, T = 500 °C, sample foam: Co 580 µm.

It is well evident that the measured temperatures using helium are higher than those measured using nitrogen at equal flow rate. Moreover the helium profiles present a more significant concavity. It has to be considered that these tests are performed using the same volumetric flow rate, which means, according the perfect gases law, also the same molar flow. However, since helium is a monoatomic gas, it presents a lower specific heat capacity than nitrogen ($c_{p_{He}} = \frac{5}{2}R$ kJ/(mol K), $c_{p_{N_2}} = \frac{7}{2}R$ kJ/(mol K)), which means that helium has a lower total heat capacity so it requires less heat to increase its temperature. Besides, the conductivity of helium is more than five times higher than the nitrogen one. An increase in the gas conductivity induce the system to have a better penetration of the heat in the bulk region. This two reasons explain why the higher temperature is reached in case of tests performed with helium.

5.1.5 Influence of different set point of the thermostatic chamber: 300°C and 500 °C

In order to evaluate the effect of different temperature set points of the oven, which affects the average temperature of the foam and the thermodynamic properties, tests were performed at 300 °C and 500 °C. The following graph (figure 5.9) shows the how the temperature of the thermostatic chamber affects the internal profile.

Effect of different temperature set point

Gas: N$_2$, Sample foam: Cu 580 µm

Legend:
- ◆ 10 SLM, 300 °C
- ◆ 15 SLM, 300 °C
- ◆ 20 SLM, 300 °C
- ◆ 25 SLM, 300°C
- ◆ 30 SLM, 300 °C
- ◆ 35 SLM, 300 °C
- ● 10 SLM, 500 °C
- ● 15 SLM, 500 °C
- ● 20 SLM, 500 °C
- ● 25 SLM, 500°C
- ● 30 SLM, 500 °C
- ● 35 SLM, 500 °C
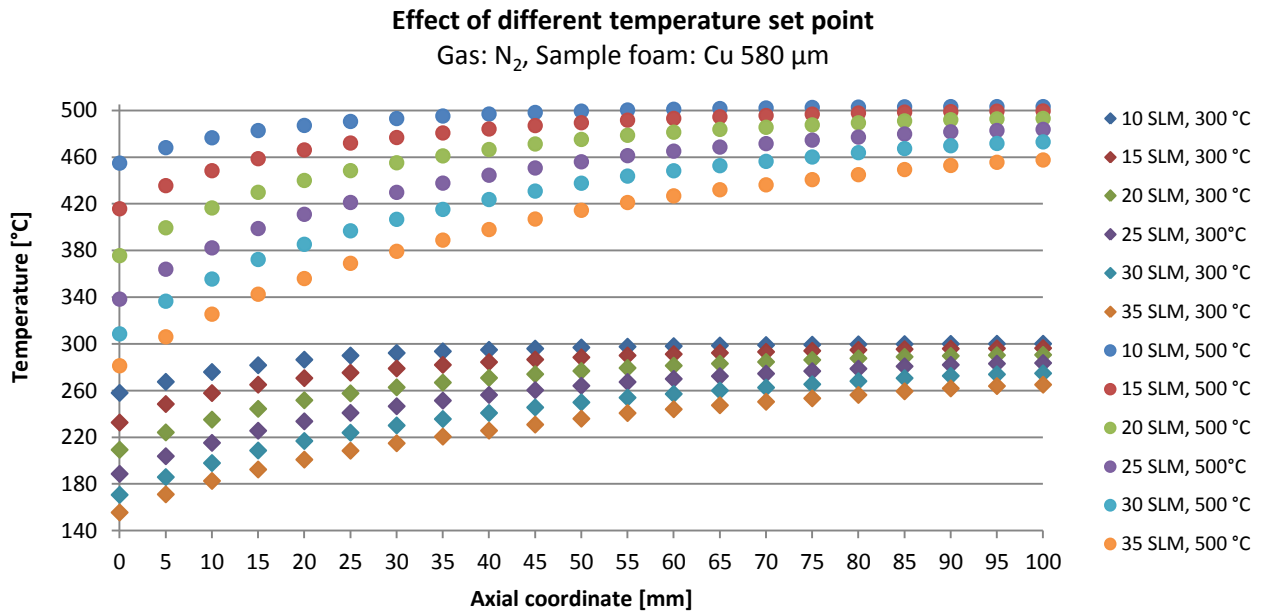
Figure 5.9 - Effect of different temperature set point of the thermostatic chamber, gas: N$_2$, sample foam: Cu 580 µm.

As expected, the temperature of the profile is always higher in case of tests at 500 °C with the same flow rate. In fact, while the mass of flowing gas is constant, the thermal power transferred from the oven, which depends on the temperature set point, increases.

5.1.6 Influence of cell diameter: 1200 µm and 580 µm

The sample foams have been provided in two different nominal cell diameters, 1200 µm and 580 µm. In this way it has been possible to study also the effect of the geometry on the temperature profile. The next comparison graphs (figure 5.10 and 5.11) represent this influence. As representative examples, two kind of materials and two different flow rates are chosen.

Effect of different cell diameters

T_{oven} = 500°C, Flow rate = 15 SLM, Gas: N_2, Foam: Co
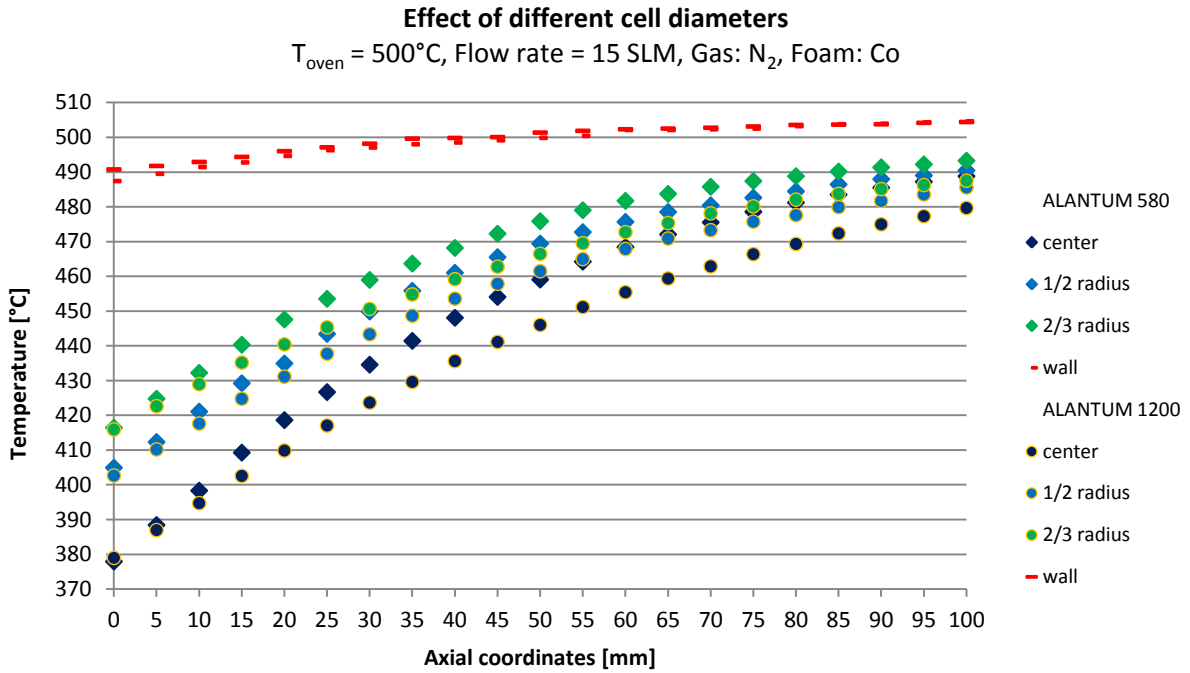
Figure 5.10 - Effect of different cell diameters, T = 500 °C, flow rate = 15 SLM, gas: N_2, foam material: cobalt.

Effect of different cell diameters

T_{oven} = 500°C, Flow rate = 35 SLM, Gas: N_2, Foam: NiCr
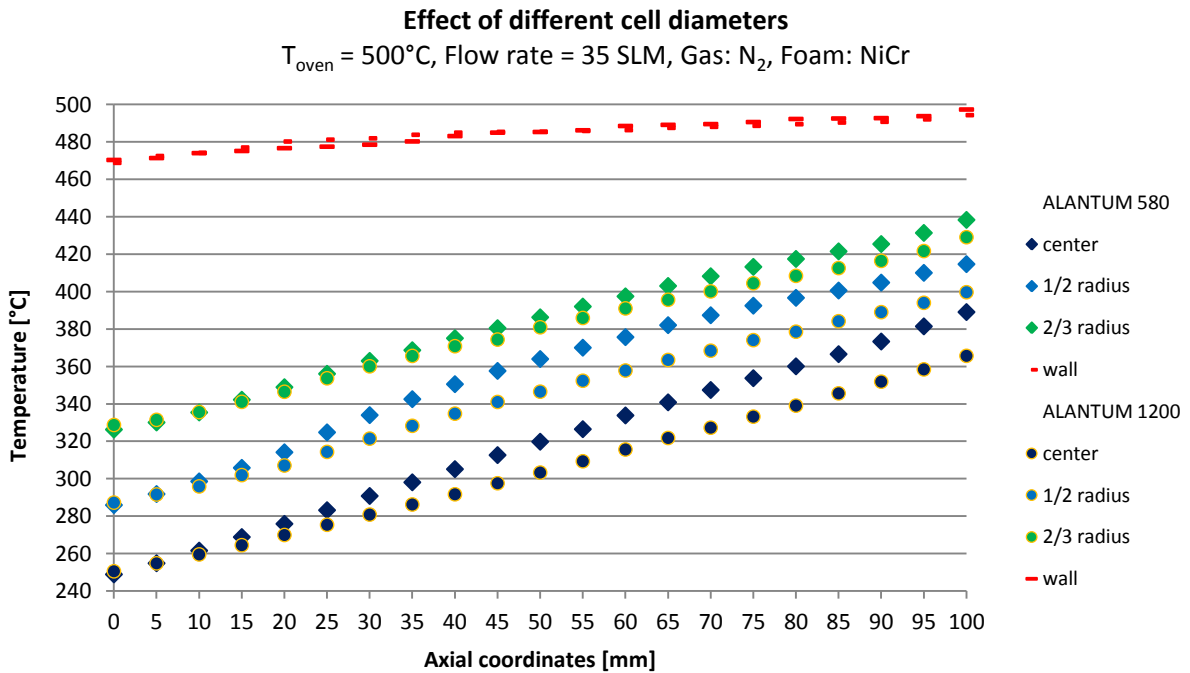
Figure 5.11 - Effect of different cell diameters, T = 500 °C, flow rate = 35 SLM, gas: N_2, foam material: NiCr alloy.

In both cases, the foam with the lower cell diameter reaches an higher temperature at the end of the bed in all the three radial positions. Such behavior can be attributed to two different effects. Accordingly to the proposed in the Bianchi thesis work, the wall heat transfer coefficients increases on decreasing the cell size.

Moreover, from the measurements made by the gravimetric analysis (chapter 2), foams with lower cell diameter have also a lower porosity, for instance, for the FeCr alloy foam, the porosity increases from 0.925 to 0.945 increasing the cell diameter. This results in having less amounts of pores per inch and less solid fraction $(1 - \varepsilon_T)$. Since the conductive heat transfer is proportional to the solid fraction, (i.e. Lemlich theory), also the radial effective conductivity is expected to decrease on increasing the cell diameter. It is also interesting to notice that the profiles with the same radial position start at the same point. This is correct, since the upstream conditions are the same and the material is the same, while the starting point probably is a function of material conductivity. The wall temperature, as it is not a measurement of the foam, it is not so affected to the cell diameters and the difference between the two kind of foam is very slight.

5.2   Model results

In this section, a brief discussion of the model estimations and its fitting of the experimental data is done. As described in chapter 4, at this stage the model try to find the best fit based on the experimental data, and from this estimate the three parameters, k_{ea}, k_{er} and h_w. The following sketch (figure 5.12) shows the physical meaning of these three parameters.
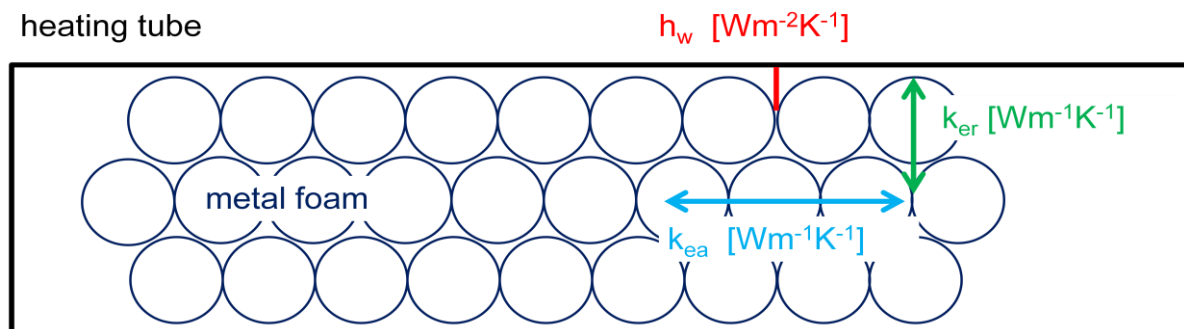
Figure 5.12 - Sketch of heating tube with the three estimated parameter.

The two effective conductivities, k_{ea} and k_{er} are the sum of contributions of conduction, convection and radiation in the two direction, axial and radial, respectively. The wall heat transfer coefficient, h_w, correspond to the specific resistance at the foam-tube interface.

5.2.1 Model regression results

In the next pages it is shown the model fitting ability, comparing the experimental axial temperature profiles with the regression results. Regression have been made constraining the radial effective conductivity (k_{er}) to be higher than the axial radial conductivity (k_{ea}), a part the wall profile which is only used as data input. Since the model doesn't give reasonable results for tests at low flow rate with helium, model for flow rate lower than 20 SLM of helium are not used. From the following results it is well evident that the model is able to provide a very good fit of experimental results for all the investigated conditions.

5.2.1.1 FeCr alloy foam, dc =1200 µm: regression results

T = 300 °C, flow rate = 10 SLM, gas: N_2.

T = 300 °C, flow rate = 15 SLM, gas: N_2.

T = 300 °C, flow rate = 20 SLM, gas: N_2.

T = 300 °C, flow rate = 25 SLM, gas: N_2.

T = 300 °C, flow rate = 30 SLM, gas: N_2.

T = 300 °C, flow rate = 35 SLM, gas: N_2.

T = 500 °C, flow rate = 10 SLM, gas: N_2.

T = 500 °C, flow rate = 15 SLM, gas: N_2.
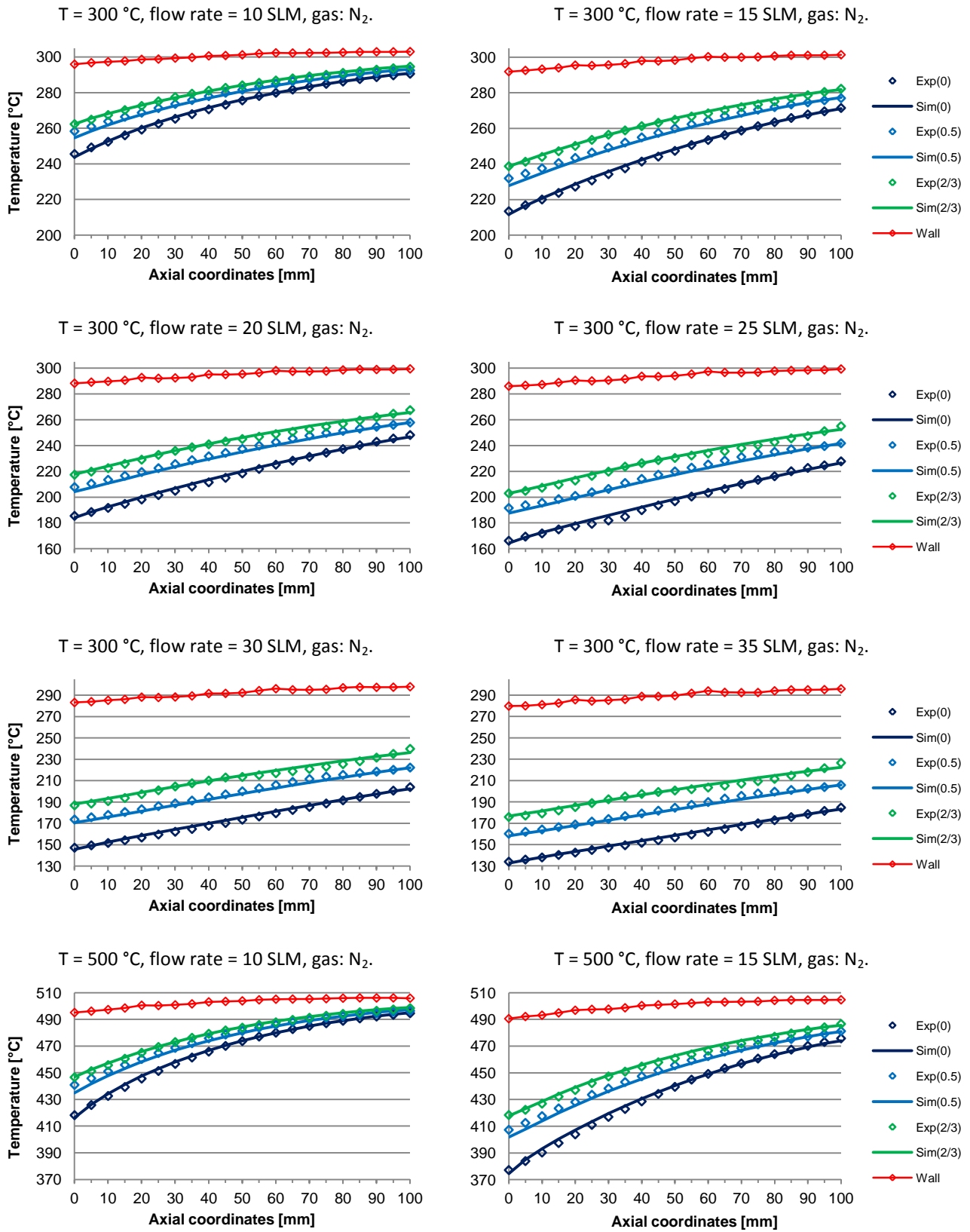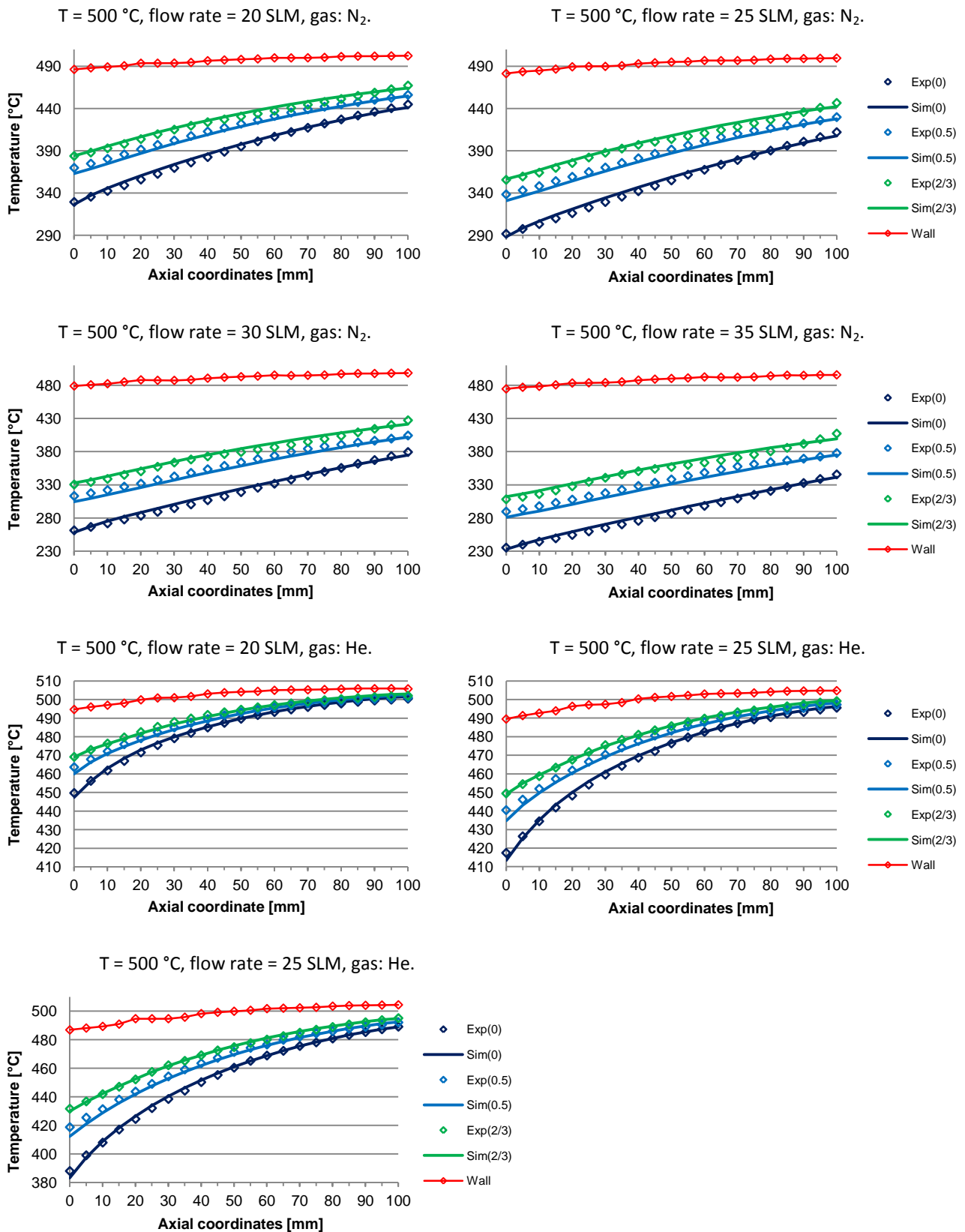
Figure 5.13 - Axial temperature profiles of FeCr alloy foam with cell diameter of 1200 μm with the optimal fit based on the experimental data.

5.2.1.2 FeCr alloy foam, d_c =580 μm: regression results
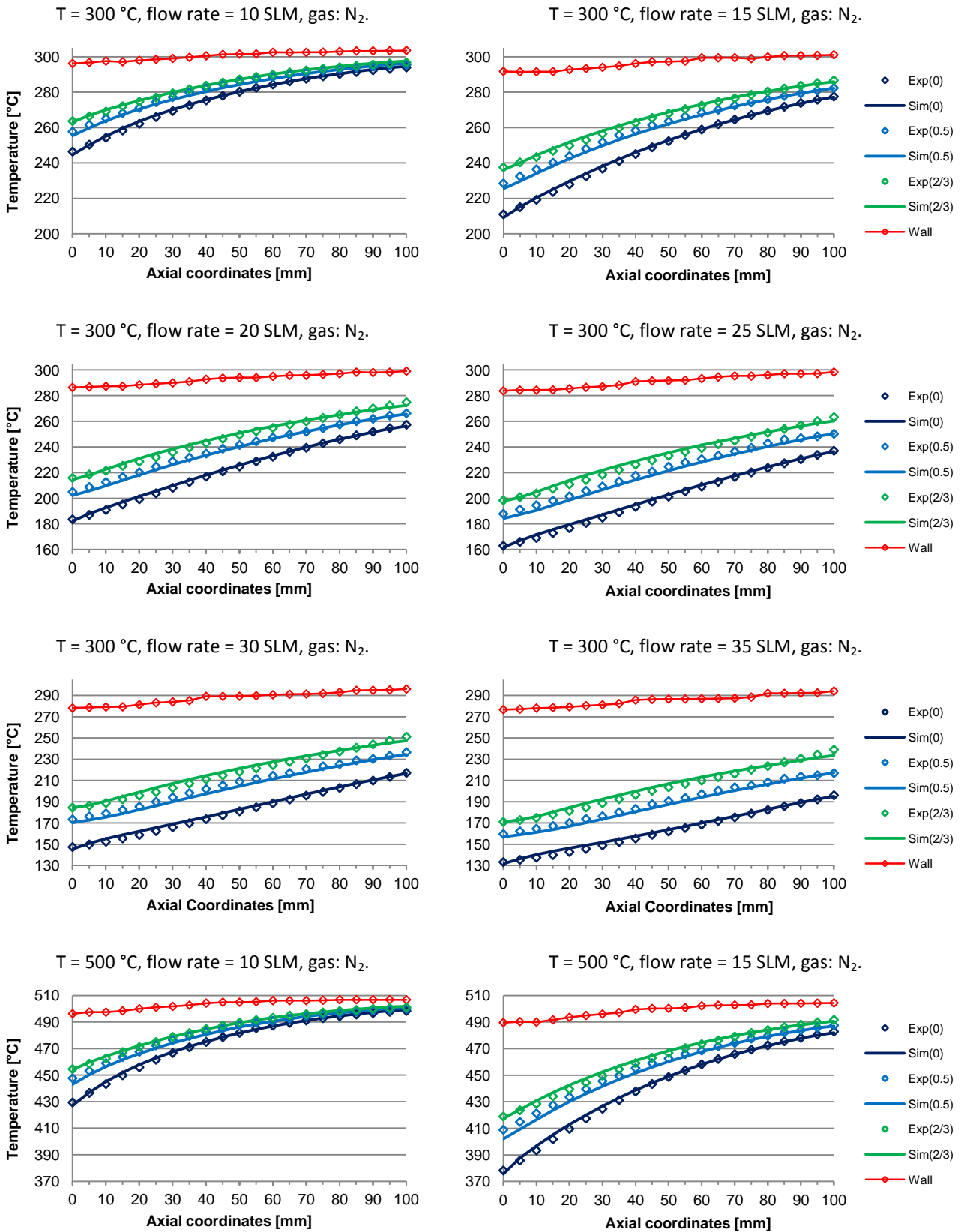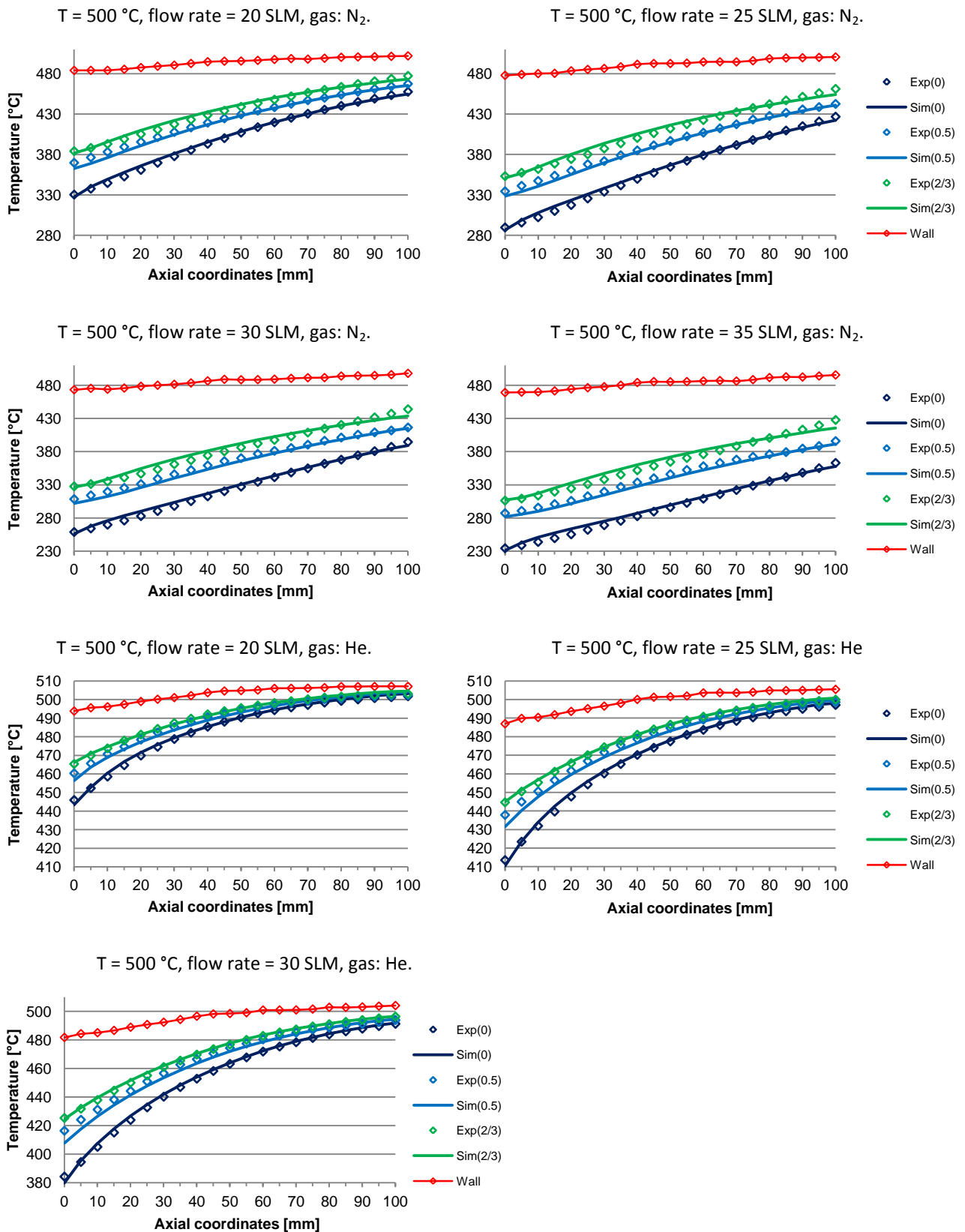
Figure 5.14 - Axial temperature profiles of FeCr alloy foam with cell diameter of 580 μm with the optimal fit based on the experimental data.

5.2.1.3 NiCr alloy foam, d_c =1200 μm: regression results

T = 300 °C, flow rate = 10 SLM, gas: N_2.

T = 300 °C, flow rate = 15 SLM, gas: N_2.

T = 300 °C, flow rate = 20 SLM, gas: N2.

T = 300 °C, flow rate = 25 SLM, gas: N2.

T = 300 °C, flow rate = 30 SLM, gas: N2.

T = 300 °C, flow rate = 35 SLM, gas: N2.

T = 500 °C, flow rate = 10 SLM, gas: N2.

T = 500 °C, flow rate = 15 SLM, gas: N2.
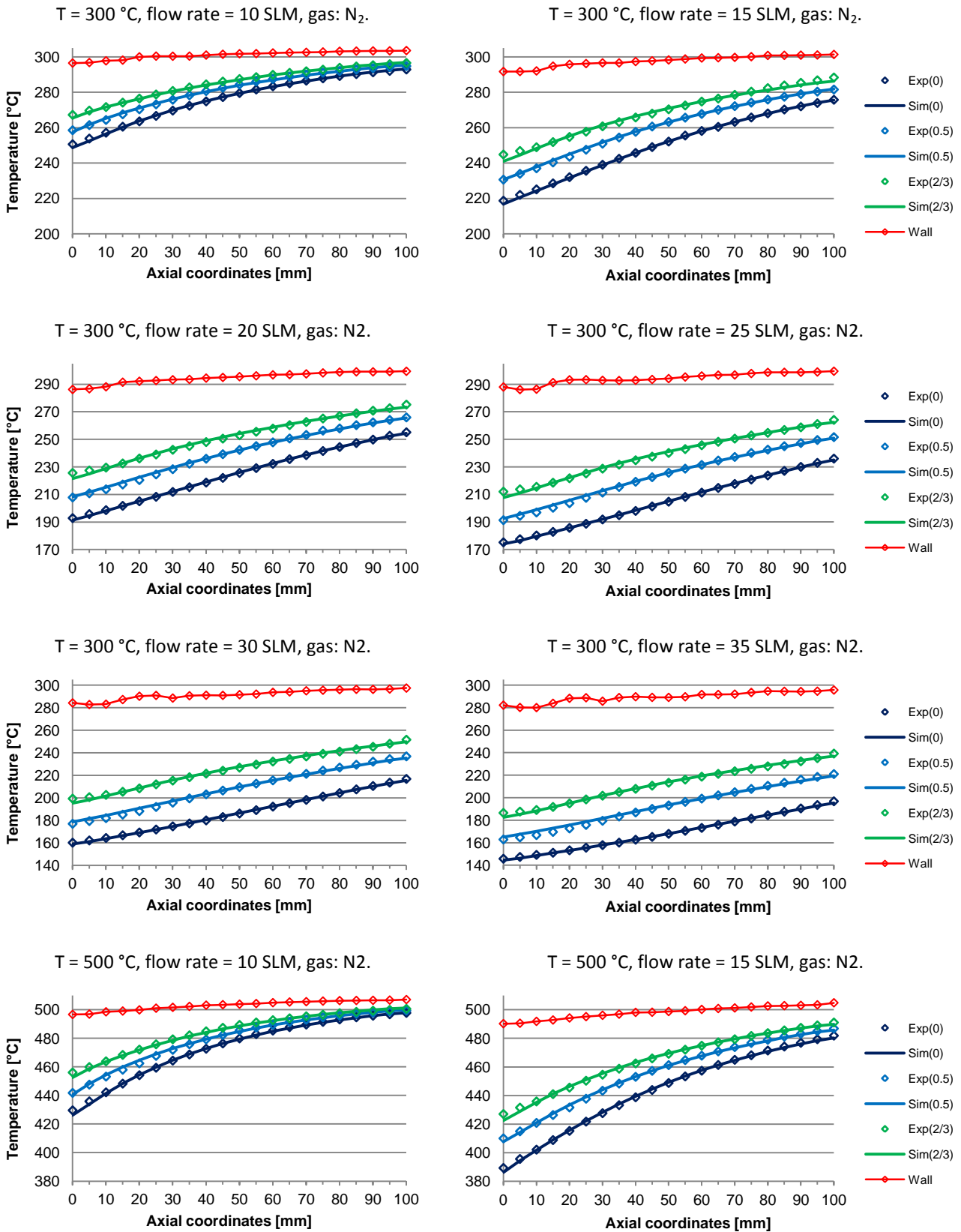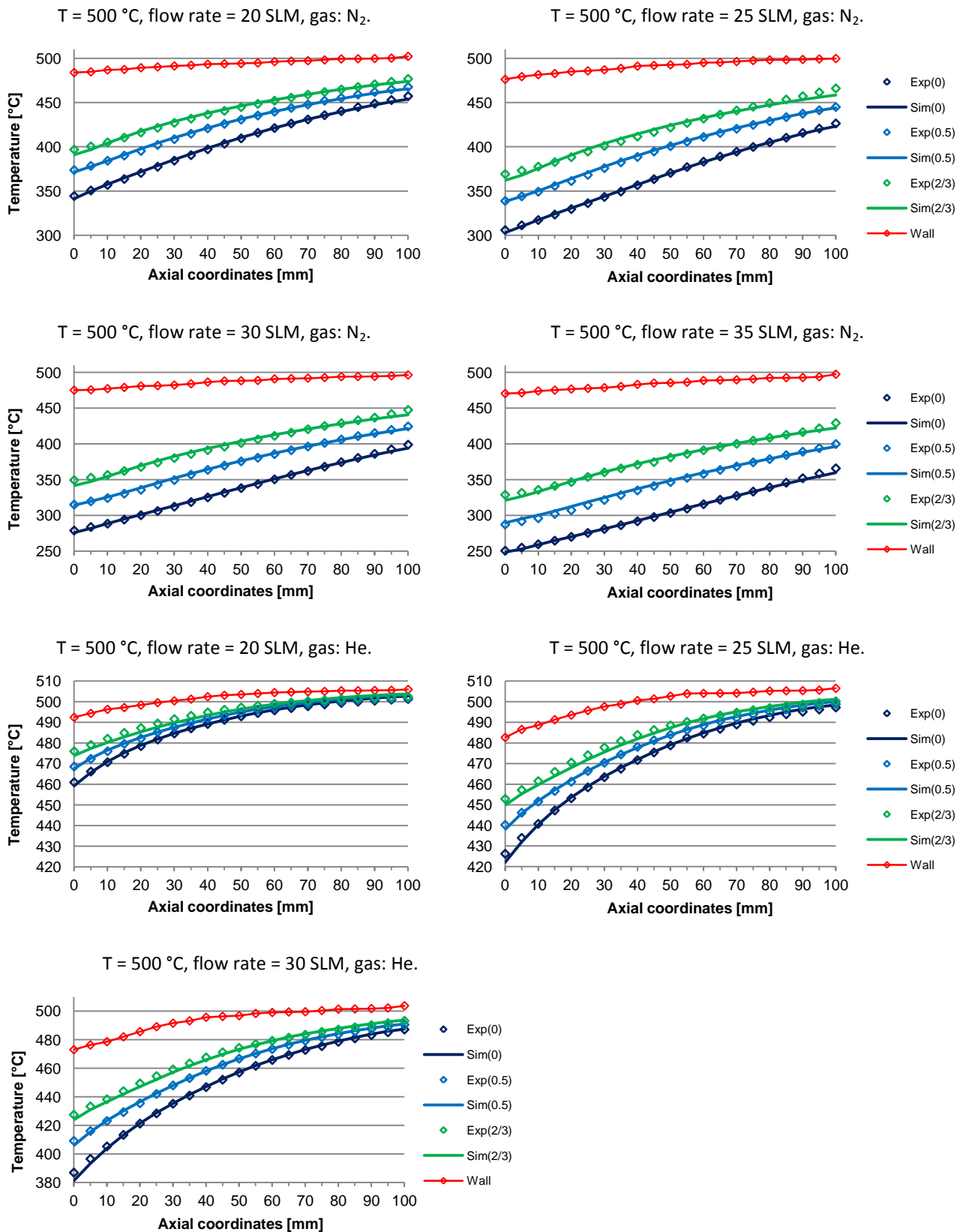
Figure 5.15 - Axial temperature profiles of NiCr alloy foam with cell diameter of 1200 μm with the optimal fit based on the experimental data.

5.2.1.4 NiCr alloy foam, d_c =580 µm: regression results

T = 300 °C, flow rate = 10 SLM, gas: N_2.

T = 300 °C, flow rate = 15 SLM, gas: N_2.

T = 300 °C, flow rate = 20 SLM, gas: N_2.

T = 300 °C, flow rate = 25 SLM, gas: N_2.

T = 300 °C, flow rate = 30 SLM, gas: N_2.

T = 300 °C, flow rate = 35 SLM, gas: N_2.

T = 500 °C, flow rate = 10 SLM, gas: N_2.

T = 500 °C, flow rate = 15 SLM, gas: N_2.
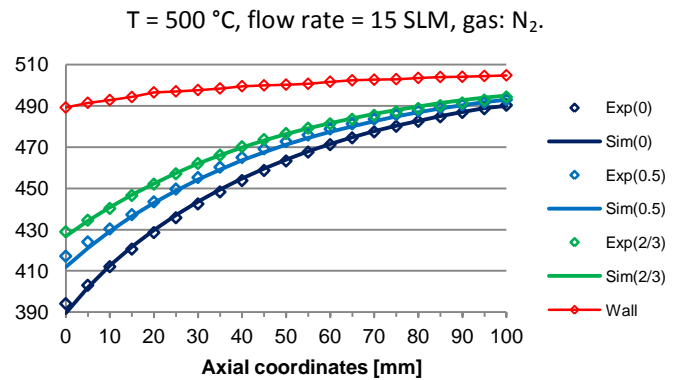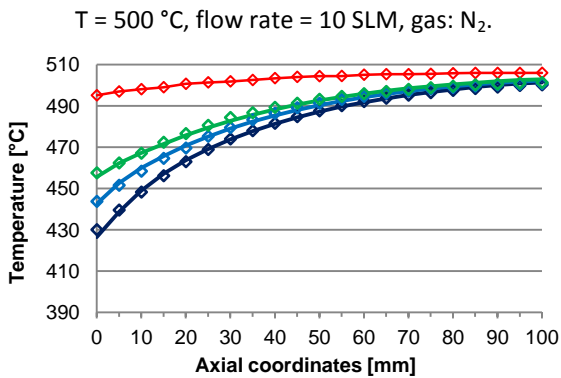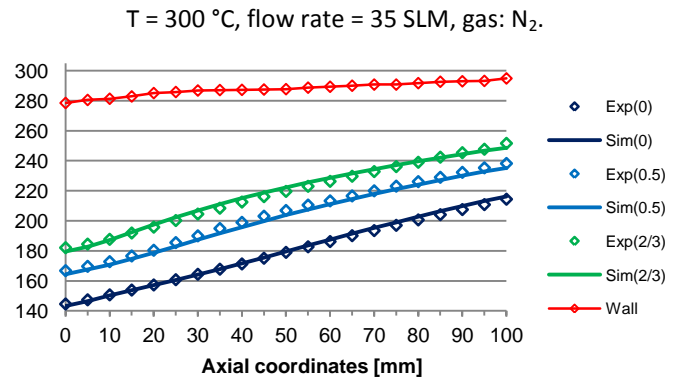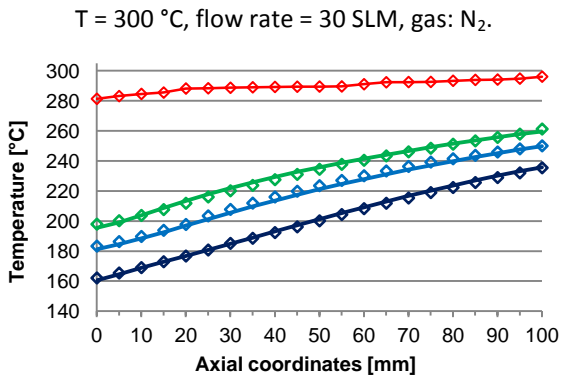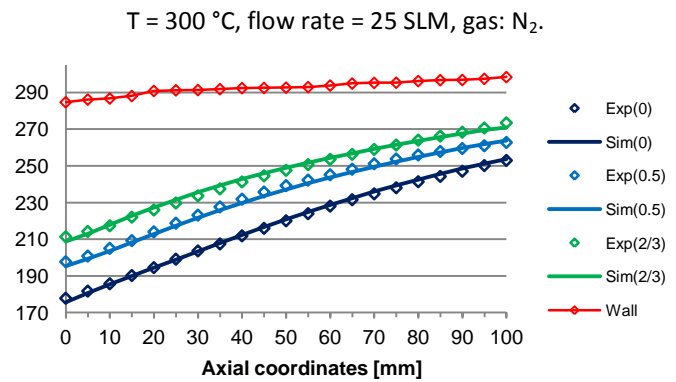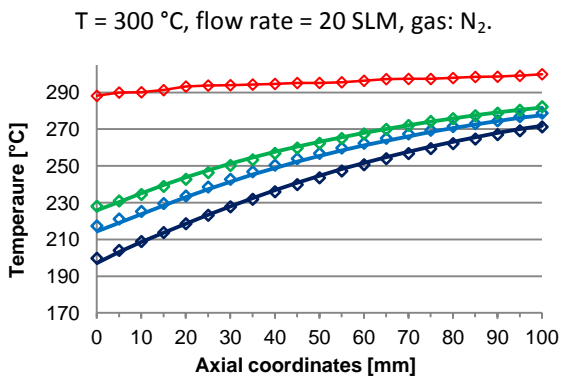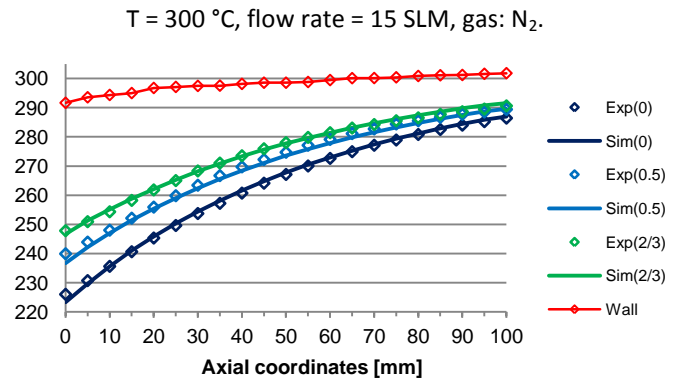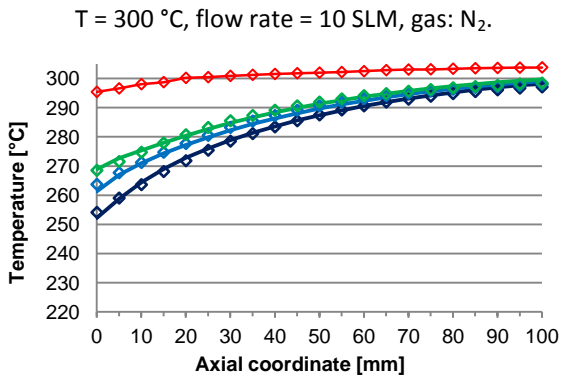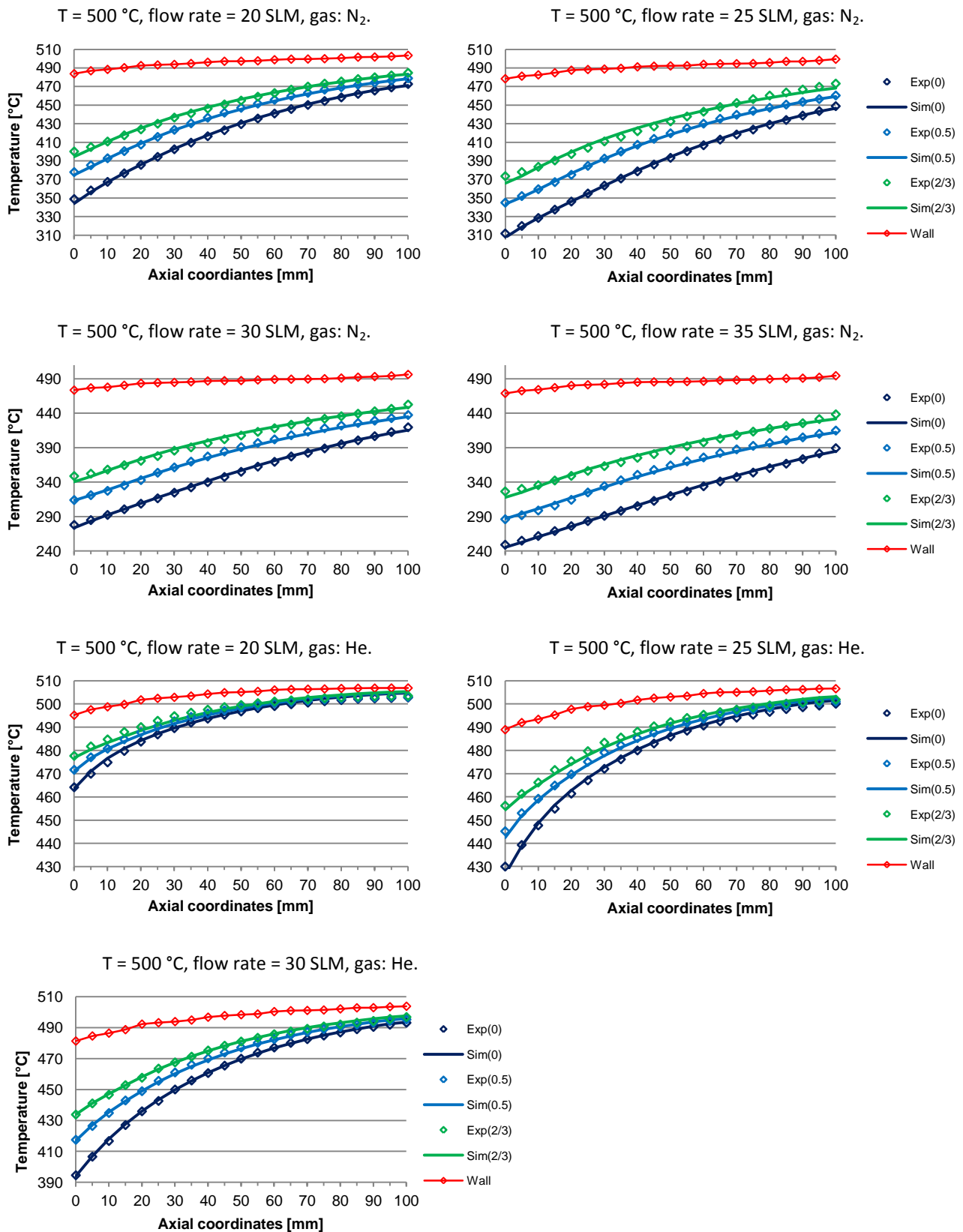
Figure 5.16 - Axial temperature profiles of NiCr alloy foam with cell diameter of 580 μm with the optimal fit based on the experimental data.

5.2.1.5 Co foam, d_c =1200 μm: regression results

T = 300 °C, flow rate = 10 SLM, gas: N_2.

T = 300 °C, flow rate = 15 SLM, gas: N_2.

T = 300 °C, flow rate = 20 SLM, gas: N_2.

T = 300 °C, flow rate = 25 SLM, gas: N_2.

T = 300 °C, flow rate = 30 SLM, gas: N_2.

T = 300 °C, flow rate = 35 SLM, gas: N_2.

T = 500 °C, flow rate = 10 SLM, gas: N_2.

T = 500 °C, flow rate = 15 SLM, gas: N_2.
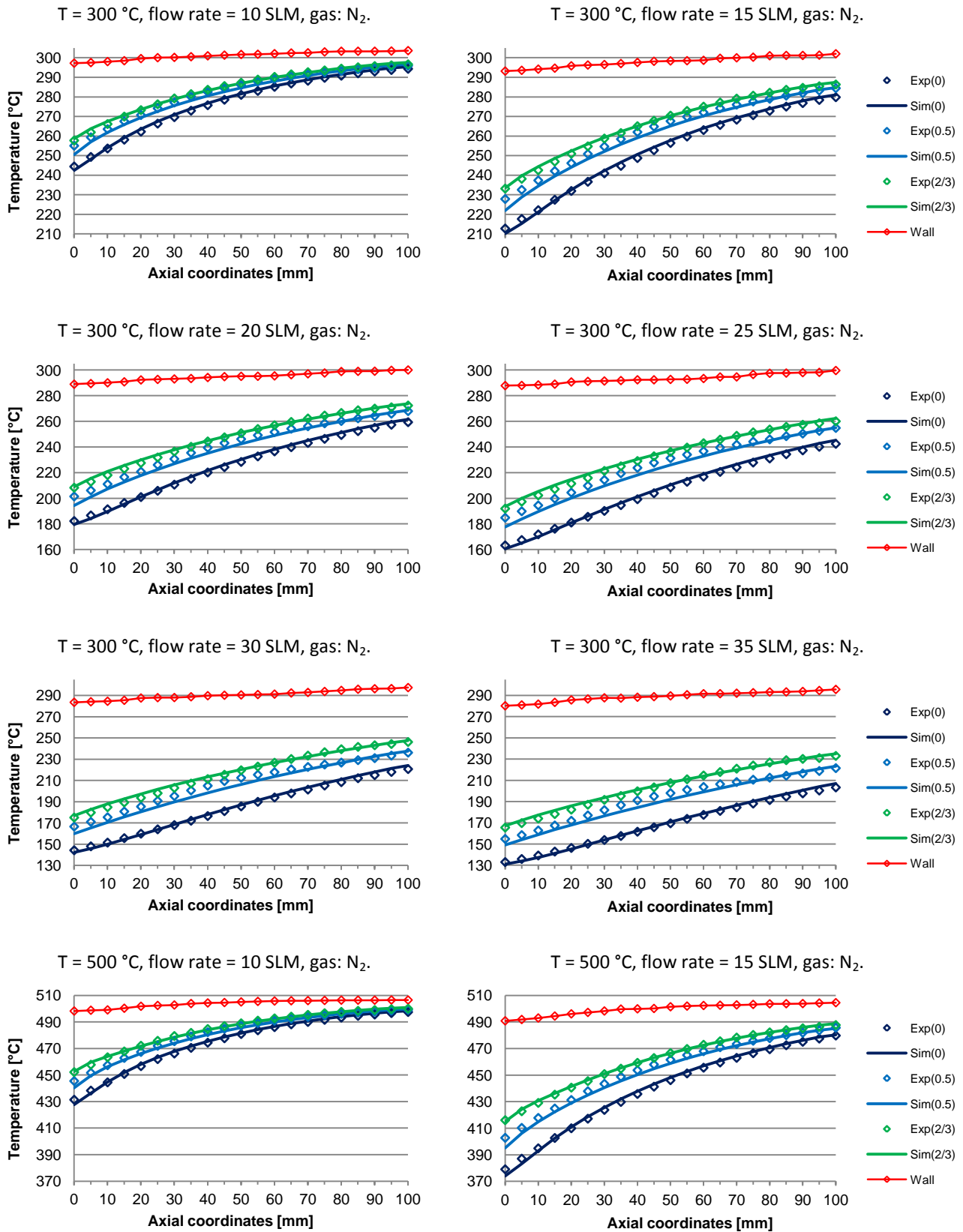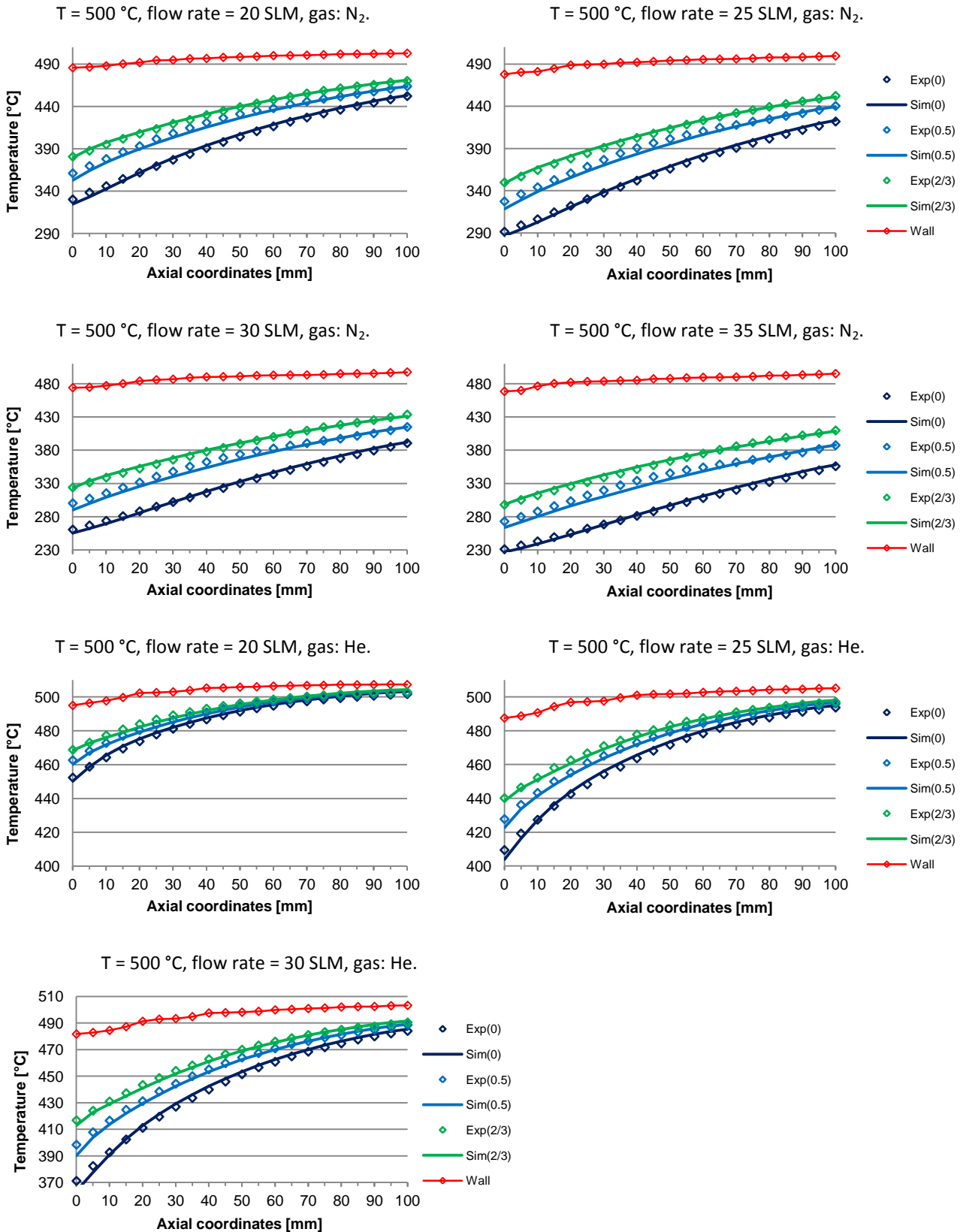
Figure 5.17 - Axial temperature profiles of Co foam with cell diameter of 1200 µm with the optimal fit based on the experimental data.

5.2.1.6   Co foam, d_c = 580 µm: regression results
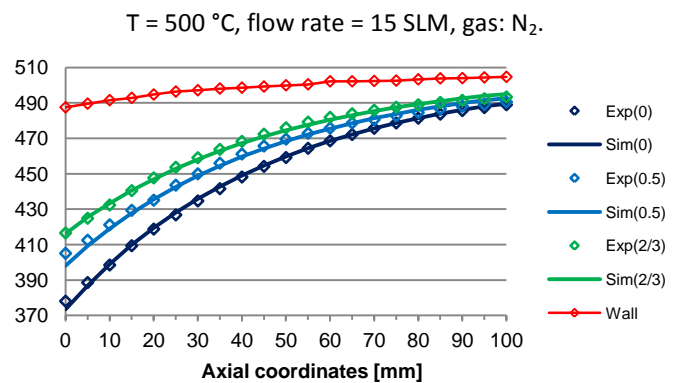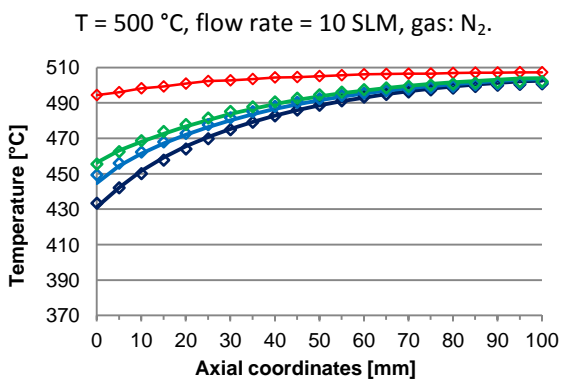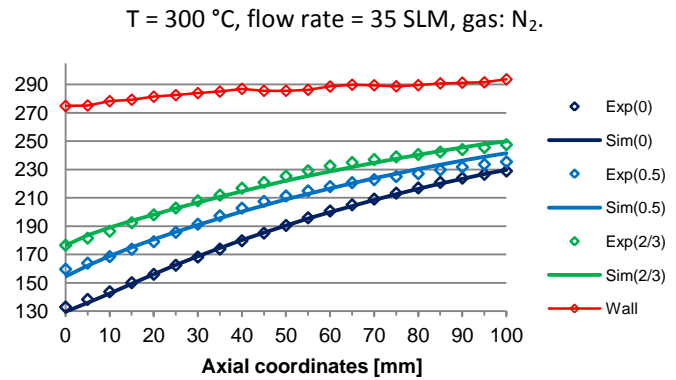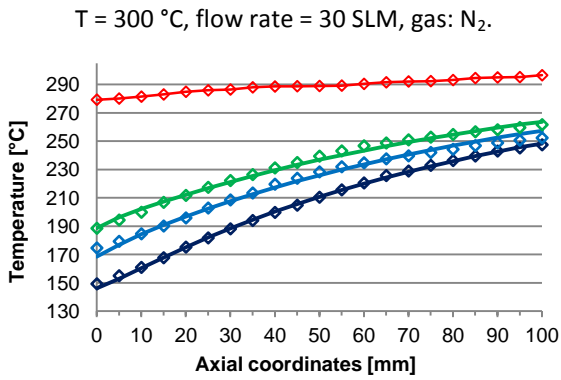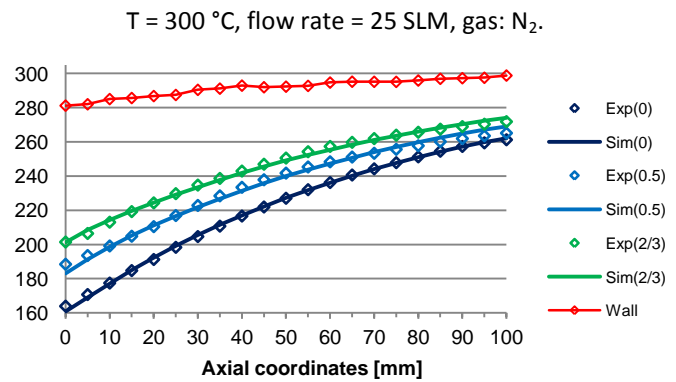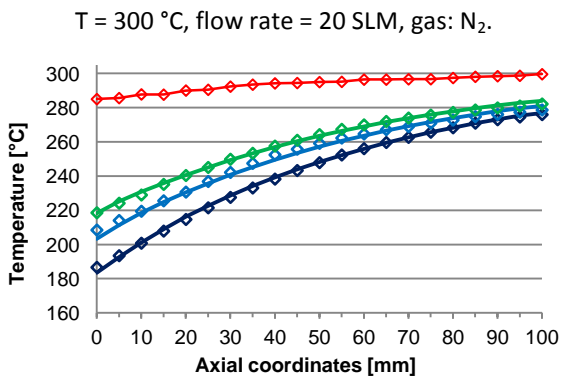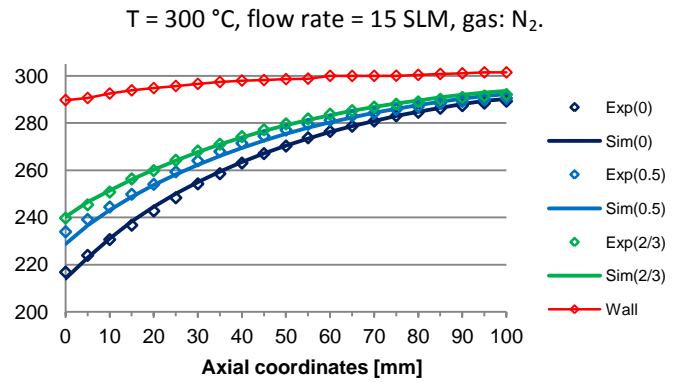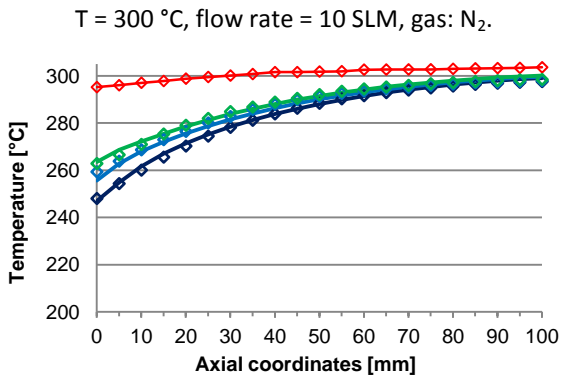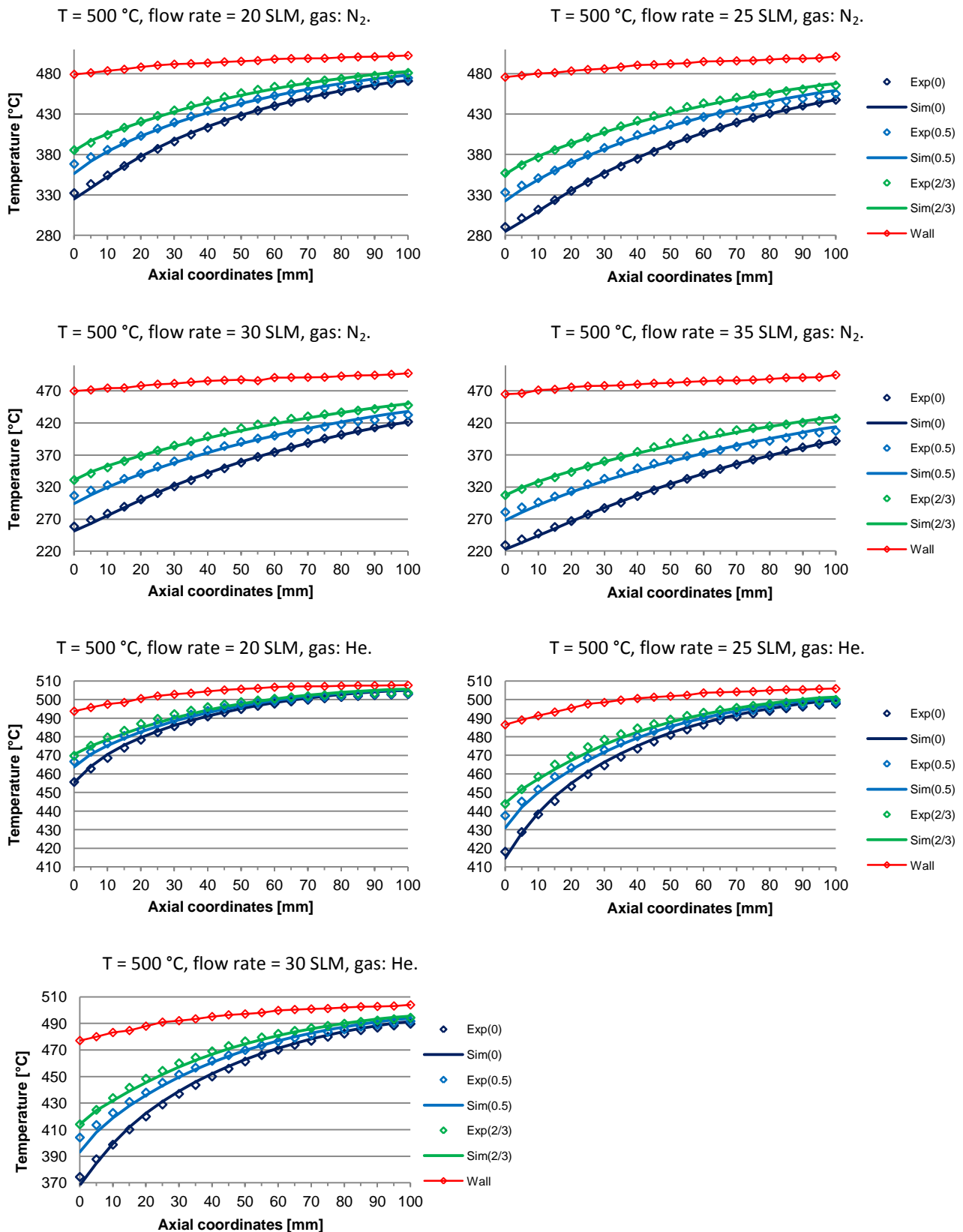
Figure 5.18 - Axial temperature profiles of Co foam with cell diameter of 580 µm with the optimal fit based on the experimental data.

5.2.1.7 Cu foam, d_c = 1200 μm: regression results

T = 300 °C, flow rate = 10 SLM, gas: N_2.

T = 300 °C, flow rate = 15 SLM, gas: N_2.

T = 300 °C, flow rate = 20 SLM, gas: N_2.

T = 300 °C, flow rate = 25 SLM, gas: N_2.

T = 300 °C, flow rate = 30 SLM, gas: N_2.

T = 300 °C, flow rate = 35 SLM, gas: N_2.

T = 500 °C, flow rate = 10 SLM, gas: N_2.

T = 500 °C, flow rate = 15 SLM, gas: N_2.
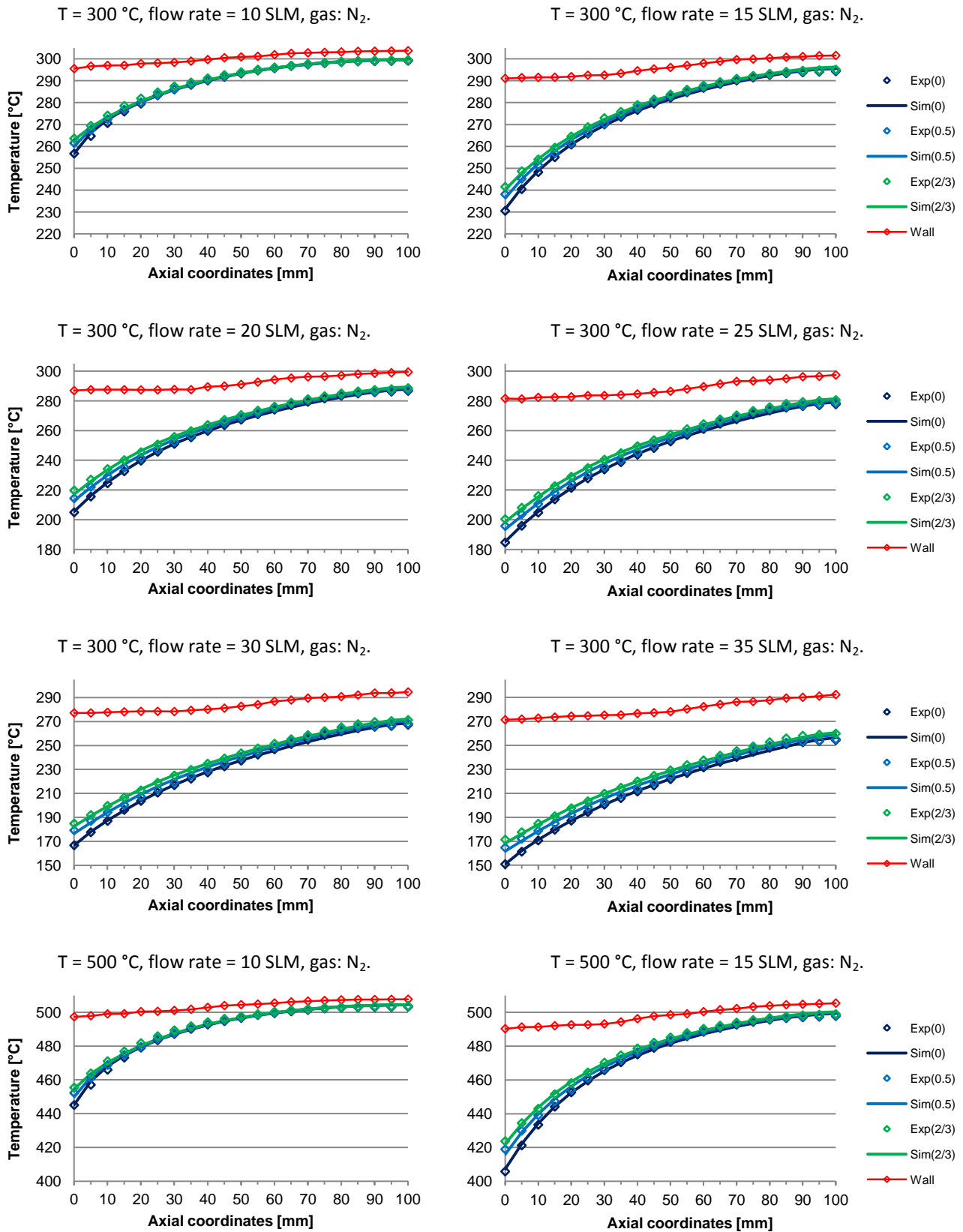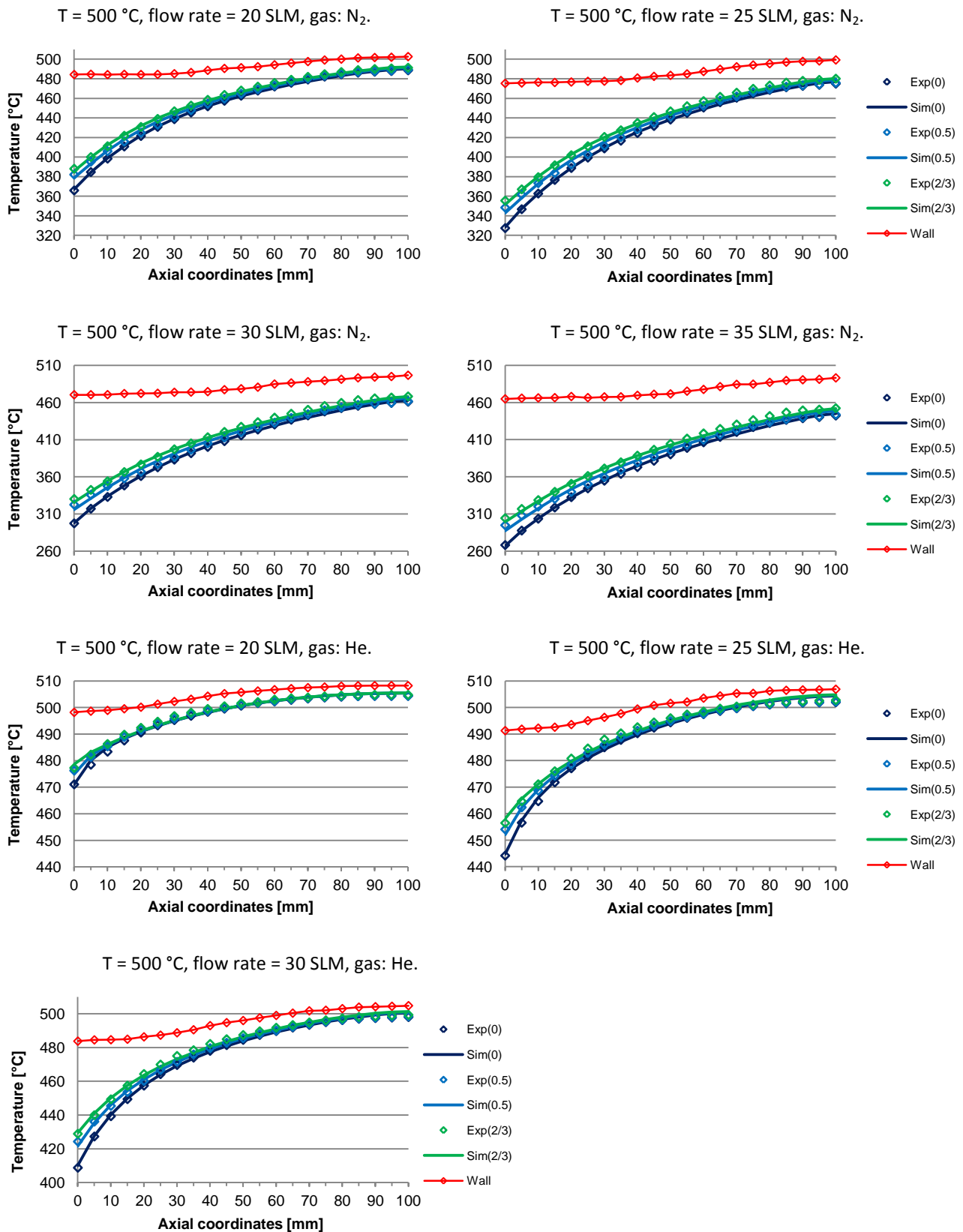
Figure 5.19 - Axial temperature profiles of Cu foam with cell diameter of 1200 μm with the optimal fit based on the experimental data.

5.2.1.8 Cu foam, d_c = 580 μm: regression results

T = 300 °C, flow rate = 10 SLM, gas: N_2.

T = 300 °C, flow rate = 15 SLM, gas: N_2.

T = 300 °C, flow rate = 20 SLM, gas: N_2.

T = 300 °C, flow rate = 25 SLM, gas: N_2.

T = 300 °C, flow rate = 30 SLM, gas: N_2.

T = 300 °C, flow rate = 35 SLM, gas: N_2.

T = 500 °C, flow rate = 10 SLM, gas: N_2.

T = 500 °C, flow rate = 15 SLM, gas: N_2.
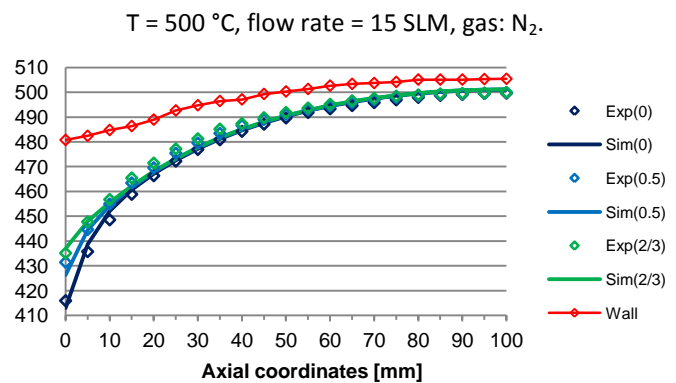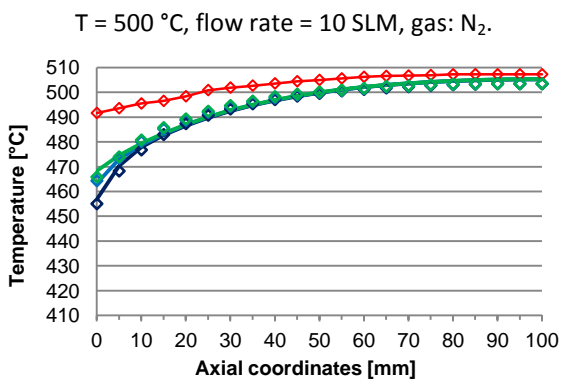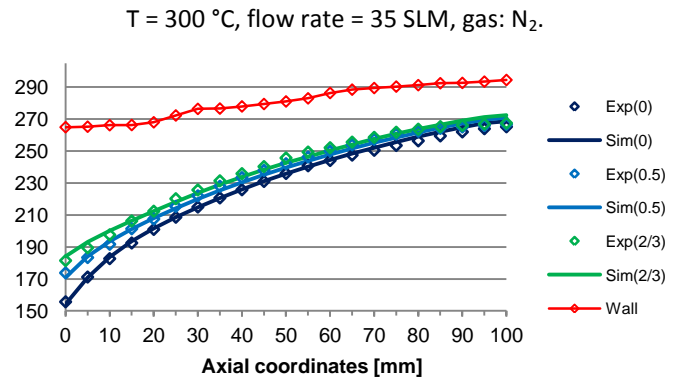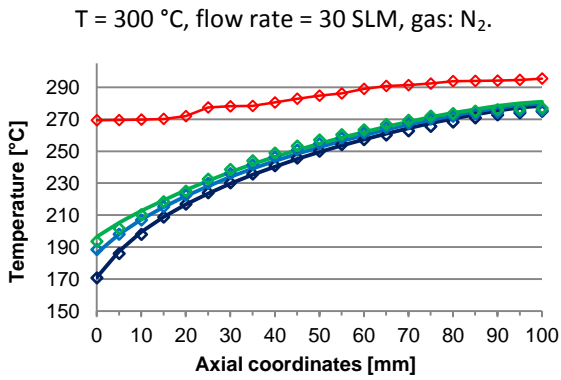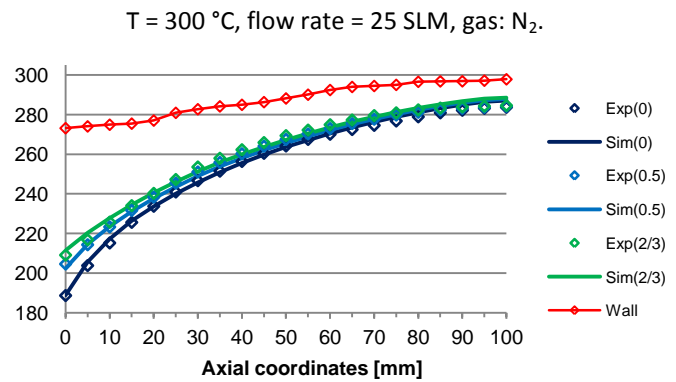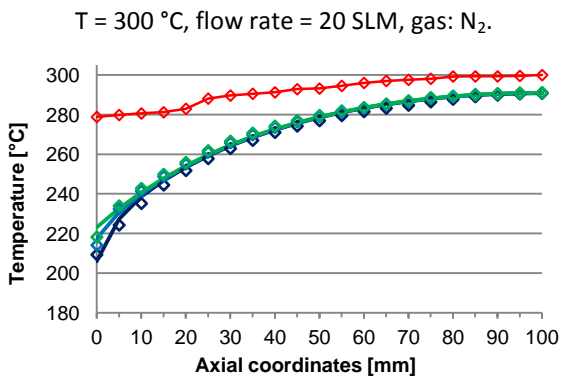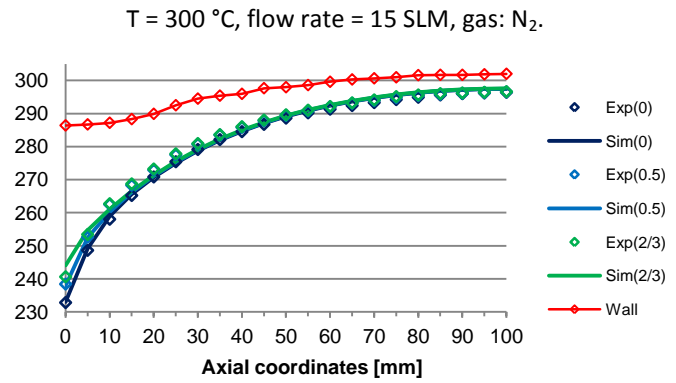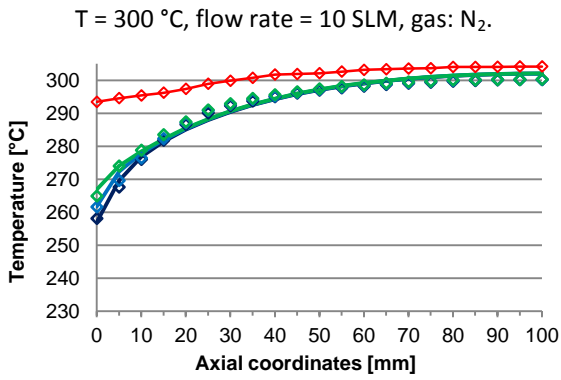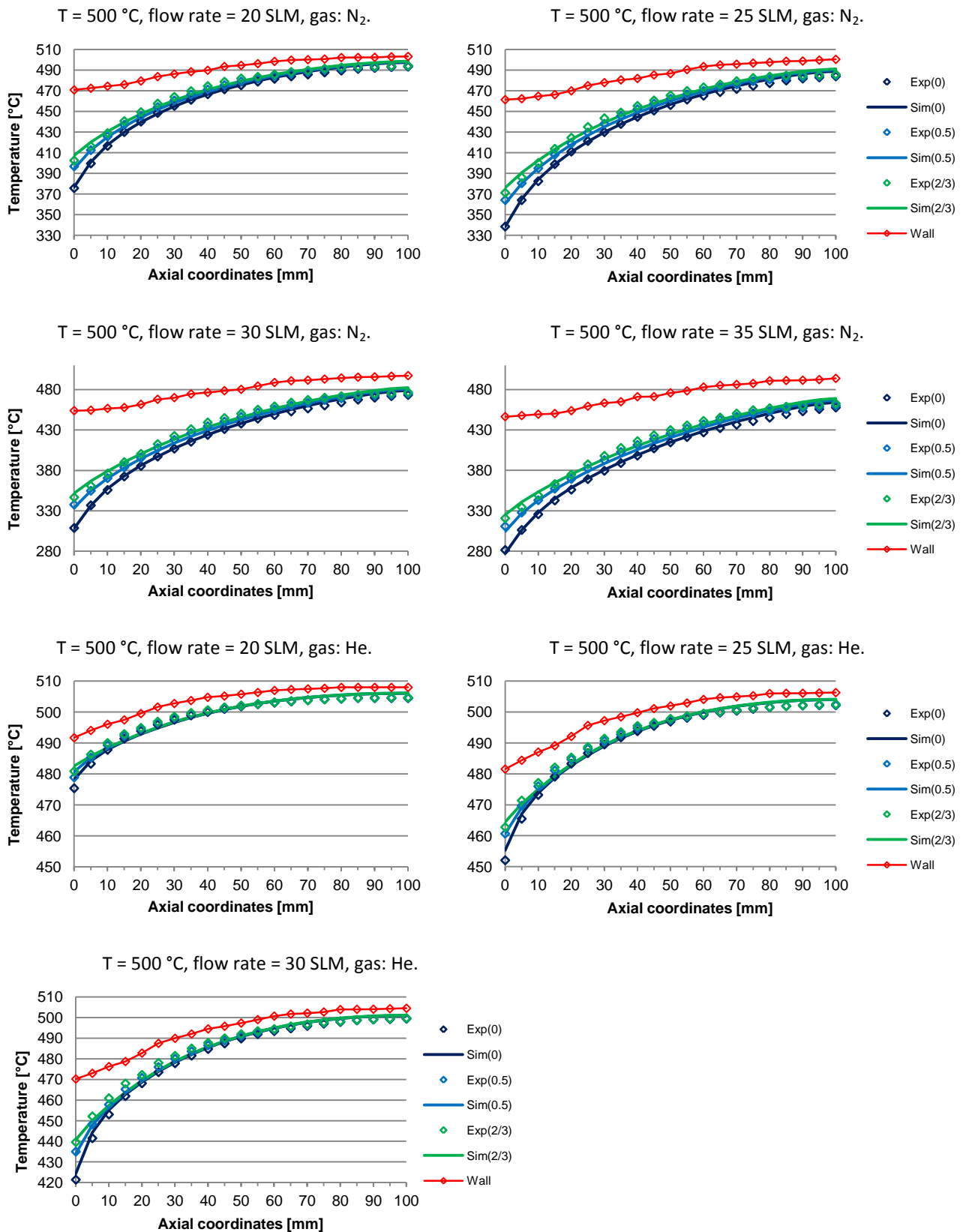
Figure 5.20 - Temperature Axial temperature profiles of Cu foam with cell diameter of 580 μm with the optimal fit based on the experimental data

5.2.2 Model estimations: effective axial conductivity

As already mentioned, the model is able to estimate three parameters, k_{ea}, the effective axial conductivity, k_{er}, the effective radial conductivity and h_w, the wall heat transfer coefficient. At the end, having all the estimation for every foam, it will be possible to define a correlation that describes the phenomena. The first parameter to be discussed is the axial effective conductivity since it is the most controversial. The assumption of constant geometrical properties of the foam samples both in the axial and in the radial direction should result also in an isotrope effective thermal conductivity (Calmidi [27]). However, some authors simplify the energy equation for foam beds by neglecting the axial coefficients [16], this could be valid only in case of common packed beds, with a non continuous matrix or with a low conductive material. This should not be the case of the metal foam with high conductivity. However, since many disks are used with imperfect thermal contact one to each other such approximation could be applied also in this case. Figure 5.21 shows the estimated effective axial conductivity of FeCr 580 μm.
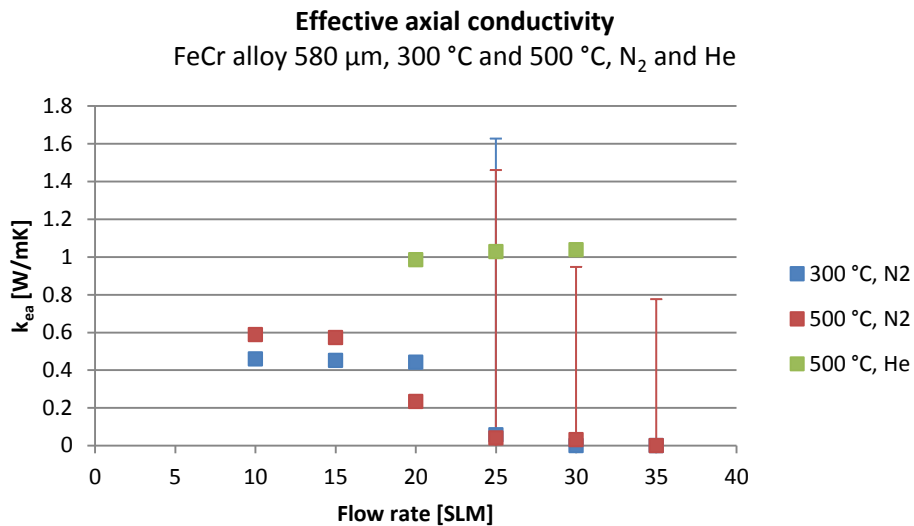
Figure 5.21 - Effective axial conductivity estimations.

Estimates of effective axial conductivity are affected by significant uncertainty and it is very difficult to find a reasonable trend. It seems that has a strong dependence on the gas type but also a dependence on flow rate, which makes it higher al low flow rate. However the uncertainties are too many (for example, the confidence interval of axial conductivity estimated at 20 SLM, at 25 SLM and at 35 SLM includes a negative value, which is physically impossible) and further simulations by adding some constraint must be done. As in this work the foam is used in disks, which obviously present a discontinuity between two adjacent disks, an interesting investigation should be to impose the effective axial conductivity to be equal or close to zero. This approach will be developed in a future work.

5.2.3 Model estimations: effective radial conductivity

Another parameters estimated by the model is the effective radial conductivity. The following graphs shows the k_{er} trend as function of gas, flow rate and temperature set point and their corresponding confidential intervals. Results without physical meaning are not plotted.

Effective radial conductivity — FeCr 1200 μm — FeCr 580 μm

Effective radial conductivity — NiCr 1200 μm — NiCr 580 μm

Effective radial conductivity — Co 1200 μm — Co 580 μm
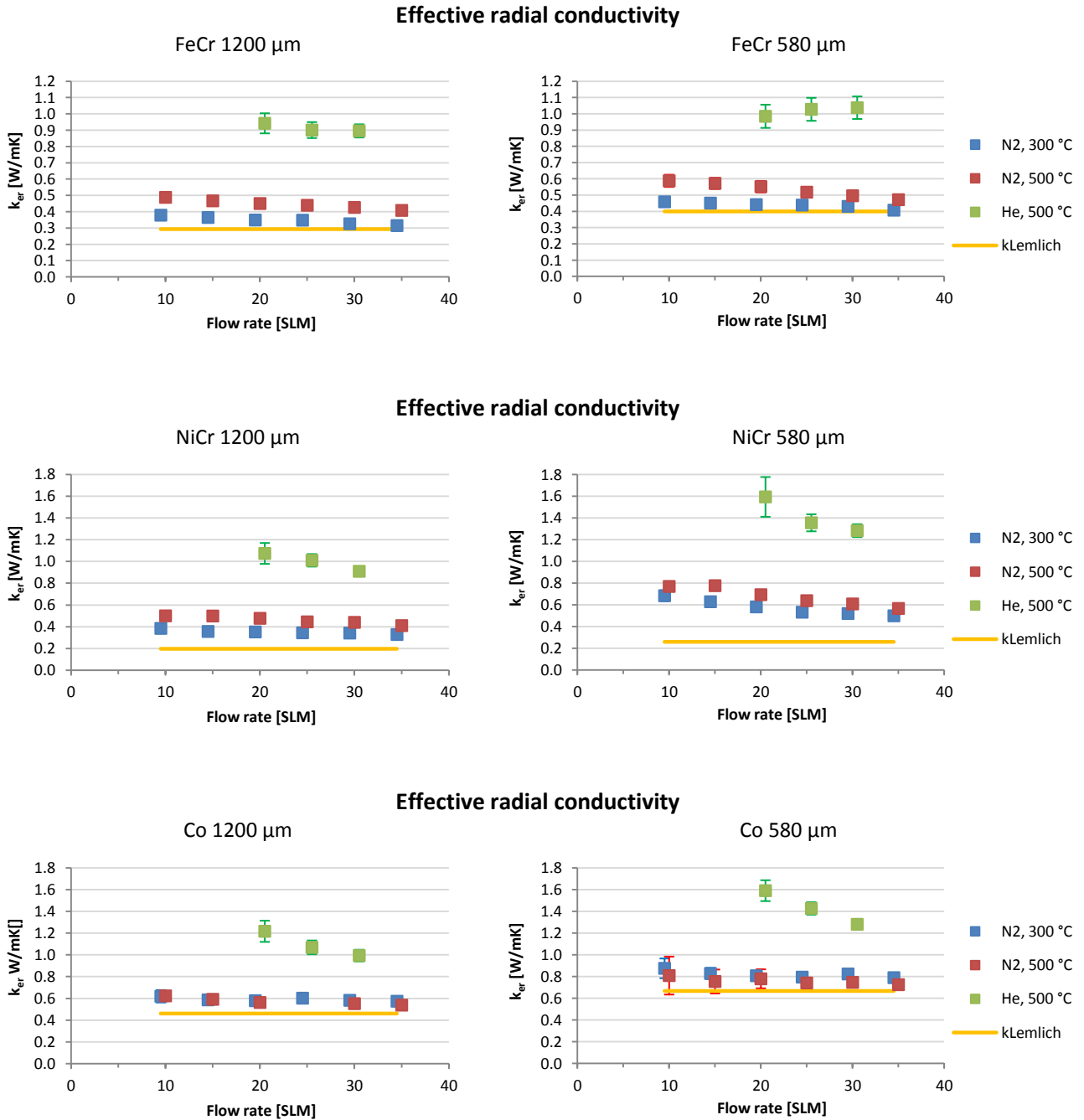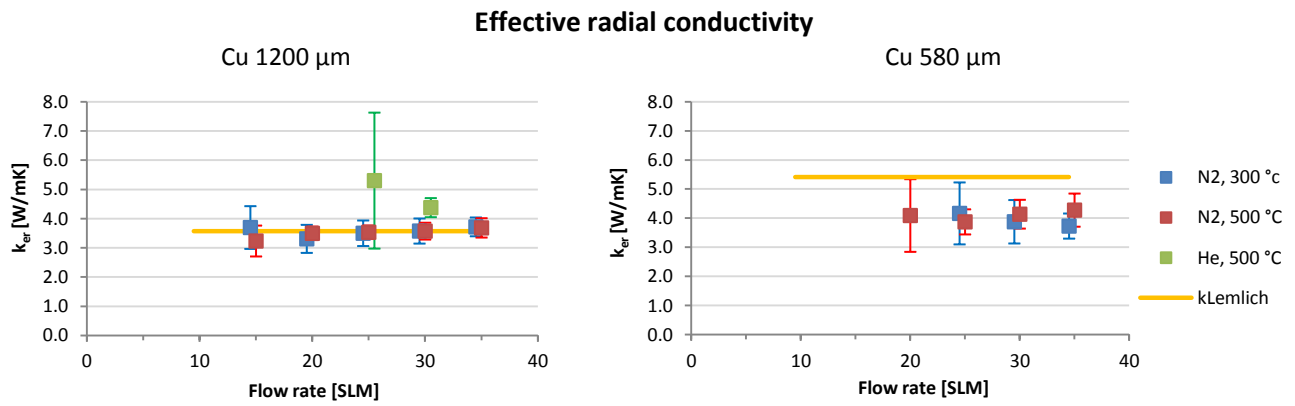
Figure 5.22 - Effective radial conductivity estimations for all kind of foam.

Estimated values of effective radial conductivity of the investigated foams are plotted in figure 5.22 as a function of the flow rate at different oven temperature and for the two different gas types. As a general trend the estimated k_{er} values scarcely depend on the flow rate suggesting that static heat transfer mechanisms, such as conduction and radiations prevail with respect to dynamic ones such as convection/dispersion. This is partly in line with results obtained in previous studies [2, 44] where a small but significant influence of convective terms were observed only for poorly conductive FeCr alloy foams.

A small enhancement of the effective radial conductivity is observed on increasing the oven temperature, i.e. the average temperature of the foam in the corresponding test, particularly for the least conductive FeCr alloy and NiCr alloy foams. It is difficult to attribute this effect to a specific contribution. Indeed all the possible contributions to effective conductivity, radiation, conduction and convention, should increase on increasing temperature at least for stainless steel like materials whose thermal conductivity typically increase with temperature. On the other hand in the case of cobalt and copper foams made of materials whose thermal conductivity decrease on increasing the temperature the effect of oven temperature disappears, possibly due to compensation between increasing contribution of radiation (and convection) and decreasing conduction.

Finally, except of highly conductive copper foam, a marked increase of effective radial conductivity is obtained in tests made using He. However this effect seems contradictory with respect to other evidences. On one hand static conduction of He (k_f = 0.15 W/mK) in foam with high void fraction (higher than 0.9) should be responsible of a 0.1 W/mK increment with respect to N_2 (k_f = 0.05 W/mK), which is much less than the increment obtained in many cases. On the other hand a major effect of the convective dynamic contribution has been previously excluded. In this respect, it is worth noting that estimates of radial effective conductivity in He tests typically decrease on increasing the flow rate, which is again strongly contradictory to a major role of the convective mechanism.

85

A possible explanation relies on scarce reliability on results of model regression on data collected in He tests. As shown in previous chapters the new experimental set up developed in this thesis work include a preheating and flow distribution section more efficient than that previously adopted in Bianchi thesis work. For the specific effect of He tests this is a drawback, since under most flow conditions the gas enter the measuring section at a temperature which is already very close to the oven one, resulting in small temperature differences all along the measured profiles, much smaller than those observed in N_2 tests. This combined with statistical correlations of the effective radial conductivity and the wall heat transfer coefficient parameters makes the estimated values affected by wide statistical uncertainties.

As a whole all the results confirm a major role of solid thermal conductivity in determining the radial effective conductivity of the different foams. This is clearly evident in figure 5.23 where the effective radial conductivity of foams made of different materials is compared, showing that the more conductive is the material (table 5.1) the higher is the effective radial conductivity.
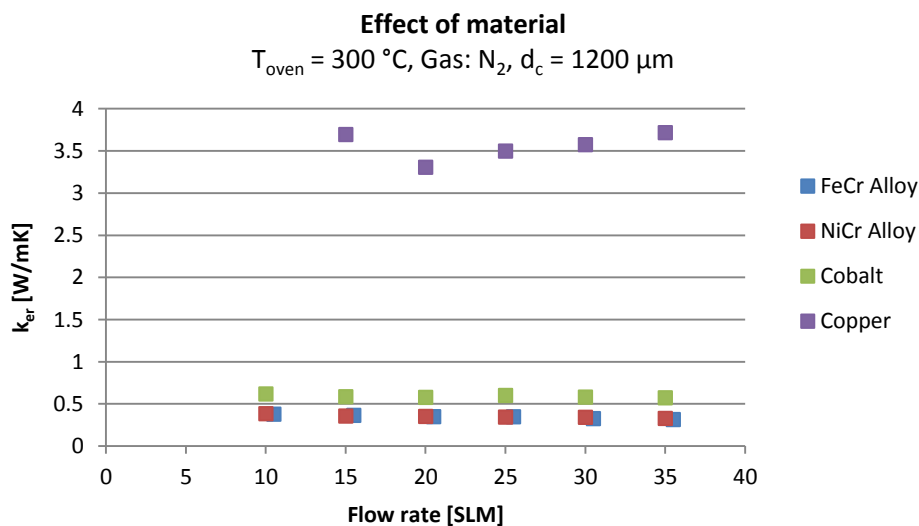
Figure 5.23 - Effect of foam material on effective radial conductivity, T = 300 °C, gas: N₂, cell diameter = 1200 μm.

This is qualitatively consistent with the Lemlich's correlation proposed in the Bianchi thesis work:

$$k_{Lemilch} = \frac{(1 - \varepsilon_T)}{3} k_s \tag{5.1}$$

Where k_s is the conductivity of the solid material and whose quantitative predictions are the yellow lines plotted in figure 5.22. An overall analysis can be obtained by plotting the prediction of the Lemlich's correlation compared with the estimated values of effective radial conductivity. Such parity plot is reported in Figure 5.24.
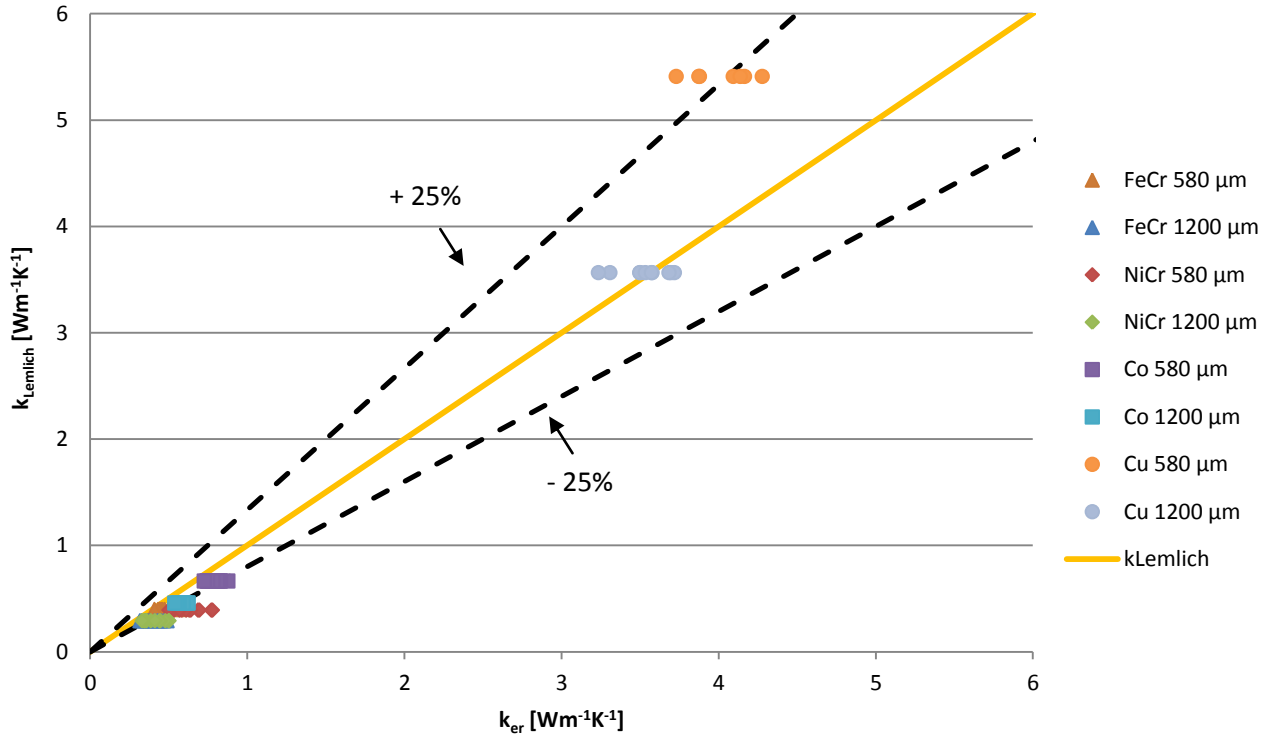
Figure 5.24 - Parity plot: estimate of k_{er} versus the predictions of Lemlich's model.

A reasonable match is observed, but significant positive deviations (effective radial conductivity higher than the valued predicted by Lemlich's correlation) are evident for low conductive foams, whereas negative deviations (effective radial conductivity lower than the valued predicted by Lemlich's correlation) occur for the most conductive copper foams. Positive deviations can be attributed to significant contributions of mechanisms other than solid conduction such as radiation, which has been proposed by Glicksman et al. [43] to be calculated by the formula:

$$k_{rad} = \frac{16\sigma T^3}{3\beta} \tag{5.2}$$

where $\sigma = 5.669 \cdot 10^{-8}$ is the Stefan–Boltzmann constant and β [m^{-1}] is the Rosseland mean extinction coefficient, and convection. On the other hand negative deviations observed for highly conductive copper foams, where contribution of mechanisms other than solid conductivity is likely negligible, can be tentatively associated with uneven distribution of solid material which makes struts thinner and intersections (nodes) thicker resulting in lower effective conductivity with respect to predictions of the Lemlich's model, which assumes uniform distribution of the material.

5.2.4 Model estimations: wall heat transfer coefficient

The last estimated parameter is the wall heat transfer, the capacity of the system to transfer heat outer.

The next graph (figure 5.25) shows this coefficient in the different operative conditions.

Wall heat transfer coefficient

FeCr 1200 μm / FeCr 580 μm / NiCr 1200 μm / NiCr 580 μm / Co 1200 μm / Co 580 μm

Legend: N2, 300 °C; N2, 500 °C; He, 500 °C

Wall heat transfer coefficient
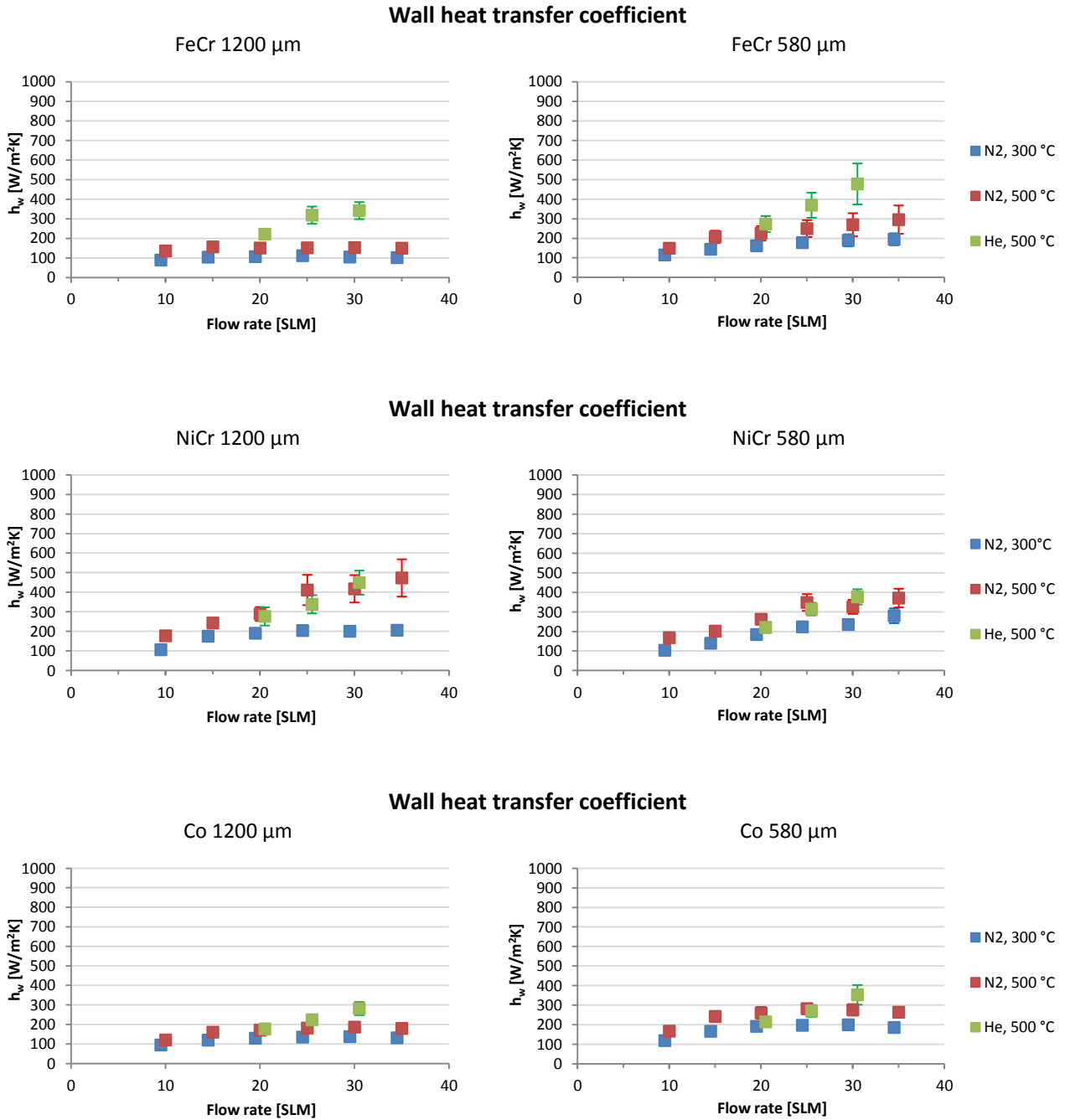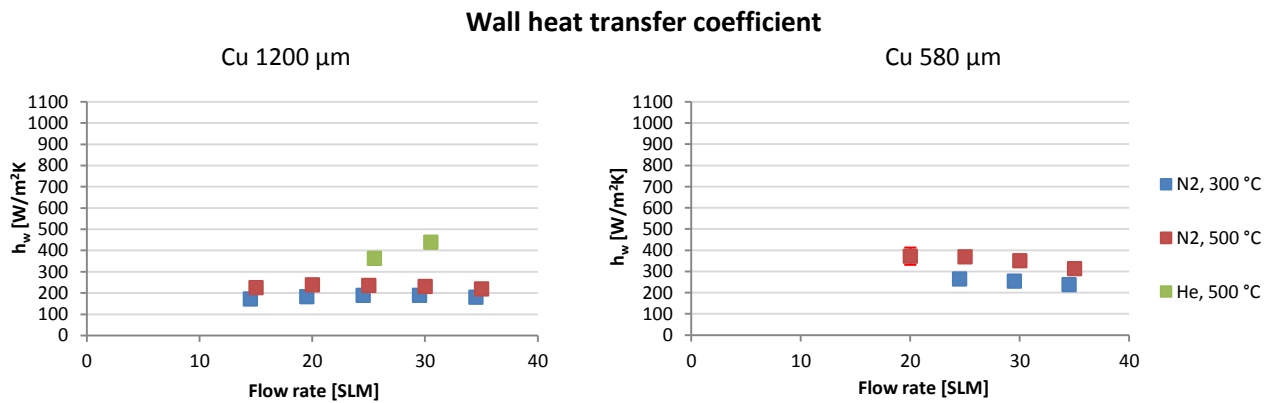
Figure 5.25 - Wall heat transfer coefficient estimations.

What it is possible to see as a general trend, is a very weak dependence of the wall heat transfer coefficient on the flow rate, which suggests again that contribution of static mechanisms are dominant respect to dynamic ones at the studied conditions.

Estimates show an influence of the foam properties: estimated values presents an inverse dependence on the cell diameter, as already found in the previous work [44] for the most of the studied cases.

Figures also exhibit a positive weak dependency on the temperature: this might be related to the beneficial effect of temperature either on the gas properties, specifically on its conductivity, and this would explain the higher value found in the some case of helium, or on the irradiative contribution. However, since the helium conductivity is five times higher than the nitrogen one, the wall heat transfer coefficient should be expected higher than the found value. It is worth noticing that this three parameters are very correlated to each other. Due to this, the model could increase the value of k_{er} finding a lower value in h_w and this occurs especially in case of helium as flowing gas because the temperature profiles are too hot at the entrance and they develop themselves in a temperature range which is not enough for the model to find good estimations.

The dependency of this value on the Reynolds number is investigated in the following graphs (figure 5.26), which compares Nusselt values calculated from hw estimates, using cell diameter as characteristic lengths, with the predictions from Nu vs Re Bianchi correlation ($Nu = 7.18 + 0.029Re^{0.8}$).
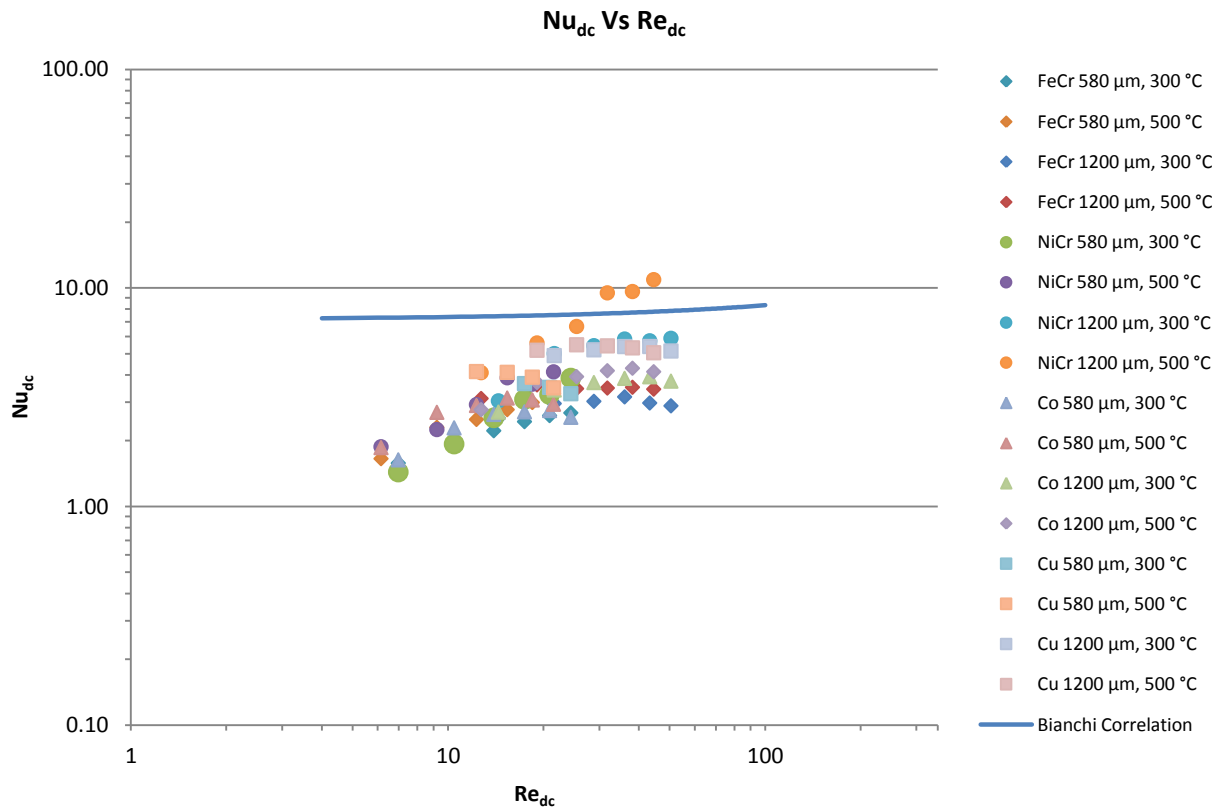
Figure 5.26 - Dimensionless wall coefficient in function of Reynolds number. The Nusselt number is based on cell diameter and fluid conductivity.

It is evident that the wall heat resistance estimated in the present work is of the same order of that found in Bianchi thesis work. However systematically lower Nusselt values have been here obtained also showing a positive dependence of Reynolds number, which was not observed in previous studies. Further work it is necessary to clarify this trend.

6. Conclusion

In this work the heat transfer properties of eight different foams have been analyzed in view of their use as catalyst supports in tubular reactors. Foams made of FeCrAl, NiCrAl, cobalt and copper, which cover the range of one order of magnitude in intrinsic solid conductivity ratio, with two different geometrical features, from 580 to 1200 μm of nominal cell diameters, were studied. First of all each foams has been geometrically and gravimetrically characterized. Results showed an high cell density with a very high total porosity, from 93% to 98%. Heat transfer tests were performed in a dedicated rig at two different oven set point temperatures, 300 °C and 500 °C, six different flow rates, from 10 to 35 SLM, by flowing two gases, nitrogen and helium, providing measurements of temperature profiles both in axial and in radial direction, for a total of 126 runs.

These data were analyzed in order to study the effect of different flow rates, gas types, types of foams, the temperature of the furnace on the temperature profiles. It was shown that the profiles are greatly affected by the solid conductivity of the foam material, which play a principal role. This, not only affects the temperature of the foam, which reaches the highest value in case of the highest conductivity, but also the relative radial position of the T-profile, which in case of high solid conductivity are closer to each other. Differences are noticed also by using different gases: on flowing helium higher temperature are reached. This is due to the conductivity of helium, which is five times higher than the nitrogen one.

By fitting the data according to a pseudo-homogeneous 2D heat transfer model it was possible to estimate the effective radial (k_{er}) and axial (k_{ea}) conductivities of the foam bed, as well as the wall heat transfer coefficients (h_W). The results were obtained running the model under the constraint that radial effective conductivity is higher than the axial radial conductivity. From the results, the effective radial conductivity is firstly greatly affected by the solid conductivity and secondly, by the gas conductivity, while it is very weakly conditioned by the flow rates and by the different oven temperature set points. This shows that the biggest contribute of this parameter is given by conduction, while forced convection and radiation have a secondary importance. Concerning the wall heat transfer coefficient, a very slightly dependence of the flow rate has been found. This parameter has a positive influence of the oven temperature, because an increase of temperature enhances the conductivities of gas and material. Since foam with high cell density has more contact surface, coefficients estimated in foams with 580 μm cell diameter are higher than the corresponding foam with 1200 μm cell diameter. An evident influence of solid conductivity was not found. For the effective axial conductivity it was more difficult to find a reasonable trend. It has to be considered that this has been only a preliminary analysis of the results, and further analysis and regression will be done varying some constrains, in order to find the best configuration.

Once estimated these parameters, the next step will be to try to find one or more correlation to describe satisfactorily the heat transfer in open celled foam. In parallel, different foams will be analyzed, in order to broaden the field of studied foams and find a cheaper way to manufacture the foam, for example, a close celled foam converted in open celled foam by cutting it in slice and randomly rearranged will be testes sooner. Moreover, it could be interesting to investigate the effect of very high flow rate and different pipe diameters, which are more interesting from an industrial point of view.

References

[1] L.P. Lefebvre, J. Banhrat, D. Dunand, *Porous metals and metallic foams: current status and recent developments*, Adv. Eng. Mater., **10 (9)**, 775-787, 2008

[2] E. Bianchi, T. Heidig, C.G. Visconti, G. Groppi, H. Freund, E. Tronconi, *An appraisal of the transfer properties of metallic open-cell foams for strongly exo-/endo-thermic catalytic processes in tubular reactors, Chemical Engineering Journal*, **198-199**, 512-529, 2012

[3] M.V. Twigg, J.T. Richardson, *Fundamentals and Applications of Structured Ceramic Foam Catalysts*, Ind. Eng. Chem. Res, **46**, 4166-4177, 2007

[4] V.C. Srivastava, K.L. Sahoo, *Processing, stabilization and applications of metallic foams. Art of science*, Material Science-Poland, **25 (3)**, 733-753, 2007

[5] S.K. Hyun, K. Murakami, H. Nakajima, *Anisotropic mechanical properties of porous copper fabricated by unidirectional solidification*, Mater. Sci. Eng. A, **299**, 241-248, 2001

[6] L.J. Gibson, M.F. Ashby, *Cellular Solids*, 2nd Edn., Cambridge University Press, UK, 1997

[7] G. Groppi, E. Tronconi, *Nano-and Micro-structured Catalytic Materials for Process Intensification*, NANOTEC 2008, 2008

[8] *http://www.reade.com/Products/Foam/foam-metal.html*

[9] J.T. Richardson, Y. Peng, D. Remue, *Properties of ceramic foam catalyst supports: pressure drop*, Applied Catalysis A: General, **204**, 19-32, 2000

[10] F.C. Buciuman, B. Kraushaar-Czarnetzki, *Ceramic Foam Monoliths as Catalyst Carriers. 1. Adjustment and Description of the Morphology*, Ind. Eng. Chem. Res., **42**, 1863-1869, 2003

[11] *Intensificazione di Processi Catalitici per Energia Pulita, Trasporti a Basse Emissioni e Chimica Sostenibile usando Schiume a Celle Aperte quali Nuovi Materiali Strutturati Avanzati (IFOAMS)*, Progetto di Ricerca, 2010

[12] J. Banhart, *Manufacture, characterization and application of cellular metals and metal foams,* Progress In Materials Science, **46(6)**, 559-U3, 2001

[13] J. Banhart, *Aluminum foams for lighter vehicles,* International Journal Of Vehicle Design, **37**, 114-125, 2005

[14] J. Banhart, *Aluminum foams: On the road to real applications,* MRS Bulletin, **28(4)**, 290-295, 2003

[15] J. Banhart, D. Weaire, *On the road again: Metal foams find favor,* Phys. Today, **55(7)**, 37-42, 2002

[16] Y. Peng, J.T. Richardson, *Properties of ceramic foam catalyst supports: one-dimensional and two-dimensional heat transfer correlations*, Applied Catalysis A: General, **266**, 235-244, 2004

[17] O. Smorygo, V. Mikutski, A. Marukovich, Y. Vialiuha, A. Ilyushchanka, N. Mezentseva, G. Alikina, Z. Vostrikov, Y. Fedorova, V. Pelipenko, R. Bunina, V. Sadykov, *Structured catalyst supports and catalysts for the methane indirect internal steam reforming in the intermediate temperature SOFC*, International journal of Hydrogen Energy, **34**, 9505-9514, 2009

[18] Haydn N.G. Wadley, *Cellular metals manufacturing*, Advanced Engineering Materials, **4(10)**, 1-8, 2002

[19] J. Grosse, B. Dietrich, G. Incera Garrido, P. Habisreuther, N. Zarzalis, H. Martin, M. Kind, B. Kraushaar-Czarnetzki, *Morphological characterization of ceramic sponges for applications in chemical engineering*, Ind. Eng. Chem. Res., **48 (23)**, 10395-10401, 2009

[20] T.J. Lu, H.A. Stone, M.F. Ashby, *Heat transfer in open-cell metal foams*, Acta Materalia, **46**, 3619-3635, 1998

[21] J.A.F. Plateau, *Statique expérimentale et théorique des liquides soumis aux seules forces moléculaires*. **Vol. 2.** Gauthier-Villars, 1873

[22] Lord Kelvin (Sir William Thomson), *On the division of space with minimum partitional area*, Philosophical Magazine, **24 (151)**, 503, 1887

[23] R. Phelan, D. Weaire, K. Brakke, *Computation of equilibrium foam structures using the surface evolver.* Experimental Mathematics, **4**, 181-192, 1995

[24] L. Giani, G. Groppi, E. Tronconi, *Mass-transfer characterization of metallic foams as supports for structured catalysts*, Ind. Eng. Chem. Res, **44**, 4993-5002, 2005

[25] M. Lacroix, P. Nguyen, D. Schweich, C.P. Huu, S. Savin-Poncet, D. Edouard, *Pressure drop measurements and modeling on SiC foams*, Chemical Engineering Science, **(62)**, 3259-3267, 2007

[26] V.V. Calmidi, R.L. Mahajan, *Forced convection in high porosity metal foams*, Journal of Heat Transfer, **122(3)**, 557-565, 2000

[27] A. Inayat, H. Freund, T. Zeiser, W. Schwieger, *Determining the specific surface area of ceramic foams: The tetrakaidecahedra model revisited*, Chemical Engineering Science, **66**, 1179-1188, 2011

[28] C.Y. Zhao, T.J. Lu, H.P. Hodson, *Thermal radiation in ultralight metal foams with open cells,* International Journal of Heat and Mass Transfer, **47**, 2927-2939, 2004

[29] K. Schwartzwalder, A.V. Somers, *Method of making porous ceramic articles*, U.S. Patent 3090094, 1963

[30] G. Incera Garrido, F.C. Patcas, S. Lang, B. Kraushaar-Czarnetzki*, Mass transfer and pressure drop in ceramic foams: A description for different pore sizes and porosities*, Chemical Engineering Science, **63**, 5202 – 5217, 2008

[31] Sartorius YDK 01, YDK 01-0D, YDK 01LP, *Density Determination Kit User's Manual*

[32] *http://www.alantum.com/en/special/applications-services/batteryfuel-cell.html*

[33] C. Yuan , J. Li , L. Hou , X. Zhang , L. Shen , X.W. Lou, *Ultrathin Mesoporous NiCo$_2$O$_4$ Nanosheets Supported on Ni Foam as Advanced Electrodes for Supercapacitors*, Advanced Functional Materials, **22**, 4592–4597, 2012

[34] G.W. Yang, C.L. Xu, H.L Li, *Electrodeposited nickel hydroxide on nickel foam with ultrahigh capacitance*, The Royal Society of Chemistry, 6537-6539, 2008

[35] G.F. Yang, J.S. Song, H.Y. Kim, S.K. Joo, *Metal Foam as Positive Electrode Current Collector for LiFePO$_4$-Based Li-Ion Battery*, Japanese Journal of Applied Physics, **52**, 10-13, 2013

[36] F. Salvatori*, Study of heat transfer properties of structured supports for highly exothermic catalytic reactions,* Master Thesis, 2013

[37] L. Giani, G. Groppi, E. Tronconi, *Heat transfer characterization of metallic foams,* Ind. Eng. Chem. Res, **44 (24)**, 9078-9085, 2005

[38] B.A. Finlayson, *Nonlinear analysis in chemical engineering,* McGraw-Hill, London and New York, 1980

[39] Athena Visual Studio, Software for modeling, estimation and optimization, Version 12.1, www.AthenaVisual.com.

[40] C.Y. Zhao, T.J. Lu, H.P. Hodson, J.D. Jackson, *The temperature dependency of effective thermal conductivity of open-celled steel alloy foams*, Mater. Sci. Eng. A, **367 (1–2)**, 123-131, 2004.

[41] Kanthal. Available from: heatingelements.hitempproducts.com/

[42] Efunda. *Co and Cu element*. Available from: www.efunda.com/materials/elements

[43] L. Glicksman, M. Schuetz, M. Sinofsky, *Radiation heat transfer in foam insulation*, Int. J. Heat Mass Transfer, **30 (1)**, 187–197, 1987.

[44] E. Bianchi, T. Heidig, C.G. Visconti, G. Groppi, H. Freund, E. Tronconi, *Heat transfer properties of metal foam supports for structured catalysts: wall heat transfer coefficient,* Catalysis Today, **216**, 121-134, 2013.

Appendix A: Nomenclature

List of symbols

a	Fitting parameter
b	Fitting parameter
c_P [kJ kg^{-1} K^{-1}]	Specific heat capacity
d_c [m]	Average cell diameter
d_p [m]	Average pore diameter
D_{FOAM} [m]	External diameter of disk foam sample
h_{FOAM} [m]	Height of foam sample
h_w [W m^{-1} K^{-1}]	Wall heat transfer coefficient
k [W m^{-1} K^{-1}]	Material thermal conductivity
k_{ea} [W m^{-1} K^{-1}]	Effective axial thermal conductivity
k_{er} [W m^{-1} K^{-1}]	Effective radial thermal conductivity
k_{rad} [W m^{-1} K^{-1}]	Radiative thermal conductivity
k_f [W m^{-1} K^{-1}]	Fluid thermal conductivity
$\dot{n}$ [mol s^{-1}]	Molar flow rate
Nu_w^f	Convective Nusselt number at wall
Nu_w^s	Static Nusselt number at wall
Nu_S	Nusselt referred to specific surface
P [bar]	Pressure
R [J mol^{-1} K^{-1}]	Gas constant
S_V [m^{-1}]	Specific surface area
T [K]	Temperature
T_1 [°C]	Standard temperature (25 °C)
T_2 [°C]	Gas temperature
$T_{x,r}$ [K]	Temperature at axial coordinate x and radial coordinate r
$T_{x,w}$ [K]	Wall temperature at axial coordinate x
t_s [m]	Average strut thickness in the middle
t [s]	Time
$\dot{V}_1$ [SLM]	Volumetric flow rate
V_2 [l]	Bubble flow meter volume
V_{FOAM} [m^2]	Volume of foam sample
$W_{FOAM}^{in\ Air}$ [kg]	Weight of foam sample saturated with air
$W_{FOAM}^{in\ EtOH}$ [kg]	Weight of foam sample saturated with ethanol
W_{in} [kg s^{-1} m^{-2}]	Specific mass velocity

Greek symbols

α [-]	Coefficient of shape struts
β [m^{-1}]	Rosseland mean extinction coefficient
ε_H [-]	Hydraulic porosity of foam sample
ε_T [-]	Total porosity of foam sample
ε [-]	Void fraction
ρ_{FOAM} [kg m^{-3}]	Foam mass density
ρ [kg m^{-3}]	Mass density
ρ_{SOLID} [kg m^{-3}]	Mass density of bulk material
ρ_{EtOH} [kg m^{-3}]	Mass density of ethanol
ρ_{HS} [kg m^{-3}]	Mass density of hollow struts
σ [-]	Standard deviation
σ [W m^{-2} K^{-4}]	Stefan-Boltzmann constant

Superscripts

$in\ Air$	Saturating fluid is air
$in\ EtOH$	Saturating fluid id ethanol
c	Convective contribute
s	Static contribute

Subscripts

c	Referred to cell
p	Referred to pore
s	Referred to struts
$EtOH$	Referred to ethanol
HS	Hollow struts
H	Hydraulic
T	Total
$SOLID$	Referred to the bulk material
$FOAM$	Referred to foam
$-\infty$	Undisturbed condition
f	Referred to fluid

Appendix B: Measures

1. Characterization

Here, all the measurements and the photos which show how the measures are taken, are reported for each foam sample. Each geometrical parameter of the studied foam is the average of sufficiently replicated measurements, such as at least 40.

FeCr Alloy 1200 µm							
Cell Diameter [µm]		Pore Diameter [µm]				Strut thickness in the middle [µm]	
1014.091	1151.367	702.8268	879.9319	680.984	483.7251	160.266	172.5046
1383.167	1494.074	305.8207	599.7908	449.5885	325.5341	151.0031	275.983
1475.505	1024.61	574.5845	223.5549	189.3377	908.8911	156.8565	164.2275
1098.023	1746.027	336.2805	134.5979	139.7218	457.5347	174.168	147.2571
1732.904	1210.647	649.4887	827.4554	908.6466	950.7721	162.3514	211.6292
1014.873	1524.166	391.6815	484.2712	472.9252	565.5755	182.9154	179.7686
1577.067	1246.77	886.2985	591.8363	665.1699	299.2287	160.3784	185.7828
1125.663	1477.82	392.6465	403.377	310.0537	291.7478	173.8573	172.1211
1585.242	1083.557	448.4648	546.1897	680.8428	523.4802	172.6786	195.211
1147.605	1496.846	277.3075	303.8305	631.596	313.7514	158.4188	204.7038
1448.706	1115.219	849.7605	786.3173	606.1268	670.7096	161.2748	166.5158
1230.578	1447.889	427.902	395.5729	413.2628	412.5937	177.0753	152.6647
1525.741	1072.115	439.8089	680.4104	159.6652	778.3243	198.6274	197.5965
1212.873	1501.642	331.8934	453.579	184.7777	542.7475	169.8729	135.3545
1422.357	1378.491			169.979	193.7593	168.1313	149.6846
1105.161	1788.47					189.7497	167.3076
1068.192	827.0269					181.7293	187.9685
1190.257	1677.368					184.2243	235.7948
1448.08	1058.146					175.4052	155.0075
992.6834	1573.448					201.9266	172.1909
1641.924	798.3787					188.6384	193.9143
						149.2022	185.3944
						188.6384	179.7352
							157.1626
Cell Diameter [µm]		Pore Diameter [µm]				Strut thickness in the middle [µm]	
Number of measure	42	58				47	
Average	1312.773	494.9402				177.2951	
Standard Deviation	257.9737	221.458				24.1504	

FeCr Alloy 580 μm							
Cell Diameter [μm]		**Pore Diameter [μm]**				**Strut thickness in the middle [μm]**	
495.9512	682.0769	155.2011	245.8714	180.1358	197.5965	93.64812	73.44476
672.427	473.3315	125.5943	173.2343	199.5928	132.4384	100.5161	76.56804
679.6507	625.2779	336.8516	120.3182	143.6226	308.4804	94.28736	81.21267
586.1763	480.9355	218.4726	263.7861	360.4882	206.02	79.71966	116.4621
432.593	675.3062	270.9085	187.4565	159.4393	273.8417	74.41973	81.13867
538.4474	595.2065	195.3648	215.5942	326.4738	222.0722	121.5104	86.65181
630.8061	692.3561	136.195	151.0031	152.6647	158.4188	90.98027	81.58165
490.2379	584.0512	84.61761	234.3126	220.634	114.3279	72.37372	90.71579
611.1502	549.7851	164.3372	134.8654	144.7889	291.9124	79.19046	74.17719
482.5316	676.204	130.5196	286.1767	218.3901	142.1512	70.09698	91.50694
728.6753	729.4003	211.4588	179.0655	242.6498	99.97681	95.86682	76.09588
625.3259	573.7371	126.4998	301.4686	244.9167	114.4329	85.25411	94.28736
605.641	573.7371	149.0814	171.8417	217.1488	226.8094	71.45491	90.71579
599.6405	556.615	179.0655	412.4626	285.5253	273.9075	79.03861	87.47971
556.6689	690.3751	191.2317	240.7611	127.2573	121.708	72.78752	80.02049
468.1764	527.4014	141.431	82.3876	197.6877	195.334	79.11457	76.9593
619.3028	540.4073	141.431	119.1139	124.8267	138.6429	73.68971	90.11788
537.9563	697.9813	125.2591	142.2779	257.2377	101.0525	77.89029	86.09545
695.196	712.1999	74.98261	136.7672	152.389	204.6157	89.11244	72.12429
485.4729	502.7239	88.2318	291.6654	318.954	187.2	62.77324	66.21922
638.0963	799.1233	373.9826	208.3395	259.9785	229.521	67.29895	86.65181
649.5997	509.5244	143.2876	123.8606	277.3724	158.7597	86.65181	74.66148
743.6805	822.8911	236.6086	206.1075	204.5276	158.7219	77.50373	73.11688
558.0484	602.9372	194.8722	293.6359	150.485	71.45491	72.78752	79.03861
615.7622	813.7523	351.9216	152.2707	151.9548	164.6658		83.76142
561.8994	595.6201	279.1211	183.5383	228.498	195.334		
543.1569	779.0725	156.6266	117.2844	175.7131	171.2464		
546.8931	468.5868	102.8787	265.4206	213.4662	154.8912		
675.0393	646.0298	254.1839	262.0497	156.7416	111.6161		
497.6923	505.2982	154.4251	164.3372	222.2615	127.8224		
632.3469	711.9721	346.7632	182.4221	163.0528	96.11713		
516.4448	575.9628	187.6807	242.1294	317.3113	181.8945		
754.2511	609.5263			177.0413	238.7568		
598.979	530.5016						
660.6392	797.9874						
523.4802	478.3305						
724.4837	679.8628						
524.6951	554.2465						
679.5712	695.2651						
646.0298	505.0604						
638.2187	688.7374						
575.7437	507.8121						
640.436	704.6449						
564.5018	559.5855						
721.5177	787.4929						
521.2148	467.0074						
611.8575	527.7657						

	Cell Diameter [μm]	**Pore Diameter [μm]**	**Strut thickness in the middle [μm]**
Number of measure	94	130	49
Average	608.1916	194.3529	24.1504
Standard Deviation	92.9468	69.74604	11.44746

NiCr Alloy 1200 µm							
Cell Diameter [µm]		Pore Diameter [µm]				Strut thickness in the middle [µm]	
845.7003	1154.535	386.1055	252.6669	675.3951	265.7146	161.5725	165.6841
1090.894	866.5181	331.7667	290.2616	363.9211	284.9778	145.1204	138.035
815.522	1377.196	395.9523	202.8467	326.345	212.6486	157.8491	138.3827
998.9266	867.3565	275.983	286.68	207.7331	311.3297	161.2376	117.8465
1421.094	1354.365	315.3173	258.9367	302.6618	294.8607	133.3425	104.7878
1102.478	1078.968	232.6403	630.9109	308.4804	205.202	161.684	123.8606
1231.437	1258.375	380.0845	406.4773	568.531	182.4221	167.5228	104.9024
1047.855	1057.607	274.6739	483.3276	337.0833	365.7158	144.7889	108.8369
1223.45	1148.965	349.7128	326.6946	354.2862	242.2534	143.4971	96.30443
948.0896	1040.728	283.3289	285.5253	202.105	502.3055	147.1347	114.3804
1262.093	1117.99	295.6135	203.8805	149.524	394.5998	165.103	146.2748
857.2628	1381.507	247.6484	368.921	223.1515	310.4022	128.2915	140.7499
1141.196	1258.432	322.4751	318.1432	339.622	367.42	149.0814	118.3043
983.5954	1035.492	240.2616	457.5347	242.1294	438.1121	144.1653	313.4832
1060.426	1237.781	256.2316	367.6652	228.0507	487.3377	177.448	135.2213
1057.169	1075.762	147.2571	220.307	159.778	357.2746	129.4103	114.4329
1024.926	1159.913	287.1824	167.4152	277.3724	253.047	255.6449	133.3875
1012.307	981.5107	201.0621	449.0537	228.8658	421.1242	119.5167	100.0369
1245.073	1347.121	275.7434	243.2432	269.1958	233.8764	157.2008	90.11788
967.1522	1005.758	237.1665	358.6338	161.8325	385.732	122.8379	141.1334
1058.021	1095.827	228.997	274.0828	332.3275	294.106	131.5282	121.0647
1227.386	1305.679	300.6106	438.7013	175.4052	437.3986	141.1334	116.2039
				239.1841	308.8502	128.8055	132.665
						117.8974	98.64615
						115.3739	131.7563
							103.0537
Cell Diameter [µm]		Pore Diameter [µm]				Strut thickness in the middle [µm]	

	Cell Diameter [µm]	Pore Diameter [µm]	Strut thickness in the middle [µm]
Number of measure	44	90	51
Average	1109.76	308.7491	138.3675
Standard Deviation	154.894	100.9315	36.74331

NiCr Alloy 580 μm							
Cell Diameter [μm]		Pore Diameter [μm]				Strut thickness in the middle [μm]	
747.427	624.0856	196.8656	299.9505	176.7357	223.5549	42.87295	63.72296
489.4899	701.321	245.8714	163.3473	197.5965	387.7821	65.94652	81.80224
686.816	648.2204	265.33	285.8196	156.1272	236.5579	68.79957	74.66148
480.5856	601.9401	379.7525	147.4609	151.9152	256.0675	76.09588	69.40804
550.3311	538.0568	65.85537	173.4422	195.1494	164.2275	78.19816	79.19046
407.6726	714.5491	103.9822	199.0504	302.2646	160.2285	71.3708	49.6266
652.6992	482.3946	193.7593	206.6314	230.9819	116.4621	76.25359	70.69428
620.0008	689.8877	282.8196	162.2773	261.981	218.8023	68.27371	66.21922
602.8276	542.3268	198.6577	313.1765	332.9054	221.4492	74.09616	73.11688
584.2054	729.0626	174.4437	237.3184	322.9405	419.1655	86.85952	57.37371
725.9994	568.4781	228.2613	228.2876	197.1705	236.2275	85.74589	101.9402
589.4871	542.1496	223.6893	137.9915	295.7557	251.7142	77.50373	80.02049
517.1886	504.1914	203.3495	124.2479	424.0099	169.1287	69.32145	76.72478
750.7228	704.3636	281.1794	173.8573	193.9143	439.9182	79.71966	63.24989
645.0248	655.1244	165.6841	203.4381	249.7978	217.1488	72.78752	71.45491
545.6835	598.9088	266.3243	120.3182	222.2885	302.2447	69.061	63.72296
582.3105	539.2055	182.9154	177.0753	375.5214	138.6429	100.9336	76.33233
450.9892	737.7199	307.2317	115.8415	391.6662	179.3337	51.52687	66.94098
616.24	547.8149	240.6363	248.0362	197.5661	105.8146	66.94098	61.32108
671.023	830.9398	420.1246	177.5495	221.4492	177.9888	79.03861	81.58165
706.2798	522.3775	236.7609	100.7549	274.0828	226.3587	88.36785	74.41973
532.1183	668.6915	312.8118	133.7922	308.4804	237.7736	63.62863	72.37372
542.5815	511.5246	154.8912	217.5633	201.3009	184.5175	72.78752	85.60567
613.6514	772.7476	178.9313	183.9632	291.3357	130.4736	65.85537	90.98027
621.1623	523.1818	155.2011	227.9453	211.686	103.9822	79.03861	85.60567
560.658	680.0748	169.0221	153.8405	235.7948	170.1556	56.84781	80.61879
684.3189	644.7267	191.7336	309.1612	136.2832	108.2836		63.91122
592.6578	884.6161	284.4714	196.1319	153.4496	271.7056		
742.031	671.703	299.4895	422.0077	162.9423	189.3377		
546.0577	734.5621	222.7204	237.4449	372.0179	298.5856		
545.6615	539.5173	213.2409	153.9186	218.912	153.0184		
481.1852	874.014	309.7242	107.0001	193.1072	321.3743		
925.4478	535.9427	218.8023	110.5346	170.6843	395.5729		
668.6017	875.9911	174.5469	112.8471	227.8663	130.6576		
728.4032	518.4067	179.9689	296.1616	150.0053	164.3372		
		193.1072	183.7018	251.1886	279.9806		
		120.3182	324.5917	160.5656	246.4814		
Cell Diameter [μm]		Pore Diameter [μm]				Strut thickness in the middle [μm]	
Number of measure	70	148				53	
Average	626.6623	220.6855				73.02815	
Standard Deviation	109.9341	77.9233				11.32561	

Co 1200 μm							
Cell Diameter [μm]		**Pore Diameter [μm]**				**Strut thickness in the middle [μm]**	
1247.632	1118.903	338.9847	184.5175	503.4403	212.5638	123.8606	125.2111
1239.328	968.8711	338.9847	494.3863	400.0274	403.4067	103.4029	220.1979
1249.499	924.5322	298.1024	625.8636	474.2443	459.6435	110.7517	100.7549
1172.972	1022.233	343.2112	260.9011	221.4492	464.7252	114.7997	119.5167
1005.185	1166.481	167.3076	173.8573	413.9164	299.6499	137.9915	112.2601
972.2441	1047.035	242.6498	520.8459	423.2726	429.7091	121.0647	110.9685
883.6377	1140.343	393.8685	303.1575	452.6245	486.7457	138.6862	121.3125
1125.364	960.5024	357.829	221.9369	473.0776	306.429	107.5041	106.3243
973.8923	1000.945	434.0901	158.0772	497.6802	200.3438	107.5041	96.67795
1081.842	873.3196	457.5347	601.5009	304.0676	384.7496	150.1654	131.7563
844.0794	1092.847	268.1674	492.9627	241.384	520.892	122.1022	118.3043
1150.846	1058.157	259.4234	467.2518	223.2592	509.8073	131.9841	116.2556
1188.181	1198.96	279.3792	380.0845	332.2371	388.2156	117.6934	133.882
1054.837	846.8006	201.9266	473.7881	440.614	415.6542	109.6068	111.8849
1100.799	995.0707	237.7736	382.7304	272.9408	266.5272	129.7812	114.3804
1056.84	901.1788	350.3306	229.5995	170.1556	394.5998	104.2706	123.715
1280.45	1059.468	308.8502	325.8845	511.689	339.9579	103.0537	108.8369
868.2217	975.6486	236.5579	294.4734	526.7746	244.1306	129.5032	106.0981
1130.864	1265.42	215.5942	181.4316	402.1241	192.7336	104.7878	128.9919
1059.967	936.5453	149.2022	496.266	279.9806	389.1428	124.8267	115.6858
957.753	1137.558	441.0092	369.1652	532.1296	235.6929	103.0537	112.8471
1187.103	957.4519	395.9523	273.9075	359.4703	401.7804	129.4103	119.5167
853.4213	1150.036	341.1045	214.9244	272.0591	453.579	127.8224	107.9502
868.3877	1220.102	209.0303	272.8528	291.8507	283.6679	130.7954	147.3794
1004.683	1163.202	287.5796	466.7372	392.7842	382.3692	149.0411	137.4681
813.3093	1096.123	211.0038	409.9354	395.9371	466.9946	104.2706	129.4103
1099.86	1091.785	334.8305	477.6268	142.2357	365.124	117.8465	117.8974
1023.783	925.0778	206.8638	459.735	222.5316	324.5917	107.0562	111.9922
1048.428	1140.717	240.0615	363.9541	115.4259	370.1564	121.0647	110.9685
837.4564	970.3146	209.3749	494.6293	68.62473	475.9133	128.6655	142.6153
1216.433	1201.683	124.7786	394.1581	277.5673	349.9188	157.8491	120.5675
931.9159	1016.151	163.0528	286.4285	247.7211	329.441	140.3652	122.5442
1046.323	1172.096	276.4396	356.6014	306.1348	564.9698	129.4103	150.485
1147.354	957.6025	155.7806	374.1111	350.9131	326.0504	106.3243	100.9336
846.3252	1266.023			259.4234	118.5579	103.9822	114.7474
1116.296	1095.904					125.9764	152.0338
1076.292	1188.984					144.7474	96.5536
864.8319	1109.473					98.64615	124.006
1147.605	1092.379					138.122	151.5986
1159.726	1112.242					119.6674	153.0184
839.3479	1093.786						139.0323
1171.948	984.389						
911.3068	1077.815						
904.0803	972.6888						
Cell Diameter [μm]		**Pore Diameter [μm]**				**Strut thickness in the middle [μm]**	
Number of measure	90	138				81	
Average	1051.22	337.095				123.0128	
Standard Deviation	121.7818	115.7492				18.72995	

Co 580 μm							
Cell Diameter [μm]		Pore Diameter [μm]				Strut thickness in the middle [μm]	
491.7427	711.9721	351.0158	457.5347	218.8023	211.8845	76.09588	86.92865
673.2751	692.5556	475.206	230.9819	224.1185	277.3075	52.79364	63.72296
590.6985	601.401	229.4948	235.7184	282.1178	93.84035	72.87	77.89029
553.0205	475.5471	309.1224	124.971	166.5158	65.85537	81.21267	56.84781
530.4903	498.006	179.7686	289.8681	335.7978	391.7735	55.88874	52.79364
604.9066	610.0681	205.2313	457.5347	188.3197	183.0467	55.88874	55.88874
654.7942	630.1201	189.4962	173.0608	418.075	194.0072	64.75158	68.09752
651.1513	510.2077	272.9408	272.9408	167.9883	296.1414	49.6266	80.842
510.5961	691.2186	285.5673	143.7898	187.5847	391.2979	51.52687	66.94098
398.4174	525.6102	393.5175	208.0221	117.8974	413.8583	126.4998	84.61761
571.4817	661.4025	253.8528	304.7385	456.6016	502.7717	54.14178	51.99109
597.6538	565.3524	326.0504	368.9699	355.2344	291.1501	62.48551	72.87
552.6728	678.4034	66.58108	120.3182	293.6359	478.431	69.75336	61.71166
607.6609	541.2958	73.68971	108.8369	369.1815	355.5893	74.82222	66.67123
550.3311	612.2697	224.7608	343.7009	284.3025	242.6251	70.18262	80.842
598.7082	568.4781	254.7504	375.953	197.5965	315.4316	52.9073	82.3876
598.3469	681.2221	235.7184	269.1958	158.0772	367.6325	66.21922	64.47267
558.7261	611.7299	346.3645	204.7625	165.8652	211.544	79.03861	81.58165
530.3204	563.6179	96.5536	204.0572	249.942	391.4207	63.24989	60.53235
519.7953	513.2246	183.0467	361.0876	211.686	300.9701	59.83369	54.14178
580.9059	667.2527	296.3847	175.3709	323.3866	303.8305	92.2913	69.75336
614.3558	443.8738	501.1442	119.7176	505.6309	221.4492	59.02509	66.58108
610.8651	740.5724	236.2275	129.4103	319.8004	284.3447	69.32145	65.39772
526.8886	483.1287	340.4876	93.58395	366.7164	179.9689	86.92865	65.7641
585.7662	572.3324	368.807	121.362	246.3107	539.5507		
519.9109	499.3551	255.7623	104.213	319.5561	314.7262		
583.8043	642.3465	111.8849	199.0504	166.6961	346.0869		
474.7507	597.2315	133.9268	140.194	183.7345	176.0888		
716.8823	608.0265	284.2391	234.7992	174.03	162.9423		
571.3555	526.2155	152.0338	360.0213	210.833	135.2213		
627.158	599.8609	302.5824	275.2201	239.3347	241.1848		
469.5984	568.869	127.1628	205.9325	220.4433	159.4393		
613.0638	728.8401	205.202	463.4957	245.8714	171.5618		
573.0876	518.1633	290.5098	228.8658	364.4654	127.8224		
749.0727	681.1251	264.5365	255.0097	270.3759	277.2208		
577.8266	498.3556	68.27371	284.3447	90.18451	149.524		
621.5973	618.2544	81.80224	137.5991	423.5421	393.8685		
681.3367	634.6699						
712.7984	620.1945						
537.8781	571.6918						
649.0539	654.6107						
454.201	507.8121						
667.6577	651.7691						
464.4149	537.4089						
730.429	578.7407						
508.4623	596.98						
753.2869	653.4259						
454.2142	525.8615						
725.7595	678.2617						
550.7675	566.276						
639.0088	565.8303						
471.2456	661.6114						
759.8371	786.9206						
609.2898	788.2934						
475.8755	551.9659						
672.9895	728.0567	656.855	613.9255				
523.331	506.5804	634.5279	631.4723				
498.7412	711.8877	491.2783	671.3541				
750.4667	615.4109						
Cell Diameter [μm]		Pore Diameter [μm]				Strut thickness in the middle [μm]	
Number of measure	124	149				48	
Average	596.6444	254.3216				68.47133	
Standard Deviation	82.6344	106.8654				13.9473	

Cu 1200 μm							
Cell Diameter [μm]		**Pore Diameter [μm]**				**Strut thickness in the middle [μm]**	
1232.607	1329.382	530.8412	463.8325	794.3282	369.2465	125.2111	105.6442
967.3385	792.7234	522.5039	486.1035	214.0001	398.1309	139.5498	142.2779
1316.104	1206.318	424.4205	305.7225	373.7738	267.4272	142.7837	128.6655
1053.623	875.8471	500.1844	378.1833	114.3279	126.4998	101.9992	126.9264
1177.552	1154.582	419.7956	302.2646	91.50694	123.715	108.8369	115.2176
926.8358	882.0184	327.0804	381.6616	182.6525	156.5882	72.12429	102.8787
991.6844	1074.203	173.3383	535.4605	225.6943	214.8406	121.5104	161.2748
1117.286	762.9769	145.74	397.9347	353.6923	337.9198	94.66884	119.5167
1169.978	1066.796	281.6917	138.6429	558.1345	183.0467	139.0323	137.5991
980.3533	1262.079	220.1979	184.5175	403.4514	430.2958	126.1669	126.4998
1174.728	1415.465	397.7535	299.9505	498.9459	571.9124	155.0075	142.9098
853.8435	1182.175	283.3289	361.8188	287.7049	262.0497	158.0772	137.1181
1238.106	1137.511	267.3373	623.0163	224.1185	289.3703	140.3652	143.7898
949.8619	1095.378	303.4744	400.1625	262.256	140.7499	146.2748	115.4259
984.1021	1180.466	85.60567	424.3498	404.7001	83.33003	135.1768	123.715
942.5487	1022.215	82.67872	301.4686	356.2644	365.8472	137.4681	130.2432
1175.08	1340.837	447.5396	241.4338	395.1018	273.3806	143.7898	100.0369
1131.661	1057.493	457.3114	377.945	561.3967	382.4635	152.0338	169.1287
1255.929	1317.659	349.7128	609.5658	298.1024	377.5633	102.6449	126.4998
966.5868	1118.172	183.309	468.1251	364.7455	288.4347	126.4998	128.4319
1242.62	1223.528	592.1306	402.3332	523.4228	234.9271	119.1139	126.4998
914.4258	1106.807	663.8954	436.0369	392.4169	404.982	120.7169	157.3536
1203.726	1162.23	392.6465	245.3088	266.9776	415.4229	136.4154	132.7103
969.0756	983.6137	386.8516	423.7265	219.7883	625.9788	113.537	118.0502
765.2802	1334.132	404.21	194.8722	255.3157	400.7625	118.5579	149.6846
1131.008	959.1506	202.9355	236.1003	404.1654	636.6261	163.1633	113.537
1145.908	809.6748	259.4234	400.4176	477.7777	349.3863	122.5442	99.7964
		399.005	256.7	98.64615	446.0877	138.6862	134.8209
		410.4626	441.404	68.09752	516.5494	135.9301	111.7775
		191.4201	463.6382	86.65181	320.8692	131.7107	137.5991
		406.3591	431.926	79.79498	411.8651		133.882
				63.91122	103.4029		
Cell Diameter [μm]		**Pore Diameter [μm]**				**Strut thickness in the middle [μm]**	

	Cell Diameter [μm]	Pore Diameter [μm]	Strut thickness in the middle [μm]
Number of measure	54	126	61
Average	1089.46	339.2011	129.0018
Standard Deviation	160.067	146.7843	18.40119

Cu 580 μm							
Cell Diameter [μm]		Pore Diameter [μm]				Strut thickness in the middle [μm]	
654.9409	686.5274	286.8685	167.4152	111.9922	149.6846	107.6158	56.42357
585.6329	659.2922	210.7475	324.4436	167.5228	183.9632	64.75158	76.72478
775.6571	749.9302	134.5979	378.3738	200.9425	198.4156	86.92865	90.18451
569.4178	617.4378	76.9593	246.1888	234.3126	177.0413	72.78752	73.11688
674.1845	693.5783	288.518	173.719	256.2316	204.8211	72.87	105.4165
819.4311	580.5749	314.669	252.3339	155.0075	229.8348	92.09583	73.68971
740.3128	588.957	221.9369	181.7293	191.0117	178.9313	81.58165	83.83311
699.0218	556.3559	137.5991	211.8845	258.8671	153.5278	83.90473	61.71166
673.391	828.4203	103.9822	137.337	284.9778	181.4647	74.82222	59.22827
600.5114	554.7665	62.48551	173.4422	237.4449	212.818	67.29895	68.62473
721.1596	674.4517	403.8681	119.1139	212.4507	190.7285	67.29895	76.9593
630.4537	576.4319	310.0149	134.999	312.1198	148.8395	84.97181	59.63256
596.1745	769.5383	291.8507	107.0001	235.54	282.6284	111.8849	63.72296
470.0843	524.5234	171.2464	268.5256	182.3563	260.0478	60.53235	85.74589
659.4652	837.9369	123.4233	217.5633	285.2516	229.4948	84.33318	62.3893
454.4257	552.7598	95.86682	202.105	283.2017	189.623	67.29895	79.19046
566.5094	835.0357	382.1649	284.4925	244.9167	264.7408	63.62863	81.13867
387.6117	620.8431	293.2264	60.53235	169.0221	238.5303	78.5813	68.36163
744.1085	887.7612	123.8606	69.061	159.3263	179.7686	69.75336	70.09698
598.9188	534.7308	100.7549	190.9174	271.7056	189.3377	91.76913	64.75158
612.4364	743.5594	187.2	166.5519	323.7579	288.3514	90.38411	90.11788
539.5507	571.6078	173.4422	212.4507	97.60548	303.8305	54.80342	71.45491
746.5666	718.414	266.3243	212.4507	115.6858	320.1195	74.41973	70.09698
660.9937	571.1557	230.1482	308.8502	264.4456	342.6507	64.47267	112.4739
625.518	679.7745	152.0338	253.5924	251.5232	206.3696	64.47267	73.11688
757.1603	629.2807	107.8389	100.5161	146.2338	181.8945	74.41973	66.94098
542.1496	890.4299	231.2938	117.8974	118.3043	348.1635	74.98261	70.09698
599.1495	602.997	218.61	239.1841	191.4201	274.6739	80.02049	60.53235
572.0805	781.1208	94.28736	164.7752	146.2338	205.2313	73.11688	66.21922
651.6308	661.2118	85.74589	346.919	139.3344	160.041	85.60567	69.32145
633.3435	691.4532	232.6403	255.5744	100.5758	263.6266	95.61586	93.64812
572.1645	788.9027	169.9436	239.5605	312.4275	319.5749	60.6315	81.80224
652.7361	856.0708	217.0105	262.1872	226.6504	124.7786	55.88874	104.2706
567.939	633.002	165.539	284.2179	266.9101	156.0118	90.98027	73.11688
629.4143	742.654	220.5795	235.3358	215.0083	160.5656	99.7964	56.42357
662.9537	527.9023	266.1664	385.9966	220.1433	230.1743	66.21922	68.79957
605.3235	797.385	222.2885	316.3444	151.9152	139.3344	81.13867	58.92323
474.0923	621.8196	191.0117	199.1409	231.9162	121.7574	68.09752	48.15222
646.2622	651.1513	231.9162	236.024	236.5579	173.3383	49.6266	45.05894
597.3824	554.6257	160.7899	150.6446	127.8224	129.9199	61.41896	55.99611
758.777	649.5719	160.266	113.3252	90.98027	254.939	80.02049	59.83369
886.7525	512.3812	139.7218	197.6877	271.4402	279.4437	121.362	60.53235
636.4845	586.0123	241.135	249.6535	236.9384	260.3249	76.25359	48.64864
516.5727	464.4149	232.4595	176.7697	221.8557	187.4565	83.47408	53.02071
		241.384	142.109	149.9652	211.686	96.67795	59.83369
		244.7204	131.5282	231.683	200.9724	103.9822	66.58108
		152.8613	131.7563	193.418	273.4465	68.27371	55.99611
		111.4007	182.4221	193.9143	313.4257	71.3708	65.7641
		223.1515	165.6841	234.1075	170.1556	104.2706	55.99611
		210.1766	174.168	128.2447	292.3442	91.76913	66.67123
		191.0117	122.1022	144.8304	194.8722	76.09588	56.42357
		140.4508	241.1848	202.8467	177.9888	68.36163	56.84781
		260.5325	242.179	167.5228	172.6786		69.32145
		218.5825	169.3062	212.4507	177.0753		
		143.6226	243.8105	291.3357	242.6498		
		124.4412	154.4251	225.5345	246.7736		
		198.6274	146.2748	223.2323	176.5317		
		197.8092	226.6504	289.3703	222.0722		
		137.9915	217.1488	216.1785	221.4492		
Cell Diameter [μm]		Pore Diameter [μm]				Strut thickness in the middle [μm]	
Number of measure	88	236				105	
Average	648.0182	205.8595				73.9591	
Standard Deviation	105.3229	65.7626				15.5205	
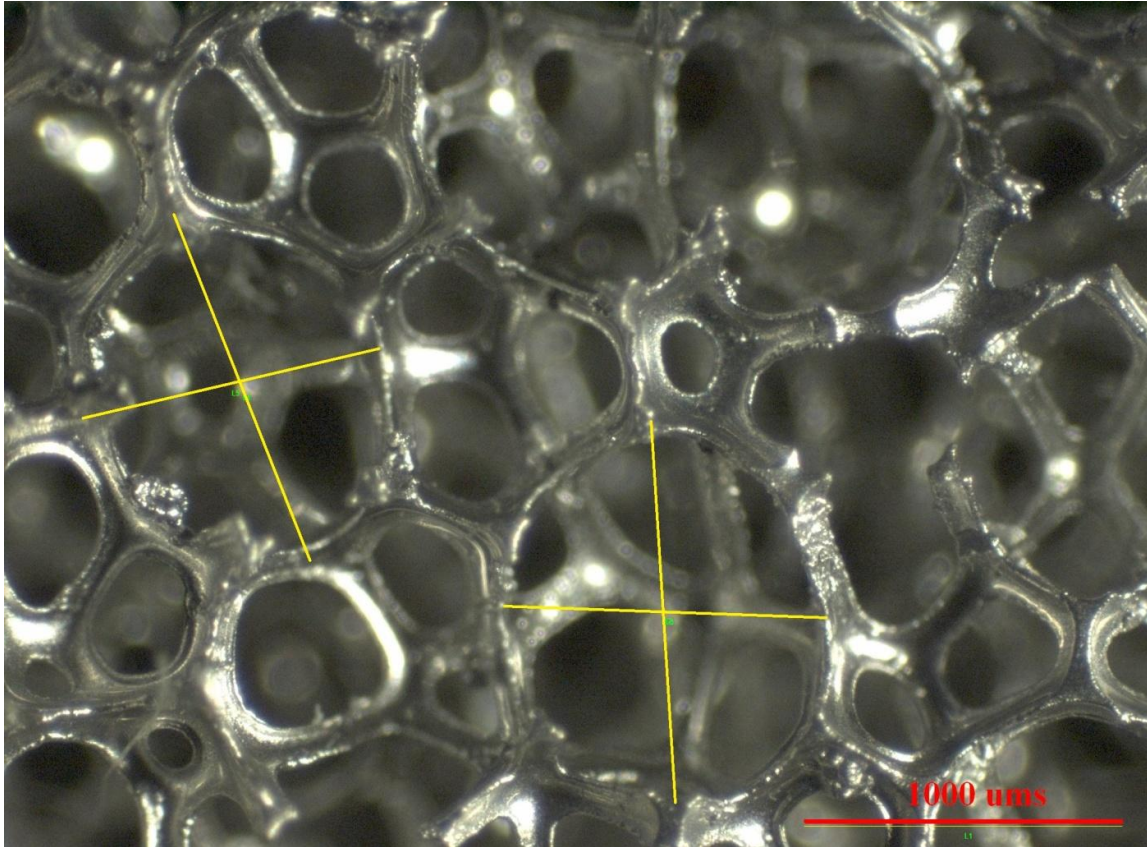
Figure B.1 How to measure cell diameter.
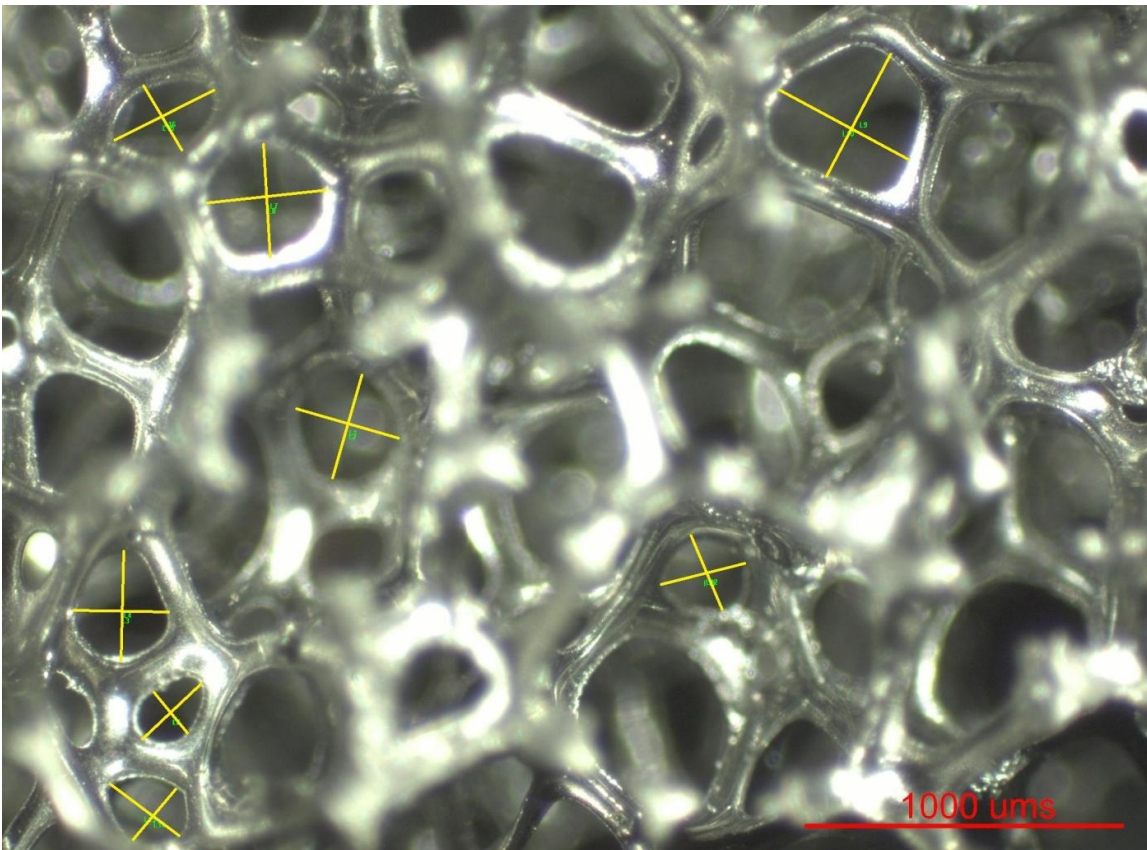
Figure B.2 - How to measure pore diameter
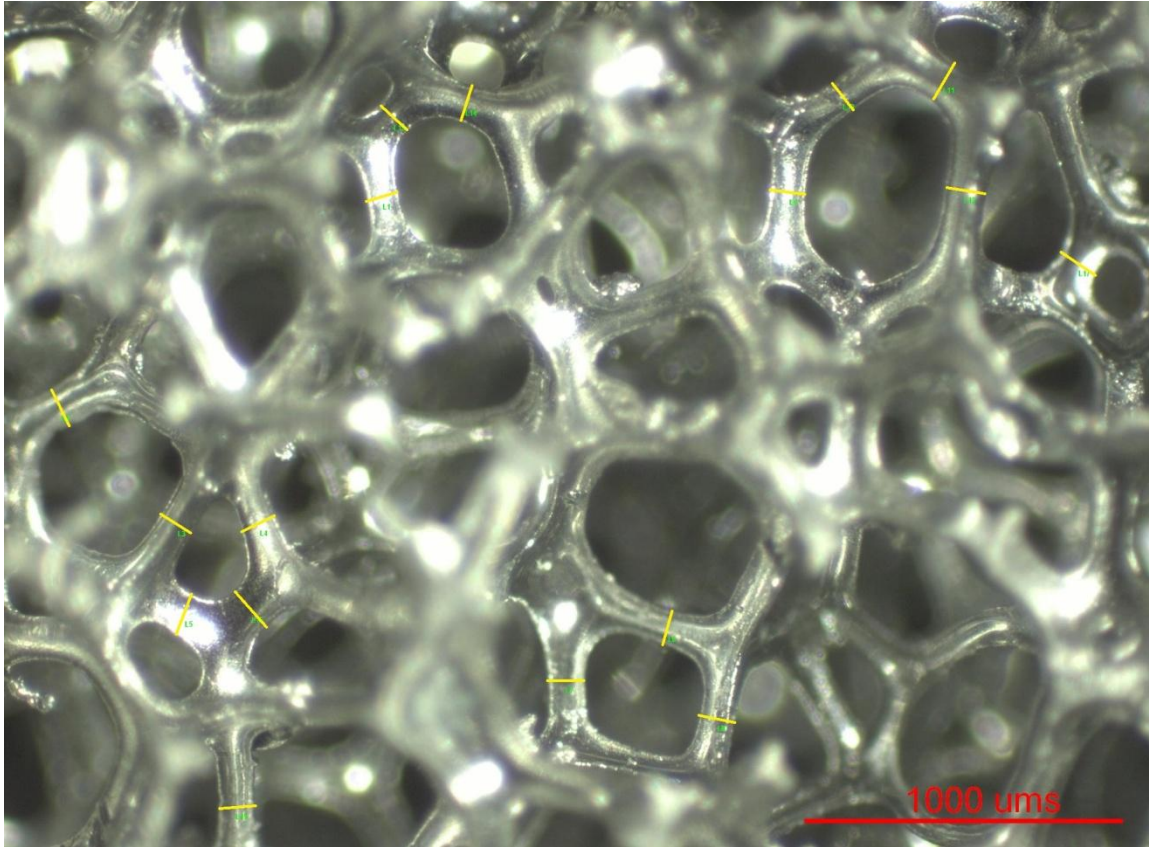
Figure B.3 - How to measure average strut thickness in the middle.

2. Heat exchange measurements

2.1 FeCr 1200 µm

Flow rate = 10 SLM, T_{oven} = 300 °C, Gas: N_2				
coordinates	Position of thermocouples			
[mm]	center	1/2 radius	2/3 radius	wall
-5	242.8	255.5	259.4	294.6
0	245.5	258.3	262.3	296.0
5	249.2	260.9	264.8	296.8
10	252.4	263.8	267.4	297.3
15	256.0	266.4	270.2	297.8
20	259.2	268.7	272.5	298.7
25	262.5	271.3	275.1	298.9
30	265.3	273.6	277.5	299.4
35	267.9	275.8	279.4	299.8
40	270.6	278.0	281.1	300.7
45	273.2	279.9	282.7	300.9
50	275.6	281.6	284.1	301.3
55	278.1	283.4	285.5	302.0
60	279.9	284.9	286.8	302.4
65	281.7	286.4	288.0	302.3
70	283.3	287.5	289.1	302.3
75	284.9	288.7	290.0	302.4
80	286.2	289.5	291.1	302.6
85	287.6	290.4	292.0	302.9
90	288.7	291.2	292.9	303.0
95	289.7	291.9	293.7	303.0
100	290.6	292.5	294.6	303.1
105	291.4	293.4	295.3	303.2

Flow rate = 15 SLM, T_{oven} = 300 °C, Gas: N_2				
coordinates	Position of thermocouples			
[mm]	center	1/2 radius	2/3 radius	wall
-5	210.8	229.2	235.9	289.9
0	213.4	231.9	238.7	291.9
5	216.8	234.6	241.2	292.5
10	220.0	237.5	243.9	293.3
15	223.7	240.5	247.1	294.0
20	227.2	243.4	250.1	295.5
25	230.7	246.4	253.5	295.3
30	234.2	249.2	256.4	295.6
35	237.5	252.0	258.8	296.3
40	241.3	254.9	261.2	298.0
45	244.1	257.4	263.1	297.8
50	247.3	260.0	264.8	298.2
55	250.6	262.3	266.6	299.4
60	253.4	264.5	268.4	300.2
65	256.2	266.9	270.2	299.9
70	258.7	268.7	271.9	299.9
75	261.2	270.4	273.4	300.1
80	263.4	271.9	275.1	300.6
85	265.8	273.4	277.0	301.0
90	267.8	274.5	278.6	301.0
95	269.5	275.7	280.4	301.1
100	271.4	276.9	282.2	301.3
105	273.0	278.5	284.1	301.5

Flow rate = 20 SLM, T_{oven} = 300 °C, Gas: N_2				
coordinates	Position of thermocouples			
[mm]	center	1/2 radius	2/3 radius	wall
-5	183.4	205.3	215.4	286.1
0	185.4	207.7	217.3	288.3
5	188.4	210.5	219.7	289.1
10	191.6	213.4	222.4	289.7
15	194.7	216.5	225.7	290.6
20	198.1	219.4	229.0	292.7
25	201.5	222.4	232.7	292.1
30	204.8	225.6	235.8	292.4
35	208.2	228.6	238.6	293.0
40	211.4	231.6	240.9	295.2
45	214.9	234.3	243.1	295.0
50	218.3	237.3	245.0	295.4
55	221.8	239.9	246.8	296.4
60	225.1	242.6	248.8	298.1
65	228.2	245.4	250.6	297.5
70	231.2	247.6	252.5	297.5
75	234.4	249.7	254.6	297.7
80	237.2	251.3	256.9	298.6
85	240.2	253.1	259.4	299.1
90	242.9	254.5	261.9	298.9
95	245.4	256.0	264.6	299.0
100	248.1	257.8	267.4	299.4
105	250.6	260.2	270.6	299.5

Flow rate = 25 SLM, T_{oven} = 300 °C, Gas: N_2				
coordinates	Position of thermocouples			
[mm]	center	1/2 radius	2/3 radius	wall
-5	164.4	189.2	200.5	283.1
0	166.1	191.5	202.9	286.0
5	169.3	193.7	204.8	286.7
10	171.8	195.6	207.2	287.3
15	174.9	198.4	209.6	288.9
20	177.4	200.9	212.8	290.5
25	179.2	203.7	216.4	290.1
30	181.8	206.3	219.7	290.6
35	184.7	210.9	223.6	291.6
40	189.8	214.1	226.3	293.7
45	193.5	217.3	228.6	293.5
50	196.7	219.9	230.3	294.1
55	200.4	222.8	232.2	295.4
60	203.3	225.3	233.8	297.4
65	206.3	228.3	235.5	296.6
70	210.1	231.1	238.0	296.5
75	213.3	233.5	240.2	296.8
80	216.1	235.1	242.6	297.8
85	220.0	237.1	245.5	298.2
90	222.6	238.3	247.2	298.5
95	224.6	239.5	251.1	298.7
100	227.7	241.7	255.0	299.3
105	231.0	244.6	258.8	299.8

Flow rate = 30 SLM, T_{oven} = 300 °C, Gas: N_2			
coordinates	Position of thermocouples		
[mm]	center	1/2 radius	2/3 radius	wall
-5	145.6	171.9	185.8	279.8
0	147.3	173.7	186.9	283.2
5	149.5	175.8	188.6	284.0
10	151.7	178.0	190.9	285.3
15	154.2	180.7	193.8	286.1
20	156.8	183.3	197.4	288.2
25	159.6	186.2	201.0	287.9
30	162.2	188.8	204.6	288.4
35	164.8	191.4	207.6	289.4
40	167.7	194.5	210.1	291.6
45	170.4	197.2	213.0	291.7
50	173.5	200.1	213.5	292.3
55	176.5	202.9	215.2	294.4
60	179.5	206.0	217.0	296.1
65	182.6	208.9	218.8	295.1
70	185.4	211.6	220.9	295.0
75	188.7	213.9	223.1	295.5
80	191.6	215.5	225.5	297.0
85	194.8	217.2	228.2	297.6
90	197.7	218.5	231.6	297.4
95	200.7	220.2	235.1	297.5
100	204.0	222.3	239.8	298.0
105	207.2	225.6	244.7	298.5

Flow rate = 35 SLM, T_{oven} = 300 °C, Gas: N_2			
coordinates	Position of thermocouples		
[mm]	center	1/2 radius	2/3 radius	wall
-5	132.6	158.5	175.2	275.9
0	134.0	160.2	175.9	279.8
5	136.0	162.0	177.2	280.1
10	138.0	164.2	179.2	281.2
15	140.3	166.4	182.0	282.6
20	142.5	168.9	185.2	285.8
25	145.0	171.6	188.9	284.5
30	147.3	174.0	192.5	285.2
35	149.4	176.7	195.1	286.1
40	151.7	179.2	197.5	288.9
45	154.1	181.8	199.3	288.9
50	156.7	184.6	200.7	289.6
55	159.4	187.3	201.9	291.8
60	161.9	189.9	203.5	294.0
65	164.6	193.2	205.2	292.7
70	167.2	195.7	207.1	292.4
75	170.0	198.0	209.4	292.5
80	172.9	199.6	211.6	294.1
85	175.8	201.2	214.6	295.0
90	178.6	202.4	217.9	295.1
95	181.6	203.9	221.6	295.2
100	184.7	205.8	226.6	296.0
105	188.0	209.1	232.3	296.2

Flow rate = 10 SLM, T_{oven} = 500 °C, Gas: N_2			
coordinates	Position of thermocouples		
[mm]	center	1/2 radius	2/3 radius	wall
-5	413.0	435.4	442.2	492.9
0	418.2	440.9	446.6	495.1
5	425.8	445.8	451.2	496.2
10	432.6	451.0	455.7	497.3
15	439.3	455.9	460.5	498.5
20	445.6	460.3	465.0	500.6
25	451.3	464.8	469.3	500.4
30	456.6	468.6	473.0	500.9
35	461.4	472.1	476.2	501.6
40	465.8	475.8	479.2	503.1
45	470.1	478.6	481.7	503.5
50	473.7	481.3	483.8	503.9
55	477.1	483.8	485.9	504.7
60	480.0	486.0	487.8	505.1
65	482.7	488.0	489.6	505.2
70	485.0	489.7	491.2	505.3
75	487.1	491.2	492.7	505.5
80	488.9	492.4	494.1	505.9
85	490.7	493.6	495.3	506.1
90	492.1	494.6	496.4	506.1
95	493.4	495.6	497.4	506.1
100	494.6	496.4	498.4	505.9
105	495.7	497.3	499.2	506.0

Flow rate = 15 SLM, T_{oven} = 500 °C, Gas: N_2			
coordinates	Position of thermocouples		
[mm]	center	1/2 radius	2/3 radius	wall
-5	371.8	402.1	415.1	487.8
0	377.2	407.3	418.4	490.6
5	383.9	412.5	422.3	492.2
10	390.3	417.6	426.9	493.2
15	397.4	423.4	432.2	494.9
20	403.9	428.1	437.1	496.9
25	411.0	433.6	442.3	497.6
30	417.0	438.3	447.3	497.7
35	422.9	443.1	450.9	498.7
40	428.6	447.4	454.7	500.4
45	434.2	451.8	457.9	501.0
50	439.5	455.6	460.8	501.5
55	444.9	459.4	463.8	502.2
60	449.2	462.5	466.6	503.0
65	453.3	465.9	469.4	503.0
70	457.0	468.5	472.0	503.2
75	460.7	471.3	474.5	503.5
80	464.0	473.2	477.0	504.2
85	467.4	475.3	479.5	504.5
90	470.2	477.1	481.8	504.5
95	473.1	479.1	484.1	504.6
100	475.8	481.2	486.6	504.7
105	478.5	483.8	488.9	504.7

Flow rate = 20 SLM, T_{oven} = 500 °C, Gas: N_2				
coordinates	Position of thermocouples			
[mm]	center	1/2 radius	2/3 radius	wall
-5	324.7	364.6	380.7	482.7
0	329.5	369.9	383.9	486.4
5	335.7	374.9	388.0	488.2
10	342.5	380.5	393.0	489.3
15	349.2	385.9	398.1	490.7
20	356.0	391.7	403.9	493.7
25	362.7	397.2	409.7	493.7
30	369.7	402.3	415.1	493.9
35	376.2	407.6	419.7	494.6
40	382.6	412.9	423.9	496.6
45	388.9	417.4	427.2	497.5
50	395.1	422.1	430.7	498.2
55	401.2	426.5	433.9	498.8
60	406.8	431.2	437.4	500.0
65	412.3	435.2	440.8	500.0
70	417.3	439.1	444.6	500.1
75	422.3	442.2	447.9	500.6
80	427.2	445.0	451.4	501.6
85	431.8	447.7	455.1	502.0
90	436.2	450.4	458.9	502.1
95	440.4	452.7	462.9	502.3
100	445.0	456.2	467.3	502.5
105	449.9	460.4	472.2	502.5

Flow rate = 25 SLM, T_{oven} = 500 °C, Gas: N_2				
coordinates	Position of thermocouples			
[mm]	center	1/2 radius	2/3 radius	wall
-5	287.6	333.4	352.6	477.3
0	291.8	338.5	355.7	481.4
5	297.6	343.3	359.6	483.7
10	303.3	348.3	364.2	485.0
15	310.0	354.2	369.8	486.8
20	316.2	359.3	375.6	489.5
25	322.9	365.0	382.1	490.0
30	329.4	370.3	387.8	489.9
35	335.7	375.7	392.7	490.8
40	342.2	381.2	397.1	493.1
45	348.6	386.6	400.7	494.2
50	355.0	391.6	403.9	495.0
55	361.8	396.6	407.3	495.6
60	367.6	401.5	411.0	496.9
65	373.7	406.1	414.7	496.7
70	379.1	410.2	418.4	496.9
75	384.9	413.9	422.7	497.3
80	390.3	416.9	426.6	498.6
85	396.0	419.9	431.2	499.2
90	400.9	422.6	435.8	499.2
95	406.3	425.9	441.0	499.5
100	412.1	429.9	446.7	499.7
105	419.0	436.2	453.8	499.6

Flow rate = 30 SLM, T_{oven} = 500 °C, Gas: N_2				
coordinates	Position of thermocouples			
[mm]	center	1/2 radius	2/3 radius	wall
-5	257.5	308.9	327.4	473.6
0	261.4	313.1	330.4	478.8
5	266.5	317.4	334.1	480.5
10	271.8	322.0	338.8	482.2
15	277.7	327.2	344.9	484.9
20	283.3	331.8	350.2	488.0
25	289.2	337.2	357.1	487.3
30	294.7	342.6	363.5	487.2
35	300.4	347.9	368.1	488.2
40	306.7	353.4	372.7	490.5
45	312.6	358.5	376.3	491.8
50	318.9	363.9	379.2	492.8
55	325.5	368.9	382.9	493.6
60	331.6	373.8	386.5	495.2
65	337.8	379.7	390.4	494.5
70	343.9	384.2	394.8	494.8
75	349.6	387.9	399.1	495.3
80	355.4	390.5	403.6	496.9
85	361.7	393.8	408.9	497.6
90	367.2	396.4	414.2	497.6
95	373.1	399.5	420.1	498.0
100	379.3	404.2	427.1	498.4
105	386.7	411.8	435.1	498.4

Flow rate = 35 SLM, T_{oven} = 500 °C, Gas: N_2				
coordinates	Position of thermocouples			
[mm]	center	1/2 radius	2/3 radius	wall
-5	232.3	285.9	305.8	469.0
0	235.3	289.6	308.1	474.4
5	239.8	293.5	311.7	476.9
10	244.3	297.8	315.9	478.2
15	249.3	302.8	321.4	480.5
20	254.4	307.7	327.6	483.3
25	259.7	312.6	334.5	483.6
30	265.0	317.5	340.6	483.9
35	270.3	322.5	345.9	485.0
40	275.6	328.3	350.4	487.6
45	281.1	333.1	353.8	489.0
50	286.7	338.0	356.7	490.1
55	292.3	343.2	359.8	490.9
60	298.2	348.4	363.2	492.4
65	303.7	353.0	366.8	491.9
70	309.3	357.6	370.8	491.9
75	315.0	361.1	375.5	492.5
80	320.7	364.1	380.3	494.1
85	326.7	366.6	385.6	495.0
90	332.6	369.3	391.6	494.8
95	338.7	372.4	398.6	495.4
100	345.6	377.7	407.1	495.6
105	354.6	386.0	417.2	495.8

Flow rate = 10 SLM, T_{oven} = 500 °C, Gas: He				
coordinates	Position of thermocouples			
[mm]	center	1/2 radius	2/3 radius	wall
-5	496.8	498.7	499.9	504.4
0	498.1	499.9	500.8	505.7
5	499.4	500.8	501.7	506.2
10	500.4	501.6	502.4	506.5
15	501.4	502.4	503.1	506.8
20	502.2	502.9	503.6	507.4
25	502.8	503.4	504.2	507.6
30	503.3	503.9	504.5	507.6
35	503.7	504.2	504.7	507.7
40	504.1	504.5	505.0	508.1
45	504.4	504.7	505.2	508.2
50	504.7	504.9	505.3	508.2
55	504.8	505.0	505.4	508.3
60	504.9	505.1	505.5	508.4
65	505.0	505.2	505.6	508.4
70	505.1	505.2	505.6	508.3
75	505.1	505.2	505.6	508.4
80	505.1	505.2	505.6	508.4
85	505.1	505.1	505.5	508.4
90	505.0	505.0	505.4	508.3
95	504.8	504.8	505.2	508.3
100	504.6	504.6	505.0	508.0
105	504.4	504.4	504.7	507.9

Flow rate = 15 SLM, T_{oven} = 500 °C, Gas: He				
coordinates	Position of thermocouples			
[mm]	center	1/2 radius	2/3 radius	wall
-5	476.3	482.5	485.9	498.2
0	479.6	485.7	488.1	500.6
5	483.1	488.1	490.3	501.5
10	486.1	490.4	492.2	502.1
15	488.8	492.4	494.0	502.7
20	491.1	494.2	495.6	503.9
25	493.1	495.7	497.1	504.5
30	494.8	497.0	498.4	504.7
35	496.3	498.2	499.4	505.0
40	497.6	499.3	500.3	505.8
45	498.6	500.1	501.0	506.1
50	499.6	500.8	501.6	506.3
55	500.5	501.5	502.1	506.5
60	501.2	501.9	502.6	506.7
65	501.8	502.4	503.0	506.8
70	502.2	502.7	503.3	506.8
75	502.6	503.0	503.6	506.8
80	502.9	503.2	503.8	507.0
85	503.1	503.3	503.9	507.0
90	503.3	503.4	504.0	507.0
95	503.4	503.5	504.1	506.9
100	503.4	503.5	504.1	506.6
105	503.4	503.4	503.9	506.7

Flow rate = 20 SLM, T_{oven} = 500 °C, Gas: He				
coordinates	Position of thermocouples			
[mm]	center	1/2 radius	2/3 radius	wall
-5	443.9	458.0	465.4	491.9
0	449.8	463.7	469.2	494.7
5	456.3	467.9	473.0	496.1
10	461.9	472.2	476.4	497.0
15	467.0	476.0	479.7	498.1
20	471.6	479.2	482.6	499.9
25	475.5	482.4	485.4	500.9
30	479.2	485.0	488.0	501.1
35	482.1	487.4	489.9	501.7
40	485.0	489.6	491.8	503.1
45	487.5	491.6	493.2	503.8
50	489.7	493.2	494.6	504.2
55	491.7	494.6	495.9	504.5
60	493.3	495.9	497.1	505.0
65	494.7	496.9	498.0	505.2
70	496.0	497.9	499.0	505.3
75	497.1	498.6	499.7	505.5
80	497.9	499.3	500.3	505.7
85	498.8	499.8	500.9	505.9
90	499.5	500.3	501.4	505.9
95	500.0	500.7	501.8	506.0
100	500.5	501.1	502.1	505.8
105	500.9	501.4	502.4	505.8

Flow rate = 25 SLM, T_{oven} = 500 °C, Gas: He				
coordinates	Position of thermocouples			
[mm]	center	1/2 radius	2/3 radius	wall
-5	409.7	433.6	444.5	485.1
0	417.5	440.5	449.5	489.6
5	426.4	446.2	454.5	491.4
10	434.5	452.0	458.8	492.7
15	441.9	457.3	463.4	494.0
20	448.3	461.9	467.6	496.4
25	454.2	466.5	471.8	497.2
30	459.6	470.4	475.5	497.5
35	464.3	474.2	478.4	498.4
40	468.7	477.7	481.1	500.4
45	472.2	480.6	483.5	501.2
50	476.4	483.3	485.7	501.7
55	479.7	485.6	487.9	502.3
60	482.6	487.8	489.8	503.0
65	485.0	489.8	491.5	503.3
70	487.2	491.4	493.2	503.4
75	489.3	492.2	494.2	503.6
80	490.5	493.3	495.4	504.2
85	492.4	494.4	496.4	504.6
90	493.3	495.4	497.4	504.7
95	494.6	496.4	498.4	504.8
100	495.6	497.3	499.2	504.8
105	496.5	498.2	500.0	504.8

coordinates	Position of thermocouples			
Flow rate = 30 SLM, T$_{oven}$ = 500 °C, Gas: He				
[mm]	center	1/2 radius	2/3 radius	wall
-5	379.0	411.3	426.2	483.2
0	388.1	418.8	431.7	486.9
5	399.1	425.5	436.8	488.2
10	408.0	431.4	441.9	489.3
15	417.1	438.1	447.1	490.9
20	424.5	443.7	452.2	494.7
25	432.1	449.1	457.5	494.7
30	438.5	454.3	462.1	494.7
35	444.3	459.2	465.2	495.8
40	450.3	463.5	469.1	498.3
45	455.3	467.3	472.5	499.2
50	460.4	471.4	474.8	499.9
55	465.2	474.3	477.6	500.6
60	468.9	476.6	480.1	501.8
65	472.2	479.9	482.5	502.1
70	475.6	482.1	484.9	502.3
75	478.1	484.4	487.0	502.7
80	480.8	485.9	488.9	503.5
85	483.3	487.7	490.7	503.9
90	485.3	489.0	492.2	504.1
95	487.3	490.4	493.7	504.3
100	489.1	492.1	495.1	504.4
105	490.8	493.8	496.6	504.4

2.2 FeCr 580 µm

coordinates	Position of thermocouples			
Flow rate = 10 SLM, T$_{oven}$ = 300 °C, Gas: N$_2$				
[mm]	center	1/2 radius	2/3 radius	wall
-5	243.1	254.3	261.3	294.0
0	246.4	257.7	263.6	296.2
5	250.3	261.5	266.3	296.7
10	254.2	265.1	269.0	297.5
15	258.3	268.2	272.0	297.1
20	262.1	271.0	274.6	297.9
25	265.9	274.3	276.9	298.5
30	269.3	277.1	279.3	299.0
35	272.5	279.7	281.6	299.6
40	275.3	282.2	283.6	300.5
45	277.9	284.3	285.4	301.3
50	280.2	286.0	287.1	301.5
55	282.4	287.4	288.6	301.6
60	284.3	288.6	289.9	302.5
65	286.0	290.0	291.1	302.4
70	287.5	291.0	292.2	302.5
75	288.9	292.1	293.2	302.6
80	290.2	292.9	294.0	303.0
85	291.3	293.8	294.8	303.2
90	292.3	294.3	295.5	303.3
95	293.1	295.1	296.2	303.4
100	293.9	295.4	296.7	303.5
105	294.6	296.0	297.3	303.7

coordinates	Position of thermocouples			
Flow rate = 15 SLM, T$_{oven}$ = 300 °C, Gas: N$_2$				
[mm]	center	1/2 radius	2/3 radius	wall
-5	207.9	224.6	235.1	286.9
0	211.0	228.4	237.5	291.7
5	215.0	232.4	240.3	291.5
10	219.2	236.4	243.3	291.5
15	223.6	240.1	246.8	291.6
20	227.9	243.8	249.8	292.7
25	232.4	248.0	252.9	293.3
30	236.7	251.8	256.4	294.0
35	241.0	255.7	259.7	294.8
40	245.0	258.4	262.6	296.1
45	248.8	261.3	265.4	297.2
50	252.3	263.5	267.9	297.3
55	255.7	266.3	270.4	297.5
60	258.8	268.4	272.4	299.4
65	261.9	270.0	274.6	299.4
70	264.5	272.4	276.5	299.4
75	267.1	274.2	278.5	298.9
80	269.4	275.9	280.3	299.9
85	271.7	277.8	282.0	300.6
90	273.8	279.3	283.6	300.6
95	275.7	280.9	285.1	300.7
100	277.5	282.3	286.6	301.1
105	279.4	284.0	288.3	301.3

Flow rate = 20 SLM, T_{oven} = 300 °C, Gas: N_2			
coordinates	Position of thermocouples		
[mm]	center	1/2 radius	2/3 radius	wall
-5	180.9	201.6	213.7	281.9
0	183.6	205.0	215.9	286.5
5	187.1	208.8	218.6	286.9
10	190.9	212.7	221.5	287.4
15	195.2	216.7	225.3	287.4
20	199.3	220.3	228.6	288.5
25	203.9	224.8	232.0	289.3
30	208.2	228.9	235.9	290.0
35	212.7	231.8	239.6	291.0
40	216.9	234.9	243.1	292.8
45	221.0	238.7	246.4	293.7
50	224.8	241.6	249.4	294.1
55	228.8	244.4	252.3	294.1
60	232.4	247.4	254.9	295.1
65	236.2	249.8	257.5	295.8
70	239.4	251.9	260.0	295.9
75	242.9	254.6	262.7	296.6
80	246.0	257.6	265.2	297.2
85	249.1	260.2	267.8	298.3
90	251.9	262.0	270.1	298.1
95	254.7	264.5	272.4	298.3
100	257.4	266.3	274.9	299.2
105	260.4	268.6	277.4	299.4

Flow rate = 25 SLM, T_{oven} = 300 °C, Gas: N_2			
coordinates	Position of thermocouples		
[mm]	center	1/2 radius	2/3 radius	wall
-5	161.0	184.9	196.4	275.8
0	163.0	187.9	198.4	283.8
5	166.0	191.3	200.9	284.4
10	169.1	194.6	203.8	284.4
15	172.9	198.2	207.5	284.6
20	176.7	201.6	210.9	285.5
25	180.8	205.9	214.3	286.6
30	184.9	209.3	218.3	287.1
35	189.1	213.1	222.3	288.3
40	193.3	217.7	226.3	291.0
45	197.4	220.8	229.6	291.5
50	201.3	224.7	233.2	291.8
55	205.4	227.9	236.3	292.1
60	209.1	230.5	239.1	293.4
65	212.9	233.4	242.2	294.6
70	216.6	236.6	245.0	295.4
75	220.2	239.4	248.1	295.3
80	223.7	242.9	251.1	296.1
85	227.3	245.9	254.1	297.2
90	230.4	246.9	257.0	297.2
95	233.8	248.3	260.2	297.3
100	237.1	250.3	263.3	298.4
105	240.7	253.2	266.7	299.2

Flow rate = 30 SLM, T_{oven} = 300 °C, Gas: N_2			
coordinates	Position of thermocouples		
[mm]	center	1/2 radius	2/3 radius	wall
-5	145.5	170.7	183.2	271.2
0	147.4	173.4	184.5	278.2
5	149.8	176.2	186.3	278.7
10	152.4	179.0	188.8	279.2
15	155.5	182.3	192.3	279.3
20	158.7	185.4	195.7	281.4
25	162.4	189.9	199.1	283.2
30	166.0	194.1	203.0	284.0
35	169.8	198.2	207.1	285.2
40	173.6	202.0	211.0	289.2
45	177.3	205.4	214.8	289.2
50	181.0	209.1	218.2	289.3
55	184.7	211.5	221.4	289.8
60	188.5	214.5	224.4	290.7
65	192.1	217.0	227.5	291.2
70	195.8	220.9	230.6	291.4
75	199.2	223.4	234.0	291.9
80	203.0	225.4	237.3	293.1
85	206.6	228.9	240.8	294.8
90	209.9	230.3	244.0	294.9
95	213.4	233.4	247.6	295.2
100	217.2	236.6	251.2	296.0
105	221.1	238.5	255.7	296.6

Flow rate = 35 SLM, T_{oven} = 300 °C, Gas: N_2			
coordinates	Position of thermocouples		
[mm]	center	1/2 radius	2/3 radius	wall
-5	131.7	157.4	170.1	269.4
0	133.2	159.6	171.0	276.7
5	135.3	162.2	172.8	277.1
10	137.4	164.6	174.8	278.1
15	139.8	167.2	177.9	278.6
20	142.7	170.1	181.3	279.3
25	145.6	173.9	184.6	280.4
30	148.9	176.4	188.5	281.2
35	152.1	180.1	192.4	282.4
40	155.4	183.3	196.4	285.7
45	158.9	187.7	200.3	286.3
50	162.0	190.6	203.6	286.6
55	165.3	193.6	206.8	286.7
60	168.4	197.2	209.9	286.9
65	171.9	200.5	213.1	287.1
70	175.3	203.6	216.3	287.4
75	178.9	205.4	220.2	288.5
80	182.3	208.3	223.5	292.0
85	185.8	211.7	227.1	292.0
90	188.8	213.8	230.6	292.2
95	192.2	214.9	234.4	292.4
100	196.1	216.9	239.0	294.1
105	200.7	220.2	244.1	294.6

Flow rate = 10 SLM, T_{oven} = 500 °C, Gas: N_2				
coordinates	Position of thermocouples			
[mm]	center	1/2 radius	2/3 radius	wall
-5	423.5	441.8	450.0	491.8
0	429.3	447.6	454.5	496.2
5	436.5	453.2	458.5	497.4
10	443.2	458.9	462.5	497.4
15	449.8	463.5	467.3	498.4
20	455.8	467.5	471.1	500.0
25	461.5	472.3	474.9	501.1
30	466.6	476.4	478.7	501.7
35	470.9	479.4	481.6	502.6
40	474.9	482.4	484.7	504.2
45	478.5	485.1	487.4	504.9
50	481.8	487.6	489.5	504.9
55	485.3	489.4	491.4	505.2
60	487.2	490.8	493.1	506.1
65	489.3	492.4	494.8	506.1
70	491.1	494.4	495.9	506.1
75	492.8	495.4	497.1	506.4
80	494.2	496.8	498.2	506.8
85	495.6	497.7	499.0	506.8
90	496.6	498.7	499.8	506.8
95	497.6	499.2	500.4	506.8
100	498.3	499.8	501.0	506.7
105	499.1	500.3	501.5	506.7

Flow rate = 15 SLM, T_{oven} = 500 °C, Gas: N_2				
coordinates	Position of thermocouples			
[mm]	center	1/2 radius	2/3 radius	wall
-5	372.2	401.5	414.6	482.6
0	378.2	408.8	418.8	489.6
5	385.7	414.8	423.5	490.3
10	393.3	421.2	428.4	489.9
15	401.7	427.4	434.0	491.6
20	409.5	433.5	439.3	493.5
25	417.3	439.6	444.3	494.9
30	424.6	445.5	449.6	496.0
35	431.1	449.6	454.5	497.2
40	437.6	455.2	459.0	499.5
45	443.3	459.0	463.1	500.2
50	448.6	462.4	466.7	500.3
55	453.6	465.8	470.3	500.8
60	458.1	468.5	473.3	502.2
65	462.1	471.7	476.2	502.6
70	465.8	474.2	479.0	502.8
75	469.2	477.5	481.7	502.9
80	472.4	479.6	483.9	503.9
85	475.5	482.1	486.2	503.9
90	478.0	483.8	488.0	504.1
95	480.5	485.7	489.8	504.2
100	482.8	487.4	491.6	504.4
105	485.3	489.6	493.5	504.4

Flow rate = 20 SLM, T_{oven} = 500 °C, Gas: N_2				
coordinates	Position of thermocouples			
[mm]	center	1/2 radius	2/3 radius	wall
-5	325.0	362.9	379.9	476.0
0	330.4	369.8	384.2	484.0
5	337.7	376.4	388.2	484.1
10	344.7	383.2	393.1	484.2
15	352.8	389.5	399.2	485.5
20	360.9	395.6	405.2	487.6
25	369.7	401.5	410.8	489.2
30	377.9	407.8	417.5	490.6
35	385.6	413.5	423.1	492.7
40	393.2	419.3	428.9	494.8
45	400.2	424.7	434.2	495.5
50	407.0	429.7	439.1	495.6
55	413.8	434.3	443.6	496.5
60	419.7	438.5	447.9	497.6
65	425.4	442.7	452.0	498.7
70	430.5	447.1	456.5	498.0
75	435.5	450.2	460.1	499.1
80	440.3	454.1	463.7	500.3
85	445.1	457.7	467.3	500.7
90	449.1	461.3	470.6	501.0
95	453.4	464.3	473.7	501.5
100	457.6	467.4	477.3	502.0
105	462.3	471.2	480.9	502.0

Flow rate = 25 SLM, T_{oven} = 500 °C, Gas: N_2				
coordinates	Position of thermocouples			
[mm]	center	1/2 radius	2/3 radius	wall
-5	285.4	328.4	350.3	469.2
0	289.8	334.5	353.2	478.0
5	295.8	341.3	357.5	479.1
10	302.3	347.4	362.1	480.1
15	310.1	353.8	368.7	480.5
20	317.5	360.1	374.4	483.6
25	325.6	368.1	380.2	485.3
30	333.9	371.9	387.4	486.5
35	341.8	379.1	393.8	488.6
40	349.8	385.1	400.4	491.7
45	357.4	391.4	406.4	492.6
50	364.8	396.8	412.1	492.6
55	372.3	402.4	417.5	493.1
60	379.1	407.0	422.6	494.5
65	385.7	412.4	427.5	494.7
70	391.8	417.4	432.4	494.6
75	398.0	423.3	437.6	496.0
80	403.7	427.8	442.3	498.6
85	409.7	431.6	447.0	499.4
90	415.1	435.8	451.5	499.7
95	420.9	438.7	456.0	500.2
100	426.8	442.6	461.2	500.7
105	433.4	448.7	467.0	500.8

Flow rate = 30 SLM, T_{oven} = 500 °C, Gas: N_2			
coordinates [mm]	Position of thermocouples		
	center	1/2 radius	2/3 radius	wall
-5	254.9	303.2	324.8	465.2
0	258.9	308.4	327.6	473.2
5	264.2	314.1	331.1	475.2
10	269.8	319.6	335.0	473.9
15	276.1	325.3	340.9	475.7
20	282.8	331.1	346.6	478.4
25	290.4	339.2	353.3	479.9
30	298.0	345.8	360.9	481.3
35	305.3	352.2	367.0	483.4
40	312.5	359.1	374.2	486.5
45	320.2	365.6	380.2	488.8
50	327.1	370.1	386.2	488.2
55	334.5	376.6	392.1	488.4
60	341.4	381.1	397.5	489.0
65	348.5	385.4	402.8	490.3
70	354.7	390.4	408.6	491.2
75	361.8	396.3	414.7	491.4
80	367.8	401.1	420.3	493.7
85	374.4	405.5	425.8	494.2
90	380.6	408.9	431.5	494.7
95	387.2	411.8	437.1	495.8
100	394.5	416.3	443.8	497.8
105	402.8	423.1	451.2	497.8

Flow rate = 35 SLM, T_{oven} = 500 °C, Gas: N_2			
coordinates [mm]	Position of thermocouples		
	center	1/2 radius	2/3 radius	wall
-5	231.1	283.4	304.4	456.9
0	234.4	287.2	306.2	468.9
5	238.8	290.8	309.2	469.6
10	243.8	295.6	313.7	469.9
15	249.5	301.0	319.4	471.4
20	255.3	305.8	324.4	474.3
25	262.1	312.8	330.8	476.2
30	269.0	319.6	338.1	477.8
35	275.6	326.9	345.2	479.9
40	282.6	333.5	351.8	484.0
45	289.6	339.9	358.4	485.4
50	296.0	345.9	364.4	485.1
55	302.6	352.3	370.3	485.4
60	309.0	357.9	375.9	486.3
65	315.7	363.0	381.8	486.9
70	322.0	367.9	388.0	486.2
75	328.6	372.2	394.5	488.3
80	335.3	376.0	400.5	491.5
85	341.7	379.2	406.9	492.6
90	348.2	384.5	413.1	492.3
95	355.0	388.4	419.6	493.8
100	362.9	395.8	427.6	495.4
105	372.2	399.1	436.7	495.5

Flow rate = 10 SLM, T_{oven} = 500 °C, Gas: He			
coordinates [mm]	Position of thermocouples		
	center	1/2 radius	2/3 radius	wall
-5	495.1	497.3	498.6	503.6
0	496.7	498.8	499.7	505.4
5	498.3	500.0	500.8	506.2
10	499.6	501.2	501.8	506.5
15	500.8	502.1	502.7	506.9
20	501.7	502.8	503.3	507.5
25	502.5	503.5	503.9	507.8
30	503.2	504.0	504.4	508.1
35	503.8	504.4	504.8	508.4
40	504.2	504.7	505.1	508.7
45	504.5	505.0	505.3	508.8
50	504.8	505.3	505.6	508.8
55	505.1	505.5	505.8	508.9
60	505.4	505.6	505.9	508.9
65	505.5	505.7	506.0	508.9
70	505.5	505.7	506.0	508.9
75	505.6	505.7	506.0	509.0
80	505.5	505.6	505.9	509.0
85	505.4	505.5	505.7	508.8
90	505.3	505.4	505.6	508.6
95	505.2	505.2	505.4	508.5
100	505.0	505.0	505.2	508.1
105	504.7	504.7	504.9	508.1

Flow rate = 15 SLM, T_{oven} = 500 °C, Gas: He			
coordinates [mm]	Position of thermocouples		
	center	1/2 radius	2/3 radius	wall
-5	470.4	478.4	481.9	495.8
0	474.7	482.2	484.7	500.2
5	479.0	485.7	487.8	501.5
10	482.8	488.7	490.1	502.1
15	486.3	491.0	492.7	502.9
20	489.3	493.2	494.5	504.0
25	492.0	495.3	496.4	504.8
30	494.2	497.0	498.1	505.4
35	496.0	498.5	499.3	506.0
40	497.5	499.7	500.5	506.9
45	498.9	500.8	501.4	507.4
50	500.0	501.6	502.2	507.4
55	501.0	502.4	502.9	507.6
60	501.9	503.0	503.5	508.2
65	502.5	503.5	504.0	508.2
70	503.1	503.9	504.3	508.2
75	503.5	504.2	504.6	508.3
80	503.9	504.4	504.8	508.3
85	504.2	504.6	505.0	508.4
90	504.3	504.6	505.0	508.3
95	504.4	504.7	505.0	508.3
100	504.4	504.7	505.0	508.3
105	504.4	504.6	504.8	507.9

Flow rate = 20 SLM, T_{oven} = 500 °C, Gas: He				
coordinates [mm]	Position of thermocouples			
	center	1/2 radius	2/3 radius	wall
-5	439.5	455.0	460.9	487.9
0	446.0	460.4	465.4	493.9
5	452.4	465.7	470.0	495.6
10	458.6	470.7	473.8	496.2
15	464.7	474.7	478.0	497.5
20	469.9	478.5	481.2	499.0
25	474.6	482.3	484.3	500.2
30	478.8	485.3	487.4	501.1
35	482.2	488.0	489.8	502.2
40	485.4	490.6	492.1	503.8
45	488.1	492.6	493.8	504.7
50	490.4	494.4	495.5	504.9
55	492.6	496.1	496.9	505.2
60	494.3	497.2	498.2	506.1
65	495.8	498.4	499.2	506.1
70	497.1	499.3	500.2	506.2
75	498.4	500.2	501.1	506.5
80	499.3	500.7	501.6	507.0
85	500.1	501.3	502.1	507.0
90	500.8	501.7	502.5	507.1
95	501.3	502.1	502.9	507.2
100	501.8	502.4	503.1	507.1
105	502.1	502.6	503.4	507.1

Flow rate = 25 SLM, T_{oven} = 500 °C, Gas: He				
coordinates [mm]	Position of thermocouples			
	center	1/2 radius	2/3 radius	wall
-5	405.2	431.1	439.1	479.0
0	413.6	437.9	444.7	487.0
5	423.5	445.0	450.5	489.9
10	432.0	450.6	455.4	490.4
15	439.7	456.6	461.2	491.9
20	447.8	461.7	465.8	493.7
25	454.3	466.9	470.1	495.2
30	460.2	471.6	474.4	496.5
35	465.3	475.5	477.7	498.0
40	470.2	478.8	481.1	500.1
45	474.1	482.0	484.0	501.3
50	477.5	484.7	486.5	501.6
55	481.1	487.2	488.8	502.0
60	483.7	489.2	490.8	503.6
65	486.3	491.1	492.7	503.7
70	488.5	492.6	494.2	503.7
75	490.4	494.1	495.6	504.0
80	492.2	495.2	496.7	504.9
85	493.7	496.2	497.7	504.9
90	495.0	497.0	498.6	505.0
95	496.1	497.7	499.3	505.3
100	497.1	498.6	500.0	505.5
105	498.0	499.4	500.7	505.6

Flow rate = 30 SLM, T_{oven} = 500 °C, Gas: He				
coordinates [mm]	Position of thermocouples			
	center	1/2 radius	2/3 radius	wall
-5	374.3	408.1	418.5	472.6
0	384.3	416.4	425.3	481.7
5	394.5	424.1	431.8	484.3
10	405.1	431.2	437.9	485.0
15	415.1	438.2	444.5	486.6
20	423.9	444.2	450.0	488.9
25	432.7	450.9	455.1	490.8
30	440.2	456.6	461.0	492.4
35	446.9	462.7	465.5	494.3
40	452.8	466.4	469.7	496.6
45	458.2	470.5	473.5	498.1
50	463.2	474.3	476.7	498.5
55	467.7	477.4	480.0	499.0
60	471.8	480.3	482.8	500.9
65	475.3	482.9	485.2	500.9
70	478.3	485.0	487.3	501.0
75	481.3	487.1	489.4	501.6
80	483.8	488.6	491.0	502.8
85	485.9	490.0	492.6	502.8
90	487.8	491.2	493.9	503.1
95	489.6	492.4	495.1	503.6
100	491.2	493.8	496.3	504.0
105	492.8	495.2	497.4	504.2

2.3   NiCr 1200 µm

coordinates [mm]	Flow rate = 10 SLM, T$_{oven}$ = 300 °C, Gas: N$_2$ Position of thermocouples			
	center	1/2 radius	2/3 radius	wall
-5	248.1	254.6	265.5	293.2
0	250.6	258.5	267.2	296.5
5	253.8	261.4	269.6	296.8
10	257.1	264.3	271.6	297.7
15	260.5	267.5	274.1	298.1
20	263.5	270.3	276.4	300.0
25	266.6	273.1	278.7	300.4
30	269.6	275.7	280.7	300.3
35	272.3	278.2	282.7	300.4
40	274.8	280.6	284.4	301.0
45	277.2	282.5	286.0	301.4
50	279.5	284.3	287.4	301.7
55	281.5	286.0	288.5	301.8
60	283.3	287.4	289.8	302.2
65	285.0	288.7	290.9	302.4
70	286.5	289.9	291.8	302.5
75	287.8	291.0	292.7	302.7
80	289.1	291.9	293.8	303.1
85	290.2	292.7	294.5	303.2
90	291.2	293.5	295.2	303.3
95	292.0	294.1	295.8	303.4
100	292.8	294.7	296.5	303.5
105	293.5	295.3	297.1	303.6

coordinates [mm]	Flow rate = 15 SLM, T$_{oven}$ = 300 °C, Gas: N$_2$ Position of thermocouples			
	center	1/2 radius	2/3 radius	wall
-5	216.1	227.0	243.0	287.6
0	218.7	230.6	244.8	291.7
5	222.0	233.9	246.8	291.7
10	225.1	237.0	248.9	292.0
15	228.5	240.3	251.8	294.7
20	232.0	243.5	254.7	295.7
25	235.6	247.5	257.7	296.2
30	239.0	250.9	260.7	296.6
35	242.4	254.4	263.1	296.6
40	245.7	257.6	265.7	297.3
45	249.0	260.6	267.9	297.7
50	252.1	263.2	270.3	298.2
55	255.5	265.6	272.5	298.8
60	258.1	267.7	274.7	299.3
65	260.4	270.0	276.4	299.5
70	263.2	272.1	278.5	299.7
75	265.7	274.1	280.3	300.1
80	268.0	275.8	282.3	300.8
85	270.2	277.4	283.8	300.8
90	272.0	278.9	285.3	300.9
95	273.9	280.3	286.7	301.0
100	275.7	281.5	288.3	301.3
105	277.5	282.9	289.5	301.8

coordinates [mm]	Flow rate = 20 SLM, T$_{oven}$ = 300 °C, Gas: N$_2$ Position of thermocouples			
	center	1/2 radius	2/3 radius	wall
-5	190.9	204.2	224.0	282.8
0	192.9	207.9	225.7	286.3
5	195.8	210.9	227.5	286.8
10	198.7	213.8	229.6	288.3
15	201.8	217.3	232.6	291.6
20	205.1	220.5	236.2	292.3
25	208.4	224.6	239.1	292.8
30	211.9	228.4	242.5	293.4
35	215.3	232.4	245.2	293.6
40	218.7	236.0	248.1	294.6
45	222.1	239.3	250.6	295.1
50	225.7	242.4	253.0	295.6
55	229.2	245.2	255.6	296.2
60	232.3	247.9	257.9	296.9
65	235.7	250.7	260.4	297.1
70	238.6	253.3	262.7	297.6
75	241.6	256.4	265.2	298.3
80	244.5	258.0	267.1	298.9
85	247.4	260.4	269.0	299.1
90	249.9	262.4	270.9	299.1
95	252.7	264.2	272.7	299.3
100	255.2	266.0	275.3	299.5
105	257.7	268.2	278.5	299.6

coordinates [mm]	Flow rate = 25 SLM, T$_{oven}$ = 300 °C, Gas: N$_2$ Position of thermocouples			
	center	1/2 radius	2/3 radius	wall
-5	173.6	188.3	210.8	282.1
0	175.3	191.4	212.1	288.1
5	177.6	194.5	213.8	286.2
10	180.3	197.0	215.6	286.5
15	182.9	200.4	218.6	291.3
20	185.8	203.7	221.8	293.3
25	188.8	207.6	225.3	293.4
30	191.9	211.4	228.8	293.0
35	195.0	215.5	231.7	292.8
40	198.1	219.3	234.9	293.0
45	201.4	222.6	237.5	293.6
50	204.8	225.8	240.2	294.2
55	208.3	228.8	243.0	295.4
60	211.4	231.5	245.8	296.1
65	214.8	234.7	248.3	296.7
70	217.7	237.3	250.6	296.9
75	220.9	240.2	252.9	297.9
80	223.9	242.6	254.8	298.7
85	227.2	245.1	256.9	298.8
90	230.1	247.4	258.8	298.8
95	233.0	249.6	261.2	299.0
100	236.1	251.7	264.2	299.6
105	239.2	254.5	268.1	300.1

Flow rate = 30 SLM, T$_{oven}$ = 300 °C, Gas: N$_2$			
coordinates [mm]	Position of thermocouples		
	center	1/2 radius	2/3 radius	wall
-5	158.7	174.1	198.4	278.7
0	160.2	177.0	199.3	284.2
5	162.2	179.4	200.6	282.8
10	164.4	182.0	202.6	283.1
15	166.8	185.1	205.4	287.2
20	169.3	188.2	208.4	290.2
25	171.9	191.9	212.0	290.9
30	174.7	195.7	215.3	288.6
35	177.3	199.5	218.3	290.6
40	180.0	203.1	221.5	291.1
45	183.0	206.5	224.1	291.0
50	186.1	209.5	226.8	291.6
55	189.1	212.6	229.6	292.1
60	192.2	215.5	232.2	293.6
65	195.3	218.5	234.5	294.1
70	198.2	221.3	236.7	295.0
75	201.2	224.2	239.1	295.5
80	204.3	226.9	241.1	296.0
85	207.5	229.4	243.2	296.3
90	210.5	232.1	245.3	296.3
95	213.5	234.4	248.0	296.6
100	216.8	236.8	251.6	297.4
105	220.2	239.9	256.4	297.9

Flow rate = 35 SLM, T$_{oven}$ = 300 °C, Gas: N$_2$			
coordinates [mm]	Position of thermocouples		
	center	1/2 radius	2/3 radius	wall
-5	144.5	160.3	186.0	273.0
0	145.8	162.9	186.5	282.2
5	147.4	164.7	187.7	280.2
10	149.2	166.8	189.1	280.1
15	151.1	169.6	191.8	283.9
20	153.3	172.7	194.9	288.3
25	155.6	175.8	198.5	288.8
30	157.9	179.5	201.8	285.8
35	160.1	183.3	205.0	289.0
40	162.7	186.9	207.9	289.7
45	165.2	190.1	210.7	289.2
50	167.9	193.2	213.3	289.1
55	170.6	196.3	216.1	289.7
60	173.2	199.2	218.7	291.7
65	176.0	202.1	221.2	291.7
70	178.8	204.9	223.5	292.0
75	181.5	207.8	225.7	293.5
80	184.5	210.6	227.9	294.7
85	187.6	213.3	230.0	294.5
90	190.5	216.1	232.3	294.4
95	193.5	218.5	235.1	294.6
100	196.8	221.0	239.2	295.7
105	200.2	224.4	244.2	297.3

Flow rate = 10 SLM, T$_{oven}$ = 500 °C, Gas: N$_2$			
coordinates [mm]	Position of thermocouples		
	center	1/2 radius	2/3 radius	wall
-5	424.2	435.8	451.8	491.1
0	429.5	441.7	456.0	496.6
5	435.8	447.5	459.8	496.9
10	442.1	453.1	463.8	498.5
15	448.2	457.9	468.3	499.0
20	454.1	462.4	472.0	499.8
25	459.3	467.6	475.7	501.0
30	464.3	471.8	479.2	501.6
35	468.6	475.7	482.0	502.3
40	472.6	479.1	484.8	503.1
45	476.3	482.2	487.3	503.5
50	479.8	485.4	489.3	503.8
55	482.8	487.4	491.0	504.3
60	485.3	489.3	492.6	504.9
65	487.7	491.3	493.9	505.3
70	489.5	492.9	495.3	505.6
75	491.4	494.6	496.4	506.0
80	493.1	495.7	497.5	506.3
85	494.6	497.0	498.4	506.4
90	495.7	497.8	499.2	506.5
95	496.7	498.6	499.8	506.7
100	497.7	499.3	500.5	507.0
105	498.6	499.9	501.0	507.0

Flow rate = 15 SLM, T$_{oven}$ = 500 °C, Gas: N$_2$			
coordinates [mm]	Position of thermocouples		
	center	1/2 radius	2/3 radius	wall
-5	384.4	403.5	423.7	483.0
0	389.3	410.0	427.0	490.2
5	395.6	414.9	431.5	490.5
10	402.1	420.8	435.8	491.8
15	408.8	426.3	440.9	492.8
20	415.2	431.6	445.5	494.2
25	421.7	437.7	450.3	495.1
30	427.6	443.3	454.5	496.1
35	433.2	448.3	458.7	496.9
40	438.7	453.0	462.4	498.1
45	443.8	457.2	465.9	498.2
50	448.7	461.2	469.1	498.7
55	453.3	464.7	472.0	499.3
60	457.3	467.8	474.8	500.2
65	461.3	470.8	477.1	500.8
70	464.9	473.8	479.3	501.2
75	468.1	476.7	481.6	501.9
80	471.4	478.9	483.6	502.6
85	474.2	481.1	485.5	502.8
90	476.8	483.1	487.3	503.0
95	479.3	485.0	489.0	503.4
100	481.8	486.8	491.0	504.8
105	484.2	488.8	493.2	504.8

Flow rate = 20 SLM, T$_{oven}$ = 500 °C, Gas: N$_2$			
coordinates [mm]	Position of thermocouples		
	center	1/2 radius	2/3 radius	wall
-5	339.9	367.4	393.4	476.1
0	344.4	373.8	396.9	483.9
5	350.7	378.4	400.5	484.7
10	356.9	384.3	405.0	486.8
15	363.6	390.1	410.4	487.4
20	370.5	395.3	416.2	489.3
25	377.5	402.1	421.4	490.2
30	384.4	408.6	427.0	491.3
35	390.6	414.8	431.8	492.1
40	397.2	420.8	436.5	493.3
45	403.5	425.9	440.6	493.7
50	409.6	430.7	444.8	494.1
55	415.8	435.4	448.5	494.7
60	421.2	439.6	452.1	496.2
65	426.3	443.9	455.5	496.8
70	430.9	447.8	458.9	497.3
75	435.7	452.1	461.9	498.2
80	440.2	455.2	464.8	499.3
85	444.8	459.0	467.6	499.5
90	448.8	461.9	470.6	499.7
95	452.8	464.7	473.5	500.2
100	457.2	467.6	476.7	502.2
105	461.5	471.5	481.5	502.4

Flow rate = 25 SLM, T$_{oven}$ = 500 °C, Gas: N$_2$			
coordinates [mm]	Position of thermocouples		
	center	1/2 radius	2/3 radius	wall
-5	301.3	332.9	366.2	471.2
0	305.9	338.9	369.2	476.2
5	311.3	344.1	373.2	479.3
10	317.3	349.3	377.6	481.5
15	323.5	355.7	382.7	482.8
20	329.7	361.3	388.3	485.0
25	336.3	368.3	394.6	485.8
30	343.4	375.9	401.0	487.0
35	349.5	382.5	406.1	488.6
40	356.6	388.5	411.5	491.2
45	363.4	394.7	416.6	491.9
50	370.5	400.7	421.7	492.6
55	377.1	405.8	426.8	493.2
60	383.2	411.1	431.9	495.0
65	389.0	415.6	436.4	495.4
70	394.5	420.4	441.0	496.3
75	399.8	424.8	445.3	497.5
80	405.0	428.9	449.3	498.2
85	410.3	433.5	453.4	498.3
90	415.7	437.4	457.2	498.7
95	420.6	441.3	461.5	499.2
100	426.4	445.0	466.0	499.7
105	432.3	450.5	472.3	500.9

Flow rate = 30 SLM, T$_{oven}$ = 500 °C, Gas: N$_2$			
coordinates [mm]	Position of thermocouples		
	center	1/2 radius	2/3 radius	wall
-5	274.5	307.6	346.9	466.3
0	278.8	315.1	349.4	475.2
5	283.8	319.7	352.8	475.6
10	288.5	324.2	356.6	477.2
15	294.2	330.4	362.1	479.0
20	300.3	335.8	367.7	480.9
25	306.1	343.0	374.0	481.4
30	312.2	349.4	380.2	482.3
35	318.6	357.0	385.8	484.1
40	325.2	363.7	391.2	486.5
45	331.5	369.7	396.1	487.9
50	338.2	375.6	401.2	488.3
55	343.8	380.6	406.3	488.8
60	350.4	385.7	411.2	490.9
65	356.7	391.2	415.8	491.4
70	362.1	396.3	420.5	491.9
75	368.1	401.3	425.0	492.8
80	374.4	406.1	428.9	494.0
85	380.4	410.9	433.0	494.2
90	386.1	415.1	436.7	494.4
95	392.4	419.6	441.8	495.2
100	398.9	424.4	447.5	496.4
105	406.9	430.9	455.7	498.9

Flow rate = 35 SLM, T$_{oven}$ = 500 °C, Gas: N$_2$			
coordinates [mm]	Position of thermocouples		
	center	1/2 radius	2/3 radius	wall
-5	247.1	282.9	326.3	460.7
0	250.6	287.3	328.8	470.5
5	254.9	291.7	331.6	471.5
10	259.6	296.0	335.7	474.1
15	264.6	302.0	341.2	475.3
20	270.0	307.2	346.6	476.8
25	275.5	314.4	353.8	477.6
30	280.9	321.5	360.2	478.6
35	286.3	328.4	365.7	480.4
40	291.8	334.9	370.9	483.2
45	297.7	341.1	374.5	485.1
50	303.4	346.6	381.0	485.4
55	309.4	352.5	386.0	486.3
60	315.7	357.9	391.1	488.6
65	321.9	363.6	395.7	489.2
70	327.4	368.5	400.2	489.6
75	333.3	374.2	404.6	490.7
80	339.2	378.7	408.5	492.4
85	345.7	384.3	412.7	492.6
90	352.0	389.1	416.5	492.8
95	358.5	394.1	421.8	493.9
100	365.8	399.8	429.2	497.4
105	374.5	407.4	439.0	497.6

Flow rate = 15 SLM, T_{oven} = 500 °C, Gas: He					Flow rate = 20 SLM, T_{oven} = 500 °C, Gas: He			
coordinates	Position of thermocouples				coordinates	Position of thermocouples		
[mm]	center	1/2 radius	2/3 radius	wall	[mm]	center	1/2 radius	2/3 radius	wall
-5	482.5	485.5	489.5	496.4	-5	456.4	464.2	472.0	488.3
0	485.1	487.8	491.4	498.9	0	461.0	468.6	476.0	492.4
5	487.7	490.1	493.3	500.7	5	466.2	472.3	479.1	494.4
10	490.0	492.1	494.9	501.7	10	470.7	476.0	482.1	496.3
15	492.2	493.9	496.5	502.1	15	474.8	479.6	484.9	497.2
20	494.0	495.4	497.7	502.9	20	478.5	482.2	487.3	498.4
25	495.6	496.8	498.8	503.5	25	481.7	485.3	489.5	499.6
30	496.9	498.0	499.7	504.0	30	484.6	487.6	491.6	500.4
35	498.0	499.0	500.5	504.5	35	487.1	490.0	493.2	501.3
40	499.1	499.9	501.2	505.0	40	489.2	491.9	494.8	502.4
45	499.9	500.7	501.8	505.4	45	491.2	493.5	496.1	503.1
50	500.6	501.2	502.2	505.6	50	492.9	494.9	497.2	503.5
55	501.2	501.8	502.6	505.8	55	494.5	496.2	498.1	504.0
60	501.8	502.2	502.9	506.1	60	495.8	497.2	499.0	504.4
65	502.2	502.6	503.2	506.1	65	496.9	498.2	499.6	504.7
70	502.5	502.9	503.4	506.2	70	497.8	499.0	500.3	504.8
75	502.8	503.1	503.6	506.3	75	498.7	499.7	500.8	505.0
80	503.0	503.3	503.7	506.4	80	499.4	500.2	501.3	505.3
85	503.2	503.4	503.8	506.3	85	500.0	500.8	501.7	505.4
90	503.3	503.4	503.8	506.3	90	500.5	501.2	502.0	505.5
95	503.3	503.4	503.8	506.3	95	501.0	501.5	502.2	505.6
100	503.3	503.4	503.8	506.4	100	501.3	501.8	502.4	505.9
105	503.1	503.2	503.5	506.4	105	501.5	501.9	502.6	505.9

Flow rate = 25 SLM, T_{oven} = 500 °C, Gas: He					Flow rate = 30 SLM, T_{oven} = 500 °C, Gas: He			
coordinates	Position of thermocouples				coordinates	Position of thermocouples		
[mm]	center	1/2 radius	2/3 radius	wall	[mm]	center	1/2 radius	2/3 radius	wall
-5	418.9	433.8	448.1	477.5	-5	378.5	401.3	422.6	465.8
0	426.3	440.3	452.9	482.7	0	387.0	409.2	427.5	473.0
5	434.0	446.2	457.2	486.6	5	396.6	416.1	433.3	476.3
10	440.8	451.6	461.5	488.6	10	405.3	423.1	438.3	478.6
15	447.3	456.7	466.0	491.3	15	413.4	429.3	444.0	482.0
20	453.2	461.2	470.5	493.5	20	421.3	435.5	449.4	485.7
25	458.5	466.4	474.1	495.7	25	428.4	442.0	454.5	489.1
30	463.4	470.4	477.8	497.6	30	435.2	448.0	459.2	491.6
35	467.5	474.4	480.9	498.8	35	440.9	453.1	463.4	493.2
40	471.7	478.1	483.9	500.6	40	446.8	458.2	467.6	495.7
45	475.4	481.3	486.3	501.4	45	452.0	462.5	471.2	496.3
50	478.8	484.0	488.5	502.7	50	457.0	466.7	474.3	496.8
55	482.5	486.3	490.2	503.9	55	461.7	470.3	476.9	498.4
60	484.5	488.4	491.9	504.0	60	465.8	473.4	479.2	499.1
65	486.8	490.5	493.3	504.1	65	469.3	476.4	481.4	499.4
70	488.9	492.1	494.7	504.1	70	472.8	479.2	483.5	499.6
75	490.7	493.8	495.9	504.6	75	475.5	481.6	485.5	500.4
80	492.4	495.0	496.9	505.2	80	478.5	483.7	487.1	501.4
85	493.9	496.2	497.9	505.3	85	480.9	485.7	488.7	501.6
90	495.1	497.1	498.6	505.4	90	483.2	487.4	490.2	501.8
95	496.2	498.0	499.4	505.6	95	485.2	488.9	491.6	502.2
100	497.2	498.8	500.2	506.5	100	487.1	490.5	493.2	503.7
105	498.1	499.5	500.9	506.5	105	488.9	492.1	495.0	503.7

2.4 NiCr 580 µm

Flow rate = 10 SLM, T_{oven} = 300 °C, Gas: N_2					**Flow rate = 15 SLM, T_{oven} = 300 °C, Gas: N_2**			
coordinates	Position of thermocouples				coordinates	Position of thermocouples		
[mm]	center	1/2 radius	2/3 radius	wall	[mm]	center	1/2 radius	2/3 radius	wall
-5	249.8	259.4	265.2	293.7	-5	221.8	235.6	244.5	289.5
0	254.1	263.7	268.5	295.4	0	226.0	239.9	247.8	291.7
5	259.0	267.7	271.5	296.6	5	230.7	243.9	250.9	293.6
10	263.6	271.2	274.7	298.1	10	235.6	248.0	254.3	294.4
15	268.1	274.7	277.9	298.8	15	240.6	252.1	258.2	295.0
20	271.8	277.7	280.7	300.2	20	245.3	255.9	261.8	296.8
25	275.4	280.5	283.2	300.5	25	249.6	259.8	265.0	297.1
30	278.5	283.2	285.5	300.9	30	253.7	263.4	268.3	297.5
35	281.1	285.4	287.3	301.3	35	257.2	266.7	271.0	297.6
40	283.4	287.3	289.1	301.6	40	260.7	269.7	273.5	298.2
45	285.5	289.1	290.6	301.8	45	264.1	272.2	275.9	298.6
50	287.5	290.6	291.9	302.0	50	267.1	274.7	278.0	298.6
55	289.2	291.9	293.0	302.2	55	270.0	277.1	279.8	298.8
60	290.6	293.1	294.1	302.5	60	272.6	279.1	281.4	299.5
65	291.9	294.1	294.8	302.9	65	274.9	281.1	283.0	300.1
70	292.9	294.9	295.6	303.1	70	277.1	282.7	284.2	300.2
75	293.9	295.7	296.2	303.2	75	278.9	284.4	285.5	300.4
80	294.8	296.3	296.8	303.4	80	280.8	285.5	286.5	300.9
85	295.5	296.9	297.2	303.5	85	282.5	286.7	287.7	301.1
90	296.1	297.2	297.6	303.6	90	284.0	287.7	288.6	301.2
95	296.7	297.6	298.1	303.7	95	285.2	288.5	289.5	301.6
100	297.1	298.0	298.4	303.8	100	286.4	289.4	290.6	301.8
105	297.4	298.2	298.8	303.9	105	287.5	290.2	291.5	301.9

Flow rate = 20 SLM, T_{oven} = 300 °C, Gas: N_2					**Flow rate = 25 SLM, T_{oven} = 300 °C, Gas: N_2**			
coordinates	Position of thermocouples				coordinates	Position of thermocouples		
[mm]	center	1/2 radius	2/3 radius	wall	[mm]	center	1/2 radius	2/3 radius	wall
-5	195.8	213.1	225.1	286.7	-5	174.5	193.8	208.7	283.2
0	199.8	217.4	228.1	288.2	0	177.9	197.8	211.4	284.7
5	204.1	221.2	231.0	290.0	5	181.8	200.9	214.3	286.2
10	208.9	225.3	234.5	290.2	10	185.8	205.1	217.4	286.8
15	213.8	229.6	238.9	291.3	15	190.3	209.3	222.1	288.1
20	218.6	233.7	242.8	293.3	20	194.6	214.1	226.0	290.9
25	223.2	238.6	246.4	293.8	25	199.2	218.8	229.8	291.2
30	227.8	242.8	250.3	294.0	30	203.7	223.2	233.7	291.4
35	231.9	246.9	253.4	294.4	35	207.5	227.7	237.5	291.9
40	236.0	250.5	256.9	294.7	40	211.9	231.9	241.3	292.4
45	239.9	254.0	259.8	295.2	45	216.0	235.8	244.6	292.5
50	243.6	256.9	262.4	295.3	50	220.1	239.3	247.6	292.7
55	247.3	259.8	265.0	295.6	55	224.0	242.3	250.7	293.0
60	250.7	262.4	267.5	296.4	60	228.1	245.2	253.6	293.8
65	254.0	265.1	270.0	297.3	65	231.6	248.2	256.3	294.9
70	256.8	267.5	272.1	297.4	70	234.8	251.2	259.0	295.3
75	259.5	269.5	274.3	297.4	75	238.1	253.8	261.4	295.4
80	262.2	271.5	275.8	297.9	80	241.4	256.0	264.1	296.3
85	264.7	273.1	277.4	298.5	85	244.3	257.9	266.3	296.8
90	267.1	274.6	278.8	298.6	90	247.1	259.5	268.4	296.9
95	269.2	276.9	280.4	299.1	95	250.2	261.0	270.7	297.5
100	271.3	278.8	282.3	300.0	100	253.0	262.8	273.5	298.4
105	273.2	279.9	284.8	300.2	105	255.7	265.2	277.1	298.9

Flow rate = 30 SLM, T_{oven} = 300 °C, Gas: N_2				
coordinates	Position of thermocouples			
[mm]	center	1/2 radius	2/3 radius	wall
-5	159.4	179.9	195.3	279.4
0	162.1	183.3	197.9	281.3
5	165.4	186.3	200.2	283.1
10	169.0	189.7	203.7	284.6
15	172.9	193.8	207.6	285.5
20	176.7	197.7	211.8	288.2
25	180.7	203.4	216.0	288.3
30	185.1	207.7	220.1	288.7
35	188.5	211.9	223.7	289.0
40	192.3	216.0	227.5	289.2
45	196.1	219.8	231.0	289.4
50	200.1	223.5	234.4	289.5
55	204.3	227.0	237.7	289.6
60	208.2	230.1	240.4	291.0
65	211.8	233.3	243.3	292.3
70	215.3	236.3	246.0	292.5
75	218.9	239.2	248.4	292.6
80	222.3	241.4	251.1	293.3
85	225.6	243.7	253.3	293.9
90	228.9	245.9	255.6	294.1
95	232.0	248.0	257.8	294.8
100	235.4	250.0	261.2	296.1
105	238.5	252.8	265.7	296.3

Flow rate = 35 SLM, T_{oven} = 300 °C, Gas: N_2				
coordinates	Position of thermocouples			
[mm]	center	1/2 radius	2/3 radius	wall
-5	141.9	163.3	179.5	276.3
0	144.6	166.8	182.1	278.5
5	147.4	169.7	184.5	280.5
10	150.7	172.8	187.7	281.3
15	153.9	176.6	191.9	282.9
20	157.3	180.4	195.8	285.1
25	160.8	185.5	200.2	285.8
30	164.4	190.0	204.5	286.8
35	167.8	194.9	208.4	287.1
40	171.3	199.0	212.5	287.3
45	175.1	203.1	216.1	287.5
50	179.0	206.9	219.6	287.7
55	182.7	210.5	223.0	288.7
60	186.2	213.3	226.3	289.3
65	190.1	216.6	229.7	290.0
70	193.5	220.0	232.8	290.8
75	197.0	223.1	236.1	290.8
80	200.6	226.1	239.0	291.7
85	204.1	229.0	242.4	292.7
90	207.5	232.3	245.4	293.0
95	210.8	235.3	247.7	293.2
100	214.4	238.2	251.6	294.9
105	218.0	241.6	257.2	295.4

Flow rate = 10 SLM, T_{oven} = 500 °C, Gas: N_2				
coordinates	Position of thermocouples			
[mm]	center	1/2 radius	2/3 radius	wall
-5	421.4	435.6	452.2	492.9
0	430.0	443.7	457.5	495.1
5	439.5	451.5	462.3	496.9
10	448.2	458.3	467.0	498.0
15	456.1	464.5	472.3	499.0
20	462.9	469.5	476.5	500.6
25	468.8	475.2	480.5	501.3
30	473.9	479.4	484.3	501.8
35	477.9	483.2	486.6	502.5
40	481.5	486.3	489.2	503.4
45	484.7	489.0	491.2	504.0
50	487.5	491.2	493.1	504.3
55	490.0	493.0	494.5	504.4
60	492.0	494.5	495.8	505.0
65	493.6	496.0	496.9	505.3
70	495.1	497.0	497.9	505.3
75	496.3	498.1	498.7	505.4
80	497.4	498.8	499.4	505.7
85	498.3	499.5	500.1	505.9
90	499.0	500.1	500.5	505.9
95	499.8	500.4	500.9	505.9
100	500.1	500.7	501.2	505.9
105	500.4	501.0	501.5	506.0

Flow rate = 15 SLM, T_{oven} = 500 °C, Gas: N_2				
coordinates	Position of thermocouples			
[mm]	center	1/2 radius	2/3 radius	wall
-5	385.6	409.4	423.4	487.0
0	394.1	417.1	428.9	489.1
5	403.0	424.0	434.5	491.4
10	412.0	430.3	440.2	492.8
15	420.5	437.2	446.5	494.2
20	428.5	443.4	452.0	496.5
25	435.7	449.6	457.0	497.0
30	442.4	455.2	462.0	497.6
35	448.2	460.2	466.0	498.4
40	453.7	464.9	470.1	499.5
45	458.6	469.1	473.6	499.9
50	463.2	472.6	476.5	500.2
55	467.5	475.8	479.1	500.6
60	471.1	478.7	481.2	501.6
65	474.4	481.2	483.4	502.3
70	477.3	483.5	485.3	502.6
75	480.0	485.7	487.0	502.9
80	482.4	487.4	488.6	503.5
85	484.6	489.0	490.0	503.9
90	486.7	490.4	491.3	504.0
95	488.5	491.6	492.7	504.4
100	490.2	492.9	494.2	504.7
105	491.9	494.3	495.8	504.8

Flow rate = 20 SLM, T_oven = 500 °C, Gas: N_2				
coordinates [mm]	Position of thermocouples			
	center	1/2 radius	2/3 radius	wall
-5	341.0	370.1	394.9	481.1
0	348.9	377.9	400.1	483.8
5	358.2	385.3	404.9	487.0
10	367.4	392.8	410.8	488.5
15	376.6	400.5	417.5	490.3
20	385.7	407.5	423.9	492.6
25	394.3	415.8	430.0	493.3
30	402.5	423.4	436.6	493.8
35	409.6	430.4	441.1	494.8
40	416.5	436.5	446.3	496.2
45	423.0	441.9	450.8	497.2
50	429.5	447.1	454.9	497.3
55	435.6	451.6	459.1	497.7
60	441.0	455.7	463.0	498.9
65	445.8	459.9	466.7	499.5
70	450.2	463.2	470.0	499.7
75	454.4	466.7	473.2	500.0
80	458.3	469.3	475.5	500.7
85	462.1	471.9	478.1	501.7
90	465.6	474.2	480.0	501.8
95	469.0	476.3	482.0	502.5
100	472.7	478.9	484.8	503.5
105	476.2	482.3	486.5	503.6

Flow rate = 25 SLM, T_oven = 500 °C, Gas: N_2				
coordinates [mm]	Position of thermocouples			
	center	1/2 radius	2/3 radius	wall
-5	304.7	337.6	368.9	475.4
0	311.8	345.0	373.5	478.4
5	319.9	352.1	378.0	481.2
10	328.5	359.5	383.6	482.6
15	337.5	367.1	390.4	484.9
20	346.2	375.0	397.3	487.6
25	354.9	384.6	404.0	488.4
30	363.4	392.5	410.9	488.9
35	371.0	400.0	415.8	489.7
40	378.7	407.3	421.9	491.2
45	386.1	413.7	427.0	492.0
50	393.3	419.7	432.5	492.2
55	400.4	425.1	437.8	492.6
60	406.8	430.1	442.9	494.0
65	412.9	435.3	448.0	494.5
70	418.4	439.6	452.3	494.6
75	423.7	443.8	456.5	494.8
80	429.0	447.2	460.3	495.8
85	434.0	450.6	463.6	497.1
90	438.8	453.5	466.8	497.1
95	443.6	456.5	469.8	498.1
100	448.9	460.4	473.2	499.5
105	454.6	465.6	479.3	499.7

Flow rate = 30 SLM, T_oven = 500 °C, Gas: N_2				
coordinates [mm]	Position of thermocouples			
	center	1/2 radius	2/3 radius	wall
-5	271.7	307.2	343.6	470.2
0	277.8	313.9	348.7	473.5
5	284.8	321.0	352.2	476.8
10	292.3	327.3	358.1	477.8
15	300.5	335.1	364.5	480.6
20	308.6	342.9	370.9	483.4
25	316.4	353.6	377.7	484.2
30	324.6	361.3	385.6	484.7
35	332.3	369.7	390.4	485.6
40	339.8	377.2	396.6	486.8
45	347.4	384.4	402.2	487.2
50	354.9	390.6	407.6	487.4
55	362.4	396.8	412.9	488.3
60	369.4	402.0	418.2	489.2
65	377.2	408.0	423.4	489.4
70	382.4	413.2	427.7	489.6
75	388.9	418.2	431.9	490.1
80	394.9	422.0	435.6	491.0
85	400.6	425.8	439.3	492.3
90	406.6	429.2	442.8	493.2
95	412.6	432.8	446.4	494.2
100	419.6	437.4	452.6	496.2
105	427.7	445.1	461.6	496.7

Flow rate = 35 SLM, T_oven = 500 °C, Gas: N_2				
coordinates [mm]	Position of thermocouples			
	center	1/2 radius	2/3 radius	wall
-5	243.7	279.5	322.0	465.2
0	249.0	286.0	326.4	468.9
5	254.9	291.9	330.2	472.6
10	261.7	298.7	335.5	474.3
15	268.9	305.9	342.3	477.1
20	276.0	314.2	349.0	480.3
25	283.3	324.9	356.2	481.3
30	290.9	334.1	363.1	482.0
35	298.2	342.6	368.8	483.9
40	305.2	350.6	375.2	485.1
45	312.7	357.7	380.6	485.5
50	319.9	364.1	386.4	485.6
55	326.6	370.1	392.1	486.0
60	333.9	375.8	397.6	486.4
65	340.9	382.2	403.1	487.6
70	347.5	387.5	408.3	488.2
75	353.8	392.6	413.3	488.7
80	360.2	396.8	417.6	489.6
85	366.7	400.7	421.6	490.5
90	373.4	404.9	425.5	490.9
95	381.5	410.1	431.5	492.2
100	389.2	414.8	438.4	494.4
105	399.4	422.7	449.1	495.9

Flow rate = 15 SLM, T_{oven} = 500 °C, Gas: He				
coordinates [mm]	Position of thermocouples			
	center	1/2 radius	2/3 radius	wall
-5	483.7	487.4	491.0	499.8
0	487.1	490.5	493.1	501.7
5	490.3	493.3	495.3	503.5
10	492.9	495.4	497.2	504.2
15	495.3	497.2	498.8	505.0
20	497.1	498.7	500.0	505.9
25	498.8	500.2	501.2	506.5
30	500.1	501.2	502.2	506.7
35	501.0	502.0	502.9	507.0
40	501.9	502.7	503.4	507.6
45	502.6	503.3	504.0	507.8
50	503.2	503.8	504.3	507.9
55	503.7	504.2	504.7	508.0
60	504.1	504.5	504.9	508.3
65	504.4	504.8	505.2	508.4
70	504.7	504.9	505.3	508.4
75	504.9	505.1	505.4	508.4
80	505.1	505.2	505.5	508.5
85	505.1	505.3	505.6	508.5
90	505.1	505.2	505.5	508.4
95	505.1	505.1	505.5	508.4
100	504.9	504.9	505.3	508.2
105	504.7	504.7	505.1	508.2

Flow rate = 20 SLM, T_{oven} = 500 °C, Gas: He				
coordinates [mm]	Position of thermocouples			
	center	1/2 radius	2/3 radius	wall
-5	458.2	466.2	473.5	492.2
0	464.2	471.7	477.7	495.2
5	470.0	477.1	481.8	497.6
10	474.9	480.8	484.8	498.8
15	479.8	484.8	488.0	499.9
20	483.8	487.8	490.1	501.8
25	486.9	490.4	492.8	502.5
30	489.6	492.6	494.8	502.9
35	492.0	494.5	496.3	503.5
40	493.7	496.0	497.6	504.3
45	495.4	497.3	498.7	504.9
50	496.8	498.5	499.6	505.2
55	498.2	499.4	500.4	505.5
60	499.1	500.3	501.1	506.1
65	499.9	500.9	501.6	506.3
70	500.6	501.4	502.0	506.4
75	501.2	501.9	502.5	506.5
80	501.7	502.3	502.8	506.7
85	502.2	502.6	503.1	506.8
90	502.4	502.8	503.3	506.9
95	502.6	503.0	503.4	506.9
100	502.8	503.0	503.5	506.9
105	502.8	503.1	503.6	506.9

Flow rate = 25 SLM, T_{oven} = 500 °C, Gas: He				
coordinates [mm]	Position of thermocouples			
	center	1/2 radius	2/3 radius	wall
-5	420.9	437.6	449.8	485.0
0	430.0	445.2	456.2	489.0
5	439.3	453.0	461.3	492.0
10	447.7	459.2	466.2	493.4
15	454.9	464.9	471.6	495.3
20	461.4	469.7	475.4	497.8
25	467.1	475.1	479.7	498.9
30	472.1	479.1	483.4	499.5
35	476.2	482.2	485.6	500.3
40	480.0	485.3	488.1	501.7
45	483.0	487.6	490.4	502.6
50	486.0	490.0	492.2	503.0
55	488.5	491.9	494.0	503.4
60	490.7	493.6	495.4	504.5
65	492.5	495.1	496.5	505.0
70	494.1	496.6	497.6	505.1
75	495.4	497.5	498.5	505.3
80	496.6	498.4	499.4	505.8
85	497.8	499.3	500.2	506.2
90	498.6	500.0	500.7	506.3
95	499.3	500.5	501.3	506.5
100	500.1	501.0	501.9	506.6
105	500.6	501.4	502.4	506.8

Flow rate = 30 SLM, T_{oven} = 500 °C, Gas: He				
coordinates [mm]	Position of thermocouples			
	center	1/2 radius	2/3 radius	wall
-5	383.7	407.0	426.6	476.8
0	394.6	417.5	433.8	481.3
5	406.6	426.4	441.0	484.6
10	416.7	434.8	446.6	486.4
15	427.0	442.9	452.8	488.7
20	435.9	448.9	457.6	492.2
25	442.6	455.6	463.5	493.2
30	450.0	461.0	467.5	493.9
35	455.8	466.0	471.2	494.9
40	460.6	470.1	475.2	496.7
45	465.4	473.9	478.3	497.8
50	469.9	477.1	481.0	498.3
55	473.8	480.1	483.4	498.8
60	477.1	482.5	485.7	500.3
65	480.1	485.2	487.5	500.9
70	482.5	487.1	489.2	501.1
75	484.8	489.0	490.7	501.4
80	486.8	490.4	492.0	502.1
85	488.9	491.9	493.2	502.8
90	490.4	493.1	494.3	502.9
95	491.8	494.2	495.6	503.5
100	493.1	495.2	496.8	503.8
105	494.3	496.3	498.1	504.1

2.5   Co 1200 µm

coordinates [mm]	Flow rate = 10 SLM, T_{oven} = 300 °C, Gas: N_2 Position of thermocouples			
	center	1/2 radius	2/3 radius	wall
-5	240.8	250.8	252.3	294.7
0	244.4	255.0	257.7	297.2
5	249.3	259.3	261.9	297.5
10	253.6	263.5	266.1	298.0
15	258.1	267.5	269.9	298.5
20	262.2	270.7	273.2	299.6
25	266.3	274.1	276.2	300.0
30	269.6	277.1	279.2	300.2
35	272.9	280.1	281.4	300.5
40	275.7	282.5	283.6	301.0
45	278.5	284.4	285.5	301.3
50	281.0	286.0	287.2	301.7
55	283.0	287.8	288.8	301.8
60	285.1	289.2	290.2	302.1
65	286.8	290.5	291.5	302.4
70	288.2	291.5	292.6	302.5
75	289.7	292.5	293.5	303.0
80	290.8	293.2	294.4	303.3
85	292.0	294.1	295.1	303.3
90	292.9	294.7	295.7	303.3
95	293.7	295.4	296.1	303.4
100	294.3	295.9	296.6	303.6
105	294.9	296.4	297.0	303.6

coordinates [mm]	Flow rate = 15 SLM, T_{oven} = 300 °C, Gas: N_2 Position of thermocouples			
	center	1/2 radius	2/3 radius	wall
-5	209.4	223.4	227.5	290.2
0	212.7	227.8	233.1	293.2
5	217.6	232.5	238.1	293.6
10	222.1	237.3	242.5	294.2
15	227.4	242.1	246.9	294.7
20	231.9	246.1	250.9	295.9
25	236.6	250.8	254.7	296.3
30	240.9	254.6	258.7	296.5
35	244.7	258.4	261.5	297.0
40	248.7	262.0	265.0	297.6
45	252.7	264.8	267.8	298.2
50	256.4	267.6	270.4	298.4
55	259.7	269.8	272.8	298.5
60	263.0	272.0	275.0	298.7
65	265.6	274.2	277.1	299.7
70	268.3	276.0	279.1	300.0
75	270.6	277.6	280.6	300.3
80	272.8	279.0	282.1	301.0
85	275.0	280.6	283.6	301.2
90	276.8	281.9	284.6	301.2
95	278.4	283.2	285.4	301.3
100	279.8	284.4	286.3	302.0
105	281.1	285.6	287.4	302.0

coordinates [mm]	Flow rate = 20 SLM, T_{oven} = 300 °C, Gas: N_2 Position of thermocouples			
	center	1/2 radius	2/3 radius	wall
-5	179.1	197.6	201.7	285.9
0	182.3	201.5	208.3	289.0
5	186.7	206.2	213.0	289.5
10	191.5	211.1	218.1	290.1
15	196.4	216.6	223.1	290.9
20	201.0	220.8	227.6	292.4
25	205.9	226.1	231.9	292.8
30	210.7	230.7	236.5	293.1
35	215.2	235.5	240.2	293.5
40	220.2	239.5	244.4	294.3
45	224.3	243.1	247.6	294.9
50	228.4	246.2	250.8	295.2
55	232.7	249.2	254.1	295.2
60	236.6	251.7	257.0	295.5
65	239.9	254.3	259.6	296.4
70	243.2	256.2	262.3	297.1
75	246.4	258.5	264.6	297.8
80	249.4	260.3	266.6	298.9
85	252.4	262.4	268.7	299.1
90	255.0	264.2	270.0	299.2
95	257.4	266.0	271.0	299.9
100	259.4	268.0	272.4	300.1
105	261.3	270.0	274.0	300.1

coordinates [mm]	Flow rate = 25 SLM, T_{oven} = 300 °C, Gas: N_2 Position of thermocouples			
	center	1/2 radius	2/3 radius	wall
-5	160.4	181.4	186.4	283.0
0	163.3	184.9	192.0	287.9
5	167.5	189.9	197.4	288.1
10	171.9	194.5	202.3	288.5
15	176.3	199.8	207.2	289.1
20	181.1	204.5	211.5	290.8
25	185.6	209.8	215.9	291.2
30	190.2	214.4	221.4	291.5
35	194.7	219.5	225.0	291.9
40	199.3	223.8	229.1	292.5
45	204.0	227.8	232.8	292.5
50	208.5	231.3	236.2	292.8
55	212.9	234.1	239.6	292.9
60	216.9	236.8	243.0	293.5
65	220.6	239.6	245.8	294.7
70	224.2	241.8	248.8	294.7
75	227.9	244.2	251.5	296.6
80	231.1	246.0	253.7	297.6
85	234.4	248.5	255.8	297.7
90	237.4	250.5	257.4	298.1
95	240.2	252.6	258.6	298.3
100	242.5	254.9	260.1	299.7
105	244.8	257.5	262.0	299.9

Flow rate = 30 SLM, T$_{oven}$ = 300 °C, Gas: N$_2$				
coordinates [mm]	Position of thermocouples			
	center	1/2 radius	2/3 radius	wall
-5	142.1	163.8	170.0	279.2
0	144.3	166.6	175.1	283.6
5	148.0	171.0	179.8	284.1
10	151.5	175.4	184.8	284.6
15	155.7	180.8	189.3	285.5
20	159.9	185.4	193.7	287.6
25	164.0	190.8	198.0	288.0
30	168.0	195.3	203.0	288.1
35	172.1	200.6	207.1	288.8
40	176.5	205.0	211.3	289.8
45	181.1	209.4	215.4	290.2
50	185.6	212.5	219.6	290.5
55	189.9	215.4	223.1	290.9
60	194.0	217.8	226.7	291.3
65	197.8	220.5	230.2	292.4
70	201.4	222.7	233.4	292.9
75	205.2	225.0	236.6	293.8
80	208.4	226.8	239.4	294.8
85	212.1	229.1	241.6	295.9
90	215.0	231.0	243.1	296.3
95	218.0	233.4	244.3	296.5
100	220.7	236.2	246.2	297.4
105	223.4	239.3	248.1	297.5

Flow rate = 35 SLM, T$_{oven}$ = 300 °C, Gas: N$_2$				
coordinates [mm]	Position of thermocouples			
	center	1/2 radius	2/3 radius	wall
-5	130.9	152.2	161.3	275.4
0	133.0	154.8	165.5	280.2
5	135.9	158.4	169.7	281.0
10	139.2	162.8	174.0	281.8
15	142.9	167.5	178.2	283.5
20	146.3	171.9	182.4	285.8
25	150.2	177.0	187.0	286.7
30	153.8	182.0	191.6	287.8
35	157.6	186.7	195.3	287.5
40	161.6	191.1	199.7	288.3
45	165.8	195.0	203.4	288.9
50	169.5	198.0	207.4	289.6
55	173.7	201.1	211.0	290.7
60	177.5	203.8	214.6	291.6
65	181.2	206.4	217.8	291.7
70	184.5	208.4	221.0	292.1
75	188.1	210.6	224.0	292.6
80	191.4	212.5	226.8	293.3
85	194.7	214.4	229.0	293.3
90	197.7	216.5	230.2	293.8
95	200.4	218.8	231.0	294.7
100	203.3	221.5	233.0	295.7
105	205.9	224.7	234.5	295.7

Flow rate = 10 SLM, T$_{oven}$ = 500 °C, Gas: N$_2$				
coordinates [mm]	Position of thermocouples			
	center	1/2 radius	2/3 radius	wall
-5	425.5	439.2	445.0	494.8
0	431.3	445.4	452.1	498.2
5	438.2	451.6	457.7	498.8
10	444.4	457.3	463.3	499.0
15	450.7	462.8	467.7	500.3
20	456.6	467.3	472.0	501.8
25	461.9	471.9	475.7	502.4
30	466.1	475.4	479.3	502.7
35	470.4	479.0	481.7	503.8
40	474.3	482.2	484.6	504.3
45	477.6	484.8	486.8	504.6
50	480.8	487.1	488.9	505.0
55	483.6	489.1	490.9	505.4
60	486.0	490.8	492.6	505.7
65	488.1	492.4	493.9	505.9
70	489.9	493.7	495.3	506.0
75	491.5	494.9	496.5	506.2
80	493.2	496.0	497.5	506.4
85	494.5	497.0	498.3	506.4
90	495.5	497.7	498.9	506.4
95	496.6	498.5	499.5	506.5
100	497.4	499.1	499.9	506.5
105	498.2	499.8	500.4	506.4

Flow rate = 15 SLM, T$_{oven}$ = 500 °C, Gas: N$_2$				
coordinates [mm]	Position of thermocouples			
	center	1/2 radius	2/3 radius	wall
-5	372.9	395.4	407.6	488.1
0	379.0	402.7	416.0	490.8
5	387.0	410.2	422.7	491.8
10	394.8	417.7	429.0	493.0
15	402.6	424.8	435.2	494.4
20	409.9	431.2	440.5	496.1
25	417.1	437.8	445.4	497.2
30	423.7	443.4	450.7	498.2
35	429.7	448.7	454.8	499.7
40	435.7	453.6	459.2	499.9
45	441.2	457.9	462.8	500.1
50	446.1	461.5	466.5	501.4
55	451.2	465.0	469.6	501.9
60	455.5	467.9	472.8	502.4
65	459.4	470.9	475.4	502.6
70	462.9	473.3	478.2	502.8
75	466.4	475.8	480.2	503.2
80	469.4	477.7	482.1	503.6
85	472.4	480.0	483.8	503.7
90	475.0	481.8	485.2	503.8
95	477.4	483.6	486.3	504.2
100	479.7	485.6	487.6	504.5
105	481.9	487.7	489.1	504.3

Flow rate = 20 SLM, T_{oven} = 500 °C, Gas: N_2				
coordinates	Position of thermocouples			
[mm]	center	1/2 radius	2/3 radius	wall
-5	324.2	353.7	372.2	482.0
0	330.3	361.2	380.8	485.8
5	338.5	369.8	387.8	486.6
10	346.0	378.1	395.1	488.1
15	354.5	386.3	401.9	490.4
20	361.9	393.3	407.9	492.0
25	369.6	401.7	413.5	494.7
30	377.0	408.3	419.7	494.9
35	383.8	414.7	424.3	496.5
40	390.9	421.0	430.0	496.8
45	398.1	426.5	435.0	498.1
50	404.3	431.1	439.4	498.6
55	410.8	435.1	443.7	499.2
60	416.6	438.0	448.0	500.1
65	422.0	442.8	451.5	500.3
70	427.0	445.9	455.5	500.7
75	431.7	449.1	458.7	501.2
80	436.1	451.7	461.6	502.0
85	440.6	454.9	463.9	502.1
90	444.5	457.6	465.7	502.2
95	448.4	460.6	468.5	502.6
100	452.3	463.9	470.3	502.9
105	456.3	467.6	473.3	503.0

Flow rate = 25 SLM, T_{oven} = 500 °C, Gas: N_2				
coordinates	Position of thermocouples			
[mm]	center	1/2 radius	2/3 radius	wall
-5	286.6	320.7	340.4	475.2
0	291.5	327.4	349.8	477.9
5	299.2	336.0	356.9	480.4
10	306.3	344.2	364.5	481.1
15	314.5	352.8	371.9	484.8
20	322.1	360.6	378.1	488.8
25	330.1	368.5	384.4	489.5
30	337.4	376.7	391.0	489.8
35	344.6	384.3	396.4	491.7
40	352.0	390.7	402.7	492.1
45	359.2	396.6	407.8	493.1
50	366.0	401.5	412.9	494.1
55	372.9	406.1	418.4	494.7
60	379.2	410.5	423.4	495.5
65	385.5	414.8	427.7	495.9
70	390.7	417.9	432.1	496.1
75	396.7	421.9	435.6	496.8
80	401.6	424.7	439.4	497.8
85	407.1	428.6	442.8	498.0
90	411.9	431.8	445.9	498.3
95	416.7	435.6	449.0	499.0
100	422.0	440.4	452.3	499.6
105	427.0	445.7	456.6	499.5

Flow rate = 30 SLM, T_{oven} = 500 °C, Gas: N_2				
coordinates	Position of thermocouples			
[mm]	center	1/2 radius	2/3 radius	wall
-5	255.7	293.6	314.1	469.7
0	260.6	300.2	323.9	473.9
5	266.9	307.2	331.5	474.5
10	273.8	315.3	338.7	477.0
15	280.8	323.8	345.8	480.0
20	288.0	331.4	352.2	483.9
25	295.0	340.3	358.8	485.7
30	302.0	347.8	365.6	486.6
35	308.9	355.5	370.9	489.0
40	315.7	362.3	377.7	490.1
45	323.0	368.4	383.4	490.5
50	330.2	373.7	389.5	491.1
55	337.6	378.4	394.7	492.1
60	343.7	382.6	399.9	492.7
65	350.2	386.9	405.0	492.9
70	355.8	390.4	409.4	493.0
75	362.1	394.1	414.5	493.5
80	367.6	397.2	418.1	494.9
85	373.7	401.5	421.3	495.0
90	379.3	405.1	425.1	495.3
95	385.0	409.7	429.3	496.3
100	390.5	414.8	433.5	497.4
105	396.4	421.4	437.9	497.5

Flow rate = 35 SLM, T_{oven} = 500 °C, Gas: N_2				
coordinates	Position of thermocouples			
[mm]	center	1/2 radius	2/3 radius	wall
-5	226.9	267.4	289.5	464.6
0	231.1	272.9	297.9	468.4
5	236.8	279.8	305.2	469.7
10	242.9	287.8	312.0	476.2
15	249.2	295.9	319.3	480.3
20	255.2	303.4	325.6	481.9
25	262.0	312.0	331.8	483.2
30	268.3	319.6	338.9	483.7
35	274.5	327.2	344.7	484.5
40	281.2	334.0	351.1	485.0
45	288.0	340.0	357.3	487.2
50	294.9	345.3	363.5	487.6
55	301.9	350.2	369.2	488.7
60	307.9	354.1	374.9	489.5
65	314.3	358.4	380.5	489.8
70	320.1	361.7	385.9	490.0
75	326.1	365.4	390.6	490.8
80	331.9	368.2	394.8	492.1
85	338.4	372.4	398.7	492.2
90	343.6	376.5	402.2	493.2
95	349.7	381.7	405.6	494.0
100	355.8	387.3	409.6	495.0
105	362.6	395.0	415.1	494.0

Flow rate = 20 SLM, T$_{oven}$ = 500 °C, Gas: He			
coordinates [mm]	Position of thermocouples		
	center	1/2 radius	2/3 radius	wall
-5	446.1	457.0	463.1	491.0
0	452.4	462.7	468.8	495.0
5	458.8	468.1	473.0	496.4
10	464.3	472.8	477.3	497.7
15	469.5	477.0	480.9	499.7
20	473.8	480.4	484.0	502.3
25	477.8	483.7	486.7	502.6
30	481.2	486.4	489.2	503.0
35	484.1	488.9	491.1	503.9
40	486.7	490.9	493.1	505.3
45	489.2	493.0	494.7	505.4
50	491.3	494.6	496.2	505.8
55	493.3	496.0	497.4	506.0
60	494.8	497.2	498.5	506.4
65	496.2	498.3	499.4	506.6
70	497.4	499.2	500.3	506.8
75	498.5	500.0	501.0	506.9
80	499.3	500.6	501.6	507.2
85	500.1	501.2	502.0	507.2
90	500.7	501.7	502.4	507.3
95	501.3	502.1	502.7	507.4
100	501.7	502.4	502.9	507.3
105	502.0	502.7	503.2	507.2

Flow rate = 25 SLM, T$_{oven}$ = 500 °C, Gas: He			
coordinates [mm]	Position of thermocouples		
	center	1/2 radius	2/3 radius	wall
-5	400.1	419.6	431.7	483.5
0	409.5	427.8	440.2	487.6
5	419.3	436.2	446.5	488.8
10	427.4	443.3	452.2	490.7
15	435.5	450.0	458.1	494.3
20	442.6	455.2	462.6	496.8
25	448.3	461.0	466.7	497.2
30	454.3	465.2	471.0	497.6
35	458.7	469.3	474.2	499.5
40	463.7	473.0	477.8	501.0
45	468.2	476.3	480.4	501.5
50	471.7	479.4	483.2	501.8
55	475.6	482.1	485.4	502.0
60	478.4	484.5	487.5	502.7
65	481.6	486.6	489.3	503.1
70	483.7	488.3	491.0	503.4
75	485.9	490.0	492.4	503.7
80	487.8	491.4	493.7	504.2
85	489.8	492.8	494.8	504.4
90	491.2	493.9	495.6	504.6
95	492.4	494.9	496.3	505.0
100	493.7	496.0	497.1	505.2
105	494.8	497.1	498.0	504.9

Flow rate = 30 SLM, T$_{oven}$ = 500 °C, Gas: He			
coordinates [mm]	Position of thermocouples		
	center	1/2 radius	2/3 radius	wall
-5	360.4	387.5	405.7	476.4
0	371.2	398.4	416.8	481.7
5	382.4	407.8	424.0	482.8
10	392.7	416.6	431.0	484.5
15	402.4	424.7	437.2	487.2
20	411.1	431.2	443.4	491.3
25	419.5	438.5	448.6	492.9
30	427.0	444.3	454.0	493.3
35	433.6	450.0	458.1	494.8
40	439.9	455.1	462.8	497.5
45	445.9	459.7	466.5	497.8
50	451.4	464.0	469.9	498.1
55	456.6	467.3	473.1	498.8
60	460.8	470.9	476.0	499.9
65	464.9	474.1	478.6	500.3
70	468.4	476.4	481.0	500.9
75	471.7	479.0	483.2	501.3
80	474.6	480.9	484.9	502.0
85	477.5	483.2	486.6	502.3
90	479.9	484.9	487.4	502.4
95	482.1	486.7	489.1	503.0
100	484.0	488.5	490.4	503.2
105	486.0	490.7	492.1	503.1

2.6 Co 580 µm

coordinates	Flow rate = 10 SLM, T_{oven} = 300 °C, Gas: N_2			
	Position of thermocouples			
[mm]	center	1/2 radius	2/3 radius	wall
-5	243.4	253.7	256.4	294.6
0	248.0	259.3	262.8	295.2
5	254.3	263.8	266.5	296.0
10	260.0	268.6	270.9	297.0
15	265.5	272.9	275.3	297.8
20	270.2	276.4	279.0	298.8
25	274.4	280.0	281.9	299.5
30	278.1	282.7	284.8	300.1
35	281.1	285.7	286.7	300.7
40	283.8	287.9	288.8	301.5
45	286.2	289.8	290.4	301.5
50	288.3	291.2	292.0	301.8
55	290.2	292.5	293.4	301.9
60	291.5	293.5	294.4	302.6
65	292.8	294.4	295.2	302.6
70	293.9	295.1	295.9	302.7
75	294.8	295.9	296.6	302.7
80	295.6	296.4	297.1	302.9
85	296.3	297.0	297.5	303.1
90	296.8	297.3	297.9	303.2
95	297.2	297.6	298.2	303.3
100	297.5	297.9	298.4	303.6
105	297.7	298.1	298.6	303.7

coordinates	Flow rate = 15 SLM, T_{oven} = 300 °C, Gas: N_2			
	Position of thermocouples			
[mm]	center	1/2 radius	2/3 radius	wall
-5	211.5	228.1	234.8	289.3
0	216.8	233.9	239.7	289.7
5	223.9	239.1	245.3	290.6
10	230.6	244.4	250.7	292.5
15	236.7	249.8	256.3	293.8
20	242.7	254.0	259.8	294.8
25	248.3	259.3	264.2	295.7
30	254.2	264.0	268.1	296.6
35	258.5	267.9	271.0	297.4
40	263.0	271.4	274.2	298.0
45	267.0	274.4	277.1	298.2
50	270.2	277.0	279.6	298.6
55	273.7	279.4	281.7	298.8
60	276.4	281.1	283.7	300.0
65	278.6	283.0	285.2	299.9
70	280.8	284.2	286.7	300.0
75	283.0	285.7	287.9	300.0
80	284.5	286.9	288.9	300.4
85	286.2	288.2	290.0	300.8
90	287.3	289.1	290.8	301.0
95	288.4	289.8	291.4	301.4
100	289.2	290.5	292.0	301.4
105	289.8	291.3	292.8	301.6

coordinates	Flow rate = 20 SLM, T_{oven} = 300 °C, Gas: N_2			
	Position of thermocouples			
[mm]	center	1/2 radius	2/3 radius	wall
-5	181.5	203.5	213.2	285.0
0	186.7	208.5	218.6	285.1
5	193.5	214.1	224.2	285.7
10	200.8	219.5	229.0	287.8
15	207.9	225.6	235.2	287.7
20	214.7	230.7	240.4	290.1
25	221.5	236.9	245.1	290.5
30	227.6	242.2	249.9	292.4
35	233.1	247.5	253.4	293.5
40	238.3	252.5	257.6	294.3
45	243.3	255.8	261.0	294.5
50	247.9	259.2	264.3	295.0
55	252.4	262.3	267.4	295.2
60	256.1	264.7	270.0	296.5
65	259.7	267.2	272.0	296.5
70	262.7	269.0	274.0	296.7
75	265.7	271.0	275.7	296.7
80	268.3	272.8	277.3	297.4
85	271.0	274.8	278.7	298.1
90	273.0	276.1	279.9	298.5
95	274.6	277.4	281.0	298.7
100	276.0	278.7	282.2	299.6
105	277.1	279.8	283.5	300.4

coordinates	Flow rate = 25 SLM, T_{oven} = 300 °C, Gas: N_2			
	Position of thermocouples			
[mm]	center	1/2 radius	2/3 radius	wall
-5	159.7	183.7	196.2	281.5
0	164.0	188.5	201.5	281.3
5	170.8	193.6	206.5	282.1
10	177.5	199.2	213.1	285.1
15	184.8	204.9	219.3	285.7
20	191.3	210.5	224.4	286.9
25	198.4	217.0	229.8	287.5
30	204.7	222.9	234.8	290.5
35	210.8	228.5	238.7	291.2
40	216.7	233.5	243.0	293.0
45	222.0	237.9	247.0	292.0
50	227.1	241.8	250.6	292.4
55	232.1	245.4	254.3	292.8
60	236.3	248.4	257.4	294.8
65	240.7	251.2	259.8	295.3
70	244.3	253.4	262.0	295.2
75	247.9	255.7	264.0	295.2
80	251.3	257.8	265.7	296.0
85	254.6	260.2	267.5	297.0
90	257.4	262.0	269.0	297.3
95	259.5	263.6	270.4	297.6
100	261.3	265.2	271.9	298.9
105	262.9	267.2	274.3	300.1

Flow rate = 30 SLM, T$_{oven}$ = 300 °C, Gas: N$_2$				
coordinates	Position of thermocouples			
[mm]	center	1/2 radius	2/3 radius	wall
-5	145.5	169.7	182.6	277.9
0	149.3	174.6	188.5	279.3
5	155.0	179.3	194.3	280.1
10	160.9	184.6	199.8	281.4
15	167.7	190.1	206.8	283.0
20	175.2	195.8	211.7	284.9
25	181.7	202.8	217.4	285.9
30	188.1	208.5	222.2	286.5
35	194.0	213.4	226.4	288.0
40	199.7	219.6	231.1	288.6
45	204.8	223.8	234.9	288.8
50	210.4	228.3	239.4	288.9
55	215.6	231.9	243.1	289.2
60	220.5	234.7	246.7	290.4
65	225.7	237.5	248.7	291.5
70	228.9	239.6	250.9	292.1
75	232.9	242.0	252.8	292.4
80	236.3	244.2	254.7	293.1
85	239.5	246.8	256.6	294.5
90	243.0	248.8	258.0	295.0
95	245.2	250.6	259.6	295.2
100	247.4	252.3	261.6	296.5
105	249.2	254.2	264.2	297.4

Flow rate = 35 SLM, T$_{oven}$ = 300 °C, Gas: N$_2$				
coordinates	Position of thermocouples			
[mm]	center	1/2 radius	2/3 radius	wall
-5	129.3	156.0	170.7	274.9
0	132.9	159.6	176.5	274.8
5	138.3	163.9	181.5	275.2
10	143.7	168.5	186.4	278.2
15	150.1	173.7	192.4	279.2
20	156.0	179.0	198.0	281.4
25	162.4	185.6	202.8	282.5
30	168.2	191.4	207.9	283.9
35	173.8	197.3	211.9	285.0
40	179.7	202.7	216.8	286.9
45	185.1	207.5	220.9	285.6
50	190.5	211.3	225.3	285.6
55	195.9	214.9	229.1	286.3
60	200.7	217.9	232.5	288.6
65	205.1	220.7	234.9	289.8
70	209.1	222.8	237.0	289.4
75	213.3	225.0	238.9	288.7
80	217.0	227.0	240.6	289.5
85	220.9	229.7	242.3	290.8
90	223.9	231.7	244.0	291.3
95	226.6	233.6	245.5	291.5
100	228.9	235.4	247.5	293.6
105	230.8	237.8	251.0	295.6

Flow rate = 10 SLM, T$_{oven}$ = 500 °C, Gas: N$_2$				
coordinates	Position of thermocouples			
[mm]	center	1/2 radius	2/3 radius	wall
-5	426.6	442.2	448.0	493.6
0	433.3	449.3	455.4	494.4
5	442.0	455.9	462.4	496.0
10	450.0	462.2	468.6	498.2
15	457.6	467.9	473.8	499.3
20	463.9	472.7	477.7	500.9
25	469.7	477.6	481.4	502.3
30	474.8	481.5	485.1	502.7
35	479.0	485.0	487.7	503.5
40	482.6	488.0	490.5	504.4
45	485.9	490.3	492.6	504.6
50	488.6	492.3	494.5	505.1
55	491.1	494.1	496.0	505.6
60	493.2	495.5	497.4	506.2
65	494.7	496.8	498.4	506.3
70	496.1	497.7	499.3	506.5
75	497.3	498.6	500.0	506.6
80	498.3	499.3	500.6	506.9
85	499.2	500.2	501.1	507.1
90	499.9	500.7	501.5	507.1
95	500.4	501.1	501.8	507.3
100	500.7	501.4	502.0	507.3
105	501.1	501.9	502.2	507.4

Flow rate = 15 SLM, T$_{oven}$ = 500 °C, Gas: N$_2$				
coordinates	Position of thermocouples			
[mm]	center	1/2 radius	2/3 radius	wall
-5	369.6	396.8	409.9	535.6
0	378.0	405.0	416.5	487.5
5	388.5	412.4	424.8	489.6
10	398.4	421.1	432.3	491.5
15	409.3	429.3	440.4	492.8
20	418.7	435.0	447.6	494.7
25	426.7	443.5	453.6	496.4
30	434.6	449.9	459.0	497.1
35	441.5	455.9	463.7	498.1
40	448.1	461.1	468.2	498.6
45	454.1	465.6	472.3	499.2
50	459.1	469.5	475.9	499.9
55	464.3	472.8	479.1	500.5
60	468.5	475.7	481.8	502.2
65	472.1	478.6	483.8	502.2
70	475.6	480.5	485.8	502.4
75	478.6	482.7	487.5	502.6
80	481.3	484.5	488.9	503.3
85	483.6	486.5	490.2	503.8
90	485.6	488.0	491.4	504.0
95	487.3	489.1	492.3	504.4
100	488.9	490.5	493.3	504.7
105	489.8	491.9	494.5	504.8

Flow rate = 20 SLM, T_{oven} = 500 °C, Gas: N_2				
coordinates	Position of thermocouples			
[mm]	center	1/2 radius	2/3 radius	wall
-5	323.2	356.3	374.7	478.9
0	332.3	368.3	385.5	479.2
5	343.5	376.9	394.6	481.1
10	354.2	385.8	404.1	483.6
15	365.8	394.8	413.2	485.4
20	376.5	403.0	420.7	488.2
25	387.0	412.0	427.8	490.4
30	396.1	419.6	434.6	491.7
35	404.7	427.1	440.3	492.4
40	413.2	434.0	446.0	493.2
45	420.6	439.5	451.2	494.6
50	427.5	444.3	456.0	495.3
55	434.4	448.9	460.2	496.2
60	440.1	452.7	463.9	498.1
65	445.3	456.4	466.7	498.6
70	450.0	459.3	469.4	498.9
75	454.5	462.6	471.7	499.1
80	458.6	464.8	473.8	500.0
85	462.6	467.9	475.9	500.7
90	465.6	470.3	477.5	501.0
95	468.3	472.4	479.2	501.5
100	470.9	474.7	481.0	502.5
105	473.3	477.3	483.3	503.1

Flow rate = 25 SLM, T_{oven} = 500 °C, Gas: N_2				
coordinates	Position of thermocouples			
[mm]	center	1/2 radius	2/3 radius	wall
-5	283.6	325.6	344.4	473.7
0	290.4	333.1	357.1	475.8
5	301.2	341.6	366.9	477.7
10	311.8	350.7	376.3	480.4
15	323.6	360.3	385.6	481.2
20	335.1	369.2	393.7	483.4
25	345.8	379.4	401.2	485.1
30	355.8	388.2	408.6	486.0
35	365.4	396.6	415.0	488.3
40	374.6	404.2	421.6	490.6
45	383.4	410.9	427.7	491.2
50	391.6	416.8	433.7	492.1
55	400.0	421.9	438.9	493.0
60	407.0	426.4	443.4	495.0
65	413.4	430.5	446.9	495.3
70	419.6	434.5	450.4	495.8
75	425.4	438.7	453.1	496.1
80	430.7	441.9	456.0	497.4
85	436.1	446.0	458.4	498.6
90	440.4	449.1	460.7	498.7
95	444.1	451.9	462.8	499.3
100	447.6	455.1	465.5	501.2
105	451.3	458.9	468.6	501.9

Flow rate = 30 SLM, T_{oven} = 500 °C, Gas: N_2				
coordinates	Position of thermocouples			
[mm]	center	1/2 radius	2/3 radius	wall
-5	250.9	299.8	317.9	468.5
0	258.5	306.6	331.0	469.9
5	268.6	314.6	341.2	471.5
10	278.5	323.0	350.6	474.4
15	289.3	332.8	360.4	474.7
20	300.6	341.0	368.7	478.2
25	310.5	351.7	376.8	480.4
30	321.0	360.2	384.7	481.6
35	330.7	369.0	391.2	483.8
40	340.2	377.4	398.9	485.6
45	349.2	383.9	405.4	486.6
50	358.2	390.3	411.8	487.3
55	367.1	395.7	417.7	485.9
60	374.4	400.1	422.6	490.8
65	382.0	404.5	426.6	491.0
70	388.6	409.6	430.2	491.2
75	395.6	414.1	433.4	491.4
80	401.7	417.6	436.5	493.1
85	407.9	422.1	439.3	494.1
90	413.0	424.6	441.7	494.5
95	417.6	428.5	444.2	495.7
100	421.8	432.5	447.7	497.5
105	426.3	437.6	451.6	498.6

Flow rate = 35 SLM, T_{oven} = 500 °C, Gas: N_2				
coordinates	Position of thermocouples			
[mm]	center	1/2 radius	2/3 radius	wall
-5	222.6	275.0	293.8	463.6
0	229.1	280.7	307.2	464.9
5	238.2	288.1	316.7	466.2
10	247.2	295.9	326.0	471.2
15	257.4	305.1	335.0	472.4
20	266.7	313.3	343.3	475.7
25	276.9	324.2	351.9	477.5
30	287.0	332.8	360.1	478.2
35	295.5	341.7	367.0	478.8
40	305.7	349.1	374.8	480.3
45	314.9	356.4	382.2	481.9
50	323.3	362.6	388.9	482.5
55	332.6	368.1	395.2	484.0
60	340.5	373.1	400.5	485.2
65	348.0	377.6	404.6	486.3
70	355.1	382.9	408.6	486.4
75	362.6	387.3	411.7	487.1
80	369.0	391.8	414.8	488.6
85	376.4	396.7	417.6	490.5
90	381.7	401.5	420.3	490.8
95	387.0	404.8	422.9	491.3
100	391.8	407.3	426.8	494.8
105	397.1	411.0	432.0	495.8

Flow rate = 20 SLM, T$_{oven}$ = 500 °C, Gas: He			
coordinates [mm]	Position of thermocouples		
	center	1/2 radius	2/3 radius	wall
-5	449.6	460.7	463.1	491.6
0	455.7	466.7	469.8	493.8
5	462.9	471.9	475.2	495.8
10	468.6	476.4	479.7	497.5
15	474.1	480.5	483.3	498.5
20	478.4	483.7	487.0	500.6
25	482.4	487.1	489.7	502.0
30	485.7	489.4	492.2	502.9
35	488.4	492.0	494.1	503.5
40	490.9	494.0	496.0	504.4
45	493.1	495.6	497.4	505.2
50	494.9	497.0	498.7	505.7
55	496.6	498.2	499.6	506.1
60	497.8	499.2	500.5	506.7
65	499.0	500.1	501.3	507.0
70	499.9	500.7	501.9	507.1
75	500.7	501.4	502.4	507.2
80	501.4	501.9	502.8	507.4
85	501.9	502.4	503.2	507.6
90	502.4	502.8	503.4	507.6
95	502.7	503.0	503.6	507.6
100	502.9	503.2	503.7	507.7
105	503.1	503.4	503.8	507.8

Flow rate = 25 SLM, T$_{oven}$ = 500 °C, Gas: He			
coordinates [mm]	Position of thermocouples		
	center	1/2 radius	2/3 radius	wall
-5	408.6	429.5	433.3	483.6
0	418.2	437.6	443.9	486.5
5	428.8	445.2	451.8	489.1
10	438.3	451.7	458.5	491.4
15	445.4	458.5	465.1	493.3
20	453.4	463.3	469.5	495.4
25	459.8	468.6	474.5	497.7
30	464.6	472.9	478.5	498.5
35	469.2	476.8	481.5	499.8
40	473.6	480.2	484.6	500.6
45	477.4	483.1	486.9	501.3
50	481.0	485.7	489.3	501.8
55	483.9	487.9	491.3	502.4
60	486.5	490.1	493.0	503.6
65	489.0	491.5	494.4	504.0
70	490.9	493.0	495.6	504.2
75	492.5	494.3	496.7	504.4
80	493.9	495.4	497.6	505.0
85	495.3	496.6	498.4	505.4
90	496.2	497.4	498.9	505.4
95	497.2	498.1	499.4	505.7
100	497.8	498.7	499.9	505.9
105	498.3	499.3	500.4	506.1

Flow rate = 30 SLM, T$_{oven}$ = 500 °C, Gas: He			
coordinates [mm]	Position of thermocouples		
	center	1/2 radius	2/3 radius	wall
-5	362.9	393.3	401.1	475.4
0	374.4	404.1	414.0	477.1
5	387.7	413.5	424.9	480.0
10	398.7	422.6	433.8	483.2
15	410.1	430.9	441.6	484.7
20	419.9	437.9	448.4	487.9
25	428.9	445.4	454.3	491.0
30	436.9	451.5	460.0	492.1
35	443.6	456.7	464.3	493.4
40	450.0	461.8	469.0	495.1
45	455.9	466.0	473.0	496.5
50	461.3	469.9	476.5	497.1
55	466.1	473.5	479.5	498.1
60	470.2	476.4	482.2	499.8
65	473.8	479.1	484.4	500.5
70	476.9	481.3	486.5	500.9
75	479.9	483.6	488.2	501.2
80	482.3	485.4	489.8	501.9
85	484.9	487.5	491.2	502.6
90	486.8	489.1	492.2	502.8
95	488.4	490.4	493.2	503.1
100	489.7	491.7	494.3	504.0
105	490.9	493.3	495.6	504.5

2.7 Cu 1200 μm

coordinates [mm]	Position of thermocouples			
	center	1/2 radius	2/3 radius	wall

Flow rate = 10 SLM, T_{oven} = 300 °C, Gas: N_2

coordinates [mm]	center	1/2 radius	2/3 radius	wall
-5	248.8	253.7	256.3	293.7
0	256.7	261.5	263.6	295.5
5	264.7	267.5	269.4	296.7
10	270.6	272.4	274.1	297.0
15	275.9	276.8	278.5	297.1
20	279.5	280.1	281.9	297.8
25	283.3	283.5	284.7	298.1
30	286.0	286.2	287.4	298.4
35	288.1	288.4	289.2	299.0
40	290.1	290.4	291.1	299.7
45	291.8	292.1	292.6	300.5
50	293.3	293.5	293.9	300.9
55	294.7	294.8	295.1	301.2
60	295.7	295.8	296.1	301.9
65	296.7	296.8	296.9	302.5
70	297.4	297.6	297.7	302.8
75	298.0	298.2	298.2	303.0
80	298.5	298.6	298.7	303.2
85	298.8	298.9	299.1	303.5
90	298.9	299.0	299.3	303.5
95	299.0	299.2	299.4	303.6
100	299.1	299.3	299.5	303.7
105	299.2	299.4	299.6	303.9

Flow rate = 15 SLM, T_{oven} = 300 °C, Gas: N_2

coordinates [mm]	center	1/2 radius	2/3 radius	wall
-5	221.8	228.4	231.6	288.2
0	230.5	238.1	241.5	291.1
5	240.4	245.2	248.6	291.4
10	248.2	251.4	254.0	291.6
15	255.0	256.9	259.4	291.6
20	260.8	261.4	264.5	291.9
25	265.8	266.3	268.8	292.5
30	270.0	270.4	272.9	292.6
35	273.4	274.2	275.8	293.4
40	276.6	277.5	278.9	294.6
45	279.5	280.4	281.4	295.4
50	282.2	282.9	283.7	296.1
55	284.7	285.1	285.9	297.0
60	286.7	287.1	287.8	298.0
65	288.5	289.1	289.4	298.9
70	290.1	290.6	290.9	299.7
75	291.5	292.1	292.2	299.9
80	292.6	293.0	293.2	300.4
85	293.4	293.7	294.1	300.8
90	293.8	294.1	294.6	301.1
95	294.1	294.3	294.8	301.5
100	294.3	294.7	295.1	301.6
105	294.5	295.0	295.4	301.9

Flow rate = 20 SLM, T_{oven} = 300 °C, Gas: N_2

coordinates [mm]	center	1/2 radius	2/3 radius	wall
-5	195.8	205.0	211.7	283.4
0	205.1	214.5	219.8	286.9
5	215.7	222.2	227.1	287.5
10	224.6	229.1	234.2	287.5
15	232.7	235.4	240.2	287.5
20	239.8	241.7	245.5	287.4
25	245.8	247.3	250.7	287.4
30	251.1	252.5	255.8	287.7
35	255.5	256.6	259.7	287.6
40	259.8	261.2	263.8	289.5
45	263.7	265.1	267.2	290.0
50	267.4	268.6	270.5	291.1
55	271.0	271.9	273.5	292.7
60	274.1	275.0	276.2	294.3
65	277.0	278.1	278.8	295.4
70	279.4	280.5	281.2	296.2
75	281.7	282.8	283.2	296.5
80	283.5	284.3	285.0	297.1
85	285.0	285.6	286.4	298.1
90	285.8	286.2	287.4	298.6
95	286.2	286.7	287.9	298.9
100	286.7	287.4	288.6	299.4
105	287.1	288.1	289.1	300.0

Flow rate = 25 SLM, T_{oven} = 300 °C, Gas: N_2

coordinates [mm]	center	1/2 radius	2/3 radius	wall
-5	175.5	186.7	191.9	279.3
0	184.8	195.9	200.5	281.6
5	196.0	203.8	208.2	281.3
10	204.9	210.7	216.1	282.4
15	213.8	218.1	222.7	282.5
20	221.5	224.7	229.0	282.8
25	227.9	230.9	234.9	283.6
30	233.9	235.6	240.5	283.7
35	238.8	240.2	244.9	284.1
40	243.8	245.6	249.6	284.7
45	248.3	250.2	253.6	285.7
50	252.7	254.5	257.4	286.5
55	257.1	258.5	261.0	288.0
60	261.1	262.2	264.4	289.6
65	264.6	266.1	267.6	291.4
70	267.6	269.1	270.3	293.1
75	270.9	272.4	273.3	293.4
80	273.5	274.5	275.8	294.1
85	275.5	276.3	278.0	295.0
90	276.5	277.1	279.3	296.3
95	277.1	277.8	280.0	296.5
100	277.7	278.6	280.6	297.4
105	278.4	279.5	281.5	298.3

Flow rate = 30 SLM, T$_{oven}$ = 300 °C, Gas: N$_2$			
coordinates [mm]	Position of thermocouples		
	center	1/2 radius	2/3 radius	wall
-5	157.9	170.7	178.1	275.8
0	166.8	179.3	184.9	277.2
5	177.7	187.1	192.1	277.2
10	187.1	194.3	199.7	277.7
15	196.3	200.6	206.7	278.1
20	203.8	207.4	212.6	278.5
25	210.7	213.6	219.0	278.5
30	216.9	219.3	225.0	278.3
35	222.3	224.9	229.7	279.3
40	227.5	229.8	234.9	280.2
45	232.6	234.9	239.2	281.1
50	237.4	239.8	243.5	282.7
55	242.4	244.5	247.6	284.1
60	246.8	248.6	251.5	286.8
65	251.2	253.2	255.2	288.0
70	254.8	257.0	258.7	289.5
75	258.6	260.6	262.0	290.1
80	261.8	263.0	265.2	290.8
85	264.3	265.4	267.8	292.1
90	265.6	266.3	269.6	293.7
95	266.3	267.2	270.4	293.8
100	267.2	268.2	271.3	294.6
105	268.1	269.5	272.3	296.5

Flow rate = 35 SLM, T$_{oven}$ = 300 °C, Gas: N$_2$			
coordinates [mm]	Position of thermocouples		
	center	1/2 radius	2/3 radius	wall
-5	142.6	156.6	163.1	270.2
0	150.9	164.7	171.4	271.4
5	161.3	172.1	177.6	272.0
10	170.7	178.8	184.7	272.8
15	179.6	184.9	190.9	273.6
20	187.2	192.1	197.6	274.5
25	194.4	198.5	203.4	274.7
30	200.6	203.0	209.8	275.3
35	206.0	208.8	214.7	275.5
40	211.5	213.9	220.0	276.7
45	216.6	219.3	224.7	277.3
50	221.8	224.4	229.2	278.2
55	226.9	229.3	233.6	280.4
60	231.6	233.8	237.6	282.4
65	236.2	238.9	241.5	284.3
70	240.3	242.9	245.3	286.3
75	244.6	247.1	249.2	286.6
80	248.0	249.8	252.7	287.7
85	251.0	252.3	255.9	289.5
90	252.6	253.3	258.1	290.2
95	253.6	254.1	259.0	291.2
100	254.4	255.2	259.9	292.5
105	255.4	256.8	261.1	294.3

Flow rate = 10 SLM, T$_{oven}$ = 500 °C, Gas: N$_2$			
coordinates [mm]	Position of thermocouples		
	center	1/2 radius	2/3 radius	wall
-5	432.3	438.8	441.9	493.5
0	445.0	452.2	455.4	497.3
5	457.0	461.2	463.8	497.9
10	465.9	468.7	471.0	499.0
15	473.1	474.7	476.8	499.1
20	479.0	479.5	481.7	500.4
25	483.4	484.2	485.8	500.5
30	487.1	487.6	489.3	501.1
35	490.1	490.7	491.7	501.8
40	492.7	493.3	494.1	502.9
45	494.7	495.2	496.1	504.0
50	496.6	497.0	497.5	504.5
55	498.3	498.4	498.9	504.8
60	499.4	499.6	500.3	505.5
65	500.5	500.8	501.2	506.1
70	501.3	501.6	501.9	506.6
75	502.2	502.3	502.6	506.9
80	502.7	502.7	503.0	507.3
85	502.9	503.1	503.3	507.5
90	503.0	503.2	503.5	507.5
95	503.1	503.3	503.6	507.6
100	503.2	503.4	503.7	507.7
105	503.2	503.4	503.7	507.8

Flow rate = 15 SLM, T$_{oven}$ = 500 °C, Gas: N$_2$			
coordinates [mm]	Position of thermocouples		
	center	1/2 radius	2/3 radius	wall
-5	389.7	402.6	406.4	485.9
0	405.8	418.9	423.7	490.3
5	421.2	429.9	434.4	491.3
10	433.4	439.0	442.9	491.3
15	444.1	447.3	451.5	492.0
20	452.6	454.2	458.1	492.6
25	459.6	461.1	464.4	492.7
30	465.7	466.7	470.2	493.1
35	470.4	472.0	474.5	494.3
40	475.0	476.4	478.6	496.2
45	478.9	480.2	482.0	497.8
50	482.4	483.4	485.1	498.5
55	485.8	486.3	487.7	499.1
60	488.4	488.9	490.2	500.4
65	490.7	491.3	492.1	501.5
70	492.6	493.2	493.9	502.2
75	494.3	494.9	495.4	503.3
80	495.6	495.9	496.6	503.9
85	496.5	496.8	497.6	504.5
90	497.0	497.2	498.2	504.7
95	497.3	497.6	498.6	505.1
100	497.7	498.0	498.9	505.4
105	498.1	498.6	499.3	505.9

Flow rate = 20 SLM, T_{oven} = 500 °C, Gas: N_2				
coordinates	Position of thermocouples			
[mm]	center	1/2 radius	2/3 radius	wall
-5	348.3	365.8	373.8	478.5
0	365.9	382.1	388.1	484.3
5	384.7	395.2	400.0	484.6
10	398.4	406.0	411.1	484.3
15	410.8	415.8	421.8	484.6
20	421.5	424.8	430.8	484.4
25	430.8	433.1	439.0	484.5
30	438.7	440.7	446.8	485.2
35	445.5	447.9	452.6	486.4
40	451.8	454.5	458.5	488.6
45	457.5	459.7	463.5	490.6
50	462.7	464.7	468.0	491.3
55	467.9	469.2	472.0	492.4
60	472.1	473.1	475.8	494.3
65	475.9	477.2	479.0	496.0
70	479.2	480.3	482.0	497.6
75	482.2	483.1	484.7	499.2
80	484.5	485.1	486.9	500.1
85	486.2	486.8	488.9	501.3
90	487.2	487.6	490.0	501.7
95	487.9	488.3	490.6	502.0
100	488.6	489.3	491.3	502.7
105	489.5	490.4	492.3	503.5

Flow rate = 25 SLM, T_{oven} = 500 °C, Gas: N_2				
coordinates	Position of thermocouples			
[mm]	center	1/2 radius	2/3 radius	wall
-5	309.3	330.5	340.4	473.4
0	327.4	348.4	355.5	475.3
5	346.7	361.6	367.0	475.7
10	362.7	373.3	379.5	476.4
15	376.6	383.6	391.6	476.2
20	388.8	392.5	401.9	476.7
25	399.4	402.6	411.1	477.4
30	408.8	411.6	420.6	477.6
35	416.7	420.3	427.4	478.3
40	424.5	428.2	434.9	480.8
45	431.7	435.0	440.9	482.5
50	438.3	441.3	446.7	483.5
55	445.0	447.0	452.0	485.0
60	450.6	452.4	457.2	487.5
65	456.0	457.8	461.6	489.8
70	460.6	462.0	465.8	492.3
75	465.0	466.4	469.8	494.1
80	468.6	469.4	473.2	495.5
85	471.3	471.9	476.1	497.0
90	472.7	473.2	477.9	497.8
95	473.8	474.3	478.9	498.3
100	475.0	475.8	480.1	499.3
105	476.6	477.9	481.6	500.3

Flow rate = 30 SLM, T_{oven} = 500 °C, Gas: N_2				
coordinates	Position of thermocouples			
[mm]	center	1/2 radius	2/3 radius	wall
-5	279.5	306.1	316.2	467.8
0	297.4	322.5	330.2	470.3
5	317.1	335.6	342.4	470.4
10	332.9	347.4	354.0	470.5
15	348.3	357.8	366.4	471.9
20	361.0	366.8	376.7	472.1
25	372.7	377.3	386.9	472.3
30	383.0	386.7	397.0	473.6
35	391.7	396.2	404.9	473.9
40	400.1	404.9	413.2	474.5
45	407.9	412.7	420.4	477.1
50	415.7	419.9	427.3	478.4
55	423.5	426.6	433.5	480.5
60	430.3	432.6	439.6	484.7
65	436.7	439.2	444.8	486.2
70	442.5	444.2	450.1	487.9
75	447.8	449.5	455.2	489.3
80	452.3	453.3	459.4	491.2
85	455.4	456.7	463.2	493.1
90	457.8	458.2	465.5	494.1
95	459.3	459.6	466.6	494.9
100	460.9	461.6	468.1	496.5
105	462.9	464.5	470.3	498.0

Flow rate = 35 SLM, T_{oven} = 500 °C, Gas: N_2				
coordinates	Position of thermocouples			
[mm]	center	1/2 radius	2/3 radius	wall
-5	251.0	278.5	291.0	459.4
0	268.2	294.9	304.4	464.7
5	287.7	308.0	316.8	465.7
10	303.6	319.9	328.7	466.1
15	318.7	330.3	339.8	466.4
20	332.6	339.6	350.6	468.0
25	344.4	350.1	361.1	466.5
30	354.7	359.5	371.2	467.5
35	363.9	369.4	379.5	467.5
40	373.0	379.3	388.5	469.6
45	381.5	387.4	396.4	471.0
50	390.1	395.5	404.3	471.5
55	398.8	402.8	411.4	475.2
60	406.3	409.7	418.4	477.5
65	413.6	416.8	424.4	481.3
70	420.2	422.8	430.4	484.3
75	426.8	429.0	436.3	484.6
80	432.2	433.4	441.7	487.0
85	436.5	437.3	446.5	489.5
90	438.7	439.9	449.3	490.5
95	440.3	441.3	450.4	491.1
100	442.3	443.6	452.2	493.0
105	444.8	446.2	454.9	494.5

Flow rate = 20 SLM, T_{oven} = 500 °C, Gas: He			
coordinates [mm]	Position of thermocouples		
	center	1/2 radius	2/3 radius	wall
-5	461.7	468.2	470.7	493.4
0	471.1	476.3	477.3	498.2
5	478.5	481.4	482.3	498.7
10	483.4	485.4	486.3	499.0
15	487.6	488.9	489.8	499.6
20	490.6	491.6	492.4	500.2
25	493.3	493.9	494.7	501.3
30	495.3	495.8	496.8	502.3
35	496.9	497.5	498.1	503.2
40	498.4	498.7	499.5	504.3
45	499.6	499.9	500.5	505.3
50	500.7	501.0	501.6	505.8
55	501.7	501.8	502.1	506.3
60	502.3	502.4	503.0	506.8
65	502.9	503.1	503.5	507.2
70	503.4	503.5	503.8	507.5
75	503.8	503.9	504.2	507.8
80	504.1	504.2	504.5	508.1
85	504.3	504.3	504.7	508.2
90	504.4	504.4	504.8	508.3
95	504.4	504.4	504.8	508.3
100	504.4	504.4	504.8	508.3
105	504.4	504.4	504.8	508.3

Flow rate = 25 SLM, T_{oven} = 500 °C, Gas: He			
coordinates [mm]	Position of thermocouples		
	center	1/2 radius	2/3 radius	wall
-5	427.7	439.8	443.3	485.3
0	444.2	454.1	456.5	491.3
5	456.6	462.4	464.7	491.9
10	464.7	468.7	471.1	492.3
15	471.8	474.3	476.0	492.6
20	477.1	478.6	480.8	493.6
25	481.5	482.9	484.6	495.1
30	485.0	486.0	488.0	496.3
35	487.8	488.8	490.3	497.7
40	490.3	491.3	492.6	499.5
45	492.4	493.2	494.4	500.8
50	494.4	494.9	496.0	501.6
55	496.1	496.4	497.4	502.1
60	497.5	497.6	498.5	503.6
65	498.7	498.9	499.6	504.4
70	499.7	499.8	500.4	505.4
75	500.5	500.6	501.1	505.4
80	501.1	501.2	501.7	506.3
85	501.6	501.7	502.2	506.5
90	501.8	501.9	502.4	506.7
95	501.9	502.0	502.6	506.7
100	502.0	502.2	502.8	506.9
105	502.1	502.4	502.9	507.2

Flow rate = 30 SLM, T_{oven} = 500 °C, Gas: He			
coordinates [mm]	Position of thermocouples		
	center	1/2 radius	2/3 radius	wall
-5	386.1	404.2	411.8	476.1
0	408.8	424.3	428.9	483.8
5	427.3	436.1	439.9	484.5
10	439.3	445.4	449.3	484.6
15	449.4	453.6	457.4	484.9
20	457.4	460.2	464.3	486.3
25	464.2	466.7	469.9	487.3
30	469.6	471.5	475.0	488.7
35	474.0	475.9	478.4	490.5
40	478.0	479.6	482.1	493.0
45	481.4	482.8	484.9	494.7
50	484.5	485.5	487.4	496.0
55	487.4	488.0	489.6	497.6
60	489.7	490.0	491.7	499.0
65	491.8	492.2	493.3	500.4
70	493.4	493.8	494.8	501.7
75	495.0	495.3	496.1	502.1
80	496.2	496.4	497.2	503.0
85	497.0	497.2	498.1	503.9
90	497.4	497.6	498.5	504.2
95	497.7	498.0	498.9	504.4
100	498.0	498.4	499.3	504.8
105	498.3	498.9	499.7	505.2

2.8 Cu 580 μm

coordinates [mm]	Flow rate = 10 SLM, T$_{oven}$ = 300 °C, Gas: N$_2$ Position of thermocouples			
	center	1/2 radius	2/3 radius	wall
-5	250.0	256.3	258.7	293.0
0	258.1	261.6	264.9	293.5
5	267.6	269.6	274.0	294.6
10	276.0	276.4	278.8	295.4
15	281.8	282.3	283.5	296.3
20	286.6	287.1	287.4	297.4
25	290.1	290.8	291.0	299.0
30	292.3	292.7	292.9	299.9
35	293.7	294.2	294.5	300.8
40	295.0	295.2	295.6	301.8
45	296.1	296.3	296.5	301.9
50	297.0	297.2	297.4	302.2
55	297.7	297.9	298.1	302.7
60	298.2	298.4	298.6	303.2
65	298.7	298.9	299.1	303.4
70	299.1	299.3	299.5	303.6
75	299.4	299.6	299.7	303.7
80	299.7	299.9	300.1	304.1
85	299.9	300.1	300.1	304.1
90	300.1	300.2	300.2	304.1
95	300.2	300.2	300.2	304.2
100	300.2	300.2	300.3	304.2
105	300.2	300.3	300.3	304.2

coordinates [mm]	Flow rate = 15 SLM, T$_{oven}$ = 300 °C, Gas: N$_2$ Position of thermocouples			
	center	1/2 radius	2/3 radius	wall
-5	222.9	228.4	230.6	284.8
0	232.8	238.4	240.6	286.4
5	248.6	252.6	253.4	286.7
10	258.0	262.5	262.7	287.2
15	265.2	268.3	268.7	288.3
20	270.8	272.9	273.2	289.9
25	275.4	277.5	277.8	292.5
30	279.1	280.7	280.9	294.5
35	282.1	283.5	283.6	295.4
40	284.5	285.8	286.0	296.0
45	286.7	287.8	288.0	297.7
50	288.6	289.4	289.6	298.0
55	290.2	290.8	291.0	298.6
60	291.3	292.0	292.1	299.6
65	292.4	293.1	293.2	300.3
70	293.3	293.9	294.1	300.7
75	294.2	294.8	295.1	301.0
80	294.9	295.4	295.6	301.6
85	295.6	295.8	296.0	301.7
90	296.0	296.1	296.2	301.7
95	296.2	296.3	296.4	301.9
100	296.4	296.5	296.6	302.0
105	296.5	296.7	296.8	302.1

coordinates [mm]	Flow rate = 20 SLM, T$_{oven}$ = 300 °C, Gas: N$_2$ Position of thermocouples			
	center	1/2 radius	2/3 radius	wall
-5	195.8	213.9	218.2	278.5
0	209.4	214.2	218.3	278.8
5	224.3	232.4	234.0	279.8
10	235.2	241.5	242.8	280.6
15	244.5	248.8	249.9	281.2
20	251.8	255.1	255.9	282.9
25	257.8	261.1	261.8	288.1
30	262.9	265.8	266.6	289.6
35	267.0	269.8	270.7	290.5
40	271.0	273.5	274.2	291.2
45	274.2	276.4	277.0	292.8
50	276.9	279.0	279.6	293.1
55	279.5	281.2	281.9	294.5
60	281.5	283.1	283.6	296.0
65	283.2	285.0	285.4	297.0
70	284.7	286.5	287.0	297.5
75	286.4	288.1	288.6	298.1
80	287.7	288.9	289.4	299.2
85	289.0	289.8	290.2	299.3
90	289.8	290.3	290.6	299.3
95	290.4	290.7	290.9	299.5
100	290.7	291.0	291.1	299.9
105	291.1	291.3	291.4	300.0

coordinates [mm]	Flow rate = 25 SLM, T$_{oven}$ = 300 °C, Gas: N$_2$ Position of thermocouples			
	center	1/2 radius	2/3 radius	wall
-5	174.5	195.1	200.7	273.0
0	188.8	204.7	209.2	273.2
5	203.9	214.4	216.9	274.1
10	215.3	223.4	225.8	274.9
15	225.7	231.7	234.1	275.5
20	233.8	238.4	240.3	277.0
25	241.0	245.5	247.3	280.9
30	246.7	251.1	253.6	282.7
35	251.5	255.9	258.0	284.2
40	256.4	260.3	262.3	285.0
45	260.5	264.1	265.9	286.3
50	264.2	267.5	269.4	288.2
55	267.5	270.3	272.2	290.1
60	270.1	273.0	274.9	292.4
65	272.5	275.5	277.3	294.0
70	274.6	277.7	279.5	294.5
75	276.8	279.8	280.9	295.0
80	278.9	281.2	282.4	296.6
85	280.9	282.4	283.3	296.8
90	282.2	283.2	283.9	296.8
95	283.2	283.7	284.3	297.1
100	283.7	284.2	284.6	297.8
105	284.2	284.8	285.1	298.1

Flow rate = 30 SLM, T_{oven} = 300 °C, Gas: N_2				
coordinates [mm]	Position of thermocouples			
	center	1/2 radius	2/3 radius	wall
-5	157.3	178.7	185.8	269.0
0	170.8	188.5	193.6	269.4
5	186.0	198.1	201.7	269.5
10	198.0	207.0	210.3	269.8
15	208.8	215.3	218.4	270.2
20	216.9	222.5	225.0	271.9
25	224.0	229.9	232.5	277.4
30	230.2	236.0	238.6	278.1
35	235.7	241.5	244.0	278.3
40	240.9	246.4	248.8	280.5
45	245.7	250.7	253.2	282.8
50	250.0	254.7	257.0	284.7
55	254.1	258.3	260.3	286.1
60	257.2	261.4	263.3	289.0
65	260.1	264.7	266.7	290.8
70	262.7	267.4	269.3	291.3
75	265.5	270.1	271.9	292.3
80	268.2	271.8	273.5	293.8
85	270.8	273.3	275.0	294.0
90	272.7	274.3	275.9	294.1
95	274.0	275.1	276.5	294.6
100	274.9	275.5	276.9	295.4
105	275.6	276.3	277.3	295.7

Flow rate = 35 SLM, T_{oven} = 300 °C, Gas: N_2				
coordinates [mm]	Position of thermocouples			
	center	1/2 radius	2/3 radius	wall
-5	143.7	163.8	172.8	264.2
0	155.7	173.8	181.5	265.0
5	171.2	183.4	189.5	265.3
10	182.7	191.7	197.6	266.2
15	192.5	201.4	206.3	266.3
20	201.0	207.5	212.4	268.0
25	208.6	215.4	220.2	272.3
30	215.0	222.0	225.7	276.4
35	220.7	228.0	231.4	276.6
40	225.8	233.4	235.9	278.0
45	231.0	237.9	240.3	279.5
50	236.0	242.1	245.7	281.1
55	240.8	246.3	249.4	283.0
60	244.1	250.0	252.1	286.4
65	247.5	253.9	255.6	288.5
70	250.5	257.3	258.6	289.5
75	253.5	260.6	261.8	290.4
80	256.4	262.4	263.7	291.3
85	259.5	264.2	265.3	292.5
90	262.0	265.1	266.1	292.7
95	264.0	266.0	266.9	293.5
100	265.2	266.7	267.5	294.5
105	266.2	267.6	268.6	295.0

Flow rate = 10 SLM, T_{oven} = 500 °C, Gas: N_2				
coordinates [mm]	Position of thermocouples			
	center	1/2 radius	2/3 radius	wall
-5	439.1	452.9	455.3	489.9
0	455.0	464.3	465.8	491.6
5	468.2	473.4	473.9	493.6
10	476.7	480.1	480.7	495.5
15	482.9	485.2	485.7	496.5
20	487.3	488.7	489.2	498.4
25	490.7	491.9	492.3	500.9
30	493.2	494.2	494.6	501.9
35	495.3	496.1	496.4	502.7
40	497.0	497.7	498.2	503.6
45	498.4	498.9	499.2	504.4
50	499.5	499.9	500.1	505.0
55	500.5	500.7	500.8	505.6
60	501.1	501.4	501.5	506.2
65	501.7	502.1	502.3	506.6
70	502.2	502.5	502.5	506.7
75	502.7	502.9	503.0	506.9
80	503.0	503.1	503.2	507.2
85	503.2	503.3	503.3	507.3
90	503.4	503.4	503.4	507.2
95	503.4	503.4	503.4	507.2
100	503.4	503.4	503.4	507.2
105	503.4	503.4	503.5	507.2

Flow rate = 15 SLM, T_{oven} = 500 °C, Gas: N_2				
coordinates [mm]	Position of thermocouples			
	center	1/2 radius	2/3 radius	wall
-5	393.2	414.4	422.0	478.7
0	415.9	431.4	435.1	480.8
5	435.7	444.6	447.7	482.4
10	448.5	454.9	456.7	484.8
15	458.8	463.4	465.4	486.4
20	466.3	469.5	471.4	489.0
25	472.2	475.4	477.1	492.7
30	476.9	479.5	481.2	494.8
35	480.8	483.4	485.1	496.5
40	484.2	486.6	487.3	497.1
45	487.1	489.0	489.7	499.3
50	489.6	491.1	491.8	500.3
55	491.8	493.0	493.6	501.3
60	493.3	494.4	495.1	502.7
65	494.6	495.8	496.5	503.4
70	495.8	496.9	497.5	503.7
75	496.9	497.9	498.4	504.2
80	497.9	498.5	498.9	505.1
85	498.7	499.0	499.3	505.1
90	499.1	499.3	499.5	505.1
95	499.5	499.5	499.6	505.3
100	499.6	499.8	499.9	505.4
105	499.8	500.0	500.1	505.4

Flow rate = 20 SLM, T_{oven} = 500 °C, Gas: N_2				
coordinates	Position of thermocouples			
[mm]	center	1/2 radius	2/3 radius	wall
-5	351.1	379.5	387.8	469.4
0	375.7	396.8	402.5	470.8
5	399.6	412.5	416.3	472.4
10	416.6	425.7	429.0	474.4
15	430.0	437.0	440.6	476.0
20	440.1	445.6	449.3	479.5
25	448.5	454.2	457.6	483.7
30	455.3	460.6	464.1	486.2
35	461.2	466.2	469.7	488.4
40	466.6	471.2	474.5	489.8
45	471.4	475.4	478.7	493.5
50	475.3	478.9	481.9	494.6
55	478.8	481.7	483.5	496.2
60	481.5	484.3	485.8	498.4
65	483.9	486.6	488.2	499.7
70	485.7	488.1	489.6	500.1
75	487.7	490.1	491.4	500.7
80	489.5	491.3	492.5	502.1
85	491.1	492.3	493.2	502.2
90	492.1	492.9	493.5	502.4
95	492.9	493.5	493.9	502.9
100	493.3	493.8	494.3	503.2
105	493.8	494.5	495.0	503.2

Flow rate = 25 SLM, T_{oven} = 500 °C, Gas: N_2				
coordinates	Position of thermocouples			
[mm]	center	1/2 radius	2/3 radius	wall
-5	311.4	344.8	356.5	460.4
0	338.5	364.2	371.2	461.4
5	364.1	380.5	386.1	462.3
10	382.4	394.9	400.1	464.7
15	398.9	408.2	413.8	466.2
20	411.1	418.9	424.5	469.9
25	421.3	429.5	435.0	475.0
30	429.9	438.0	443.4	477.9
35	437.8	445.5	448.9	480.5
40	444.6	452.1	455.3	481.9
45	450.8	457.5	460.6	485.3
50	456.1	462.2	465.5	486.6
55	461.4	466.5	469.8	490.5
60	465.2	469.9	473.3	493.5
65	468.7	473.5	476.1	495.0
70	471.7	476.2	479.3	495.7
75	474.7	479.3	482.4	496.8
80	477.3	480.9	483.7	497.5
85	479.9	482.3	484.7	498.6
90	481.8	483.3	484.9	498.8
95	482.9	484.1	485.2	499.7
100	483.9	485.0	485.8	500.4
105	484.8	486.1	486.9	500.4

Flow rate = 30 SLM, T_{oven} = 500 °C, Gas: N_2				
coordinates	Position of thermocouples			
[mm]	center	1/2 radius	2/3 radius	wall
-5	282.2	319.7	331.4	453.3
0	308.7	337.6	346.6	453.9
5	336.7	354.7	360.9	454.4
10	355.7	370.3	376.0	456.6
15	372.4	383.8	390.1	457.7
20	385.4	395.4	400.4	461.6
25	397.0	407.5	412.4	467.9
30	406.8	417.7	422.5	470.0
35	415.3	426.0	430.9	474.5
40	423.8	434.6	439.2	476.3
45	431.0	440.3	444.7	478.5
50	437.8	446.1	450.1	480.2
55	443.9	451.3	455.1	484.3
60	448.4	455.3	459.1	488.7
65	452.8	460.1	463.8	490.8
70	456.5	463.5	467.1	491.6
75	460.2	467.0	469.9	492.9
80	463.9	469.1	471.7	494.3
85	467.4	471.3	473.6	495.3
90	469.9	472.5	474.6	495.6
95	471.8	473.6	475.4	496.5
100	473.2	474.9	476.5	497.2
105	474.7	476.5	477.9	497.2

Flow rate = 35 SLM, T_{oven} = 500 °C, Gas: N_2				
coordinates	Position of thermocouples			
[mm]	center	1/2 radius	2/3 radius	wall
-5	255.6	288.2	307.0	446.1
0	281.4	310.8	320.7	446.4
5	306.2	327.8	334.3	447.8
10	325.6	343.0	349.1	449.4
15	342.7	357.3	363.0	450.3
20	356.1	369.3	374.7	453.8
25	369.1	382.1	387.4	459.3
30	379.4	392.7	397.9	463.3
35	389.0	402.7	407.7	464.9
40	398.1	411.4	416.1	471.1
45	407.1	418.8	423.4	471.2
50	414.6	425.6	429.8	475.8
55	421.2	431.5	435.6	478.3
60	426.9	436.9	441.2	483.0
65	432.2	442.3	445.3	485.1
70	436.4	446.3	450.3	486.3
75	440.8	450.5	454.4	487.5
80	445.1	453.2	456.8	490.8
85	449.5	455.7	458.7	491.2
90	453.0	457.2	460.0	491.5
95	455.7	458.6	461.2	492.3
100	457.7	460.0	462.6	493.8
105	459.8	462.4	463.8	493.8

Flow rate = 20 SLM, T_{oven} = 500 °C, Gas: He			
coordinates	Position of thermocouples		
[mm]	center	1/2 radius	2/3 radius	wall
-5	463.5	471.7	472.9	488.7
0	475.4	478.9	480.9	491.7
5	483.3	485.3	486.3	494.1
10	487.8	489.3	490.0	496.1
15	491.4	492.3	492.9	497.5
20	493.9	494.5	494.9	499.5
25	495.9	496.5	496.9	501.6
30	497.5	498.1	498.5	502.8
35	498.9	499.4	499.7	503.7
40	500.0	500.4	500.6	504.8
45	501.0	501.3	501.5	505.2
50	501.8	502.0	502.1	505.8
55	502.5	502.6	502.6	506.3
60	503.0	503.1	503.1	507.0
65	503.4	503.5	503.5	507.3
70	503.8	503.8	503.8	507.5
75	504.1	504.1	504.1	507.7
80	504.3	504.3	504.3	508.0
85	504.5	504.5	504.6	508.0
90	504.5	504.5	504.6	508.0
95	504.5	504.5	504.7	508.0
100	504.5	504.5	504.7	508.0
105	504.4	504.4	504.6	508.0

Flow rate = 25 SLM, T_{oven} = 500 °C, Gas: He			
coordinates	Position of thermocouples		
[mm]	center	1/2 radius	2/3 radius	wall
-5	433.2	447.2	450.4	477.9
0	452.1	460.7	462.8	481.6
5	465.5	469.7	471.4	484.4
10	473.2	476.0	477.1	487.1
15	479.1	481.1	482.1	489.1
20	483.3	484.7	485.3	492.1
25	486.7	488.1	488.7	495.7
30	489.5	490.6	491.4	497.2
35	491.8	492.8	493.5	498.4
40	493.8	494.8	495.5	499.8
45	495.5	496.1	496.5	501.1
50	496.9	497.4	497.8	502.0
55	498.1	498.4	498.7	502.9
60	499.0	499.3	499.5	504.1
65	499.8	500.0	500.1	504.7
70	500.4	500.6	500.7	504.9
75	501.0	501.2	501.3	505.3
80	501.5	501.5	501.6	506.0
85	501.9	501.9	501.9	506.1
90	502.1	502.1	502.2	506.1
95	502.2	502.2	502.4	506.2
100	502.2	502.2	502.5	506.3
105	502.3	502.3	502.6	506.3

Flow rate = 30 SLM, T_{oven} = 500 °C, Gas: He			
coordinates	Position of thermocouples		
[mm]	center	1/2 radius	2/3 radius	wall
-5	394.3	415.3	423.4	466.9
0	421.4	435.0	439.6	470.2
5	441.5	448.2	452.1	473.0
10	453.0	457.8	460.9	476.2
15	461.9	465.2	468.0	478.7
20	468.1	470.7	472.2	482.8
25	473.5	476.0	478.0	487.5
30	477.8	480.0	481.4	489.9
35	481.5	483.6	485.0	492.0
40	484.7	486.5	487.7	494.5
45	487.4	488.9	489.9	495.8
50	489.8	491.0	491.9	497.3
55	491.9	492.7	493.4	499.0
60	493.4	494.1	494.4	500.7
65	494.7	495.4	495.7	501.7
70	495.9	496.4	496.7	502.1
75	497.0	497.4	497.7	502.7
80	497.8	498.0	498.2	503.9
85	498.6	498.7	498.8	504.0
90	499.0	499.1	499.1	504.0
95	499.2	499.3	499.4	504.3
100	499.4	499.5	499.7	504.5
105	499.6	499.8	500.1	504.5